PATHOGENESIS OF HYPERCHOLESTEROLEMIA IN IL-13-INDUCED RAT MODEL OF MINIMAL CHANGE NEPHROTIC SYNDROME

LOW DANWEI LAURETTA

(B.Sc., Second Class Honours (Upper Division), NTU)

A THESIS SUBMITTED FOR THE DEGREE OF

DOCTOR OF PHILOSOPHY

DEPARTMENT OF PAEDIATRICS

NATIONAL UNIVERSITY OF SINGAPORE

2015

Declaration

I hereby declare that this thesis is my original work and it has been written by me in its entirety. I have duly acknowledged all the sources of information which have been used in the thesis.

This thesis has also not been submitted for any degree in any university previously.

_____

Low Danwei Lauretta

11 November 2015

Acknowledgements

I sincerely express my heartfelt gratitude to my supervisor, Professor Yap Hui Kim, for her invaluable guidance and sharing of expert knowledge throughout the course of my research.

I would also like to express my gratitude to:
Associate Professor Henry Yang He and Dr Chen Jinmiao for their expertise and advice in microarray analysis.

Dr Xia Lei for his guidance in experiments involving rat primary hepatocyte cell culture.

My colleagues Chan Chang Yien, Ng Jun Li, Zhang Yaochun, Sun Zi Jin, Guinevere Sew, Liang Ai Wei, Seah Ching Ching, Joni Chong, Chin Hui Xian and Tay Siew Leng for their untiring support and fun-filled company.

My friends Stephy Chua, Tan Lay Boon, Leung Chi Ching, Pearlyn Yap, Fidelia Kuek, Gerald Lau, Ian Cheng and Nicholas Tay for their encouragement.

My family members who have always been there for me.

This work was supported by grant NMRC/1282/2010 from the National Medical Research Council, Singapore.

Table of Contents

Summary

One of the major complications of minimal change nephrotic syndrome (MCNS) is hypercholesterolemia. In non-MCNS experimental rat models of NS, hypercholesterolemia is associated with abnormalities in hepatic cholesterol metabolism, and is postulated to be secondary to massive proteinuria. Our laboratory has established an *IL-13* gene overexpression rat model of MCNS, a Th2 cytokine model similar to that in human disease, where hypercholesterolemia correlated significantly only with serum IL-13 levels, and appeared to precede the development of proteinuria. We therefore hypothesized that hypercholesterolemia in MCNS was primarily due to dysregulation of cholesterol homeostasis, mediated by the direct action of Th2 cytokines, and not solely a consequence secondary to the accompanying proteinuria.

The aims of this study were firstly to profile the molecular events in the liver of the *IL-13* transfected nephrotic rats using cDNA microarray to identify differentially expressed genes (DEGs); secondly to perform a comparative analysis of the gene expression profile of hepatic cholesterol metabolism at the onset of hypercholesterolemia in the pre-proteinuric phase (early event, termed as HC rats) and the nephrotic phase (late event); lastly to validate the *in vivo* results in rat primary hepatocyte culture.

RNA from the liver of control and *IL-13* transfected nephrotic rats were reverse transcribed and hybridized on Sentrix® BeadChip Array RatRef-12 v1. DEGs

were selected based on fold change ≥1.5 and FDR <0.05 and pathway analysis was performed using DAVID. Plasma IL-13, albumin, creatinine, total cholesterol and urine albumin excretion levels were assayed weekly. Hepatic cholesterol was extracted using hexane:isopropanol or Bligh-Dyer method, and quantified using enzymatic colorimetric assay or LC/MS respectively. Hepatocyte cholesterol efflux via ABCA1 and ABCG5 were measured using apoA-I and taurocholate as cholesterol acceptors respectively. The role of LXRa in IL-13-induced hypercholesterolemia was studied using *LXRa*-knockdown in rat primary hepatocytes. Gene and protein expressions of key molecules were studied using qPCR and Western blot respectively.

Pathway analysis of DEGs identified 'ABC transporters' as the most relevant pathway in cholesterol metabolism, of which *ABCG5* expression showed the greatest downregulation in the *IL-13* transfected nephrotic rats, and was associated with *HMGCR* upregulation.

Weekly biochemical profiling of our *IL-13* transfected rats showed that plasma cholesterol was significantly elevated from Week 1 onwards and preceded the onset of significant proteinuria. Study of these HC rats (early event) showed reduced ABCG5, accompanied by downregulation of ABCA1, *LXRa* and *RXRa*. Moreover, LXRa correlated inversely with plasma cholesterol, suggesting the role of *LXRa-ABCG5/ABCA1* pathway in initiating hypercholesterolemia.

IL-13-stimulated rat primary hepatocytes showed downregulation of *HMGCR*, *LXRa*, *RXRa* and ABCA1, accompanied by reduced ABCG5- and ABCA1-mediated cholesterol efflux. Knockdown of *LXRa* in hepatocytes diminished T0901317-induced *ABCG5* and *ABCA1* expressions.

In summary, the hypercholesterolemia observed in HC rats (early event) could be due to the downregulation of *LXRa-ABCG5/ABCA1* pathway with reduced cholesterol efflux into bile canaliculi, resulting in increased intracellular free cholesterol. This could further inhibit hepatic uptake of cholesterol, leading to hypercholesterolemia. Late event hypercholesterolemia in the *IL-13* transfected nephrotic rats could possibly be enhanced by the hepatic upregulation of *HMGCR* secondary to the gross proteinuria.

List of Tables

List of Figures

List of Abbreviations

3'UTR	3' untranslated region
^{3}H	Tritium, a radioactive isotope of hydrogen
ABC transporter	ATP-binding cassette transporter
ABCA1	ABC transporter, sub-family A, member 1
ABCG5	ABC transporter, sub-family G, member 5
ABCG8	ABC transporter, sub-family G, member 8
ACAT	Acyl CoA:cholesterol acyltransferase
ANGPTL4	Angiopoietin-like 4
Apo	Apolipoprotein
ATP	Adenosine triphosphate
BC	Bile canaliculus
BCG	Bromocresol green
BSA	Bovine serum albumin
cDNA	Complementary DNA
CM	Chylomicron
CMR	Chylomicron remnant
CNS	Congenital nephrotic syndrome
Ct	Crossing threshold
CYP7A1	Cholesterol 7-alpha hydroxylase
DAVID	Database for Annotation, Visualization and Integrated Discovery
ddH_2O	Double distilled water
DEG	Differentially expressed gene
dNTP	Deoxynucleoside triphosphate
ELISA	Enzyme linked immuno sorbent assay
ER	Endoplasmic reticulum
FBS	Fetal bovine serum
FDR	False discovery rate
FFA	Free fatty acid
FRNS	Frequently relapsing nephrotic syndrome
FSGS	Focal segmental glomerulosclerosis
GAPDH	Glyceraldehyde 3-phosphate dehydrogenase
H&E	Hematoxylin and eosin
HDL	High density lipoprotein
HIV	Human immunodeficiency virus
HMG-CoA	3-hydroxy-3-methylglutaryl-CoA
HMGCR	HMG-CoA reductase
HNF4a	Hepatocyte nuclear factor 4 alpha
HRP	Horseradish peroxidase
IDL	Intermediate density lipoprotein
Ig	Immunoglobulin

IL	Interleukin
iNOS	Inducible nitric oxide synthase
INS	Idiopathic nephrotic syndrome
KEGG	Kyoto Encyclopedia of Genes and Genomes
LB	Luria-Bertani
LC/MS	Liquid chromatography/mass spectrometry
LCAT	Lecithin cholesterol acyltransferase
LDL	Low density lipoprotein
LDLR	LDL receptor
LPL	Lipoprotein lipase
LRH-1	Liver receptor homolog-1
LXR	Liver X receptor
LXRa	LXR alpha
LXRb	LXR beta
LXRE	LXR response element
MAPK	Mitogen-activated protein kinase
MCNS	Minimal change nephrotic syndrome
MN	Membranous nephropathy
MPGN	Membranoproliferative glomerulonephritis
MsPGN	Mesangial proliferative glomerulonephritis
NaCl	Sodium chloride
NAD	Nicotinamide adenine dinucleotide
NADP	Nicotinamide adenine dinucleotide phosphate
NaOH	Sodium hydroxide
NAR rat	Nagase analbuminemic rat
NF-kB	Nuclear factor-kB
NP-40	Nonionic polyoxyethylene surfactant detergent solution
NTC	Non-targeting control siRNA
OPD	o-Diphenylenediamine
PA	Puromycin aminonucleoside
PAN	Puromycin aminonucleoside nephrosis
PBMC	Peripheral blood mononuclear cell
PBS	Phosphate-buffered saline
pCI	pCI mammalian expression vector
pCI-IL-13	pCI cloned with rat *IL-13* gene
PCR	Polymerase chain reaction
PMT	Photomultiplier tube
pSTAT6	Phosphorylated STAT6
qPCR	Quantitative real-time polymerase chain reaction
r	Spearman's rank correlation coefficient
RCT	Reverse cholesterol transport
RefSeq	NCBI Reference Sequence Database
RIN	RNA integrity number

RXR	Retinoid X receptor
RXRa	RXR alpha
S1P	Site-1 protease
S2P	Site-2 protease
SCAP	SREBF chaperone
SDNS	Steroid-dependent nephrotic syndrome
SEM	Standard error mean
siRNA	Small interfering RNA
SOC	Super optimal broth with catabolite repression
SR-BI	Scavenger receptor class B type I
SRE	Sterol regulatory element
SREBF2	Sterol regulatory element binding transcription factor 2
SRNS	Steroid-resistant nephrotic syndrome
SSNS	Steroid-sensitive nephrotic syndrome
STAT6	Signal transducer and activator of transcription 6
TBS	Tris-buffered saline
TBST	1X TBS with 0.05% Tween 20
TGFb	Transforming growth factor beta
Th cell	Helper T cell
Th1 cell	Type 1 helper T cell
Th2 cell	Type 2 helper T cell
TNFa	Tumor necrosis factor alpha
VLDL	Very low density lipoprotein
X-Gal	5-bromo-4-chloro-3-indolyl-β-d-galactopyranoside

Units of Measurement

bp	Base pair
cm	Centimeter
°C	Degree Celsius
G	Gauge
g	Gram
g/dl	Gram per deciliter
g/l	Gram per liter
g	Gravity
w/v	Mass per volume
µCi/ml	MicroCurie per milliliter
µg	Microgram
µg/24hour	Microgram per 24 hours
µg/µl	Microgram per microliter
µg/ml	Microgram per milliliter
µg/ml	Microgram per milliliter
µl	Microliter
µm	Micrometer
mg	Milligram
mg/day	Milligram per day
mg/dl	Milligram per deciliter
mg/kg	Milligram per kilogram
mg/ml	Milligram per milliliter
$mg/m^2/day$	Milligram per square meter per day
$mg/m^2/hr$	Milligram per square meter per hour
ml	Milliliter
mm	Millimeter
mM	Millimolar
mmol/l	Millimolar per liter
ng	Nanogram
ng/µl	Nanogram per microliter
ng/ml	Nanogram per milliliter
nm	Nanometer
nM	Nanomolar
N	Normality
%	Percentage
pg/ml	Picogram per milliliter
rpm	Revolutions per minute
V	Volt

List of Appendices

List of Conference Abstracts

Poster presentation at ASN Renal Week 2009, San Diego, California, USA, 29th October – 1st November 2009. Role of altered *oncostatin-M (OSM)* expression in the hypercholesterolemia of an *IL-13* overexpression rat model of minimal change nephrotic syndrome (MCNS). Chang-Yien Chan, Tarun K Maheshwari, Lauretta D Low, Jinmiao Chen, Celine Prakash, Caroline GL Lee, Henry H Yang and Hui-Kim Yap.

Poster presentation at ASN Kidney Week 2012, San Diego, California, USA, 1st November – 4th November 2012. Pathogenesis of hypercholesterolemia in *IL-13* overexpression rat model of minimal change nephrotic syndrome (MCNS). Lauretta Danwei Low, Chang Yien Chan, Tarun K Maheshwari, Jinmiao Chen, Henry He Yang, Caroline GL Lee, Hanry Yu and Hui Kim Yap.

Poster presentation at ASN Kidney Week 2014, Philadelphia, Pennsylvania, USA, 13th November – 16th November 2014. IL13-induced hepatic cholesterol transport defect in rat model of minimal change nephrotic syndrome (MCNS). Lauretta Danwei Low, Chang Yien Chan, Jinmiao Chen, Henry He Yang, Caroline GL Lee, Hanry Yu, Markus R Wenk and Hui Kim Yap.

Oral presentation at 6th ASPR Congress, ASPR2010, Taipei, Taiwan, 15th April – 18th April 2010. Down-regulation of oncostatin M (OSM) pathway in the genesis of hypercholesterolemia in the *IL-13* overexpression rat model of minimal change

nephrotic syndrome (MCNS). Lauretta D Low, Chang-Yien Chan, Tarun K Maheshwari, Henry Yang, Jinmiao Chen, Celine Prakash, Caroline GL Lee and Hui-Kim Yap.

Poster presentation at NKF 1st Scientific Meeting 2012, Singapore, 4th February 2012. Pathogenesis of hypercholesterolemia in minimal change nephrotic syndrome (MCNS). Hui-Kim Yap, Lauretta D Low, Chang-Yien Chan, Tarun K Maheshwari, Henry Yang, Jinmiao Chen, Celine Prakash, Caroline GL Lee and Hui-Kim Yap.

Poster presentation at 8th NHG Annual Scientific Congress 2009, Singapore, 16th October – 17th October 2009. Role of altered oncostatin-M (OSM) expression in the hypercholesterolemia of an *IL-13* overexpression rat model of minimal change nephrotic syndrome (MCNS). KH Ng, TK Maheshwari, CY Chan, LD Low, JM Chen, C Prakash, H Yang, C GL Lee and HK Yap.

Poster presentation at 1st Annual Graduate Scientific Congress 2011, Singapore, 25th January 2011. Role of altered *oncostatin-M* (OSM) expression in the hypercholesterolemia of an *IL-13* overexpression rat model of minimal change nephrotic syndrome (MCNS). Lauretta D Low, Chang Yien Chan, Tarun K Maheshwari, Jinmiao Chen, Celine Prakash, Henry H Yang and Hui Kim Yap.

Poster presentation at 2nd Annual Graduate Scientific Congress 2012, Singapore, 15th February 2012. Pathogenesis of hypercholesterolemia in minimal change nephrotic syndrome (MCNS). Hui-Kim Yap, Lauretta D Low, Chang-Yien Chan, Tarun K Maheshwari, Henry Yang, Jinmiao Chen, Celine Prakash, Caroline GL Lee and Hui-Kim Yap.

Poster presentation at 3rd Annual Graduate Scientific Congress 2013, Singapore, 30th January 2013. Pathogenesis of hypercholesterolemia in *IL-13* overexpression rat model of minimal change nephrotic syndrome (MCNS). Lauretta D Low, Chang Yien Chan, Tarun K Maheshwar1, Jinmiao Che2, Henry Yang, Caroline GL Lee, Hanry Yu, and Hui Kim Yap.

Poster presentation at 4th Annual Graduate Scientific Congress 2014, Singapore, 11th March 2014. Hypercholesterolemia in *IL-13* overexpression rat model of minimal change nephrotic syndrome (MCNS) is associated with hepatic cholesterol transport defect. Lauretta Low, Chang Yien Chan, Jinmiao Chen, Henry Yang, Caroline Lee, Hanry Yu, Markus Wenk and Hui Kim Yap. (Best poster award)

Chapter 1 Introduction

1.1. Nephrotic syndrome

Nephrotic syndrome is characterized by massive proteinuria, hypoalbuminemia, edema and hypercholesterolemia. In children, idiopathic nephrotic syndrome (INS) is an important cause of morbidity amongst the childhood glomerular diseases both in Singapore and worldwide (Woo et al., 2010; Yap et al., 1990; Yap et al., 1989).

1.1.1. Etiology of nephrotic syndrome

The etiology of nephrotic syndrome is usually age-dependent, and can be attributed to a primary or secondary cause. Primary causes of nephrotic syndrome can be either immunological or genetic.

Nephrotic syndrome presenting in the first three months of life is known as congenital nephrotic syndrome (CNS), and is primarily due to mutations in genes coding for podocyte slit diaphragm proteins such as podocin and nephrin, and transcriptional regulator in kidney development such as Wilms' tumor 1. CNS can also be due to multi-systemic syndromes such as Pierson syndrome, as well as congenital infections such as syphilis or cytomegalovirus.

Between the ages of 1 and 10 years, the majority of childhood nephrotic syndrome are idiopathic in nature. The proportion of secondary nephrotic syndrome due to underlying diseases such as systemic lupus erythematosus,

diabetic mellitus, viral infections (human immunodeficiency virus (HIV), hepatitis B and C), drug exposures and allergies, increases beyond the first decade of life (Gbadegesin and Smoyer, 2008).

1.1.2. Classification and epidemiology of nephrotic syndrome

Idiopathic nephrotic syndrome can be classified histologically into minimal change nephrotic syndrome (MCNS), focal segmental glomerulosclerosis (FSGS), membranoproliferative glomerulonephritis (MPGN), mesangial proliferative glomerulonephritis (MsPGN) and membranous nephropathy (MN). MCNS is the most common histologic variant among children with INS (ISKDC, 1978).

The annual incidence of nephrotic syndrome in most Western countries is estimated to range between 2 to 7 cases per 100,000 children, and the prevalence is about 16 cases per 100,000 children (Niaudet, 2004). Ethnicity, race and gender play a role in the pathogenesis of the disease. The incidence of nephrotic syndrome was reported to be six times higher in Asian than European children in the United Kingdom (Sharples et al., 1985). Hispanic and black patients were more predisposed to steroid-resistant nephrotic syndrome than white patients (Ingulli and Tejani, 1991). A higher occurrence of nephrotic syndrome was observed in boys than in girls with a ratio of 2:1, but this disparity was less obvious in adults (ISKDC, 1978).

Although the overall incidence of nephrotic syndrome has remained unchanged over the years, the histological pattern may be changing, with the incidence of FSGS reported to be on the rise in children and adults (Srivastava et al., 1999). In Singapore, there has been a significant increase in MCNS over the past three decades in adults (Table 1) (Woo et al., 2010). Similarly in Singapore children, a renal biopsy study in children with steroid-dependent and steroid-resistant nephrotic syndrome also showed that MCNS was the most common histological pattern, although in this group of children, FSGS was also an important underlying cause of INS (Yap et al., 1989).

Table 1: Distribution of the histological profile of adult INS in Singapore.

Histology	1st decade (D1)	2nd decade (D2)	3rd decade (D3)	χ^2-test (D1 vs D2 vs D3)	χ^2-test (D2 vs D3)
Minimal change nephrotic syndrome	18%	29%	30%	<0.001	0.78
Focal segmental glomerulosclerosis	10%	7%	13%	<0.05	<0.03
Focal global sclerosis	14%	19%	4%	<0.001	<0.001
Mesangial proliferative glomerulonephritis	33%	15%	8%	<0.001	<0.02
IgA nephritis	14%	17%	24%	<0.002	<0.05
Membranous nephropathy	8%	12%	19%	<0.001	<0.04
Crescenteric glomerulonephritis	1%	<1%	<1%	0.85	0.67
Others	2%	1%	2%	0.86	0.1
Total	100%	100%	100%		

1.1.3. Treatment for nephrotic syndrome

Administration of prednisone, a corticosteroid, is usually initiated in all newly diagnosed cases of nephrotic syndrome to achieve remission, after allowing time for spontaneous remission of nephrotic syndrome and elimination of other underlying factors such as occult infections. The consensus treatment starts with a daily induction of 60mg/m^2/day of prednisone for six weeks, followed by 40mg/m^2/day of prednisone on alternate days for another six weeks. Prednisone

may be stopped or slowly tapered over a variable period of time (Gipson et al., 2009; Lombel et al., 2013). An estimated 80% of nephrotic children enter into remission with corticosteroids, but up to 70% experience frequent relapses or become dependent on steroids to remain in remission (Gbadegesin and Smoyer, 2008; Koskimies et al., 1982).

Based on response to corticosteroids, nephrotic patients are classified into having (i) steroid-sensitive nephrotic syndrome (SSNS), patients who respond to corticosteroids with complete remission; (ii) steroid-resistant nephrotic syndrome (SRNS), patients who fail to go into remission after eight weeks of corticosteroid therapy; (iii) frequently relapsing nephrotic syndrome (FRNS), patients who respond to corticosteroids with remission for several weeks upon discontinuation of therapy but later relapse four or more times in a year; (iv) steroid-dependent nephrotic syndrome (SDNS), patients who respond to corticosteroids with remission but relapse while still receiving treatment or within two weeks after discontinuation of treatment, hence requiring constant low-dosage of steroids to prevent relapse (Gbadegesin and Smoyer, 2008).

In patients with FRNS and SDNS, steroid-sparing agents are often used to reduce the risk of relapse and lessen steroid-induced side effects, such as levamisole, cyclophosphamide, chlorambucil and cyclosporine. In patients with SRNS, intensive immunosuppressive treatments are used often in combination, such as

high-dose pulse methylprednisolone, cyclosporine, tacrolimus, mycophenolate mofetil and rituximab to achieve remission (Niaudet and Boyer, 2009).

Prolonged courses of corticosteroid treatment and alternative immunosuppressive agents may result in adverse side effects such as growth retardation, behavior disturbances, obesity, hypertension, cataracts, osteopenia and nephrotoxicity (Niaudet, 2004).

1.2. Hypercholesterolemia in nephrotic syndrome

One of the major pathological complications of nephrotic syndrome is hypercholesterolemia, the elevation of cholesterol level in the blood.

Although the majority of the children with nephrotic syndrome respond to corticosteroids, approximately 70% would experience one or more relapses (Gbadegesin and Smoyer, 2008; Koskimies et al., 1982). Children with FRNS will be exposed to prolonged periods of hypercholesterolemia. Similarly, in patients with SRNS, hypercholesterolemia is persistent (Merouani et al., 2003; Querfeld et al., 1988; Tsukahara et al., 1997).

Prolonged hypercholesterolemia not only increases the risk of atherosclerosis development leading to cardiovascular morbidity and mortality in the long term (Ordonez et al., 1993; Querfeld, 1999), but also progressive glomerular damage leading to renal failure (Keane et al., 1991; Moorhead et al., 1982). Even during

remission of nephrotic syndrome with resolution of proteinuria, hypercholesterolemia can still remain unabated (Merouani et al., 2003; Strauss et al., 1987; Zilleruelo et al., 1984).

Treatment with lipid-lowering medication is often indicated in addition to steroid therapy, as serum cholesterol can reach as high as 20mmol/l. Lipid-lowering agent statins is the first-line drugs to be prescribed to control the hypercholesterolemia in nephrotic syndrome (European Association for Cardiovascular et al., 2011). Alternative agents such as bile acid sequestrants, ezetimibe or nicotinic acid are used in patients who are unable to tolerate statins. These drugs target directly on cholesterol metabolism or prevent the absorption of cholesterol and bile acids.

The therapeutic effect of statins is not consistent in nephrotic patients, with a study reporting negative results in using rosuvastatin (De Backer et al., 2003; Kong et al., 2013). Coupled with insufficient validation of the efficacy of alternative agents in statin-intolerant nephrotic patients, the use of these lipid-lowering agents in managing the severe hypercholesterolemia often seen in children with nephrotic syndrome could not be firmly established. Therefore it is imperative to elucidate the molecular mechanism in the hypercholesterolemia of nephrotic syndrome in order to develop targeted therapy to control the high level of serum cholesterol.

1.2.1. Cholesterol metabolism

Cholesterol is a type of lipid, more specifically a steroid. It is an essential structural component within the plasma membrane which serves to regulate membrane fluidity, and also an important precursor in the synthesis of steroid hormones, bile acids and vitamin D.

Due to its involvement in various biological functions, cholesterol homeostasis is essential and maintained by a series of regulatory pathways that control the synthesis of endogenous cholesterol, absorption of dietary cholesterol, elimination of excess cholesterol, and transportation of cholesterol in the blood. Any imbalance in cholesterol homeostasis would result in health complications, such as cardiovascular diseases.

1.2.1.1.Regulation of cholesterol synthesis

The liver serves as a major site for cholesterol synthesis, which begins with the formation of 3-hydroxy-3-methylglutaryl-CoA (HMG-CoA) from acetyl-CoA and acetoacetyl-CoA in the cytosol (Figure 1). Reduction of HMG-CoA to mevalonate marks the irreversible step in cholesterol formation, catalyzed by HMG-CoA reductase (HMGCR). Subsequent conversion of mevalonate to cholesterol involves multiple steps catalyzed by a multitude of enzymes.

The rate-limiting enzyme HMGCR is partly involved in the main regulation of cholesterol biosynthesis. It is negatively regulated by its own end product

cholesterol, whereby increased intracellular free cholesterols bind to the sterol-sensing domain in HMGCR, activating it for proteolytic degradation (Kuwabara and Labouesse, 2002). Statins lower blood cholesterol level by inhibiting HMGCR activity.

The transcription of *HMGCR* is regulated by sterol regulatory element binding transcription factor 2 (SREBF2), which is generally involved in cholesterol biosynthesis. It binds to a DNA sequence known as sterol regulatory element (SRE) within the promoter region of *HMGCR*, as well as other genes containing SRE, to activate transcription (Eberle et al., 2004). Another crucial gene regulated by SREBF2 is the LDL receptor (LDLR), which facilitates the uptake of circulatory cholesterols into the liver.

SREBF2 is synthesized as an integral membrane protein in the rough endoplasmic reticulum (ER). When intracellular cholesterol level is high, SREBF2 binds to SREBF chaperone (SCAP), which in turn binds to Insig, an anchor protein holding the SCAP-SREBF2 complex in the ER membrane.

The sterol-sensing domain within SCAP allows it to function as a cholesterol sensor, such that when cellular cholesterol level is low, SCAP changes conformation and releases Insig, allowing the SCAP-SREBF2 complex to migrate to Golgi apparatus. SREBF2 is then cleaved by two membrane-bound proteases, site-1 protease (S1P) and site-2 protease (S2P), to release the active SREBF2,

which migrates into the nucleus, binds SRE of target genes and promotes transcription. When cellular cholesterol level returns to normal or is high, nuclear SREBF2 is rapidly degraded and SREBF2 activation is inhibited by SCAP binding SREBF2 and the retention of SCAP-SREBF2 complex in the ER.

Hence, the synthesis of endogenous cholesterol is mostly regulated by cholesterol itself through SREBF2, which in turn regulates the transcription of *HMGCR* and *LDLR* involved in increasing cellular cholesterol production and uptake respectively.

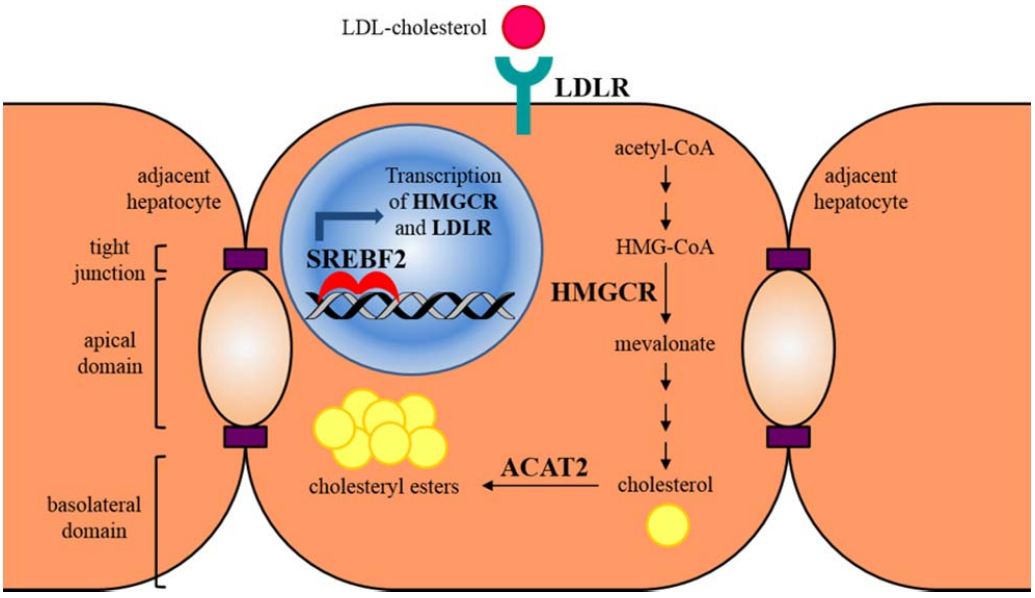

Figure 1: Regulation of cholesterol synthesis in the hepatocyte.
SREBF2 regulates the transcription of *HMGCR* and *LDLR*, whereby HMGCR catalyzes the rate-limiting step of HMG-CoA to mevalonate, and LDLR binds to LDL-cholesterol in the blood for endocytosis into the cell. ACAT2 esterifies intracellular free cholesterols to cholesteryl esters for storage within the cell.

1.2.1.2.Regulation of cholesterol elimination

Significant elimination of excess cholesterol from the body takes place in the liver, and occurs mainly via two pathways (Figure 2). The first is the conversion of excess cholesterols to bile acids, which are then excreted into the bile duct. Cholesterol 7-alpha hydroxylase (CYP7A1) catalyzes the first and only rate-limiting step in bile acid synthesis (Shefer et al., 1970). The second pathway involves the excretion of free cholesterols directly into the bile canaliculi (BC), facilitated by ATP-binding cassette, sub-family G, member 5 (ABCG5) and ATP-binding cassette, sub-family G, member 8 (ABCG8). Both ABCG5 and ABCG8 are half transporters that dimerize to form a functional transporter in the canalicular membrane of the hepatocyte (Graf et al., 2003).

Extrahepatic cells such as macrophages remove surplus intracellular cholesterols via the membrane transporter ATP-binding cassette, sub-family A, member 1 (ABCA1) into plasma high density lipoproteins (HDL) to be brought back to the liver for elimination, a process known as reverse cholesterol transport (RCT). However, ABCA1 in the liver is identified as the rate-limiting factor in the biogenesis of HDL. Hepatic ABCA1 mediates the efflux of cholesterols and phospholipids to lipid-poor apolipoproteins A-I, which combine to form plasma HDL (Fitzgerald et al., 2010; Lee and Parks, 2005).

The transcription of *ABCA1*, *ABCG5*, *ABCG8* and *CYP7A1* are collectively regulated by liver X receptor (LXR), a transcription factor known to induce the

expression of genes involved in cholesterol catabolism, efflux and elimination, hence protecting the cells from cholesterol overload (Chiang et al., 2001; Repa et al., 2002; Schwartz et al., 2000).

The accumulation of cellular oxysterols formed from excess cholesterols induces the activation of LXR, which functions as a sterol sensor (Lehmann et al., 1997). Upon activation, LXR recruits retinoid X receptor (RXR) to form an obligate heterodimer and binds to a regulatory DNA sequence known as LXR response element (LXRE) in the promoter region of target gene (Willy et al., 1995).

There are two isoforms of LXR, of which the expression of LXR alpha (LXRa) is predominantly restricted to tissues known to play important roles in lipid metabolism such as the liver, kidney, intestine, adipose tissue, lung, spleen and macrophages, whereas LXR beta (LXRb) is ubiquitously expressed (Repa and Mangelsdorf, 2000; Teboul et al., 1995; Willy et al., 1995).

Although these two isoforms are highly related, sharing almost 80% identity in the amino acid sequences in both their DNA- and ligand-binding domains, studies have shown that LXRa participates more actively in the regulation of hepatic cholesterol metabolism. When challenged with a high cholesterol diet, *LXRa*-knockout mice were unable to maintain cholesterol homeostasis, consequently accumulating large amount of liver cholesterols with hypercholesterolemia. Despite the presence of intact LXRb in the liver of these mice, it was not able to

compensate for the absence of LXRa (Peet et al., 1998). Conversely, *LXRb*-knockout mice with intact LXRa retained normal hepatic cholesterol metabolism and were able to adapt to cholesterol-rich diet (Alberti et al., 2001). LXRa is also more involved than LXRb in regulating LXR target gene expression as shown by LXRa binding LXRE in CYP7A1 with a substantially higher affinity than LXRb (Lehmann et al., 1997). When challenged with a high cholesterol diet, the expression of hepatic ABCG5/G8 was decreased in *LXRa*-knockout mice, whereas in *LXRb*-knockout mice, ABCG5/G8 expression was still maintained, demonstrating the sterol-induced upregulation of ABCG5/G8 required LXRa (Repa et al., 2002). Recently, Ma *et al.* reported that the maintenance of cholesterol efflux was predominantly mediated by the LXRa isoform but not LXRb (Ma et al., 2014).

The greater specificity of LXRa response in cholesterol metabolism may be due to a greater amount of LXRa than LXRb in the liver (Repa and Mangelsdorf, 2000), and that LXRa essentially exhibits a higher activity than LXRb in activating its target genes (Peet et al., 1998).

Hence, LXRa plays a more dominant role in preventing the accumulation of excess cholesterols within the cell by activating the transcription of genes which facilitate cholesterol removal.

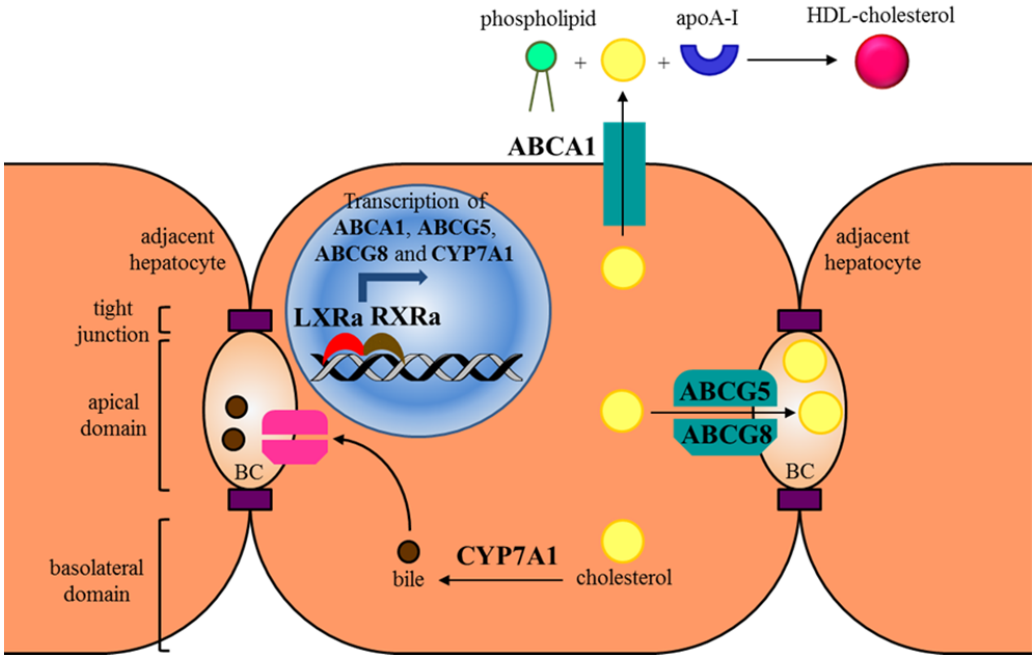

Figure 2: Regulation of cholesterol elimination in the hepatocyte.
LXRa dimerizes with RXRa to initiate transcription of *ABCA1*, *ABCG5*, *ABCG8* and *CYP7A1*. Basolateral ABCA1 transports cholesterols and phospholipids out of the hepatocyte to combine with apoA-I to form plasma HDL. Heterodimer ABCG5/G8 excretes excess cellular free cholesterols into the bile canaliculus (BC) for elimination. CYP7A1 catalyzes the rate-limiting step in bile formation involved in cholesterol degradation.

1.2.1.3.Regulation of cholesterol transport

Due to the hydrophobic nature of cholesterol, lipoprotein particles are utilized to facilitate cholesterol transport in the blood (Figure 3). A lipoprotein particle consists of a nonpolar core of cholesteryl esters and triglycerides surrounded by an amphipathic shell of cholesterols, phospholipids and apolipoproteins (apo) which are principal protein components that contain cell-targeting signals.

Besides *de novo* synthesis of cholesterol, cells also obtain cholesterol via dietary means. Dietary cholesterols, cholesteryl esters and triglycerides are transported away from the intestine and enter into the bloodstream in the form of lipoprotein

complexes called chylomicrons (CM), which function to deliver dietary triglycerides to the adipose tissue and skeletal muscles, and dietary cholesterols to the liver. They first adhere to binding sites on the inner surface of blood capillaries in adipose tissue and skeletal muscles. ApoC-II on the shell of CM activates lipoprotein lipase (LPL) on the blood capillaries, which hydrolyzes the triglycerides within CM and releases monoacylglyercols and free fatty acids (FFA) into the cells. CM shrinks as its triglycerides are progressively being hydrolyzed until it is cholesterol-enriched. The remaining molecule, known as a chylomicron remnant (CMR), is taken up by the liver via remnant receptors.

When triglycerides and cholesterols taken up by the liver are in excess, they are exported back into the blood in the form of very low density lipoprotein (VLDL), stabilized by apoB-100, apoC-II and apoE. Triglycerides in VLDL are hydrolyzed by LPL on capillary surfaces, giving rise to intermediate density lipoprotein (IDL) rich in cholesteryl esters. IDL can either be taken up by the liver for processing or converted to low density lipoprotein (LDL) by the removal of more triglycerides and all apolipoproteins, except apoB-100.

LDL is the major carrier of cholesterol in the blood. Peripheral cells generally do not synthesize their own cholesterol, but obtain it from plasma LDL. The presence of LDLR on the surface of peripheral cells binds to apoB-100 on LDL, forming a LDL-LDLR complex which is taken up by the cell via receptor-mediated endocytosis. The endocytosed LDL-LDLR vesicle fuses with another vesicle,

giving rise to an acidified endosome and triggering the dissociation of LDL from LDLR. LDLR is recycled back to the plasma membrane intact. The endosome with the LDL fuses with lysosomes containing acid lipases that hydrolyze LDL to liberate the free cholesterols which are subsequently incorporated into the membrane.

Excess free cholesterols within the cell activate acyl CoA:cholesterol acyltransferase (ACAT), which catalyzes the intracellular esterification of free cholesterols to cholesteryl esters for storage within cell. Two isoforms of ACAT have been identified – ACAT1 is expressed in most tissues, whereas ACAT2 (Figure 1) is primarily expressed in the liver and intestine (Oelkers et al., 1998).

Circulating HDL removes the excess cholesterols within peripheral cells by first extracting cholesterols from cell surface membrane via ABCA1, followed by converting them to cholesteryl esters through the action of lecithin cholesterol acyltransferase (LCAT), an enzyme activated by apoA-I on HDL. HDL transports the cholesterols back to the liver upon binding to scavenger receptor class B type I (SR-BI) for recycling or excretion from the body. The lipid-depleted HDL then dissociates from the liver and re-enters circulation (Voet and Voet, 2011).

The maintenance of lipoprotein metabolism is essential for appropriate amount of lipids to be circulated within the body for cellular use and removal. Pathway defects in lipoprotein synthesis, processing, and clearance could lead to

accumulation of atherogenic lipids in plasma and endothelium. Hence, regulation of lipoprotein metabolism is crucial to preserve cholesterol homeostasis.

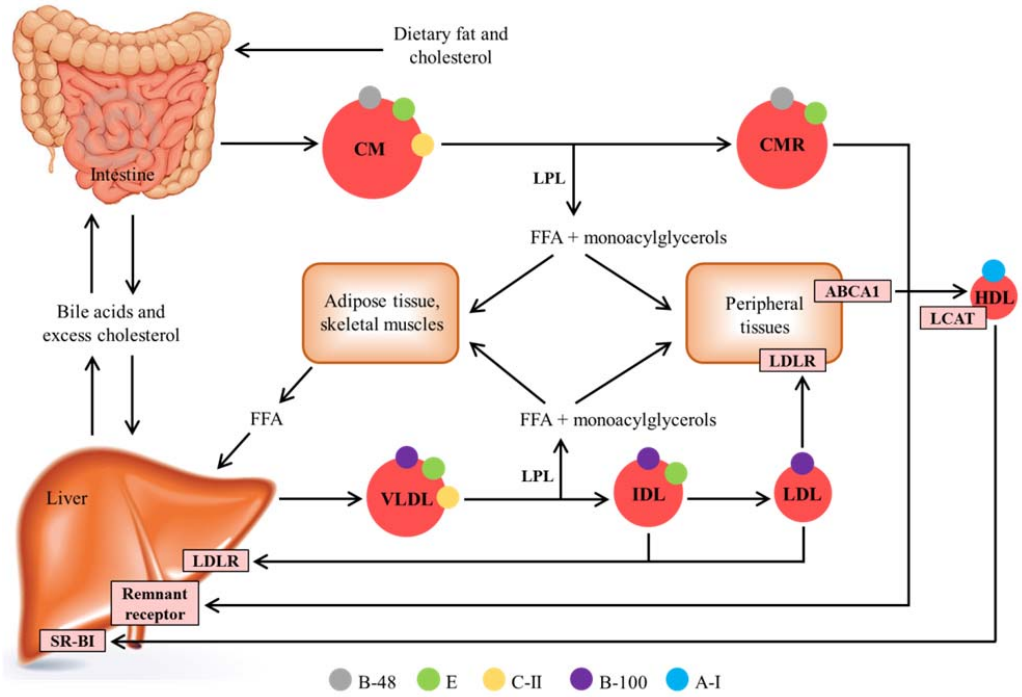

Figure 3: Lipoprotein metabolism and transport.
Different apolipoproteins in the lipoproteins are depicted with circles in different colors. CM transports dietary lipids from intestine into the bloodstream, and is hydrolyzed by LPL in the capillary surface to give CMR. The released FFA is taken up by adipose tissue and skeletal muscles. CMR is taken up into the liver via remnant receptor. Excess lipids in the liver are secreted into the blood as VLDL, which is hydrolyzed by LPL to release FFA to peripheral cells. The remaining cholesterol-enriched IDL is either taken up by the liver via LDLR or further hydrolyzed to give LDL. Cells obtain cholesterols from LDL via LDLR present on their membrane. Excess LDL return to the liver via LDLR. Circulating HDL removes excess cholesterols from peripheral cells via ABCA1 and LCAT and returns to the liver via SR-BI. Adapted and modified from reference (Berg et al., 2012).

1.2.2. Characteristics of hypercholesterolemia in nephrotic syndrome

The elevation of plasma total cholesterol, specifically LDL-cholesterol, is the major lipid abnormality in MCNS, although hypertriglyceridemia may occur as the disease progresses (Thabet et al., 1993b). In addition, recent studies have shown elevation of IDL, VLDL and triglycerides with variable levels of HDL in

the dyslipidemia of nephrotic syndrome (DK et al., 2014; Kaysen and de Sain-van der Velden, 1999; Vaziri, 2003).

Composition within the plasma lipoproteins is also altered in nephrotic syndrome, where the ratios of cholesterols to triglycerides, free cholesterols to cholesteryl esters, and phospholipids to protein are significantly higher in nephrotic subjects (Gherardi et al., 1977). Apolipoproteins are also dysregulated, with apoB in VLDL and LDL, and apoC-III involved in inhibiting lipolysis of VLDL and chylomicrons, significantly elevated in patients (Kaysen, 1991; Warwick et al., 1990; Warwick et al., 1991).

1.2.3. Causes and current knowledge of hypercholesterolemia in nephrotic syndrome

Till now, the pathogenesis of hypercholesterolemia in nephrotic syndrome is still unknown. Studies to elucidate the molecular mechanisms triggering hypercholesterolemia in nephrotic syndrome have been mostly carried out in the puromycin aminonucleoside nephrosis (PAN) model in rats, a commonly used model for MCNS.

Although the pathogenesis of nephrotic hypercholesterolemia is incompletely understood, in the experimental PAN rat model of nephrotic syndrome, hypercholesterolemia has been shown to be associated with abnormalities in hepatic cholesterol metabolism which involves the dysregulation of crucial

enzymes and transporters participating in cholesterol metabolism (Liang and Vaziri, 2003).

The mRNA and activity of hepatic HMGCR were markedly upregulated during the induction phase of nephrotic syndrome in PAN rats, but tapered down to baseline levels during the chronic phase of nephrotic syndrome (Vaziri and Liang, 1995), without any significant difference in the mRNA, protein and activity of HMGCR when compared to controls (al-Shurbaji et al., 1998; Kim et al., 2007). In contrast, Han *et al.* reported an increase in protein expression of HMGCR in the PAN rats (Han et al., 2013). This transient but significant rise in HMGCR could contribute to increased synthesis of cholesterol and lead to the initiation and maintenance of hypercholesterolemia in nephrotic syndrome.

Despite the presence of hypercholesterolemia, CYP7A1 in PAN rats did not show any rise in its mRNA, protein abundance and activity in both the induction and chronic phases of nephrotic syndrome (Liang et al., 1996; Thabet et al., 1993a). This was in contrast to rats with diet-induced hypercholesterolemia, whereby their CYP7A1 was upregulated in a feedback mechanism. Bile secretion was also unchanged in PAN nephrotic rats (Pahl et al., 1998). Hence, PAN-induced hypercholesterolemia could be associated with the absence of a compensatory rise in hepatic CYP7A1.

To account for the different responses of HMGCR and CYP7A1 in PAN-induced hypercholesterolemia and diet-induced hypercholesterolemia, hepatic cellular cholesterol levels were measured, because HMGCR and CYP7A1 are regulated by free cholesterol level. Diet-induced hypercholesterolemia displayed a 16-fold increase in hepatic cholesterol content whereas there was no increase in hepatic cholesterol level in the PAN nephrotic rats despite severe hypercholesterolemia (al-Shurbaji et al., 1998; Kim et al., 2007; Liang et al., 1996; Vaziri and Liang, 1995; Zhou et al., 2008), which led to the investigation of hepatic LDLR. Vaziri and Liang reported a gradual downregulation of LDLR protein in the course of PAN nephrosis in rats (Vaziri and Liang, 1996), hence explaining the normal hepatic cholesterol level. Decreased LDLR might lead to decreased clearance of plasma LDL, and thus contributing to hypercholesterolemia in nephrotic syndrome. However, al-Shurbaji *et al.* reported no significant difference in hepatic LDLR protein expression between the PAN nephrotic rats and controls (al-Shurbaji et al., 1998).

Hepatic SREBF2 protein expression in the PAN nephrotic rats showed no change across the microsomal, cytoplasmic and nuclear compartments in the cell (Han et al., 2013; Kim et al., 2007), which could explain the normal levels of intracellular cholesterols, as well as the non-change in LDLR mRNA expression.

There was also diminished level of plasma LCAT coupled with increase in urinary LCAT and downregulation of SR-BI, of which the former is required for HDL-mediated clearance of cellular cholesterols in peripheral cells and SR-BI to facilitate hepatic uptake of HDL, hence resulting in reduced clearance of cholesterol (Vaziri et al., 2001).

Upregulation of ACAT2 activity was observed in the livers of nephrotic rats (Vaziri and Liang, 2002), indicating that a greater amount of intracellular free cholesterols was being esterified to cholesteryl esters to be stored within the cells, decreasing the availability of free cholesterols to inhibit HMGCR, which could result in the transient upregulation of HMGCR leading to increased cholesterol synthesis (Vaziri and Liang, 1995).

These abnormalities in enzymes and transporters in cholesterol metabolism observed in PAN rats were not entirely related or solely due to the degree of hypoalbuminemia, a conclusion drawn from studies comparing Nagase analbuminemic rats (NAR) and PAN rats. Both strains of rats had very low to absence of serum albumin and hypercholesterolemia but only PAN rats had proteinuria. Moreover, PAN rats exhibited a more severe hypercholesterolemia profile than NAR rats. Hence it was postulated that these abnormalities in hepatic cholesterol metabolism were primarily due to the marked proteinuria seen in these rat models.

By comparing the protein expression and activity of crucial factors involved in cholesterol metabolism in NAR and PAN rats, LDLR and LCAT were severely reduced in PAN rats but normal in NAR rats. Although both PAN and NAR rats displayed ACAT2 upregulation, the increase was mild in NAR rats and attributed to the increase in liver free cholesterol, as opposed to the fourfold increase in PAN rats. This drastic increase occurred in the presence of a significant reduction in liver free cholesterol, suggesting a primary maladaptive phenomenon in nephrotic syndrome. This comparison between NAR and PAN rats suggested a predominant role of proteinuria in the onset of hypercholesterolemia in MCNS (Liang and Vaziri, 2003; Vaziri and Liang, 2002).

Two distinct hypotheses have been put forth to establish the relationship between proteinuria and dysregulated lipid metabolism in nephrotic syndrome. The first hypothesis states that proteinuria causes reduced serum oncotic pressure, which then directly stimulates albumin synthesis, along with synthesis of all other liver-derived exported proteins, including lipoproteins (Jones et al., 1967; Marsh and Drabkin, 1960). The second postulates that the loss of a lipid regulatory protein during proteinuria causes the defective removal of lipids from the circulation, resulting in a cascade of events leading to dysregulation of the enzymes and receptors in cholesterol metabolism (Davies et al., 1990; Staprans et al., 1980; Staprans et al., 1987).

However, until now, the definitive contribution of increased synthesis and decreased catabolism to hypercholesterolemia in nephrotic syndrome, and their mechanistic relationship to proteinuria remains unresolved.

The PAN rat model of MCNS is achieved by intravenous injection of puromycin aminonucleoside (PA), an analog of the antibiotic puromycin classified as a drug and toxin. Administration of PA induces nephrosis by causing direct damage to the podocytes, giving rise to glomerular lesions consistent with human nephrotic syndrome and coupled with proteinuria, hypercholesterolemia, hypoalbuminemia and edema (Ryan and Karnovsky, 1975; Vernier et al., 1959). Additionally, PA has been reported to cause increased reactive oxygen species in isolated rat hepatocytes by activating the enzyme protein kinase C, and inhibit endogenous protein degradation at the level of autophagic sequestration (Aoyagi et al., 2000; Kovacs et al., 1981). Hence, the hypercholesterolemia observed in PAN rats could also be attributed to the direct toxicity of PA on the hepatocytes.

The proteinuria achieved from using PA is reported to be different from the proteinuria observed in MCNS patients (Chugh et al., 2012). This, coupled with the toxic nature of PA and its direct damage to podocytes, questions the robustness of using PAN rats to study the onset of hypercholesterolemia in nephrotic syndrome.

The hypercholesterolemia observed in patients with MCNS is different and more extreme when compared to the hypercholesterolemia in other diseases with similar protein losses such as peritoneal dialysis and chronic nephropathy. Patients with MCNS relapses have extremely high serum cholesterol, typically 10 to 20mmol/l, up to four times the normal cholesterol level (Hu et al., 2010; Querfeld et al., 1988) as compared to hypercholesterolemia in peritoneal dialysis in which serum cholesterol rarely exceeds 7mmol/l (Johansson et al., 2000). During MCNS remission, the extremely high cholesterol levels often rapidly fall to normal levels of about 3 to 5mmol/l, whereas hypercholesterolemia in other diseases with comparable protein losses is often sustained and chronic. Also, in some patients with MCNS, hypercholesterolemia has been observed to precede the development of proteinuria. These clinical observations suggest that proteinuria alone could not account for the onset of severe hypercholesterolemia in MCNS, and that some other mediators involved in the pathogenic mechanism of MCNS could potentially also induce the hypercholesterolemia seen in this disease.

1.3. Minimal change nephrotic syndrome

Minimal change nephrotic syndrome, also known as minimal change disease or lipoid nephrosis, is the most common cause of nephrotic syndrome in childhood, affecting close to 80% of nephrotic children, as compared to 20-30% of nephrotic adults (Nakayama et al., 2002; Woo et al., 2010).

The glomeruli in MCNS appears normal under light microscopy, but shows the effacement of podocyte foot processes with absence of electron-dense immune deposits under electron microscopy (Mathieson, 2007). This podocyte effacement represents a permeability defect in the glomerular filtration barrier and is shown to be associated with proteinuria in MCNS (Mundel and Reiser, 2010; Mundel and Shankland, 2002). However, the pathogenic mechanism of MCNS is still largely unknown.

With a wide variety of immunological abnormalities being described in and associated with MCNS, including *in vivo* and *in vitro* observations, the hypothesis that immunological dysregulation is the cause of MCNS has long dominated the scientific literature for decades, with most studies focusing on T cell function.

1.3.1. Minimal change nephrotic syndrome and the immune system

Minimal change nephrotic syndrome was first postulated to be a disorder of T cell function by Shalhoub in 1974 when he hypothesized that an abnormal expansion of a clone of T cells produced a circulating factor that disrupted the glomerular basement membrane of the kidneys, leading to increased permeability to urinary proteins (Shalhoub, 1974). His postulate was based on clinical observations that (i) the disease remitted with measles infection, whereby the measles virus suppressed cell-mediated immunity, (ii) patients were highly susceptible to pneumococcal infection, whereby the hypothesized expansion of T cell clones suppressed the production of antibodies against pneumococcal infection, (iii)

disease remission was induced with corticosteroids and cyclophosphamide, both known to be inhibitors of T cells, and (iv) the occurrence of MCNS in Hodgkin's lymphoma, a T cell lymphoproliferative disorder.

The absence of immune complexes in the glomeruli of patients with MCNS, coupled with the lack of morphological changes in the kidney suggest that MCNS represents a generalized disorder of the immune system resulting in renal manifestations, rather than a specific disease of the kidney itself. The dysfunction in T cells seen in active MCNS has been demonstrated in many studies, including distinct T cell subset abnormalities in children with relapsing MCNS (Fiser et al., 1991), and the significant increase in percentage of CD4+CD45RO+ and CD8+CD45RO+ memory T cell subsets in INS children (Yan et al., 1998). Abnormalities in serum immunoglobulins (Ig) also occurred during MCNS relapses characterized by depressed IgG and elevated IgE (Cheung et al., 2004; Yokoyama et al., 1987).

Persistent stimulation of nuclear factor-kB (NF-kB), a crucial regulator of cytokine expression, within the peripheral blood mononuclear cells (PBMCs) during MCNS relapse could contribute to the immunologic abnormalities in MCNS (Sahali et al., 2001). Subtractive cDNA library from T cell-enriched PBMCs in MCNS patients during relapse and remission identified a number of differentially expressed transcripts involved in various tightly coordinated steps of

T cell activation during relapse, supporting MCNS as a T cell-mediated disease (Sahali et al., 2002).

The mechanism by which T cell dysregulation could increase glomerular permeability causing proteinuria in MCNS has remained elusive. The absence of inflammation, infiltration of immune cells and deposition of immunoglobulin or complement in the glomerulus alludes to the role of a soluble circulating factor mediating proteinuria. Supernatant from T cells of patients with MCNS when injected into rats caused immediate proteinuria and podocyte foot process effacement (Garin and Boggs, 1987; Koyama et al., 1991; Tanaka et al., 1992). Also, the dysregulation of T cell function, often manifested as T cell expansion, is often associated with increased synthesis of several cytokines, suggesting the role of cytokines as circulating factors involved in MCNS (Araya et al., 2006).

1.3.2. Minimal change nephrotic syndrome and Th2 cytokine bias

The role of cytokines in MCNS is postulated to involve a T helper (Th) type 2 (Th2) cytokine predominance (Mathieson, 2003). Th2 cytokines, mainly comprising of interleukin- (IL-) 4, IL-5 and IL-13, are secreted by CD4+ Th cells. Th2 cytokines are anti-inflammatory, stimulate B cells to produce antibodies, primarily IgE, IgA and IgG4, promote eosinophil proliferation, and are upregulated in allergic disorders (Abbas et al., 1996).

The close association between MCNS and atopy support the underlying Th2 predominance in the disease. There have been several reports on patients who developed nephrotic syndrome following exposure to allergens such as pollen or bee stings (Florido et al., 1992; Wittig and Goldman, 1970). Furthermore, the incidence of atopy was reportedly higher in MCNS patients than in healthy subjects (Lin et al., 1990; Yap et al., 1983). Elevation of IgE was also observed in MCNS relapse (Cheung et al., 2004).

The expression of IL-12 receptor b2 subunit, which is exclusively expressed by Th1 cells to facilitate IL-12 signaling, was downregulated in the T cell-enriched PBMCs of MCNS relapse, along with increased expression of Th2 transcriptional regulator c-Maf and histamine-releasing factor which triggers IL-13 production by basophils (Sahali et al., 2002). Together with a lack of IL-12 production during MCNS relapse (Stefanovic et al., 1998), Th1 phenotype was suggested to be depressed, with the activated T cells of MCNS committed to a Th2 phenotype. IL-4 was also found to be upregulated in the PBMCs from patients with MCNS, and this was associated with increased B-cell expression of the type II IgE receptor and high IgE production (Cho et al., 1999).

Our laboratory was the first to demonstrate that IL-13 was upregulated in CD4+ and CD8+ T cells in patients with MCNS relapse (Yap et al., 1999). Moreover, the percentage of CD3+ cells producing IL-13 was significantly higher in children with nephrotic relapse, also correlating with the elevated serum IgE levels

observed during the active phase of the disease (Cheung et al., 2004). Our findings were consistent with the study of Kimata *et al.* which showed the importance of IL-13 in the spontaneous production of IgE and IgG4 by PBMCs in the nephrotic patients (Kimata et al., 1995). Furthermore, we were able to demonstrate that genetic polymorphisms in the 3' untranslated region (3'UTR) of the *IL-13* gene correlated with long-term outcome of MCNS in Singapore Chinese children, rather than disease susceptibility (Wei et al., 2005). These findings are consistent with the well-recognized association between MCNS and Hodgkin's disease, where IL-13 is known to be an autocrine growth factor for the Reed-Sternberg cell in Hodgkin's lymphoma, being highly expressed in both the Reed-Sternberg cells in biopsy samples and tumor cell lines (Kapp et al., 1999; Skinnider et al., 2001; Skinnider et al., 2002).

Our laboratory overexpressed *IL-13* gene in rats, which subsequently developed proteinuria, hypoalbuminemia, edema and hypercholesterolemia, associated with minor abnormalities on light microscopy, and podocyte foot process effacement with downregulation of nephrin, podocin and dystroglycan (Lai et al., 2007), consistent with a possible role of IL-13 in MCNS. In addition, in this model of minimal change-like nephropathy, serum IL-13 level correlated with serum cholesterol, but not with serum albumin or urine albumin excretion, suggesting an association between IL-13 and hypercholesterolemia.

1.4. Research hypothesis and scope of thesis

The current hypothesis regarding the pathogenesis of nephrotic hypercholesterolemia is mainly derived from the PAN model of nephrotic syndrome in rats, where PA directly damages podocytes, without involvement of the immune system. On the other hand, our *IL-13* gene overexpression rat model reflects more closely to the immunological Th2 cytokine pathogenesis of human MCNS, and is a more appropriate model to study the pathogenesis of hypercholesterolemia associated with the disease.

We hypothesize that in relapse of MCNS, hypercholesterolemia is primarily due to dysregulation of cholesterol homeostasis, mediated by the direct action of Th2 cytokines like IL-13, on pathways regulating cholesterol synthesis, elimination or transport, and not solely a consequence secondary to the accompanying proteinuria (Figure 4).

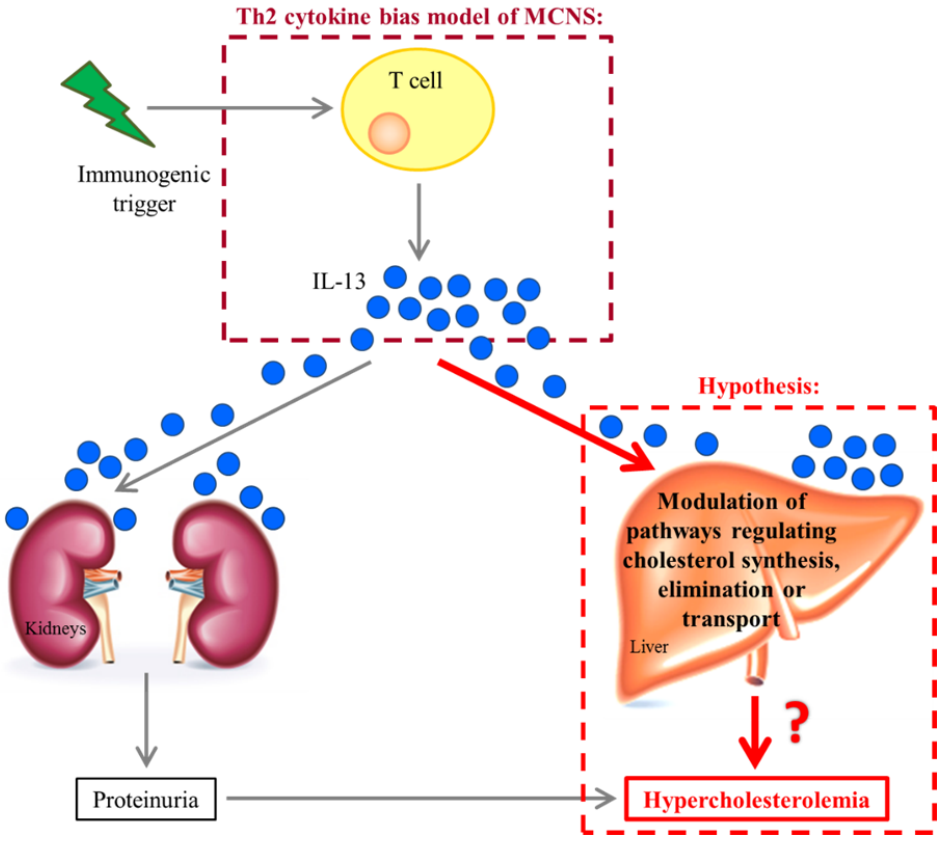

Figure 4: Hypothesis of Th2 cytokine bias model of MCNS leading to nephrotic hypercholesterolemia.
Following an immunological trigger, T cells release Th2 cytokines such as IL-13, which directly act on the liver to dysregulate pathways regulating cholesterol synthesis, elimination or transport, resulting in the hypercholesterolemia seen in MCNS.

1.4.1. Aims of study

To study the hypothesis that hypercholesterolemia in MCNS is primarily due to cytokine dysregulation, we propose to firstly establish the role of Th2 cytokines in regulating cholesterol homeostasis in the *IL-13* gene overexpression rat model of MCNS prior to the onset of proteinuria, and subsequently to validate this pathway in a rat primary hepatocyte cell culture system.

The **main objectives** will be accomplished by:

1. Profiling the genes involved in the pathways of cholesterol metabolism in the liver of the ***IL-13* transfected nephrotic rats** using cDNA microarray and identify the differentially expressed genes (DEGs).
    a. Subsequent functional clustering and pathway analysis using Database for Annotation, Visualization and Integrated Discovery (DAVID) will be performed to characterize the link between IL-13 and hepatic cholesterol metabolism in the *IL-13* transfected nephrotic rats.
    b. The microarray results will be validated using quantitative real-time polymerase chain reaction (qPCR).
2. Conducting a timeline experiment to determine if hypercholesterolemia preceded the onset of proteinuria in this cytokine-induced model of MCNS by studying plasma cholesterol and urine albumin excretion level at weekly intervals following *IL-13* transfection of the rat.
3. Performing a comparative analysis of the gene expression profile of the pathways of hepatic cholesterol metabolism between the *IL-13* transfected rats at the onset of hypercholesterolemia in the pre-proteinuric phase (early event) and the nephrotic phase (late event).
    a. qPCR will be performed to determine if the DEGs identified from the liver microarray profile in the late event could also be involved in the early event.

b. Protein detection methods such as Western bot and ELISA will be used to correlate and validate the qPCR data of the pathways of cholesterol metabolism in the early event.

4. Validating the findings of cholesterol dysregulation from both the early and late events in the *IL-13* transfected rats in an ***in vitro*** **IL-13-stimulated rat primary hepatocyte cell culture system**.
    a. Gene and protein expressions of the molecules involved in the dysregulated cholesterol metabolic pathway(s) identified in the *IL-13* gene overexpression rat model of MCNS will be studied in the hepatocytes following IL-13 stimulation.
    b. Intracellular cholesterol level will be measured in the hepatocytes.
    c. Cholesterol transport across the cells will be assayed using apoA-I and taurocholate.
    d. Functional studies using siRNA-transfected rat hepatocytes to knock down target molecules will be performed to delineate the molecular mechanism of IL-13-induced hypercholesterolemia.

Understanding the molecular mechanism of hypercholesterolemia associated with INS in children has important implications especially in the steroid-dependent and steroid-resistant child, as they tend to have prolonged hypercholesterolemia, which in the long term will result in significant atherosclerotic disease. Lowering cholesterol level during childhood may reduce the risk for atherosclerotic changes and serious cardiovascular and cerebrovascular disease in young adulthood. In

addition, hyperlipidemia has also been associated with progression of chronic kidney disease due to its effects on inflammatory and fibrogenic pathways. A better understanding of the etiology of the pathogenesis of hypercholesterolemia is thus important, so that novel molecules can be developed to tackle this complication of nephrotic syndrome, given that statins may have severe side effects when used in combination with drugs normally used to treat nephrotic syndrome such as cyclosporine.

Chapter 2 Materials and methods

2.1. *IL-13* gene overexpression rat model of MCNS

All animal studies were approved by the Institutional Animal Care and Use Committee of the National University of Singapore. Six-week-old female Wistar rats weighing between 100g to 200g were used. Induction of MCNS in rats by *IL-13* gene overexpression has been published (Lai et al., 2007).

The complete experimental protocol is illustrated in Figure 5. Prior to blood collection and electroporation, the rats were housed in metabolic cages for a 24-hour urine collection and the volume of urine recorded. After subjecting the rats to inhalational isoflurane with oxygen, 1ml of blood was drawn from the ventral artery of the tail into a heparinized tube using a 23G needle.

Electroporation of the rats was carried out every week over a period of 10 weeks with 200μg of endotoxin-free and purified plasmid DNA injected into their quadriceps. An electric current consisting of six pulses of 20 milliseconds each at 160V was generated using the "Electro Square Porator ECM830" (BTX Technologies Inc., NY, USA) and delivered though the 10mm 2-Needle Array™ tip (BTX Technologies Inc., NY, USA) connected to a 2-Needle Array™ electrode (BTX Technologies Inc., NY, USA). Treatment rats received mammalian expression plasmid pCI cloned with rat *IL-13* gene (pCI-IL-13), while control rats received pCI alone.

Both urine and blood collected were centrifuged at 3000rpm for 10 minutes to remove debris and obtain plasma respectively. Plasma IL-13, albumin, creatinine, total cholesterol and urine albumin excretion levels were assayed regularly.

To study the treatment rats in the nephrotic state (termed as 'late event'), the rats were euthanized at Week 10 by overdose of anesthetic (75mg/kg of ketamine and 10mg/kg of xylazine) via intraperitoneal injection, followed by blood collection via cardiac puncture. The liver was immediately removed, cut into small pieces and frozen in liquid nitrogen, then stored at -80°C until processed.

To study the rats which developed hypercholesterolemia in the pre-proteinuric phase (termed as 'early event'), a subgroup of treatment rats were euthanized as soon as their plasma total cholesterol levels increased to 1.5 times more than their baseline value at the start of the experiment, without the development of proteinuria. This sacrificial process could vary between Week 1 to Week 10. Blood and liver were collected as described above. Additional measurements were carried out for plasma triglycerides, HDL-cholesterol and LDL-cholesterol for this set of hypercholesterolemic rats, which were designated as HC rats.

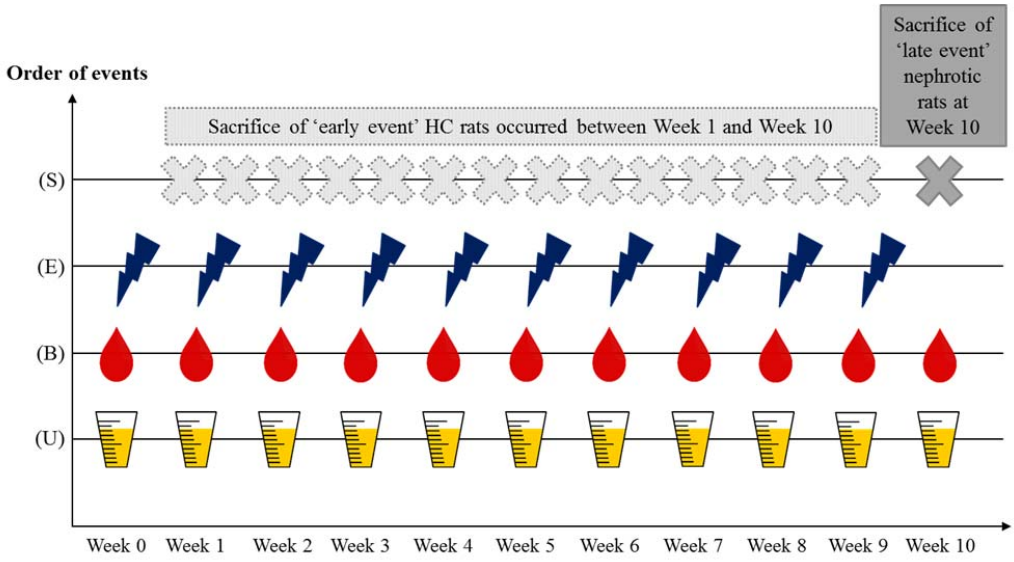

Figure 5: Experimental protocol for animal work.
The y-axis represents the order of events that occurred weekly as indicated by the x-axis. 24-hour urine was first collected (U), followed by the drawing of tail blood (B) and electroporation was carried out last (E). No electroporation was done on rats that were to be sacrificed (S). Rats were sacrificed at Week 10 to study the late event in nephrotic syndrome (solid gray cross). HC rats were sacrificed as soon as their plasma total cholesterol levels increased to 1.5 times more than their Week 0 value, without the development of proteinuria (early event) (gray crosses with dotted filling and lines).

2.2. Plasma IL-13

Plasma level of rat IL-13 was measured using a commercially available solid phase sandwich Enzyme Linked Immuno Sorbent Assay (ELISA) kit (Invitrogen, CA, USA), in which monoclonal antibody specific for rat IL-13 had been coated onto the wells of the microtiter strips provided. Briefly, 50µl of standards ranging from 7.8pg/ml to 500pg/ml, positive controls and rat plasma samples were pipetted into the wells, followed by the addition of 150µl of biotinylated secondary monoclonal antibody. Plasma from the *IL-13* transfected rats was diluted five-fold, while the control plasma was used undiluted.

After incubation at room temperature for 2 hours, the wells were washed with wash buffer provided to remove excess biotinylated antibody. Following a 30-minute incubation with 100µl of streptavidin-peroxidase enzyme, the wells were washed and then incubated with 100µl of stabilized chromogen substrate, which upon reacting with the bound enzyme, produced a color signal directly proportional to the amount of IL-13 bound. After a 30-minute incubation in the dark, 100µl of stop solution was added and the final absorbance was measured at wavelength 450nm using a microplate reader (Bio-Rad Laboratories, Inc., CA, USA). The concentration of IL-13 in the samples was determined from the standard curve, factoring in the dilution.

2.3. Plasma total cholesterol

Plasma total cholesterol level was determined by an enzymatic colorimetric endpoint method (Allain et al., 1974) using a commercial kit (Randox Laboratories, Antrim, UK). Briefly, 10µl of reagent blank consisting of 0.9% w/v sodium chloride (NaCl) in distilled water, standard and samples were each added to 1ml of Reagent R1. After incubation at room temperature for 10 minutes, 200µl of reaction mixture was transferred into the wells of a microplate in duplicate and absorbance was read at 490nm using a microplate reader (Bio-Rad Laboratories, Inc., CA, USA) against reagent blank. Sample concentration of total cholesterol was determined by multiplying the absorbance ratio of sample $\left(A_{sample}\right)$ and standard $(A_{standard})$ with the concentration of the standard provided by the manufacturer $\left(\frac{A_{sample}}{A_{standard}} \times \text{concentration of standard}\right)$.

2.4. Plasma HDL-cholesterol

Plasma HDL-cholesterol level was determined by an enzymatic clearance assay (Izawa et al., 1997) using a commercial kit (Randox Laboratories, Antrim, UK). Briefly, 15µl of reagent blank consisting of 0.9% w/v NaCl in distilled water, standard and samples were each added to 900µl of Enzyme Reagent 1 in a 1cm cuvette and mixed. After incubation at 37°C for 5 minutes, 300µl of Enzyme Reagent 2 was added immediately, mixed and incubated for exactly 30 seconds before reading the initial absorbance A_1 at 600nm using Spectronic® GENESYS™ 5 spectrophotometer (Thermo Electron Corporation, WI, USA) against reagent blank. Final absorbance A_2 was read immediately after a further incubation of 150 seconds at 600nm against reagent blank. Sample concentration of HDL-cholesterol was determined by multiplying the absorbance ratio of the sample difference $(A_2\text{-}A_1)$ and the standard $(A_{standard})$ with the concentration of the standard provided by the manufacturer $\left(\frac{A_2\text{-}A_1}{A_{standard}} \times \text{ concentration of standard}\right)$.

2.5. Plasma triglycerides

Plasma triglyceride level was determined by an enzymatic endpoint method (Jacobs and Vandemark, 1960; Koditschek and Umbreit, 1969; Tietz et al., 1990; Trinder, 1969) using a commercial kit (Randox Laboratories, Antrim, UK). Briefly, 5µl of reagent blank consisting of 0.9% w/v NaCl in distilled water, standard and samples were each added to 500µl of Reagent R1. After incubation at room temperature for 10 minutes, 200µl of reaction mixture was transferred

into the wells of a microplate in duplicate and absorbance was read at 500nm using Infinite M1000 microplate reader (Tecan, Mannedorf, Switzerland) against reagent blank. Sample concentration of triglycerides was determined by multiplying the absorbance ratio of sample (A_{sample}) and standard $(A_{standard})$ with the concentration of the standard provided by the manufacturer $\left(\frac{A_{sample}}{A_{standard}} \times \text{concentration of standard}\right)$.

2.6. Plasma LDL-cholesterol

Plasma LDL-cholesterol concentration was calculated using the formula of Friedewald *et al.* (Friedewald et al., 1972), which is the most often used formula in clinical practice and considered acceptable for patients' classification (Tremblay et al., 2004).

The concentration of plasma LDL-cholesterol in mmol/l is obtained using fasted blood samples from plasma total cholesterol (C_{TC}), plasma HDL-cholesterol (C_{HDL}) and plasma triglycerides (C_{TG}), and calculated with the formula $\left(C_{TC}\text{-}C_{HDL}\text{-}\,C_{TG}/2.2\right)$.

2.7. Plasma albumin

Plasma albumin level was determined by the bromocresol green (BCG) method using a commercial kit (Randox Laboratories, Antrim, UK). Briefly, 5µl of reagent blank consisting of 0.9% w/v NaCl in distilled water, standards and samples were each added to 1.5ml of BCG reagent and mixed. After incubation at

room temperature for 5 minutes, 200µl of reaction mixture was transferred into the wells of a microplate in duplicate and absorbance was read at 600nm using a microplate reader (Bio-Rad Laboratories, Inc., CA, USA) against reagent blank. Sample concentration of albumin was determined by multiplying the absorbance ratio of sample (A_{sample}) and standard $(A_{standard})$ with the concentration of the standard provided in the kit $\left(\frac{A_{sample}}{A_{standard}} \times \text{concentration of standard}\right)$.

2.8. Plasma creatinine

Plasma creatinine was determined by the alkaline picrate method (Archibald, 1962). Creatinine in alkaline solution reacts with picrate to form a colored complex, which is directly proportional to the creatinine concentration. Briefly, 100µl of distilled water as blank, standards of 0.5, 1, 3, 10mg/dl and samples were each added to a mixture containing 100µl of distilled water, 100µl of 5% w/v sodium tungstate in distilled water and 100µl of 2/3N sulphuric acid, and incubated at room temperature for 10 minutes. After centrifuging the mixture at 6000rpm for 2 minutes, 100µl of supernatant was transferred into the wells of a microplate in duplicate, followed by the sequential addition of 20µl of saturated aqueous picric acid and 30µl of 1N aqueous sodium hydroxide (NaOH). Incubation was carried out at room temperature for 20 minutes. The absorbance of the colored complex formed was read at 490nm using a microplate reader (Bio-Rad Laboratories, Inc., CA, USA). Sample concentration of creatinine was determined using the standard curve generated.

2.9. Urine albumin ELISA

A direct sandwich ELISA system was developed to detect the concentration of rat albumin in 24-hour urine samples (Crowther, 2001). Wells were coated with 100µl of 21.65µg/ml (total protein) rabbit antiserum to rat albumin antibody (MP Biomedicals, CA, USA) and 50µl of 0.965µg/ml (total protein) horseradish peroxidase (HRP)-conjugated sheep polyclonal antibody to rat albumin secondary antibody (MP Biomedicals, CA, USA) was used as the detecting antibody. o-Diphenylenediamine (OPD) (MP Biomedicals, CA, USA) in pH 5.0 citrate buffer was used as the substrate for color development. Rat albumin standards (MP Biomedicals, CA, USA) of known concentrations were included in each assay. Each sample was measured in triplicate. Endpoint absorbance was read at 490nm by a microplate reader (Bio-Rad Laboratories, Inc., CA, USA). The total amount of albumin excreted in a 24-hour urine sample was derived by multiplying the concentration of albumin obtained from the standard curve (mg/ml) and the volume of urine collected for 24 hours (ml) (Appendix 2.1).

2.10. RNA extraction

Extraction of total RNA from rat liver tissue was carried out by first homogenizing 300mg of liver in 3ml of TRIzol® Reagent using Heidolph Diax 600 homogenizer (Heidolph, Schwabach, Germany). For adherent monolayer cell culture in 6-well plate, 500µl of TRIzol® Reagent was used to lyse cells directly by pipetting the cells up and down several times.

The homogenized and lysed sample in TRIzol® Reagent was incubated at room temperature for 5 minutes to permit complete dissociation of the nucleoprotein complexes. Two hundred µl of chloroform (Thermo Fisher Scientific Inc., MA, USA) was added for every 1ml of TRIzol® Reagent used and the mixture was shaken vigorously for 15 seconds, followed by incubation at room temperature for 3 minutes. After centrifugation at 12,000*g* at 4°C for 15 minutes, the mixture was separated into a lower red phenol-chloroform phase, an interphase and an upper colorless aqueous phase. The aqueous phase, which contained the RNA, was carefully removed and transferred into a clean microfuge tube. Five hundred µl of isopropanol (Thermo Fisher Scientific Inc., MA, USA) was added to precipitate the RNA for every 1ml of TRIzol® Reagent used initially. The mixture was mixed by inverting repeatedly and incubated at room temperature for 10 minutes, followed by centrifugation at 12000*g* at 4°C for 10 minutes. After discarding supernatant, the RNA pellet was washed with 1ml of 75% ethanol (Merck, NJ, USA) for every 1ml of TRIzol® Reagent used initially. The sample was briefly vortexed and centrifuged at 7500*g* at 4°C for 5 minutes. After decanting ethanol, the RNA pellet was air-dried and dissolved in RNase-free water (Qiagen GmbH, Hilden, Germany). Concentration of RNA yield was measured using NanoDrop 1000 Spectrophotometer (NanoDrop products, Thermo Scientific, DE, USA).

2.11. RNA purification and cleanup

Liver tissue RNA was first isolated using TRIzol® Reagent method as described in 2.10, and further purified using RNeasy Mini Kit (Qiagen GmbH, Hilden,

Germany) according to manufacturer's protocol for microarray experiment (Appendix 2.2). Concentration and purity ratio A260/A280 of liver tissue RNA were measured using NanoDrop 1000 Spectrophotometer (NanoDrop products, Thermo Scientific, DE, USA).

2.12. RNA quantification and quality analysis

The samples were processed using Agilent RNA 6000 Nano Kit (Agilent Technologies, Waldbronn, Germany) according to manufacturer's protocol, followed by measuring the concentration of RNA in samples and checking their RNA quality using Agilent 2100 Bioanalyzer (Agilent Technologies, Waldbronn, Germany) before using them for microarray (Appendix 2.3). Purity of the RNA was checked using the ratio A260/A280, and its integrity was measured by the ratio 28S/18S and RNA Integrity Number (RIN).

2.13. RNA amplification for microarray analysis using Illumina® TotalPrep RNA Amplification Kit

2.13.1. Reverse transcription to synthesize first strand cDNA

All liver RNA samples were reconstituted to 300ng in a final volume of 11µl with nuclease-free water. Reverse Transcription Master Mix, consisting of 1µl of T7 oligo(dT) primer, 2µl of 10X first strand buffer, 4µl of dNTP mix, 1µl of RNase inhibitor and 1µl of ArrayScript™, was added to each RNA sample and incubated at 42°C for 2 hours to obtain first strand cDNA.

2.13.2. Second strand cDNA synthesis

Second Strand Master Mix, consisting of 63µl of nuclease-free water, 10µl of 10X second strand buffer, 4µl of dNTP mix, 2µl of DNA polymerase and 1µl of RNase H, was added to the first strand cDNA sample and incubated at 16°C for 2 hours. The double-stranded cDNA sample obtained was briefly put on ice before proceeding immediately to cDNA purification.

2.13.3. cDNA purification

The cDNA was transferred into a 1.5ml microfuge tube containing 250µl of cDNA Binding Buffer. The mixture was then transferred to a cDNA Filter Cartridge and centrifuged at 10,000*g* for 1 minute. This was followed by washing with 500µl of Wash Buffer and centrifuged at 10,000*g* for 1 minute. The cDNA Filter Cartridge was then transferred to a cDNA Elution Tube and 10µl of 55°C nuclease-free water was added to the center of the cDNA Filter Cartridge, incubated at room temperature for 2 minutes and centrifuged at 10,000*g* for 1.5 minutes. An additional 9µl of 55°C nuclease-free water was added to the center of the cDNA Filter Cartridge and centrifuged at 10,000*g* for 2 minutes in the same cDNA Elution Tube to collect the purified double-stranded cDNA.

2.13.4. *In vitro* transcription to synthesize cRNA

In vitro Transcription Master Mix, consisting of 2.5µl of T7 10X Reaction Buffer, 2.5µl of T7 Enzyme Mix and 2.5µl of Biotin-16-UTP, was added to the purified

cDNA sample and mixed, and incubated at 37°C for 14 hours. The reaction was stopped by adding 75µl of nuclease-free water to the newly synthesized cRNA sample to bring the final volume to 100µl, before proceeding to cRNA purification.

2.13.5. cRNA purification

cRNA was transferred into a clean 1.5ml microfuge tube containing 350µl of cRNA Binding Buffer, followed by 250µl of 100% ethanol and mixed. The mixture was passed through a cRNA Filter Cartridge by centrifugation at 10,000*g* for 1 minute and washed with 650µl of Wash Buffer by centrifugation at 10,000*g* for 1 minute. An additional spin was carried out to remove trace amount of Wash Buffer. After transferring cRNA Filter Cartridge to a cRNA Collection Tube for cRNA elution, 50µl of 55°C nuclease-free water was added to the center of the cRNA Filter Cartridge, incubated at room temperature for 2 minutes and centrifuged at 10,000*g* for 1.5 minutes. An additional 30µl of 55°C nuclease-free water was added to the center of the cRNA Filter Cartridge and centrifuged at 10,000*g* for 1.5 minutes in the cRNA Collection Tube to collect the purified cRNA.

The concentration of purified cRNA was measured using NanoDrop 1000 Spectrophotometer (NanoDrop products, Thermo Scientific, DE, USA). Samples with concentration less than 150ng/µl were concentrated by vacuum centrifugation.

2.13.6. cRNA hybridization and array scanning

Hybridization of 750ng cRNA was carried out for 18 hours on Sentrix® BeadChip Array RatRef-12 v1 (Illumina®, CA, USA) according to the manufacturer's protocol (Appendix 2.4). Array washing was performed followed by blocking, streptavidin-Cy3 detection and scanning with BeadArray™ Reader (Illumina®, CA, USA) using scan factor 1.5, PMT 531.

2.14. Microarray analysis

The raw intensity values of the array were extracted with background subtraction via BeadStudio (Illumina®, CA, USA) for analysis. The raw data was pre-processed to correct unreliable intensities for each array. The intensities with detection p-values greater than 0.05 were considered as unreliable and replaced by the intensity with detection p-value equal to 0.05. The pre-processed data was normalized by the Cross-Correlation method (Chua et al., 2006). Differentially expressed genes (DEGs) were selected based on fold change of at least 1.5 and false discovery rate (FDR) less than 0.05. Biological functional clustering and pathway analysis were carried out on the DEGs using a bioinformatics resource Database for Annotation, Visualization, and Integrated Discovery (DAVID) (Dennis et al., 2003; Huang da et al., 2009).

2.15. Plasmid DNA standard curve

Plasmid DNA standard curves were generated for copy number quantification of target genes in sample. Conventional PCR was first carried out with rat liver cDNA using specific primer sequences (Table 2). Thermal cycling conditions for *Taq* polymerase-amplification consisted of 1 cycle of 95°C for 5 minutes, followed by 35 cycles of 95°C for 30 seconds, 60°C for 30 seconds and 72°C for 30 seconds, and a final extension of 72°C for 7 minutes.

TA cloning reaction mixture was prepared with 3µl of *Taq* polymerase-amplified PCR product, 1µl of water, 1µl of salt solution and 1µl of pCR™ 2.1-TOPO® plasmid vector using the TOPO® TA Cloning® Kit (Invitrogen, Life Technologies, CA, USA), and incubated at room temperature for 15 minutes.

Transformation was carried out by adding 4µl of the cloning reaction mixture to a tube of OneShot® TOP10 Chemically Competent *E. coli* cells (Invitrogen, Life Technologies, CA, USA) and incubated on ice for 20 minutes, before being subjected to heat shock in a 42°C water bath for 30 seconds. The mixture was then incubated on ice for 2 minutes, followed by the addition of 250µl of SOC medium and shaking at 250rpm at 37°C for 1 hour.

One hundred µl of the transformation mixture was spread on a pre-warmed Luria-Bertani (LB) agar plate containing 100µg/ml of ampicillin (Sigma-Aldrich, MO, USA) and 40µg/ml of 5-bromo-4-chloro-3-indolyl-β-d-galactopyranoside (X-Gal)

(Promega, WI, USA) for blue/white colony screening. The plate was incubated overnight at 37°C.

White colonies representing successful transformation of *E. coli* cells with cloned vector were selected and cultured in LB broth containing 100µg/ml of ampicillin with shaking at 250rpm overnight at 37°C. After centrifuging at 6000*g* at 4°C for 15 minutes, *E. coli* cell pellet was lysed and plasmids were extracted and purified using QIAprep® Spin Miniprep Kit (Qiagen GmbH, Hilden, Germany) according to manufacturer's protocol. The concentration of the eluted plasmid was measured using NanoDrop 1000 Spectrophotometer (NanoDrop products, Thermo Scientific, DE, USA). Presence of insert was confirmed by EcoRI (New England BioLabs Inc., MA, USA) restriction digestion and agarose gel electrophoresis.

A 10X serial dilution was done to obtain a series of plasmid standards with copy numbers ranging from 10^9 to 10^0. Plasmid standards were run in triplicate in qPCR using LightCycler® 480 SYBR Green I Master reagent kit (Roche, Mannheim, Germany) with LightCycler® 480 Instrument machine (Roche, Mannheim, Germany).

The crossing threshold point (Ct) of plasmid standards was plotted against its copy number in the plasmid standard curve. A perfect amplification reaction produces a plasmid standard curve with a slope gradient of -3.33 and an efficiency of 2. Upon determining the Ct of an unknown sample, LightCycler® 480 Basic

Software provides the concentration of target DNA in the unknown sample using the plasmid standard curve (LightCycler® 480 Instrument Operator's Manual).

Table 2: Nucleotide sequence of primers for the respective genes of interest in rat liver.

Gene	GeneBank accession	Primer	Nucleotide sequence 5' – 3'	Product size/bp
b-actin	NM_031144	Forward Reverse	5'-GCCCTAGACTTCGAGC-3' 5'-CTTTACGGATGTCAACGT-3'	217
ABCA1	NM_178095	Forward Reverse	5'-AGACGGGCCTTCGGTGACAA-3' 5'-GCTGAAGACCAGGGCGATGC-3'	282
ABCG5	NM_053754	Forward Reverse	5'-CACTTGTGCTGCTTGGTATG-3' 5'-ATTGGGTTATTTGGCACAGA-3'	247
ACAT2	NM_153728	Forward Reverse	5'-GAGTCGAGAACCCTTCAG-3' 5'-GAAGGAAGTAGAGTTCCACCA-3'	184
CYP7A1	NM_012942	Forward Reverse	5'-TGCCACCACTACATGATATTGA-3' 5'-CCAGCTATGTGAACACCC-3'	210
HMGCR	NM_013134	Forward Reverse	5'-CTGGTAGCATAGGAGGC-3' 5'-CACACAATTCGGGCAAG-3'	301
IL-4Ra	NM_133380	Forward Reverse	5'-TCCACCCAATAGACCGT-3' 5'-GCAATCAAGTTTGCGTTC-3'	266
IL-13Ra1	NM_145789	Forward Reverse	5'-TTGGCACAACCTGAGCT-3' 5'-TGCACGAATAAGGCACC-3'	330
IL-13Ra2	NM_133538	Forward Reverse	5'-GGAATGCTGGGAAGGT-3' 5'-AGTTTAGCAGAGCGTCT-3'	190
LDLR	NM_175762	Forward Reverse	5'-CAAGATCAAGAAAGGGGGTT-3' 5'-CTGCTTCTCATCCTCCAAAA-3'	193
LXRa	NM_031627	Forward Reverse	5'-GCGAGGGCTGCAAGGGATTC-3' 5'-TTGGGGACACCGATGTGGCT-3'	240
RXRa	NM_012805	Forward Reverse	5'-CTCGGCTCTCCTCTGGGCTC-3' 5'-GCTGCTCACGGGGTTCATGG-3'	201
SREBF2	NM_001033694	Forward Reverse	5'-TCCTCCATCAACGACAAAAT-3' 5'-CAAGTCCACATCACTGTCCA-3'	228

2.16. Quantitative real-time PCR

One µg of RNA was reverse transcribed to single-stranded cDNA using Maxima® First Strand cDNA Synthesis Kit for RT-qPCR (Thermo Scientific, Thermo Fisher Scientific, PA, USA) according to manufacturer's protocol.

The qPCR was performed in a final volume of 10µl reaction mixture containing 1µM each of the forward and reverse primers, 1µl of PCR-grade water, 5µl of LightCycler® 480 SYBR Green I Master mix (Roche, Mannheim, Germany) and 2µl of single-stranded cDNA, and run in LightCycler® 480 Instrument machine (Roche, Mannheim, Germany). Thermal cycling conditions consisted of an initial pre-incubation at 95°C for 10 minutes, followed by 40 cycles of 95°C for 5 seconds, 62°C for 10 seconds and 72°C for 15 seconds, and lastly melting curve analysis was carried out before cooling to 40°C.

All samples were run in duplicate and target gene copy number for each sample was determined from the respective plasmid standard curve. Target gene expression was expressed as a ratio against the housekeeping gene b-actin.

2.17. Western blot

For Western blot analysis, liver tissue and cultured cells were homogenized and lysed in RIPA buffer with phosphatase and protease inhibitors (Pierce Thermo Scientific, IL, USA). Lysed samples were rotated at 4°C for 15 minutes, followed by centrifugation at 13,000*g* at 4°C for 10 minutes. The supernatant was

transferred into a clean 1.5ml microfuge tube, and protein concentration was measured based on Lowry method (Lowry et al., 1951).

Lysates containing equal amount of protein were fractionated on 5% and 8% Tris-glycine polyacrylamide gel at 100V for 2 hours and transferred to 0.45µm nitrocellulose membrane (Bio-Rad Laboratories, Inc., Munich, Germany). The membrane was blocked using 5% nonfat milk (Bio-Rad Laboratories, Inc., CA, USA) in 1X Tris-buffered saline (TBS) and 0.05% Tween 20 (TBST) at room temperature for 1 hour. After a 5-minute wash in TBST, the membrane was probed with the following primary antibodies at 4°C overnight: mouse anti-ABCA1 (1:5000) (Millipore, CA, USA), rabbit anti-IL-4Ra (1:1000) (Santa Cruz Biotechnology Inc., CA, USA), mouse anti-IL-13Ra2 (1:1000) (Santa Cruz Biotechnology Inc., CA, USA), rabbit anti-LXRa (1:4000) (Sigma-Aldrich, MO, USA), rabbit anti-pSTAT6 (1:5000) (Santa Cruz Biotechnology Inc., CA, USA) and rabbit anti-STAT6 (1:5000) (Santa Cruz Biotechnology Inc., CA, USA). Antibody against GAPDH (1:20,000) (Sigma-Aldrich, MO, USA) served as the loading control.

After 3 washes in TBST for 5 minutes, membrane was incubated in 2.5% nonfat milk in TBST containing HRP-linked secondary antibodies for 1 hour. After 5 washes in TBST for 5 minutes, the membrane was developed by chemiluminescent detection using Luminata™ Forte Western HRP Substrate (Millipore, MA, USA) and protein bands quantified using ImageJ software

(National Institute of Health, MD, USA). Target protein expression was expressed as an index of the GAPDH.

2.18. Hepatocyte isolation and culture

Hepatocytes were harvested from the liver of male Wistar rats (kind gift from Professor Hanry Yu, National University of Singapore, Singapore) weighing between 250g to 300g by a two-step *in situ* collagenase perfusion method (Seglen, 1976). Routinely, 200 to 300 million cells were isolated with viability above 85% as determined by trypan blue exclusion assay.

Freshly isolated rat hepatocytes were seeded at a density of 1.2 million cells on type I collagen-coated 6-well plates (Iwaki® Cell Biology, Japan) in Williams' Medium E (Sigma-Aldrich, MO, USA) supplemented with 1g/l of bovine serum albumin (BSA) (Sigma-Aldrich, MO, USA), 0.292g/l of L-glutamine (Gibco®, Life Technologies, CA, USA), 0.5g/l of insulin (Sigma-Aldrich, MO, USA), 5nM of dexamethasone (Sigma-Aldrich, MO, USA), 50ng/ml of linoleic acid (Sigma-Aldrich, MO, USA), 100units/ml of penicillin and 100µg/ml of streptomycin (Gibco®, Life Technologies, CA, USA). The cultures were incubated at 37°C and 5% CO_2 in a humidified atmosphere. After cell attachment for 3 hours, the medium was replaced with fresh Williams' Medium E, and subsequently culture medium was changed every 24 hours. Cells were photographed using an Olympus IX70 microscope equipped with the cell-F software (Soft imaging Software GmbH, Muenster, Germany).

After overnight incubation, hepatocyte cell cultures were stimulated with 25ng/ml of recombinant rat IL-13 (R&D Systems, MN, USA) for 2 to 48 hours. Cells were observed daily to ensure the absence of bacterial and fungi contamination.

2.19. Cholesterol quantification in rat liver tissue

Cholesterol in rat liver was extracted according to a modified Bligh and Dyer lipid extraction method (Bligh and Dyer, 1959; Shui et al., 2011). One hundred mg of rat liver tissue was homogenized in 1ml of ice-cold 1X Phosphate-buffered saline (PBS). The homogenized sample was vortexed for 15 seconds, before transferring 100µl of the homogenate into a clean 2ml microfuge tube. After adding 900µl of ice-cold chloroform:methanol (1:2), the tube was vortexed for 15 seconds and incubated on ice for 15 minutes in the dark, with intermittent vortexing during incubation. Three hundred µl of ice-cold chloroform and 300µl of ice-cold water were added to the mixture. The mixture was vortexed for 15 seconds and incubated on ice for 1 minute and repeated. After centrifuging at 9000rpm at 4°C for 2 minutes, the lower organic phase was transferred into a clean 1.5ml microfuge tube and dried under Savant SPD1010 SpeedVac Concentrator (Thermo Scientific, PA, USA). The dried lipid film was reconstituted in chloroform:methanol (1:1). Quantification of free cholesterol and cholesteryl esters were carried out using liquid chromatography/mass spectrometry (LC/MS), a collaboration with Professor Markus Wenk (National

University of Singapore, Singapore), and normalized against the mass of rat liver tissue used.

2.20. Cholesterol quantification in hepatocyte cell culture

Cholesterol in hepatocytes was extracted using the hexane:isopropanol method (Robinet et al., 2010). Culture medium was removed and cells were washed twice with 1X PBS, followed by the addition of 1ml of hexane:isopropanol (3:2). After incubation at room temperature for 5 minutes, the solvent extract was transferred to a clean 1.5ml microfuge tube and vacuum dried using Savant SPD1010 SpeedVac Concentrator (Thermo Scientific, PA, USA). The dried lipid film was dissolved in 1ml of isopropanol:NP-40 (Pierce Thermo Scientific, IL, USA) (9:1) and quantified using enzymatic colorimetric endpoint method as described in 2.3.

After cholesterol extraction, residual solvent remaining in the well was evaporated at room temperature. Protein from the same well was dissolved by adding 1.4ml of 0.2N NaOH. The plate was incubated at 37°C for 3 hours, followed by rocking at room temperature for 5 minutes. Protein lysate was transferred to a clean microfuge tube and protein concentration was measured using Lowry method.

2.21. Cholesterol efflux assay

This experiment was based on reported journal by Low *et al.* (Low et al., 2012). After seeding the hepatocytes and incubating at 37°C and 5% CO_2 in a humidified

atmosphere for 3 hours, the cells were labeled with 1μCi/ml of [^{3}H]-cholesterol (PerkinElmer, MA, USA) for 24 hours in culture medium containing 5% of fetal bovine serum (FBS). The cells were washed twice with 1X PBS, followed by treatment with 25ng/ml of IL-13 for 24 hours. The cells were washed twice with 1X PBS and [^{3}H]-cholesterol efflux was initiated by adding either 5μg/ml of apoA-I (cholesterol acceptor for ABCA1) (Sigma, MO, USA) for 24 hours or 10mM of taurocholate (cholesterol acceptor for ABCG5) (Sigma, MO, USA) for 30 minutes in serum-free culture medium. Culture medium was centrifuged at 14,000rpm for 10 minutes to remove cellular debris. Cells were frozen at -20°C for 30 minutes, followed by thawing and addition of 500μl of water, in which cells were scraped and homogenized. One hundred μl of centrifuged culture medium and homogenized cell lysate were aliquoted into separate scintillation vials followed by adding 5ml of scintillation liquid. Radioactivity in the vial was counted using the scintillation machine (Wallac WinSpectral 1414 Liquid Scintillation Counter, Turku, Finland). Efflux of [^{3}H]-cholesterol was calculated as the percentage of counts in the culture medium to the counts in both the culture medium and cells $\left(\frac{[^3\text{H}]\text{-cholesterol in medium}}{[^3\text{H}]\text{-cholesterol in medium} + [^3\text{H}]\text{-cholesterol in cell}} \times 100\%\right)$.

2.22. ABCG5 ELISA

Concentration of ABCG5 in rat liver and rat primary hepatocyte cell culture were measured using a commercial ELISA kit (MyBioSource, Inc., CA, USA), in which antibody specific for rat ABCG5 had been pre-coated onto the wells of the microplate. Briefly, 100μl of standards ranging from 25pg/ml to 1600pg/ml and

samples were pipetted into the wells in duplicate, followed by incubation for 2 hours. All incubation steps were carried out at 37°C. After removing unbound substances, 100µl of biotin-conjugated antibody specific for rat ABCG5 was added and incubated for 1 hour. The wells were washed to remove excess biotinylated antibody and then incubated with 100µl of avidin-conjugated HRP for 1 hour. After washing to remove unbound avidin-HRP complex, 100µl of substrate solution was added, which upon reacting with the bound HRP, produced a color signal which developed in proportion to the amount of ABCG5 bound in the initial step. Color development was halted with the stop solution and absorbance was measured at wavelengths 450nm and 540nm using microplate reader Infinite® M1000 microplate reader (Tecan, Mannedorf, Switzerland). Final absorbance value was derived after subtracting readings at 540nm from readings at 450nm. The concentration of ABCG5 in the sample was determined from the standard curve using its final absorbance value, and multiplied by its dilution factor. Samples from rat liver and cultured rat hepatocytes were diluted 2000X and 200X respectively.

2.23. Hematoxylin and eosin staining

The liver tissue structure of control and HC rats was stained with hematoxylin and eosin (H&E) to look for histological abnormality and lipid droplets. Paraffin-embedded liver tissue was cut into 7µm sections and mounted onto a slide. Sections were first dewaxed and rehydrated through alcohol, by going through incubation with 2 changes of Clearene (Leica Biosystems Richmond, Inc., IL,

USA) for 5 minutes each, 3 changes of absolute ethanol (Fisher Scientific, MA, USA) for 1 minute each, followed by 90% ethanol for 1 minute, 70% ethanol for 1 minute and 50% ethanol for 1 minute. The sections were washed in distilled water before staining with Shandon™ hematoxylin (Thermo Fisher Scientific Inc., MA, USA) for 5 minutes. After washing in distilled water, 0.25% acid alcohol was used to differentiate the section, and then submerged in aqueous ammonia. The sections were lastly stained with eosin (Fisher Scientific, MA, USA). The sections were dehydrated and cleared by going through incubation with 95% ethanol for 1 minute and 3 changes of absolute ethanol for 1 minute each, followed by 2 changes of Clearene for 1 minute each and a final incubation with Clearene for 5 minutes. The sections were then mounted with cover slip using Permount™ mounting medium (Thermo Fisher Scientific Inc., MA, USA) and viewed under Olympus BX51 light microscope (Olympus, Tokyo, Japan).

2.24. Transfection of cultured hepatocytes with siRNA

Freshly isolated hepatocytes were seeded at a cell density of 0.6 million cells per well on a type I collagen-coated 6-well plate. Culture medium was replaced with fresh medium after 3 hours of cell attachment, followed by an overnight incubation at 37°C and 5% CO_2 in a humidified atmosphere.

The cells were transfected with ON-TARGET*plus* rat LXRa small interfering RNA (siRNA) SMARTpool or ON-TARGET*plus* non-targeting control pool (GE Dharmacon, CO, USA) as negative control at a final concentration of 50nM by

using DharmaFECT 1 Transfection Reagent (GE Dharmacon, CO, USA) according to manufacturer's protocol (DharmaFECT™ Transfection Reagents – siRNA Transfection Protocol) for 24 hours. The target sequences of the pool of LXRa siRNAs were as follows: (1) GCUCAAGCCACAUCGGUGU; (2) GAGUGUCGCCUUCGCAAAU; (3) GAGACAUCGCGGAGGUACA; and (4) CGUCCACAGAAGCGGAAAA.

Briefly, the sequence specific siRNA and transfection reagent were separately diluted in serum-free and antibiotic-free culture medium and incubated at room temperature for 5 minutes. After adding the diluted siRNA into the diluted transfection reagent, the mixture was further incubated for 20 minutes to allow complex formation. siRNA-transfection agent complex was gently added to the cultured cells and incubated at 37°C and 5% CO_2 in a humidified atmosphere for 24 hours. The cells were then treated with 5μM of LXRa agonist T0901317 (Sigma-Aldrich, MO, USA) for another 24 hours, following which the cells were harvested for qPCR and Western blot analyses.

Gene knockdown percentage efficiency was calculated according to manufacturer's protocol (Demonstration of a ΔΔCq Calculation Method to Compute Relative Gene Expression from qPCR Data).

2.25. Statistical analysis

Statistical analysis was performed using SPSS software (IBM SPSS Statistics for Windows, Version 22.0, Armonk, NY, USA). All values were expressed as mean ± standard error mean (SEM). Differences between control and *IL-13* transfected rats were determined using the non-parametric Mann-Whitney test, where p-value < 0.05 was considered significant. Statistical analysis on paired samples in the cell culture work was carried out using the non-parametric Wilcoxon signed-rank test, where p-value < 0.05 was considered significant. The strength of the association between two variables was measured using Spearman's rank correlation coefficient (r), where results were considered to be statistically significant at $p < 0.05$.

Chapter 3 Delineating the molecular mechanism of IL-13-induced hypercholesterolemia in the nephrotic rat

3.1. Introduction

Hypercholesterolemia is one of the major pathological manifestations of MCNS, the most common cause of childhood INS. MCNS patients with multiple relapses or steroid-resistance will be exposed to prolonged periods of hypercholesterolemia, thus increasing the risk of atherosclerosis leading to cardiovascular and cerebrovascular diseases.

Previous studies on PAN rats suggested that the mechanism of nephrotic hypercholesterolemia is related to dysregulation of cholesterol metabolism in the liver triggered by the proteinuria (Liang and Vaziri, 2003). However, till now, the exact mechanistic pathway has not been elucidated.

Following our discovery of the upregulation of *IL-13* mRNA in CD4+ and CD8+ T cells in patients with MCNS relapse, we went on to establish an experimental model of MCNS, with the overexpression of *IL-13* gene in rats by weekly injecting a mammalian plasmid construct that contained rat *IL-13* gene into rat thigh muscle followed by electroporation for ten weeks (Lai et al., 2007). Histological examination of the renal tissue at the end of ten weeks showed no significant glomerular pathology on light microscopy, however, on electron microscopy, podocyte foot process effacement was seen in the glomeruli from rats

transfected with the *IL-13* gene, similar to MCNS. Our preliminary biochemical studies showed an elevation of serum cholesterol level consistently observed in all rats transfected with the *IL-13* gene as compared to control, as well as edema, proteinuria and hypoalbuminemia. In addition, only the level of serum cholesterol, but not serum albumin or urine albumin excretion levels, correlated significantly with the serum IL-13 level, suggesting an association between IL-13 and hypercholesterolemia.

Studies have also shown the presence of IL-13 receptor subunits in the liver, as well as the ability of IL-13 to signal through these receptors in the hepatocytes to trigger downstream processing (Akaiwa et al., 2001; Stanya et al., 2013), indicating the possible direct involvement of IL-13 acting on the liver.

We therefore hypothesized that IL-13 was able to act on the liver, in turn causing hepatic cholesterol dysregulation, thereby inducing hypercholesterolemia in the *IL-13* gene overexpression rat model of MCNS.

3.2. Aim of chapter

In this chapter, we aimed to examine the molecular mechanism of IL-13-induced hypercholesterolemia in the livers of the *IL-13* transfected nephrotic rats at Week 10, representing the 'late event' of MCNS. The objectives of this chapter are to:

1. Profile the molecular expression events involved in the liver of the *IL-13* gene overexpression rat model of MCNS using cDNA microarray and identify the DEGs in these *IL-13* transfected nephrotic rats.
2. Perform functional clustering and pathway analysis using DAVID to characterize the link between IL-13 and hepatic cholesterol metabolism in the *IL-13* transfected nephrotic rats.
3. Validate the microarray results using qPCR.

3.3. Results

3.3.1. Phenotype of rats used for microarray analysis

The serum IL-13 level of the *IL-13* transfected nephrotic rats was significantly elevated as compared to control rats (Table 3). The *IL-13* transfected nephrotic rats also displayed elevated serum cholesterol and urine albumin excretion, and decreased serum albumin classical of nephrotic syndrome. No significant difference was observed for serum creatinine and liver mass. The complete profile for every rat is shown in Appendix 3.1.

Table 3: Profile of control and *IL-13* transfected nephrotic rats used in cDNA microarray.

	Control rats (n=3)	*IL-13* transfected nephrotic rats (n=6)	p-value
Serum IL-13 (pg/ml)	0 ± 0	717 ± 305	0.018
Serum albumin (g/l)	45.3 ± 5.9	27.1 ± 1.7	0.020
Serum cholesterol (mmol/l)	1.79 ± 0.09	6.00 ± 0.77	0.020
Serum creatinine (µmol/l)	81.6 ± 7.2	71.6 ± 5.0	0.517
Urine albumin excretion (µg/24hour)	270 ± 64	5825 ± 1539	0.020
Liver mass (g)	12.3 ± 0.2	16.4 ± 1.5	0.121

3.3.2. Liver RNA transcriptional profile of *IL-13* transfected nephrotic rats

The RNA transcriptional profile in the livers of the *IL-13* transfected nephrotic rats was determined using genome-wide gene expression microarray analysis. This identified 499 DEGs (fold change ≥ 1.5 and FDR < 0.05) out of the 22,523 genes analyzed, when compared to control rats. Of the 499 DEGs, 274 (54.9%) were downregulated (with a maximum fold change of 7.39) and 225 (45.1%) were upregulated (with a maximum fold change of 18.01). The expression levels of the

DEGs are indicated by a color scale from low (green) to high (red) (Figure 6). The lists of downregulated and upregulated DEGs are available in Appendix 3.2 and Appendix 3.3 respectively.

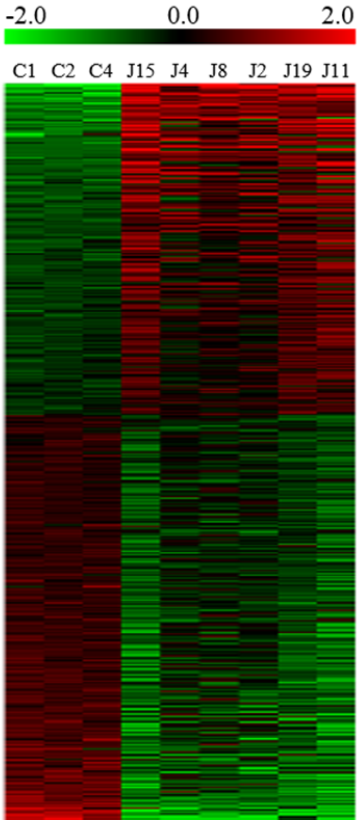

Figure 6: Heatmap of the 499 DEGs.
The data are presented in a matrix format, such that each row represents individual genes and column representing each rat. The expression level of the 499 DEGs is indicated using a log2-transformed scale colored bar from low (green) to high (red), with black representing median expression. C indicates biological replicate for control rats and J indicates biological replicate for *IL-13* transfected nephrotic rats.

Nine crucial genes that are well established to significantly affect cholesterol metabolism from pathways involving cholesterol biosynthesis, elimination and transport were selected to validate the microarray results by qPCR. Except for *RXRa* and *ABCA1*, there was good agreement between the microarray data and

the qPCR data, with qPCR confirming the up- or downregulation of each gene. The fold change was also of a comparable magnitude to the microarray data (Figure 7).

Microarray analysis showed increased expression of genes involved in both cholesterol synthesis and degradation, and decreased expression of genes involved in cholesterol transport (Figure 7). Of the nine genes validated on qPCR, *ABCG5* and *HMGCR* showed significant dysregulation in the livers of *IL-13* transfected nephrotic rats as compared to control rats.

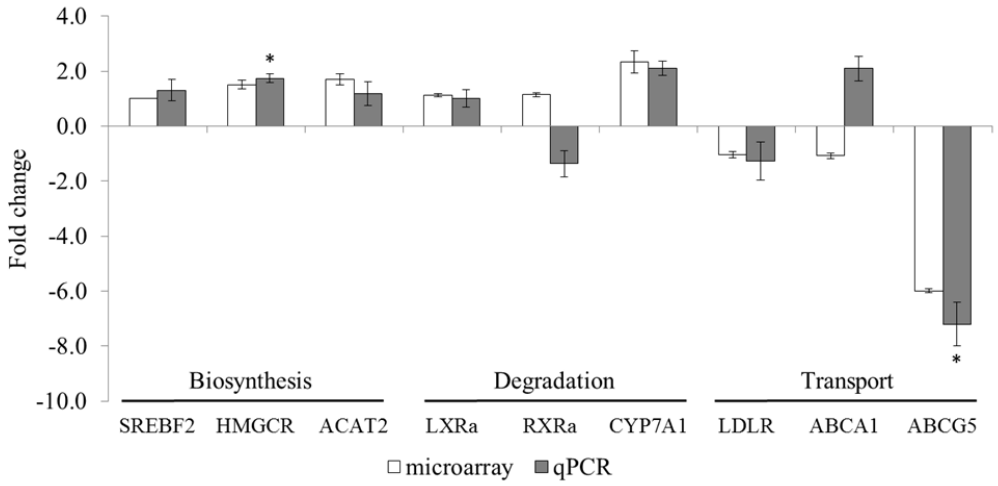

Figure 7: Validation of microarray results using qPCR.
Nine genes involved in cholesterol metabolism were selected and analyzed using qPCR to confirm the microarray results. Downregulated genes were arbitrarily assigned a negative value. For qPCR, gene expression levels were normalized against housekeeping gene b-actin and fold change was calculated using the $2^{\Delta\Delta Ct}$ method, where ΔΔCt was converted to an absolute value. Results were presented as fold change ± SEM. Asterisk (*) indicates significant difference, with p-value < 0.05, between the ΔCt values of control (n=7) and *IL-13* transfected nephrotic (n=7) rats. The transcriptional profiles observed were nearly similar between microarray and qPCR, except for *RXRa* and *ABCA1*.

3.3.3. Functional annotation clustering and pathway analyses of DEGs

The Database for Annotation, Visualization and Integrated Discovery (DAVID) v6.7 was used to understand the biological meaning behind the list of 499 DEGs. The list of DEGs was submitted to the Functional Annotation Tool in DAVID and analyzed with the functional annotation clustering and pathway options. The top ten clusters were selected from the functional annotation clustering analysis of the 499 DEGs based on enrichment score, whereby a higher enrichment score indicated closer agreement among the biological processes of the genes (Table 4). Functional annotation clustering showed that these DEGs were principally related to cofactor binding involving redox reaction, lipid and drug metabolisms, RNA processing, C-acyltransferase, CoA hydrolase and antioxidant activities, and were involved in cellular components such as peroxisome and mitochondrial matrix.

Table 4: Functional annotation clusters of the 499 DEGs with enrichment score.

Functional annotation cluster	Enrichment score
Redox reactions involving NAD/NADP	3.33
Lipid metabolism	2.97
mRNA processing and metabolic processes	2.80
C-acyltransferase activity	2.29
Peroxisome	2.28
Mitochondrial matrix	2.18
Intracellular organelle lumen	2.17
Antioxidant activity	2.10
Acyl-CoA hydrolase activity	1.86
Drug metabolism	1.83

The DAVID analysis tool was also used to identify putative pathways occurring in the livers of the *IL-13* transfected nephrotic rats, using the Kyoto Encyclopedia of Genes and Genomes (KEGG) pathway database. The 499 DEGs were mapped

to 19 pathways (Table 5), of which ‘Fatty acid metabolism’, ‘ABC transporters’, ‘Valine, leucine and isoleucine degradation’, ‘Spliceosome’ and ‘Fatty acid elongation in mitochondria’ were the top five pathways which still showed significant p-values after using the multiple testing correction technique Benjamini provided by DAVID.

Because we were interested to identify key molecular events and investigate biological signaling pathways involved in cholesterol dysregulation in the livers of *IL-13* transfected nephrotic rats, we chose to focus on ‘ABC transporters’, which was the second most significant pathway mapped out by KEGG, as the genes involved in the first pathway ‘Fatty acid metabolism’ were distinctively different from those involved in cholesterol metabolism.

The genes involved in the ‘ABC transporters’ pathway are summarized in Table 6, and the description of their functions was obtained from the NCBI Reference Sequence Database (RefSeq) (Pruitt et al., 2007). *ABCG5* showed the greatest decrease in gene expression level in the ‘ABC transporters’ pathway, with a fold change of 6.00, and it was also the fifth most downregulated gene in the entire microarray data.

Table 5: KEGG pathway analysis of the 499 DEGs.

KEGG_ID	Term	p-value	Fold enrichment	Benjamini p-value	Genes
rno00071	Fatty acid metabolism	1.26E-06	8.76	< 0.001	RGD1562373, Peci, Adh6, Adh1, Acsl4, Acat2, Hadha, Hadhb, Acadm, Adh4
rno02010	ABC transporters	1.51E-04	6.69	0.011	Abcc8, Abcc3, Abcd2, Abcb9, Abcg3, Abcg4, Abcg5, Abca6
rno00280	Valine, leucine and isoleucine degradation	2.02E-04	6.40	0.010	RGD1562373, Auh, Hmgcs2, Acat2, Hadha, Hadhb, Mcee, Acadm
rno03040	Spliceosome	3.85E-04	3.65	0.014	Isy1, Thoc1, U2surp, Ppih, Prpf38b, Sfrs5, Prpf3, LOC682323, Snrpa, Rbm8a, Cdc40, LOC306428
rno00062	Fatty acid elongation in mitochondria	9.79E-04	18.39	0.028	Mecr, Ppt1, Hadha, Hadhb
rno03320	PPAR signaling pathway	2.86E-03	4.14	0.067	Scd, RGD1562373, Pck1, Rxrb, Acsl4, Hmgcs2, Fabp7, Acadm
rno01040	Biosynthesis of unsaturated fatty acids	3.57E-03	7.66	0.072	Scd, RGD1562373, Acot5, Hadha, Acot2
rno00020	Citrate cycle (TCA cycle)	8.12E-03	6.13	0.138	Aco1, Idh1, Pck1, Acly, Cs
rno00410	beta-Alanine metabolism	2.04E-02	6.69	0.284	Cndp1, Srm, Hadha, Acadm
rno00980	Metabolism of xenobiotics by cytochrome P450	2.23E-02	3.68	0.281	Gsta4, Adh6, Adh1, Yc2, LOC687840, Cyp2c22, Adh4
rno00590	Arachidonic acid metabolism	4.00E-02	3.15	0.418	Ptgds2, Pla2g4a, Cyp4f37, Cbr1, Gpx2, Cyp2c22
rno00982	Drug metabolism	4.43E-02	3.06	0.424	Gsta4, Adh6, Adh1, Yc2, LOC687840, Cyp2c22, Adh4
rno00480	Glutathione metabolism	4.51E-02	3.68	0.405	Idh1, Gsta4, Srm, Yc2, LOC687840, Gpx2
rno00640	Propanoate metabolism	5.84E-02	4.46	0.466	Acat2, Hadha, Mcee, Acadm
rno00270	Cysteine and methionine metabolism	6.74E-02	4.20	0.493	Adi1, Ahcy, Srm, Bhmt
rno00830	Retinol metabolism	7.43E-02	3.12	0.505	Dhrs4, Adh6, Adh1, Cyp2c22, Adh4
rno04620	Toll-like receptor signaling pathway	9.54E-02	2.45	0.577	Map2k6, Ikbke, Rac1, Ripk1, Irf7, Stat1
rno04142	Lysosome	9.59E-02	2.20	0.559	Manba, Naglu, Ppt1, Ctsb, Abcb9, Slc17a5, Slc11a1
rno00310	Lysine degradation	9.79E-02	3.59	0.547	Suv420h2, Plod2, Acat2, Hadha

Table 6: List of DEGs involved in ABC transporters.

Gene symbol	GenBank accession number	Gene description	Gene function	Fold change
Abcg5	NM_053754	ATP-binding cassette, sub-family G (WHITE), member 5	Limit intestinal absorption and promote biliary excretion of sterols. Mainly expressed in intestine and liver.	-6.00
Abcd2	NM_033352	ATP-binding cassette, sub-family D (ALD), member 2	Peroxisomal import and homeostasis of fatty acids and/or fatty acyl-CoAs in the organelle (Fourcade et al., 2009).	-2.00
Abca6	XM_001081607	ATP-binding cassette, sub-family A (ABC1), member 6	Macrophage lipid homeostasis and intracellular lipid transport (Gai et al., 2013).	-1.68
Abcg4	NM_001106816	ATP-binding cassette, sub-family G (WHITE), member 4	Cholesterol transport and controls platelet production, atherosclerosis, and thrombosis. Highly expressed in megakaryocyte progenitors and brain (Westerterp et al., 2014).	1.58
Abcg3	NM_001128311	ATP-binding cassette, subfamily G (WHITE), member 3	Transport of specific peptides or hydrophobic compounds from lymphocytes. Highly expressed in thymus and spleen.	1.97
Abcb9	NM_022238	ATP-binding cassette, sub-family B (MDR/TAP), member 9	Multi-drug resistance and translocation of peptides from cytosol into lysosomal lumen.	2.21
Abcc8	NM_013039	ATP-binding cassette, sub-family C (CFTR/MRP), member 8	Multi-drug resistance and modulator of ATP-sensitive potassium channels and insulin release.	3.38
Abcc3	NM_080581	ATP-binding cassette, sub-family C (CFTR/MRP), member 3	Multi-drug resistance and transport of biliary and intestinal excretion of organic anions.	3.45

3.4. Discussion

Hypercholesterolemia, one of the pathological manifestations in MCNS, is a cause of concern in patients who frequently relapse or are steroid-resistant, as this is a highly significant risk factor for development of atherosclerosis leading to early onset cardiovascular and cerebrovascular complications. It is therefore imperative to elucidate the exact molecular mechanism of nephrotic hypercholesterolemia, which till now is still controversial.

Most of the data on nephrotic hypercholesterolemia are derived from studying PAN rats, an established model for nephrotic syndrome. In this model, hypercholesterolemia is triggered upon PA-induced damage to the kidneys resulting in heavy proteinuria and hypoalbuminemia. The PAN model is a toxic model, unlike human MCNS which appears to be associated with Th2 cytokine immune dysregulation, consistent with Shalhoub hypothesis (Shalhoub, 1974).

Our *IL-13* gene overexpression rat model of MCNS showed that high levels of circulating IL-13 in the serum were able to induce nephrosis in the rats (Lai et al., 2007). This closely mirrors the hypothesis that immune dysregulation with a Th2 cytokine bias may be involved in human MCNS. This is therefore a more appropriate endogenous model to study the pathogenesis of nephrotic hypercholesterolemia.

Microarray analysis was carried out to analyze the possible molecular mechanisms involved in cholesterol metabolism in the livers of the *IL-13* transfected nephrotic rats. Using a fold change of at least 1.5 and FDR less than 0.05, 499 DEGs were selected. This list of DEGs was analyzed using the functional annotation clustering tool provided by DAVID in order to group highly similar annotation terms into clusters, thus giving a more focused biological interpretation (Huang da et al., 2009). The top ten clusters generated predominantly showed a liver profile involving cellular components with metabolic processes.

Nephrotic hypercholesterolemia has always been associated with dysregulated metabolic activities in the liver, and this was reflected in the top three clusters. Enzymatic redox reactions involving crucial coenzymes, nicotinamide adenine dinucleotide (NAD) and nicotinamide adenine dinucleotide phosphate (NADP), were ranked as the top cluster. NAD and NADP serve as electron carriers in a variety of enzymatic reactions, and are used extensively in biosynthetic pathways such as cholesterol synthesis, rather than catabolic pathways.

The second top cluster, lipid metabolism, indicated dysregulation of lipid metabolism in the liver, whereby lipid generally encompasses cholesterol, triglycerides and fatty acids. The third top cluster, which was mRNA processing and metabolic activities, suggested dysregulated mRNA synthesis which could in

turn lead to dysregulated protein synthesis of crucial enzymes and transporters in cholesterol metabolism, possibly contributing towards hypercholesterolemia.

Mitochondrial matrix and peroxisomes were among the top cellular components in which the DEGs were involved in. Peroxisomes are small organelles which contain a variety of enzymes involved in a variety of metabolic processes including free radical detoxification, lipid catabolism and biosynthesis, and hydrogen peroxide metabolism. Mitochondrial matrix, the site of tissue respiration, contains the enzymes for the tricarboxylic acid cycle and, in some organisms, the enzymes involved in fatty acid oxidation. They are known to house numerous cellular metabolic processes.

Using the KEGG pathway analysis tool, the DEGs were mapped to 19 different pathways, of which the second most significant pathway 'ABC transporters' was the most relevant to cholesterol metabolism, and might be involved in the pathogenesis of hypercholesterolemia in the *IL-13* transfected nephrotic rats. Of the eight DEGs involved in the 'ABC transporters' pathway, *ABCG5* expression showed the greatest downregulation.

qPCR validation of crucial genes involved in cholesterol metabolism identified *HMGCR* as one of the upregulated genes, and this could explain the increased synthesis of cholesterol, as HMGCR controls the first rate-limiting step in the synthesis of cholesterol. In the PAN rat model of nephrotic syndrome, significant

but transient upregulation of hepatic *HMGCR* expression and activity was also observed, of which the hypercholesterolemia was attributed to this transient upregulation (Vaziri and Liang, 1995). However, pathway analysis could not demonstrate any significant involvement of *HMGCR* in the molecular pathogenic mechanism of hypercholesterolemia in *IL-13* transfected nephrotic rats.

Downregulation of cholesterol transporters, LDLR and ABCG5, could suggest defective clearance of cholesterol from the circulation and from the liver into bile respectively. However our microarray data in the *IL-13* transfected nephrotic rats showed that only *ABCG5* was significantly downregulated, and this was validated by qPCR. ABCG5 is highly involved in biliary cholesterol transport in the liver. It is essentially a half-transporter, belonging to the family of ATP-binding cassette (ABC) transporters, which are transmembrane proteins that transport various substrates such as lipids, sterols and drugs across cellular membranes by utilizing energy from adenosine triphosphate (ATP) hydrolysis. A fully functional transporter is formed when ABCG5 binds to ABCG8, limiting intestinal sterol absorption and promoting hepatic biliary excretion of sterols.

Since the discovery that mutation in ABCG5 and/or ABCG8 can lead to sitosterolemia, a rare autosomal recessive lipid metabolic disease whereby patients exhibit hyperabsorption and marked reduction in biliary excretion of dietary sterols but have normal biliary excretion of phospholipids, emerging evidence is suggesting the specific involvement of ABCG5 and ABCG8 in the

transport and regulation of cholesterol metabolism (Berge et al., 2000; Miettinen, 1980). Sitosterolemia patients are often hypercholesterolemic, which leads to the development of cholesterol deposits in the skin and tendons known as xanthomas, as well as in the arteries, leading to accelerated atherosclerosis and eventually premature coronary heart disease (Bhattacharyya and Connor, 1974; Miettinen, 1980; Salen et al., 1989).

Disruption of either ABCG5 or ABCG8 in mice resulted in increased intestinal absorption and decreased biliary excretion of cholesterols (Yu et al., 2002a; Yu et al., 2004). Overexpression of human ABCG5 and ABCG8 in *ABCG5/G8*-knockout mice led to reduced absorption and increased secretion of dietary cholesterol (Wu et al., 2004; Yu et al., 2005). Similarly, the overexpression of ABCG5 and ABCG8 in mice caused a selective increase in cholesterol excretion into bile (Yu et al., 2002b).

Evidence have shown that ABCG5 and ABCG8 are obligate heterodimers, only dimerizing with each other and not with other half-transporters from the G family of ATP transporters such as ABCG1, ABCG2 and ABCG4. They are also dependent on one another for transport out of endoplasmic reticulum to be expressed on membrane surface (Graf et al., 2003). The transporter is highly expressed in the liver and intestine, specifically located on the apical surface of hepatocyte facing the bile canaliculi and brush border membrane of enterocyte (Graf et al., 2003; Klett et al., 2004). ABCG5/G8 consists of two transmembrane

domains that contain the translocation site for specific substrates such as cholesterol or plant sterol, and two cytoplasmic nucleotide binding domains that hydrolyze ATP to drive the transport process (Holland and Blight, 1999).

ABCG5 and *ABCG8* genes are located adjacent to each other in a head-to-head orientation on chromosome 2 and are encoded on opposite strands, with their initiation codons separated by a 144bp intergenic region (Berge et al., 2000; Lu et al., 2001). This intergenic region not only serves as a bidirectional promoter, but also contains binding sites for GATA transcription factor, NF-kB, hepatocyte nuclear factor 4 alpha (HNF4a) and liver receptor homolog-1 (LRH-1) (Freeman et al., 2004; Remaley et al., 2002; Sumi et al., 2007).

A very prominent and well-established transcriptional regulator of ABCG5 is LXR, which is highly involved in cholesterol degradation (Repa et al., 2002). The LXRE within the intergenic region of ABCG5 and ABCG8 genes has only been recently identified (Back et al., 2013). LXR activation increases the transcription of *ABCG5* and *ABCG8* in the liver. Consistently, activation of LXR fails to increase biliary cholesterol excretion in *ABCG5/G8*-knockout mice (Yu et al., 2003). Similarly, hepatic *ABCG5/G8* expression was decreased in the *LXRa*-knockout mice when challenged with a high cholesterol diet, demonstrating that sterol-induced upregulation of ABCG5/G8 requires LXRa, whereas the expression of *ABCG5/G8* was still maintained and comparable to wild-type mice in the *LXRb*-knockout mice (Repa et al., 2002).

Although there were no significant changes in *LXRa* and *RXRa* expression levels in our microarray data, their downstream target gene *ABCG5* was drastically downregulated, which could lead to a decrease in biliary excretion of hepatic cholesterols. Hence, excess cholesterols in the circulation might not be cleared as efficiently, mounting to the hypercholesterolemia observed in the *IL-13* transfected nephrotic rats.

In summary, the pathogenesis of hypercholesterolemia in the *IL-13* transfected nephrotic rats with MCNS could be due to the downregulation of *ABCG5* which is associated with decreased hepatic clearance of cholesterol into bile, and upregulation of *HMGCR*, associated with increased synthesis of cholesterol. Upregulation of gene expression of cholesterol degradation enzymes shown in our microarray, although not significant on qPCR, could indicate a possible feedback mechanism consequent to the increased plasma cholesterol.

The next chapter will investigate the initial molecular mechanism (early event prior to the development of proteinuria) that could have resulted in the dysregulated transcriptional profile seen in the hypercholesterolemic nephrotic rats (late event), in particular the role of *ABCG5* and *HMGCR*.

Chapter 4 Delineating the initial molecular mechanism of hypercholesterolemia in IL-13-induced HC rats (without proteinuria)

4.1. Introduction

Patients with MCNS relapses have extremely high serum cholesterol, typically 10 to 20mmol/l, up to four times the normal cholesterol level (Hu et al., 2010; Querfeld et al., 1988), compared to other diseases with similar urinary protein losses such as patients on peritoneal dialysis whose protein losses can reach a similar range as nephrotic patients, yet serum total cholesterol level rarely exceeds 7mmol/l (Johansson et al., 2000). Moreover, hypercholesterolemia has been observed to precede the development of proteinuria in some of these children with MCNS following a viral infection.

This observation, together with the extreme serum total cholesterol increase during the disease phase and rapid drop to normality in remission, suggests that proteinuria could not be the sole trigger for hypercholesterolemia in MCNS as purported in the PAN rats, and that some other mediators could potentially contribute to the hypercholesterolemia seen in this disease.

Our *IL-13* gene overexpressed rat model demonstrated features consistent with MCNS, namely marked proteinuria, hypoalbuminemia, edema and hypercholesterolemia, as well as podocyte foot process effacement. Additionally,

a significant correlation was established between serum IL-13 and serum cholesterol in these *IL-13* transfected nephrotic rats, but not with serum albumin or urine albumin excretion level (Lai et al., 2007).

We therefore hypothesized that the hypercholesterolemia in our *IL-13* gene overexpression rat model of minimal change-like nephropathy was not solely secondary to the marked proteinuria, but could be due to increased level of plasma IL-13 acting on hepatic pathways of cholesterol metabolism.

4.2. Aims of chapter

The aims of this chapter are to:

1. Investigate if hypercholesterolemia preceded the onset of proteinuria in our *IL-13* gene overexpression rat model of MCNS by studying the biochemical profile at weekly intervals following *IL-13* transfection of the rat.
2. Perform a comparative analysis of the gene expression profile of the pathways of hepatic cholesterol metabolism between the *IL-13* transfected rats at the onset of hypercholesterolemia in the pre-proteinuric phase (early event) and the nephrotic phase (late event), in particular the role of the DEGs identified from the microarray profile of the *IL-13* transfected nephrotic rats in the late event, namely ABCG5 and HMGCR.
3. Investigate the plasma and liver lipid profiles and hepatic protein expressions of the selected DEGs during the early event of the *IL-13* transfected HC rats.

4.3. Results

4.3.1. Relationship of IL-13 to the development of hypercholesterolemia and proteinuria in *IL-13* transfected rats from Week 0 to Week 10

Plasma IL-13 was significantly elevated as early as Day 1 after the first electroporation of pCI-IL-13, and remained significantly higher in the *IL-13* transfected rats compared to control rats throughout the entire experiment until Week 10 (Figure 8) (Appendix 4.1).

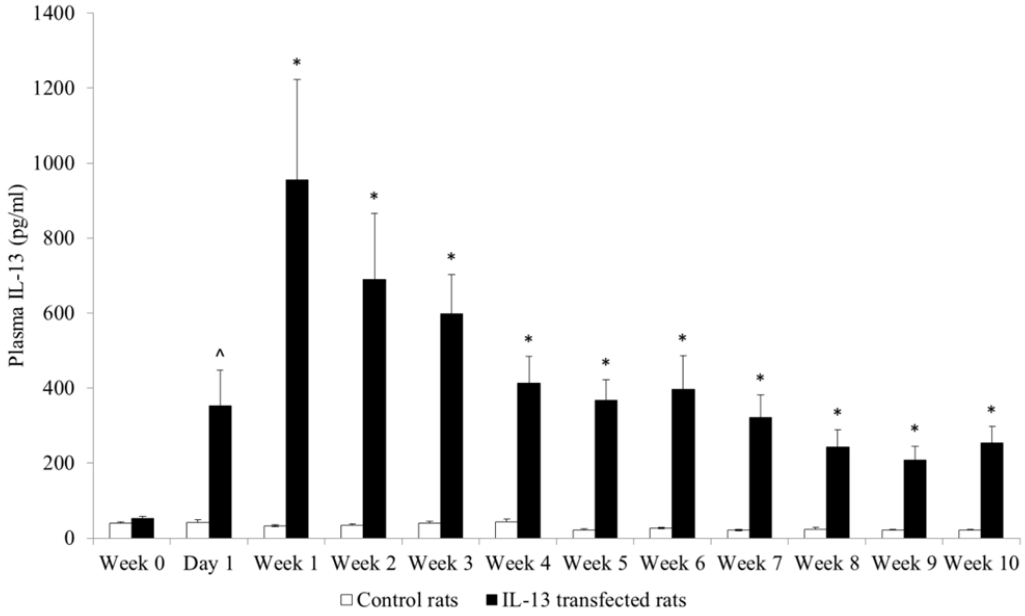

Figure 8: Weekly plasma IL-13 profile.
Plasma IL-13 was significantly elevated in the *IL-13* transfected rats compared to control rats from Day 1 to Week 10. ^ denotes p-value < 0.005, * denotes p-value < 0.001.

As shown in Figure 9, in the *IL-13* transfected rats, plasma cholesterol was significantly higher than controls from Week 1 onwards and preceded the onset of significant proteinuria which occurred at Week 10 (Figure 10) (Appendix 4.2 and Appendix 4.3).

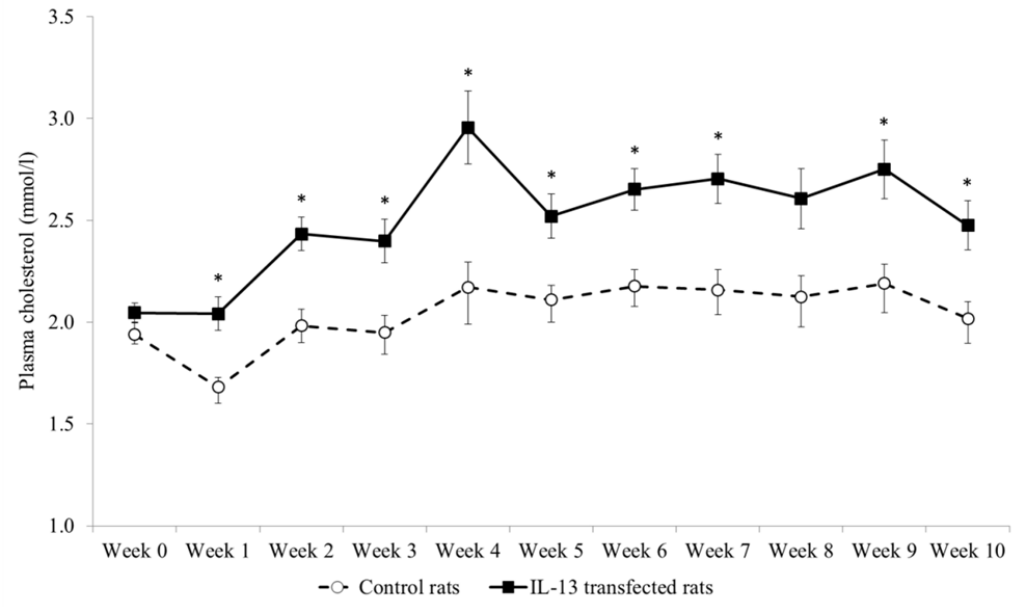

Figure 9: Weekly plasma cholesterol profile.
Plasma cholesterol was significantly elevated from Week 1 onwards in the *IL-13* transfected rats compared to control rats. * denotes p-value < 0.02.

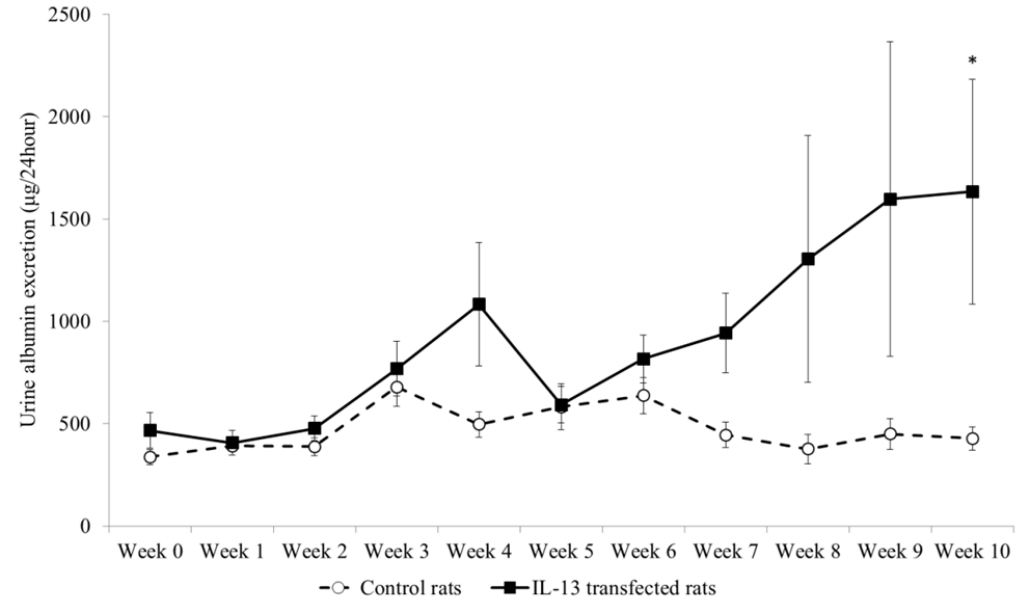

Figure 10: Weekly urine albumin excretion profile.
Urine albumin excretion was significantly elevated at Week 10 in the *IL-13* transfected rats compared to control rats. * denotes p-value < 0.05.

4.3.2. Phenotype of HC rats

In order to investigate the pathogenesis of hypercholesterolemia in the absence of proteinuria upon *IL-13* transfection, HC rats which developed hypercholesterolemia in the pre-proteinuric phase (termed as 'early event') were sacrificed as soon as their plasma total cholesterol levels were 1.5 times above their baseline values at the start of the experiment at Week 0.

The HC rats showed significant elevation in plasma IL-13, plasma total cholesterol and liver mass compared to controls. In addition, the plasma creatinine was significantly lower in this group of rats. Plasma albumin and urine albumin excretion did not differ significantly between the control rats and HC rats (Table 7) (Appendix 4.4).

Table 7: Profile of control and HC rats.
Results are shown as mean ± SEM with the range of values for each parameter in parentheses.

	Control rats (n=9)	HC rats (n=15)	p-value
Plasma IL-13 (pg/ml)	21 ± 3 (10-36)	1219 ± 290 (112-4420)	< 0.001
Plasma total cholesterol (mmol/l)	1.84 ± 0.05 (1.60-2.03)	2.97 ± 0.22 (2.14-5.07)	< 0.001
Plasma albumin (g/l)	37.1 ± 1.5 (31.0-44.2)	40.1 ± 1.3 (31.8-48.5)	0.101
Plasma creatinine (µmol/l)	95.9 ± 5.0 (70.5-116.9)	81.4 ± 3.7 (55.3-105.7)	0.029
Urine albumin excretion (µg/24hour)	254 ± 39 (133-436)	308 ± 40 (104-645)	0.421
Body mass (g)	257 ± 12 (196-311)	248 ± 7 (208-289)	0.474
Liver mass (g)	9.2 ± 0.4 (7.4-10.5)	11.9 ± 0.5 (9.0-17.2)	< 0.001

Plasma lipid profiling was carried out on a subgroup within the HC rats after overnight fasting. They exhibited significantly elevated levels of plasma LDL-cholesterol and HDL-cholesterol, without any difference in plasma triglycerides when compared to controls. There was no significant difference in the liver cholesterol levels between control and HC rats (Table 8) (Appendix 4.5 and Appendix 4.6). H&E staining carried out on the rat liver section did not show any gross abnormality in both control and HC rats, nor were there lipid droplets observed in the HC rats (Figure 11).

Table 8: Plasma lipid profile and liver cholesterol profile of control and HC rats.
Results are shown as mean ± SEM with the range of values for each parameter in parentheses.

Plasma	Control rats (n=6)	HC rats (n=5)	p-value
Total cholesterol (mmol/l)	1.85 ± 0.07 (1.60-2.03)	2.60 ± 0.24 (2.14-3.30)	0.006
LDL-cholesterol (mmol/l)	1.11 ± 0.09 (0.81-1.41)	1.68 ± 0.18 (1.33-2.30)	0.011
HDL-cholesterol (mmol/l)	0.47 ± 0.05 (0.32-0.64)	0.69 ± 0.07 (0.52-0.90)	0.045
Triglycerides (mmol/l)	0.59 ± 0.12 (0.39-1.18)	0.51 ± 0.06 (0.31-0.62)	0.855
Liver	**Control rats (n=9)**	**HC rats (n=15)**	**p-value**
Total cholesterol (mg/g liver)	1.00 ± 0.07 (0.77-1.46)	0.92 ± 0.03 (0.71-1.17)	0.493
Free cholesterol (mg/g liver)	0.82 ± 0.06 (0.66-1.19)	0.74 ± 0.03 (0.62-0.94)	0.221
Cholesteryl esters (mg/g liver)	0.17 ± 0.02 (0.10-0.28)	0.18 ± 0.01 (0.10-0.28)	0.881

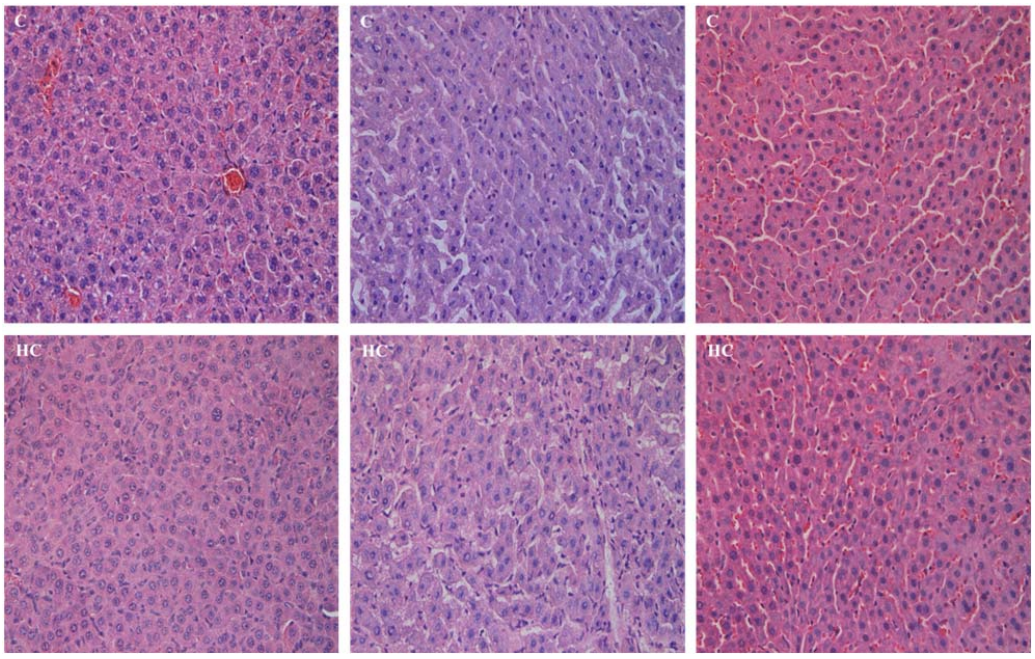

Figure 11: H&E staining of rat liver.
H&E staining of the livers of control rats (C) (n=3) and HC rats (HC) (n=3). Images were taken at 40X magnification.

4.3.3. Comparative analysis of gene expression profile and protein expression in HC rats

To establish the presence of IL-13 receptors in the liver, hepatic gene expressions of IL-13 receptor subunits, *IL-4Ra*, *IL-13Ra1* and *IL-13Ra2*, were studied. Only *IL-13Ra2* showed significant upregulation in the HC rats (Figure 12). Moreover, there was an increase in the protein level for IL-13Ra2, similar to its gene expression, although this did not reach statistical significance (Figure 13).

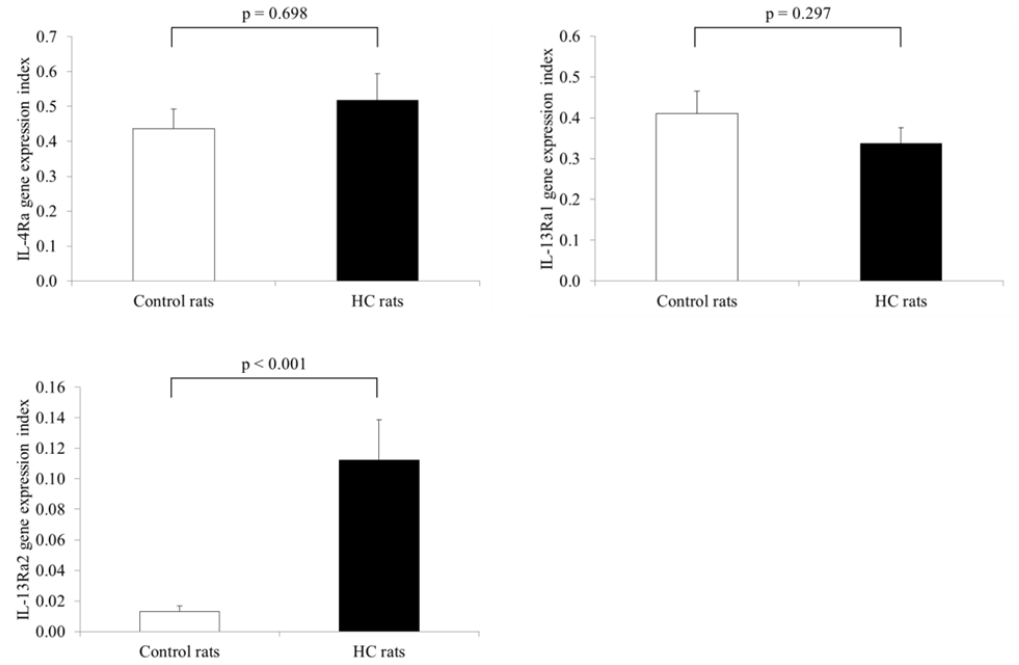

Figure 12: Hepatic mRNA expressions of IL-13 receptor subunits in HC rats.
No significant difference was observed in the hepatic mRNA expressions of *IL-4Ra* and *IL-13Ra1* between the HC rats (n=15) and control rats (n=9). Hepatic *IL-13Ra2* mRNA level was significantly elevated in HC rats compared to controls.

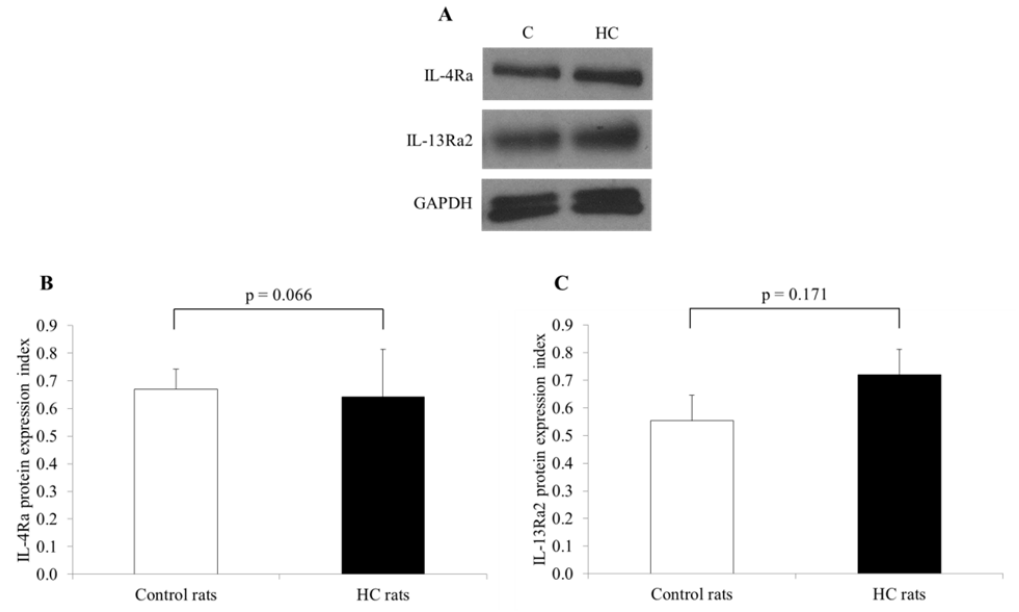

Figure 13: Hepatic protein expressions of IL-4Ra and IL-13Ra2 in HC rats.
Representative Western blot image of IL-4Ra and IL-13Ra2 in control (C) and HC rats (HC) with GAPDH as loading control (A). No significant difference in hepatic protein expressions of IL-4Ra and IL-13Ra2 was observed between the HC rats (n=13) and control rats (n=9) (B).

The nine genes selected for microarray validation by qPCR in the *IL-13* transfected nephrotic rats in Chapter 3 were further investigated in the HC rats. *ABCG5* was the only gene that showed consistent downregulation in both the microarray data and HC rats. *HMGCR* transcription was significantly upregulated in microarray data but showed a non-significant downregulation in HC rats. Significant downregulation of *LXRa*, *RXRa*, *ABCA1* and *ACAT2* was only detected in the HC rats, and not in the nephrotic rats (Figure 14) (Appendix 4.7).

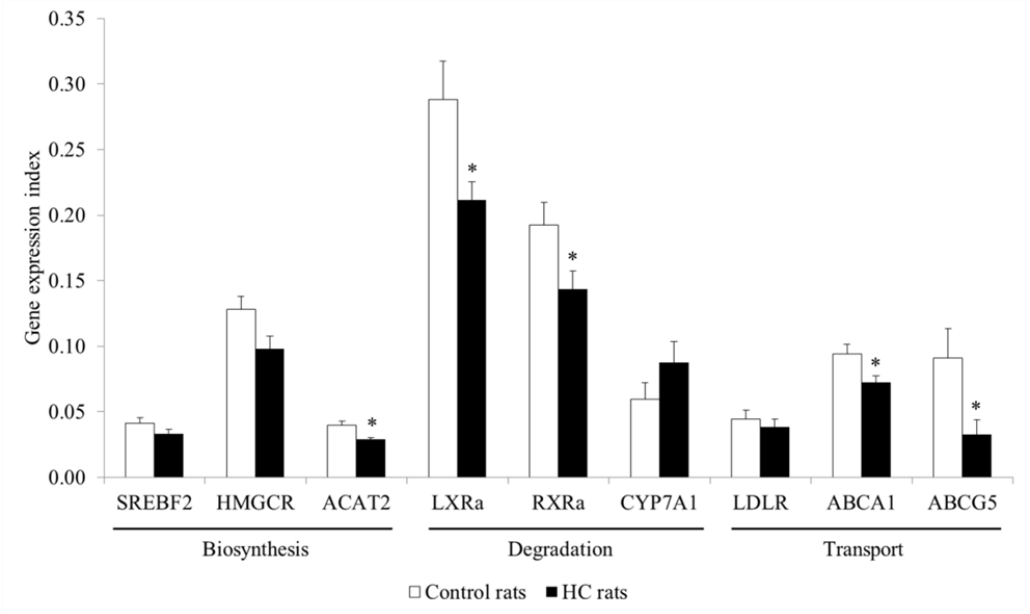

Figure 14: Hepatic mRNA expressions of cholesterol metabolic genes in HC rats.
The nine genes selected for microarray validation by qPCR in the *IL-13* transfected nephrotic rats were investigated in the HC rats (n=15) and controls (n=9). The gene expression index for *LDLR* is multiplied by a factor of 10. * indicates p-value < 0.03.

The protein expression of ABCG5 in the liver of HC rats was subsequently validated using ELISA, and this showed a significant downregulation as compared to controls (Figure 15) (Appendix 4.8).

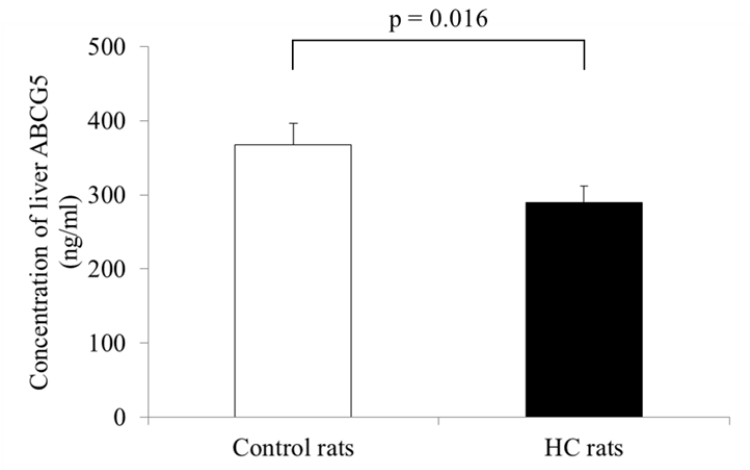

Figure 15: Hepatic protein concentration of ABCG5 in HC rats.
Hepatic protein concentration of ABCG5 was significantly decreased in the HC rats (n=15) as compared to control rats (n=9).

Using Western blot analysis, the protein expression of ABCA1 in the liver of HC rats was significantly reduced compared to control rats (Figure 16). Although there was no significant difference between the hepatic protein expression of LXRa in the HC rats compared to controls (Figure 17), a significant correlation was established between hepatic protein level of LXRa and plasma total cholesterol in the HC rats (Figure 18) (Appendix 4.9 and Appendix 4.10).

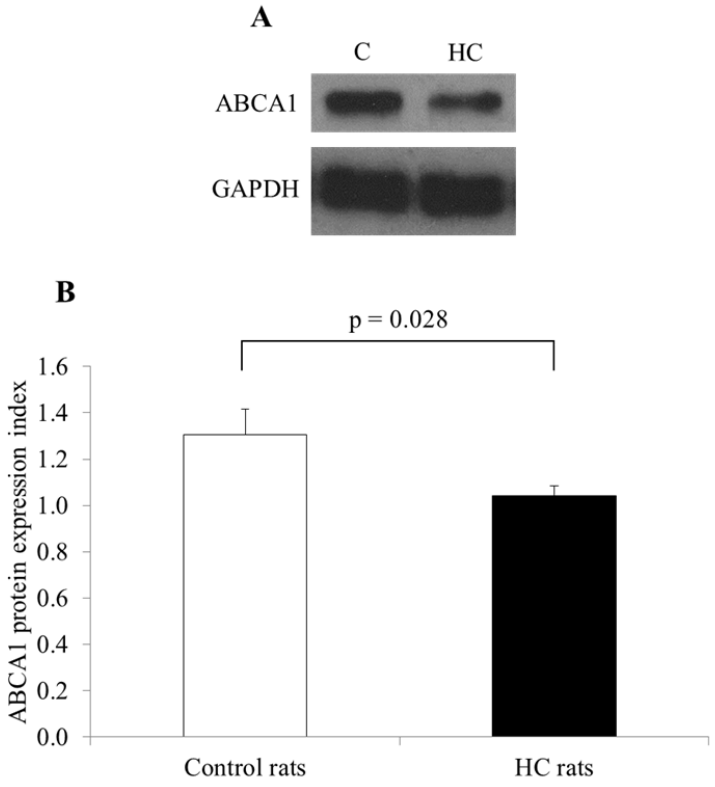

Figure 16: Hepatic protein expression of ABCA1 in HC rats.
Representative Western blot image of ABCA1 in control (C) and HC rats (HC) with GAPDH as loading control (A). Hepatic protein expression of ABCA1 was significantly downregulated in HC rats (n=15) compared to control rats (n=8) (B).

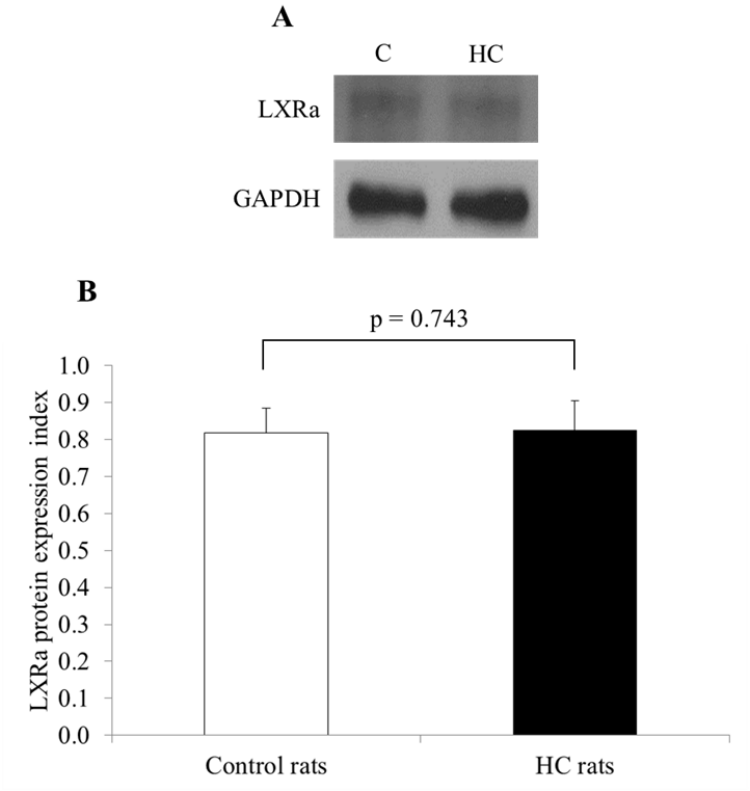

Figure 17: Hepatic protein expression of LXRa in HC rats.
Representative Western blot image of LXRa in control (C) and HC rats (HC) with GAPDH as loading control (A). No significant difference in hepatic protein expression of LXRa was observed between the HC rats (n=15) and control rats (n=9) (B).

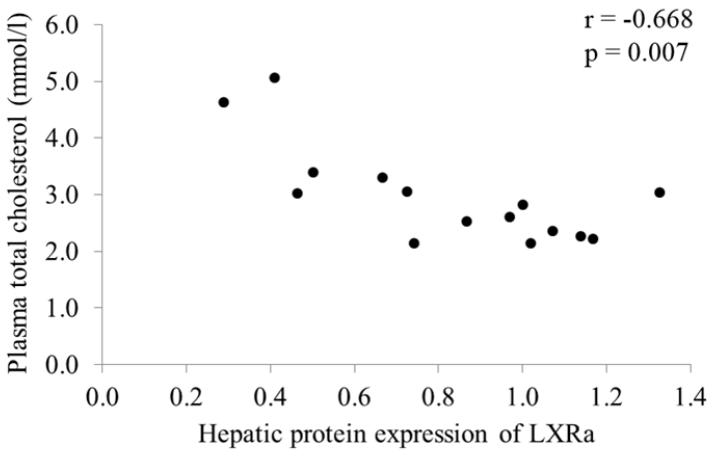

Figure 18: Correlation between hepatic protein expression of LXRa and plasma total cholesterol in HC rats.

4.4. Discussion

The overexpression of *IL-13* in rats was carried out by *in vivo* electroporation of pCI-IL-13 as reported previously by Lai *et al.* (Lai et al., 2007). Successful intramuscular electroporation of pCI-IL-13 was confirmed by the consistent significant elevation of plasma IL-13 in the *IL-13* transfected rats as compared to control rats throughout the entire experiment.

The longitudinal biochemistry profiling of the *IL-13* transfected rats from Week 0 to Week 10 showed that plasma cholesterol was significantly elevated by Week 1, whereas proteinuria was only significantly elevated at Week 10, demonstrating that the development of hypercholesterolemia preceded the onset of proteinuria. This observation was consistent with our hypothesis that the hypercholesterolemia in our *IL-13* overexpression rat model of minimal change-like nephropathy is not solely secondary to the marked proteinuria, but could be related to the increased level of plasma IL-13 acting on hepatic pathways of cholesterol metabolism.

In order to investigate the molecular mechanism of IL-13-induced hypercholesterolemia prior to the onset of significant proteinuria, that is, the 'early event', a subgroup of *IL-13* transfected rats, termed HC rats, were sacrificed as soon as their plasma total cholesterol levels were 1.5 times above their baseline values at the start of the experiment at Week 0, without the development of proteinuria. These hypercholesterolemic HC rats had significantly

heavier liver masses, suggestive of a more active or dysregulated metabolism occurring in the liver as compared to control rats.

Fasting plasma lipid profiling was carried out on a subgroup within the HC rats, and this showed that both plasma LDL-cholesterol and HDL-cholesterol were significantly elevated, but not plasma triglycerides. Therefore, the hyperlipidemia in our *IL-13* transfected rat model was consistent with that seen in human MCNS, with elevated levels of plasma LDL-cholesterol being the major lipid abnormality. The exact nature of plasma HDL-cholesterol in nephrotic syndrome has not yet been confirmed, and reported to be variable by different authors. However, upregulation of plasma HDL-cholesterol has also been shown in patients with nephrotic syndrome and PAN rats (Adigun et al., 1999; Liang and Vaziri, 1999; Michaeli et al., 1981; Oetliker et al., 1980), similar to our *IL-13* transfected rats.

Our HC rats did not demonstrate significant hypertriglyceridemia, as this has been described mainly in overtly nephrotic rats, probably secondary to the massive proteinuria. In a recent landmark study by Clement *et al.*, plasma angiopoietin-like 4 (ANGPTL4) has been identified as the molecular link between proteinuria and hypertriglyceridemia (Clement et al., 2014). These authors have shown that the increase in ANGPTL4 in circulation in response to nephrotic range proteinuria induced hypertriglyceridemia. ANGPTL4 is a known inactivator of LPL, a crucial enzyme that breaks down triglycerides to free fatty acids (FFAs) resulting in FFA uptake in the adipose tissue, heart and skeletal muscles. Inhibition of LPL by

ANGPTL4 thus results in the development of hypertriglyceridemia. However, the investigators have not been able to demonstrate any relationship between ANGPTL4 and the marked hypercholesterolemia seen in nephrotic syndrome.

In order to determine if the elevated plasma cholesterol was due to increased hepatic synthesis as the liver is the major organ regulating cholesterol production, we went on to examine the liver cholesterol profile in the *IL-13* transfected HC rats. Liver total cholesterol, cholesteryl esters and free cholesterol in the HC rats were not significantly different from the control rats, similar to that observed in PAN rats (Kim et al., 2007; Zhou et al., 2008). H&E staining also did not show any accumulation of large amounts of lipid droplets within the liver, when compared to control rats. This suggested that the severe hypercholesterolemia following IL-13 transfection in our HC rats was more likely a result of defective hepatic clearance of cholesterol from the circulation into the bile ducts rather than due to increased hepatic synthesis.

The gene and protein expressions of the IL-13 receptor subunits were detected in the liver of HC rats, with *IL-13Ra2* gene expression showing significant upregulation, indicating that circulatory IL-13 was able to act on the liver to trigger downstream intracellular event. We therefore proceeded to investigate in the HC rats, the nine crucial genes identified from the microarray profile in Chapter 3, that are well established to significantly affect cholesterol metabolism from pathways involving cholesterol biosynthesis, degradation and transport.

Although the *IL-13* transfected nephrotic rats demonstrated significant increase in *HMGCR* mRNA level, we could not show any significant difference in *HMGCR* between HC and control rats. This was consistent with our finding of downregulation of *ACAT2* gene expression, an enzyme important in the conversion of excess hepatic free cholesterols to cholesteryl esters for storage, as the liver cholesterol in the HC rats was not elevated, despite the high plasma cholesterol level. In contrast, the hypercholesterolemia in PAN rats has been attributed to the upregulation of hepatic HMGCR and ACAT2 expression and enzymatic activity (Vaziri and Liang, 2002; Vaziri and Liang, 1995). Therefore, the mechanism triggering hypercholesterolemia in our *IL-13* transfected rat model of nephrotic syndrome during the 'early event' prior to onset of proteinuria was different from that in PAN rats. Dysregulation of *HMGCR* appeared to be a late event in our *IL-13* transfected rat model, with upregulation occurring only when the rats developed frank nephrosis.

Both gene and protein expressions for ABCG5 were significantly downregulated in the HC rats, consistent with the *ABCG5* downregulation observed in the *IL-13* transfected nephrotic rats representing the late event. ABCG5 is crucial in the elimination of excess cellular free cholesterols into bile. The downregulation of ABCG5 could impede effective removal of cholesterol within the liver, leading to the buildup of intracellular cholesterols. This in turn could prevent the further uptake of excess circulatory cholesterols, leading to the significant elevation of

plasma LDL-cholesterol observed in the HC rats. Therefore, downregulation of ABCG5 could be one of the key elements in initiating and subsequently maintaining hypercholesterolemia in the *IL-13* transfected rats.

Both gene and protein expressions of ABCA1 were significantly downregulated in the HC rats. ABCA1 is a full transporter protein belonging to the ABC transporter superfamily, and is essentially involved in two main functions, of which is cell-dependent. Hepatic ABCA1 is involved in the biogenesis of HDL in the liver by mediating the efflux of cellular cholesterols and phospholipids to plasma apoA-I, whereas excess cellular cholesterols in peripheral cells are removed via ABCA1 into HDL to be transported back to the liver for either recycling or disposal from the body as bile, a process known as reverse cholesterol transport (RCT) (Lee and Parks, 2005). The study by Brunham *et al.* showed that knockout of the hepatic *ABCA1* resulted in reduced plasma HDL-cholesterol level and accelerated atherosclerosis (Brunham et al., 2009). Hence, ABCA1 is believed to be anti-atherogenic.

Although hepatic ABCA1 was downregulated in our HC rats, this was not accompanied by a decrease in plasma HDL-cholesterol level, which was instead significantly elevated. Significant elevation of plasma HDL was also reported in other experimental rat models of nephrotic syndrome such as those induced by PA, adriamycin and passive Heymann nephritis (Kaysen et al., 1995; Liang and Vaziri, 1999). The biogenesis of plasma HDL does not depend solely on hepatic

ABCA1 and is multifaceted, involving also apoA-I, whose hepatic synthesis has been shown to be increased, along with decreased catabolism in experimental nephrosis (Liang and Vaziri, 1999; Marshall et al., 1990). High levels of plasma HDL could also be due to decreased availability of hepatic SR-BI (Brundert et al., 2005; Kozarsky et al., 1997), which was also observed in the PAN nephrotic rats, coupled with significant increase in plasma HDL (Liang and Vaziri, 1999; Vaziri et al., 2011).

The gene expression of *LXRa*, a major and prominent regulator for both ABCA1 and ABCG5, was also significantly downregulated in the HC rats. Although we were unable to demonstrate any change in the LXRa protein level, we were able to demonstrate a significant inverse correlation between LXRa protein level and plasma total cholesterol in the HC rats, suggesting the regulatory role of LXRa in cholesterol metabolism. In addition, we found that levels of cognate LXRa target genes, ABCA1 and ABCG5, as well as the gene expression of *RXRa*, the obligate LXRa binding partner, were decreased during the early event of *IL-13* transfection in the rats. Previous studies have reported that cytokines, such as IL-1b and TNF-a, were able to suppress LXRa gene expression and activity (Ruan et al., 2004; Wang et al., 2005). It is therefore possible that IL-13 could be involved in the suppression of LXRa, which in turn downregulates its target genes ABCA1 and ABCG5, leading to the hypercholesterolemia seen in the *IL-13* transfected rat model of nephrotic syndrome.

In summary, we have shown that the elevation of plasma total cholesterol level preceded the onset of proteinuria in our *IL-13* transfected rats. The study of the HC rats (early event) displayed significant reduction of ABCG5 gene and protein expressions, similar to that in the *IL-13* transfected nephrotic rats. This was accompanied with the downregulation of ABCA1, and their transcriptional regulator *LXRa* and its obligate binding partner *RXRa*. Moreover, LXRa protein expression correlated inversely with plasma total cholesterol level, suggesting the possible role of *LXRa-ABCG5/ABCA1* pathway in the initiation of hypercholesterolemia following IL-13 transfection.

The next chapter will investigate the direct effect of IL-13 on the liver, using an *in vitro* rat primary hepatocyte cell culture incubated with IL-13 in order to validate these findings from our HC rats.

Chapter 5 Mechanism of IL-13-mediated cholesterol dysregulation in IL-13-stimulated rat primary hepatocyte cell culture system

5.1. Introduction

Cholesterol homeostasis is essential due to the involvement of cholesterol molecule in several biological processes such as the synthesis of steroid hormones, regulation of cell membrane fluidity and production of bile salts to emulsify dietary fats.

The liver is central to the regulation of cholesterol homeostasis, which is maintained by a series of regulatory pathways that control the hepatic synthesis of endogenous cholesterol and elimination of excess cholesterol into the bile canaliculi. In addition, the liver synthesizes various lipoproteins involved in transporting cholesterol and lipids throughout the body. Any imbalance in cholesterol homeostasis would result in health complications, such as hypercholesterolemia, a risk factor for cardiovascular diseases.

In the weekly biochemical profiling of our *IL-13* transfected rats, hypercholesterolemia was shown to precede the development of proteinuria, depicting the early event upon *IL-13* transfection. Hypercholesterolemia was sustained till the rats developed significant proteinuria and nephrotic syndrome, representing the late event following continuous *IL-13* transfection. At this time

point, there was also a significant direct correlation between serum IL-13 and serum cholesterol levels in the *IL-13* transfected rats. However, no relationship was seen between serum IL-13 and urinary albumin excretion or serum albumin levels. These observations strongly suggested that the hypercholesterolemia seen in our *IL-13* transfected rats could be due to IL-13-induced dysregulation of cholesterol metabolism in the liver, and was not solely secondary to marked proteinuria.

In the previous chapters, liver microarray profile of the *IL-13* transfected nephrotic rats (late event) demonstrated severe downregulation of *ABCG5* gene expression. Pathway analysis of the DEGs also identified 'ABC transporters' pathway to be the top most relevant pathway of cholesterol metabolism in our *IL-13* transfected nephrotic rats, suggesting the possible involvement of ABC transporters such as ABCG5 in the genesis of hypercholesterolemia. ABCG5 and its obligate binding partner ABCG8 are important for cholesterol excretion, secreting excess intracellular free cholesterols directly into the bile canaliculi. The disruption of ABCG5 could lead to increased hepatic cholesterol levels, thereby inhibiting the further uptake of circulatory cholesterols into the liver, eventually resulting in increased plasma cholesterol level.

Our studies on the early event following *IL-13* transfection in rats (HC rats) showed that the expression of ABCG5 was similarly reduced. These HC rats had high plasma cholesterol level but normal urine albumin excretion level. Therefore,

the consistent feature of ABCG5 downregulation found in both the early and late events in our *IL-13* transfected rat model suggested a possible role for ABCG5 both in initiating and sustaining the hypercholesterolemia seen in this model of minimal change-like nephropathy.

On the other hand, the other cholesterol metabolic genes investigated did not show similar consistency between both the early and late events following *IL-13* transfection. In the late event where the *IL-13* transfected rats had developed both hypercholesterolemia and proteinuria, increased gene expression of *HMGCR* was seen. On the contrary, *HMGCR* gene expression was not increased in the HC rats which developed hypercholesterolemia prior to onset of proteinuria, but instead was downregulated albeit insignificant statistically. The HC rats also showed downregulation of gene expressions of *ABCA1*, *LXRa* and *RXRa*, a finding not observed in the late event in the nephrotic rats.

We therefore hypothesized that the hypercholesterolemia seen in our *IL-13* transfected rats prior to the onset of proteinuria could be due to the IL-13-induced dysregulation of cholesterol metabolism in the liver. The hypercholesterolemia could possibly be further enhanced by another stimulus during the late events, namely the development of proteinuria.

5.2. Aim of chapter

The aim of this chapter is to investigate the direct effect of IL-13 on cholesterol homeostasis in the liver, by using an *in vitro* rat primary hepatocyte cell culture system, in order to validate the findings of cholesterol dysregulation from both the early and late events in the *IL-13* transfected rats. Specifically, the objectives of this chapter are to:

1. Validate the gene expression profile of *IL-13* transfected nephrotic rats and HC rats in the IL-13-stimulated hepatocytes.
2. Study the gene and protein expressions of molecules (LXRa, ABCA1 and ABCG5) involved in the cholesterol metabolic pathway(s) following IL-13 stimulation.
3. Determine intracellular cholesterol level in IL-13-stimulated hepatocytes.
4. Assay [^{3}H]-cholesterol transport in the IL-13-stimulated hepatocytes using apoA-I and taurocholate, which induces cholesterol efflux via ABCA1 and ABCG5 respectively.
5. Perform functional studies using LXRa siRNA-transfected rat hepatocytes and investigate the effect of *LXRa*-knockdown on its downstream targets namely, ABCA1 and ABCG5.

5.3. Results

5.3.1. Establishing rat primary hepatocyte cell culture for IL-13 stimulation

To study the direct effect of IL-13 on cholesterol metabolism in the liver, we first established the hepatocyte cell culture system. Primary hepatocytes were isolated from rat liver, followed by seeding and culturing them on a collagen-coated surface. Cells were observed under light microscope after seeding to ensure optimal confluency for re-establishment of cell polarity and cell-cell contact. The hepatocytes displayed a cuboidal morphology after a 3-hour incubation (Figure 19A).

After overnight incubation, the cells changed from the cuboidal morphology into a polygonal shape with extensive cell-cell contact and bile canaliculi network formation defined as the interconnecting bright translucent belts around each cell (Figure 19B). Cells were stimulated with 25ng/ml of IL-13 after overnight incubation. Similar cell morphology appearance was seen in IL-13-stimulated cultures at both 24-hour (Figure 19E) and 48-hour (Figure 19F) post-stimulation as compared to unstimulated cultures (Figure 19C and Figure 19D respectively). Hepatocytes still maintained their polygonal morphology with extensive cell-cell contact and bile canaliculi network formation in both unstimulated and IL-13-stimulated cultured hepatocytes till 48-hour post-stimulation. The cells did not proliferate further in culture.

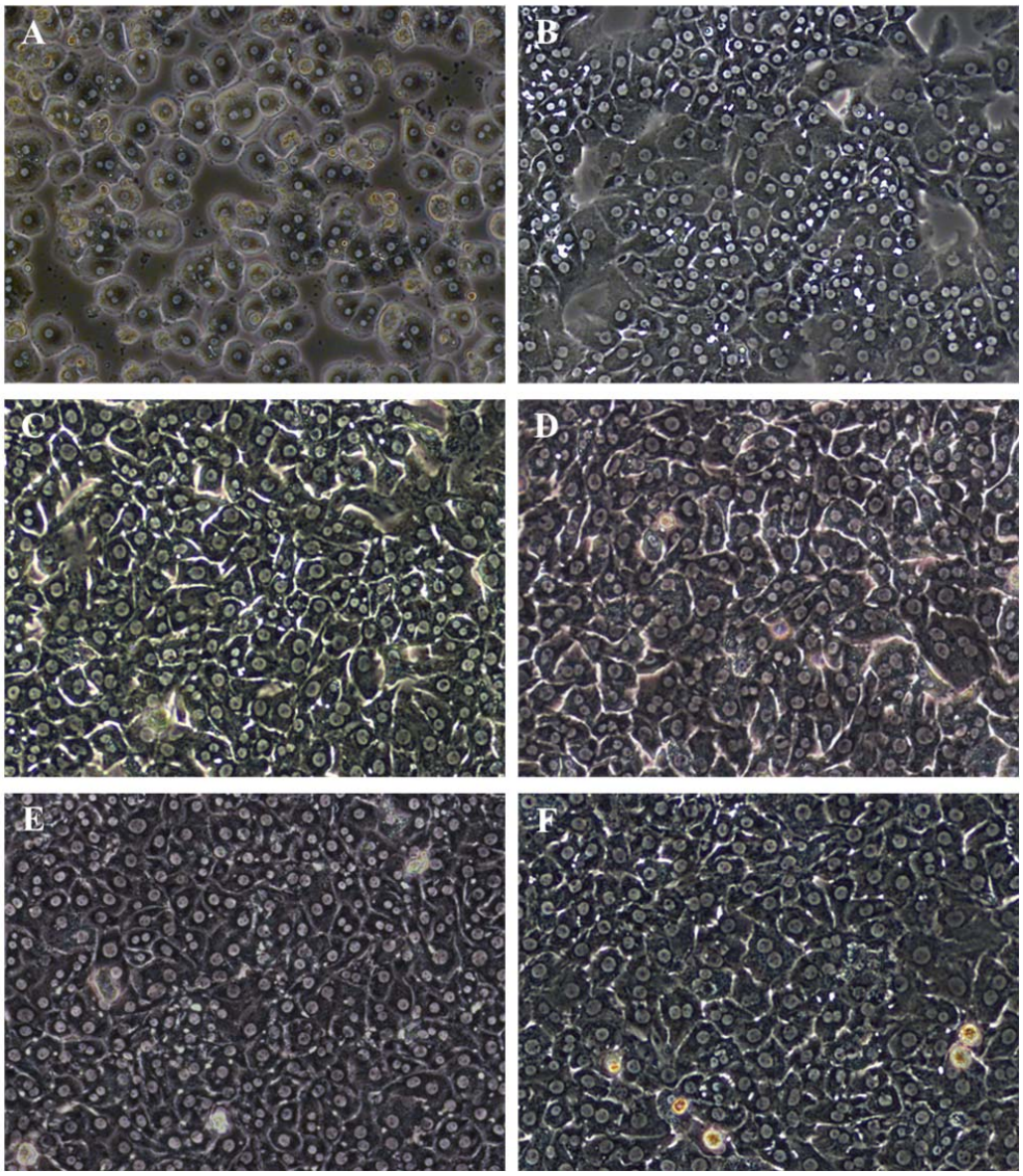

Figure 19: Morphology of cultured rat primary hepatocytes.
Images of rat primary hepatocytes after 4 hours of seeding (A), overnight incubation (B), 24 hours in unstimulated condition (C), 48 hours in unstimulated condition (D), 24-hour stimulation with 25ng/ml of IL-13 (E), 48-hour stimulation with 25ng/ml of IL-13 (F). Images were taken at 100X magnification.

5.3.2. Comparative analysis of gene and protein expression profiles in rat primary hepatocyte cell culture

Both *IL-4Ra* (Figure 20A) and *IL-13Ra1* (Figure 20B) gene expressions were not significantly different between IL-13-stimulated and unstimulated hepatocytes (Appendix 5.1). However, gene expression of *IL-13Ra2* was increased and protein expression of phosphorylated signal transducer and activator of transcription 6 (pSTAT6) was detected in IL-13-stimulated cultures but reduced and undetected respectively in unstimulated cells (Figure 21), demonstrating and verifying the occurrence of IL-13 signaling in our rat primary hepatocyte cell culture upon IL-13 incubation.

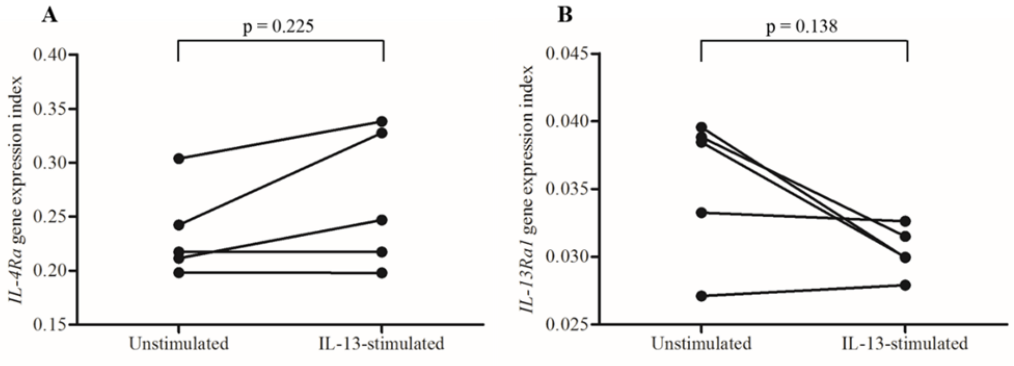

Figure 20: mRNA expression of *IL-4Ra* and *IL-13Ra1* in IL-13-stimulated hepatocytes.
No significant difference was observed for *IL-4Ra* (A) and *IL-13Ra1* expressions (B) in hepatocytes stimulated with 25ng/ml of IL-13 for 24 hours as compared to unstimulated hepatocytes (n=5).

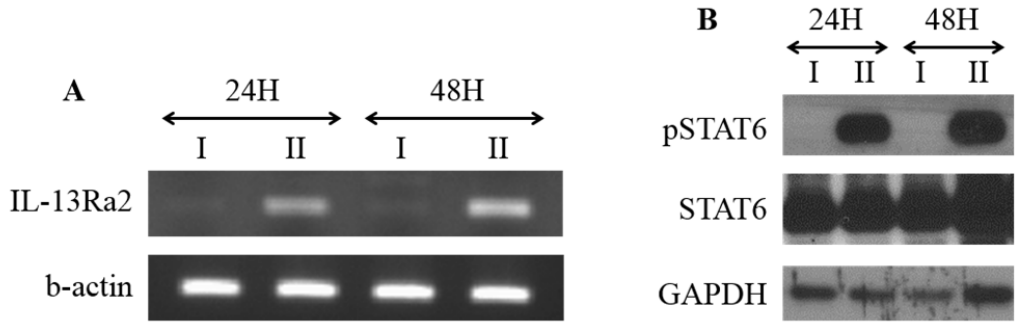

Figure 21: Representative images of *IL-13Ra2* and pSTAT6 expression in IL-13-stimulated hepatocytes.
Representative gel image of *IL-13Ra2* mRNA expression at 24-hour (24H) and 48-hour (48H) in unstimulated (I) and 25ng/ml of IL-13-stimulated hepatocytes (II). Expression of b-actin was shown as a housekeeping gene (A). Representative Western blot image of pSTAT6 protein expression at 24H and 48H in unstimulated (I) and 25ng/ml of IL-13-stimulated hepatocytes (II). Expression of STAT6 and GAPDH were shown for normalization and loading control respectively (B).

The nine genes selected for microarray validation by qPCR in the *IL-13* transfected nephrotic rats in Chapter 3 were further investigated in the IL-13-stimulated rat primary hepatocyte cell culture. These genes were grouped into those involved in cholesterol synthesis (Figure 22), elimination (Figure 23) and transport (Figure 24).

Of the genes involved in cholesterol synthesis, there was no difference in gene expression of *SREBF2* in IL-13-stimulated hepatocytes compared to unstimulated cultures (Figure 22A). On the other hand, gene expression of *HMGCR* was significantly downregulated in the IL-13-stimulated hepatocytes compared to unstimulated hepatocytes (Figure 22B), whereas gene expression of *ACAT2* was significantly upregulated in the IL-13-stimulated hepatocytes compared to controls (Figure 22C) (Appendix 5.1).

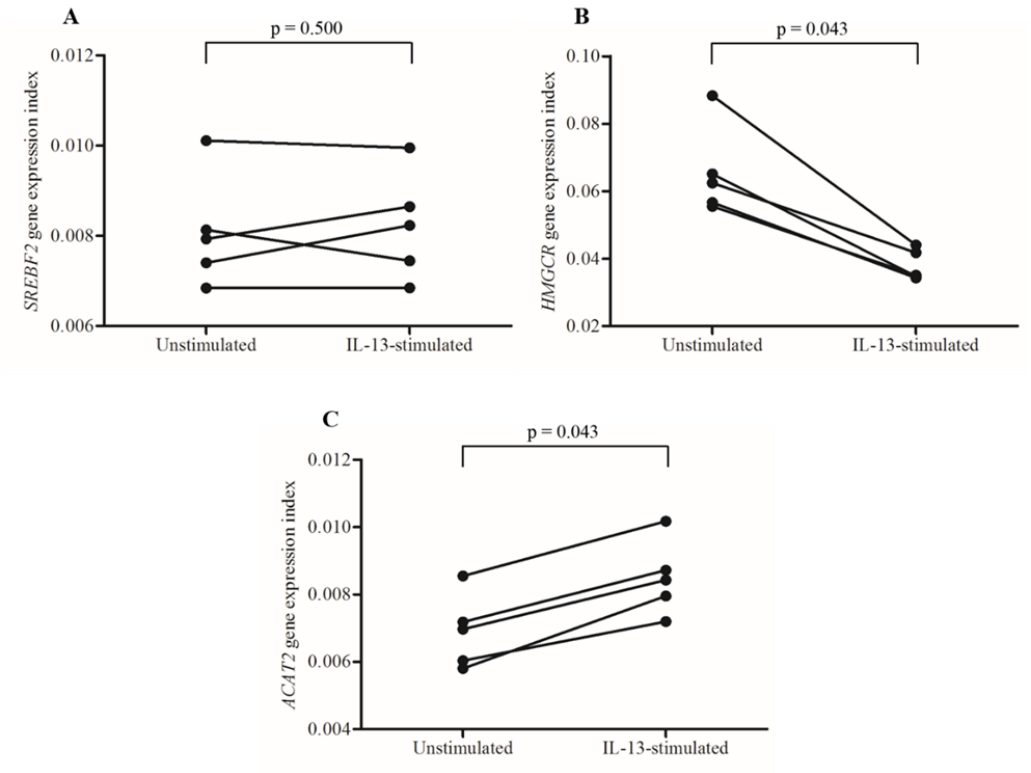

Figure 22: mRNA expression of genes involved in cholesterol synthesis in IL-13-stimulated hepatocytes.
No significant difference was observed for *SREBF2* expression (A), whereas *HMGCR* (B) and *ACAT2* expressions (C) were significantly downregulated and upregulated respectively in hepatocytes stimulated with 25ng/ml of IL-13 for 24 hours as compared to unstimulated hepatocytes (n=5).

Gene expressions of *LXRa* (Figure 23A), *RXRa* (Figure 23B) and *CYP7A1* (Figure 23C), which are involved in the cholesterol elimination pathway, demonstrated significant downregulation upon IL-13 stimulation (Appendix 5.1).

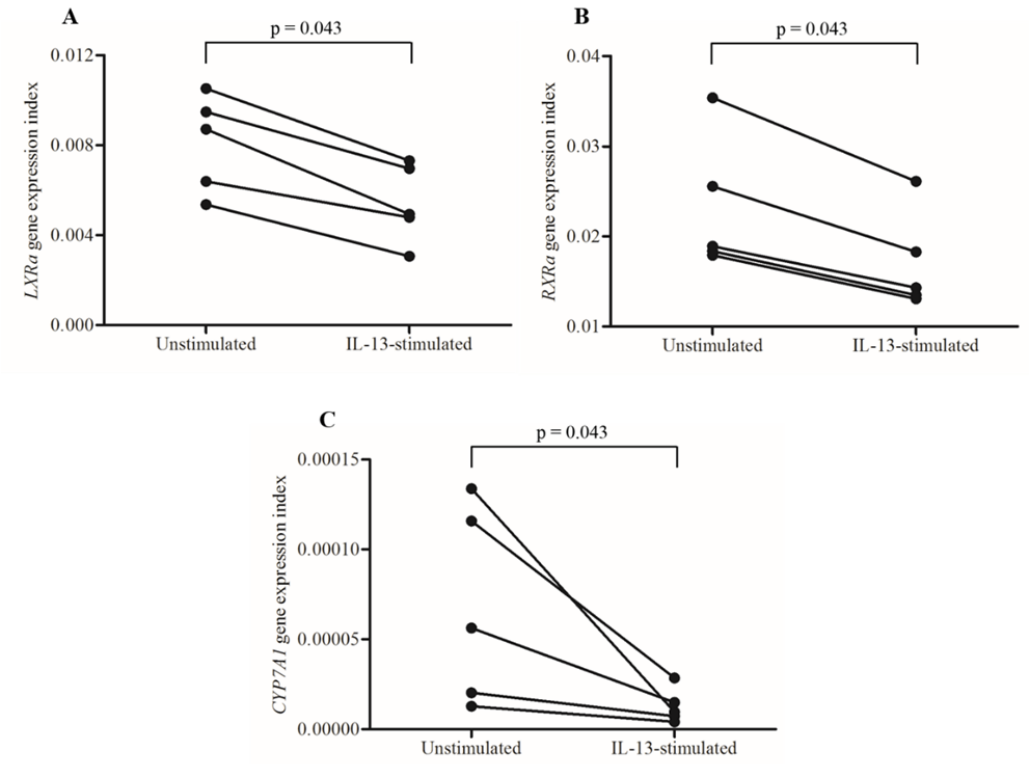

Figure 23: mRNA expression of genes involved in cholesterol elimination in IL-13-stimulated hepatocytes.
Expression levels for *LXRa* (A), *RXRa* (B) and *CYP7A1* (C) were significantly downregulated in hepatocytes stimulated with 25ng/ml of IL-13 for 24 hours as compared to unstimulated hepatocytes (n=5).

Of the genes involved in cholesterol transport, there was no significant difference in gene expression of *LDLR* in the IL-13-stimulated hepatocytes compared to unstimulated cultures (Figure 24A). Following IL-13 stimulation, *ABCA1* gene expression was significantly reduced (Figure 24B). However, the gene expression of *ABCG5* was significantly increased in the IL-13-stimulated hepatocytes compared to unstimulated hepatocytes (Figure 24C) (Appendix 5.1).

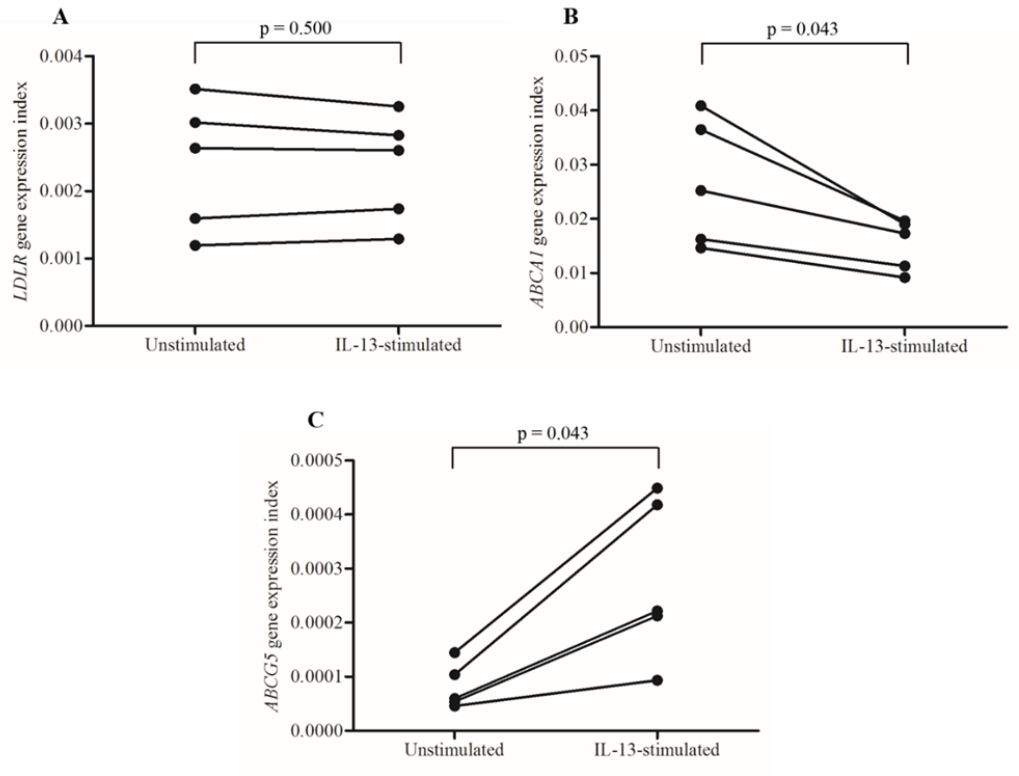

Figure 24: mRNA expression of genes involved in cholesterol transport in IL-13-stimulated hepatocytes.
No significant difference was observed for *LDLR* expression (A), whereas *ABCA1* (B) and *ABCG5* expressions (C) were significantly downregulated and upregulated respectively in hepatocytes stimulated with 25ng/ml of IL-13 for 24 hours as compared to unstimulated hepatocytes (n=5).

Western blot analysis showed significant downregulation for ABCA1 protein expression (Figure 25A and Figure 25B) in the IL-13-stimulated hepatocytes compared to controls, whereas no difference was detected for LXRa protein level (Figure 25A and Figure 25C). Protein concentration of ABCG5 measured using ELISA was not significantly different between IL-13-stimulated hepatocytes compared to unstimulated cells (Figure 25D) (Appendix 5.2).

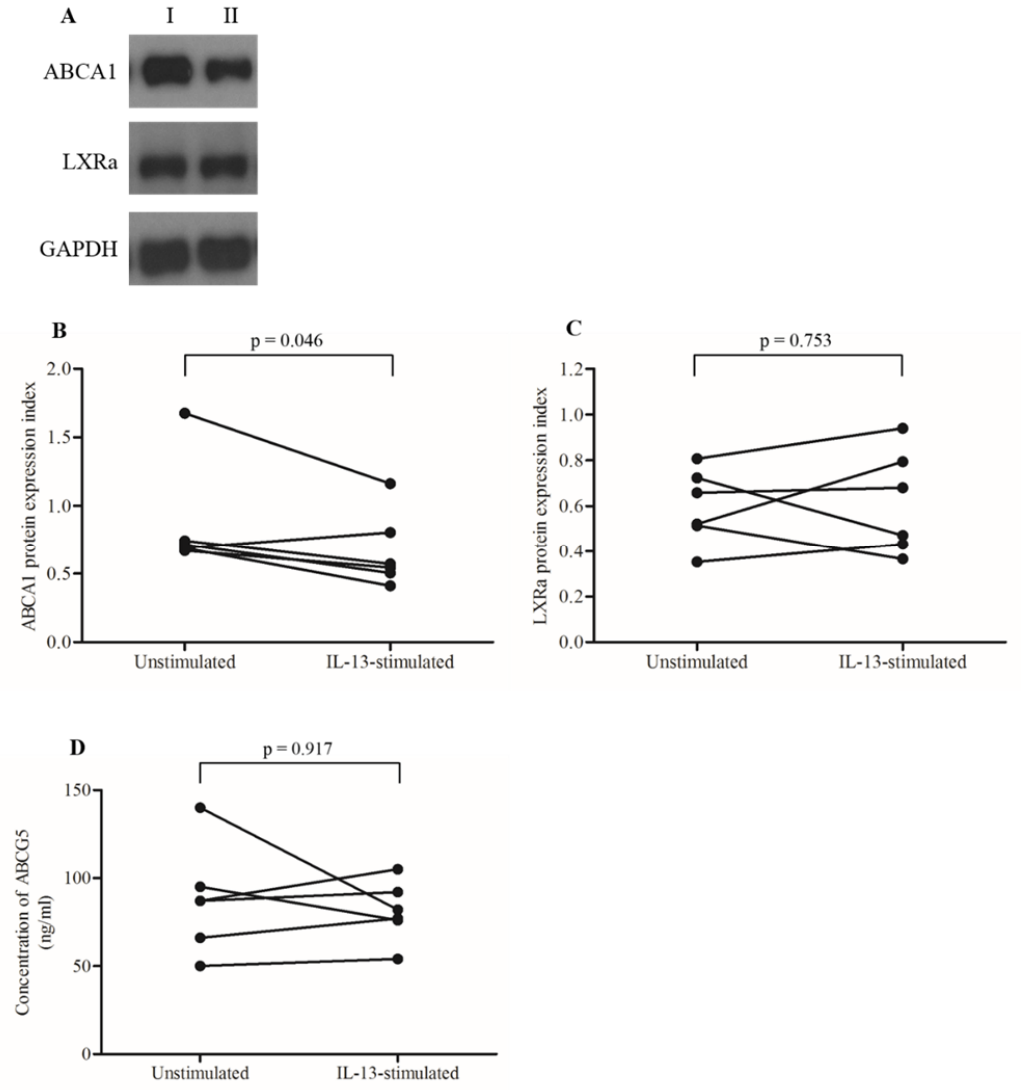

Figure 25: Protein levels of ABCA1, LXRa and ABCG5 in IL-13-stimulated hepatocytes.
Representative Western blot image of ABCA1 and LXRa at 24-hour in unstimulated hepatocytes (I) and 25ng/ml of IL-13-stimulated hepatocytes (II), with GAPDH as loading control (A). Western blot and densitometric analyses showed a decrease in ABCA1 protein expression (B) and no change in LXRa protein level (C) in IL-13-stimulated hepatocytes as compared to unstimulated cells (n=6). ELISA did not detect any difference in ABCG5 protein concentration between IL-13-stimulated and unstimulated hepatocytes (n=6) (D).

5.3.3. Temporal expressions of *LXRa* and its target genes

We next investigated the temporal gene expressions of *LXRa*, *RXRa*, *ABCA1* and *ABCG5* following IL-13 stimulation. These genes were significantly downregulated in the early events following *IL-13* transfection in rats (HC rats).

Gene expressions of *LXRa* (Figure 26A) and *RXRa* (Figure 26B) were significantly downregulated as early as 2-hour post-IL-13-stimulation compared to unstimulated hepatocytes, and was sustained till 24-hour post-stimulation. Gene expression of *ABCA1* showed significant decrease 6-hour post-stimulation (Figure 26C), while *CYP7A1* only showed significant decrease in gene expression 24-hour post-stimulation (Figure 26E). Although there was significant increase in *ABCG5* gene expression in the IL-13-stimulated hepatocytes throughout the temporal experiment, its expression showed a progressive decrease in the difference between stimulated and unstimulated cultures over time (Figure 26D) (Appendix 5.3).

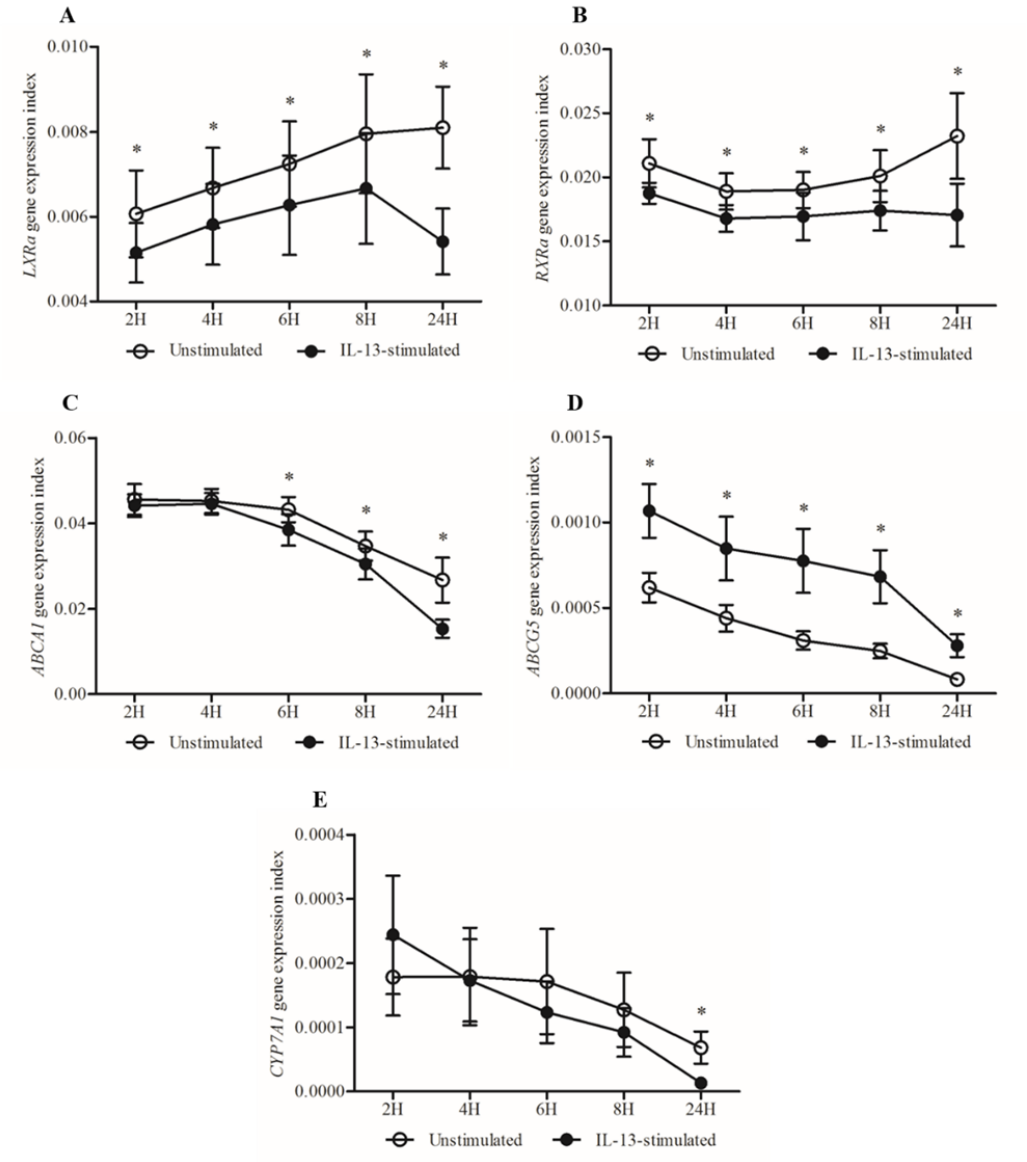

Figure 26: Temporal response curve of *LXRa, RXRa, ABCA1, ABCG5* and *CYP7A1* expression following IL-13 stimulation in hepatocytes.
Rat hepatocytes were cultured with 25ng/ml of IL-13 and harvested at various time points as indicated for gene expression detection (n=5). * indicates p-value < 0.05.

5.3.4. Effect of IL-13 on [^{3}H]-cholesterol efflux and intracellular cholesterol level

The induction of [^{3}H]-cholesterol efflux using apoA-I in culture medium was measured in the cultured hepatocytes after incubation with IL-13. ApoA-I-

meditated cholesterol efflux in the IL-13-stimulated hepatocytes was significantly reduced when compared to unstimulated hepatocytes (Figure 27). Incubation with IL-13 also demonstrated significant decrease in [^{3}H]-cholesterol efflux in the rat hepatocytes when bile acid taurocholate was used as the cholesterol acceptor in the culture medium (Figure 28). However, IL-13 stimulation of hepatocytes did not result in a change in intracellular total cholesterol levels as compared to unstimulated cells (Figure 29) (Appendix 5.4).

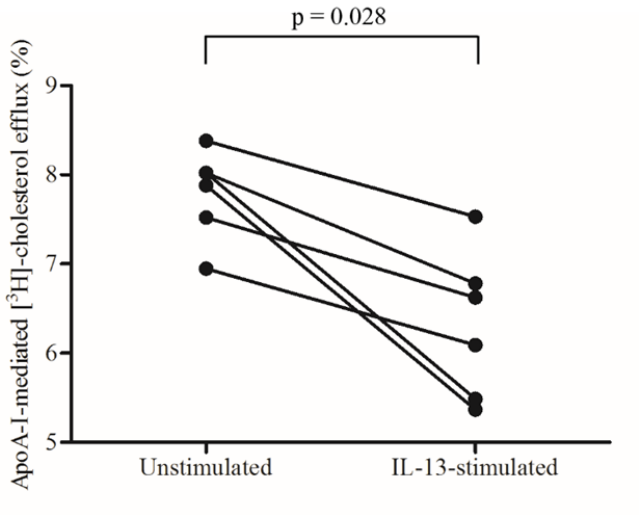

Figure 27: Reduction in apoA-I-mediated [^{3}H]-cholesterol efflux in IL-13-stimulated hepatocytes.
Following 24 hours of [^{3}H]-cholesterol labeling, cultured rat hepatocytes were stimulated for 24 hours with 25ng/ml of IL-13. Cholesterol efflux was assayed with the addition of 5µg/ml of apoA-I in culture medium for another 24 hours (n=6).

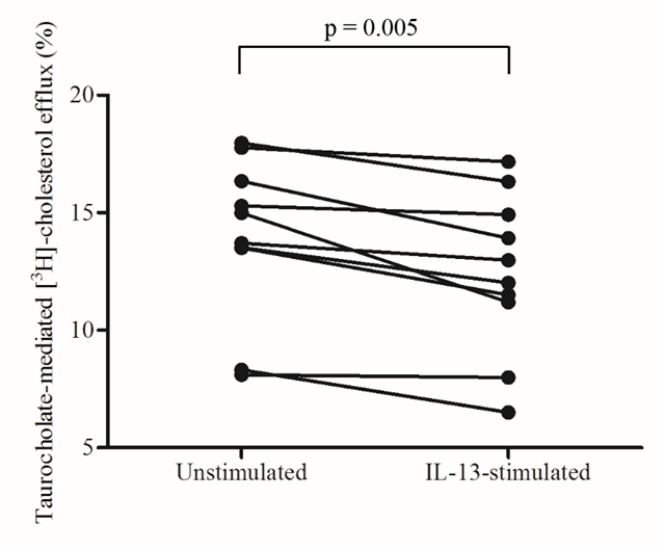

Figure 28: Reduction in taurocholate-mediated [^{3}H]-cholesterol efflux in IL-13-stimulated hepatocytes.
Following 24 hours of [^{3}H]-cholesterol labeling, cultured rat hepatocytes were stimulated for 24 hours with 25ng/ml of IL-13. Cholesterol efflux was assayed by incubating 10mM of taurocholate in culture medium for another 30 minutes (n=10).

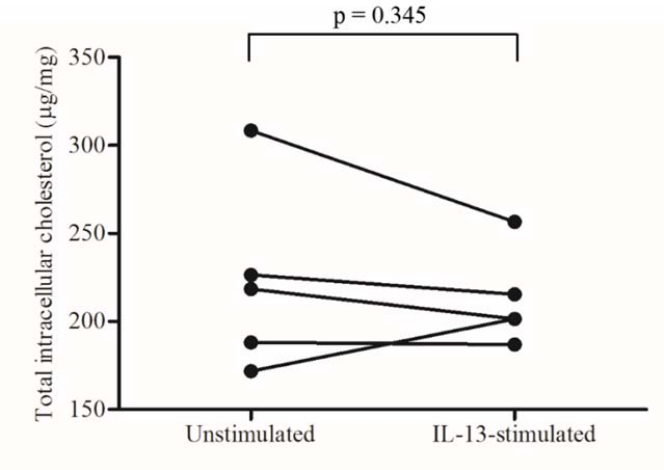

Figure 29: No difference in intracellular cholesterol level between IL-13-stimulated and unstimulated hepatocytes.
Cultured rat hepatocytes were incubated with 25ng/ml of IL-13 for 24 hours, followed by extraction of intracellular cholesterol using hexane:isopropanol. Concentration of cholesterol was normalized against protein lysate obtained after cholesterol extraction (n=5).

5.3.5. Validation of LXRa regulation on ABCA1 and ABCG5

To verify whether LXRa regulated ABCA1 and ABCG5 expressions, we used siRNA to knock down *LXRa* in our rat primary hepatocyte cell culture, and stimulated the culture with T0901317, followed by examining the gene expression of *LXRa* and its target genes *ABCA1* and *ABCG5*. T0901317 is a well-established synthetic agonist for LXRa activity and known to induce LXRa target genes. Following incubation with LXRa siRNA, we achieved a significant and reproducible gene silencing of *LXRa* in rat primary hepatocytes under both unstimulated and T0901317-stimulated conditions, achieving a gene knockdown percentage efficiency of 78.6% ± 3.8% and 80.0% ± 2.7% respectively, as compared to cells incubated with non-targeting control siRNA (NTC) (Figure 30). LXRa protein level was similarly downregulated in the *LXRa*-knockdown hepatocytes under both unstimulated and T0901317-stimulated conditions, although insignificant due to small sample size, thus validating its gene expression result (Figure 31) (Appendix 5.5).

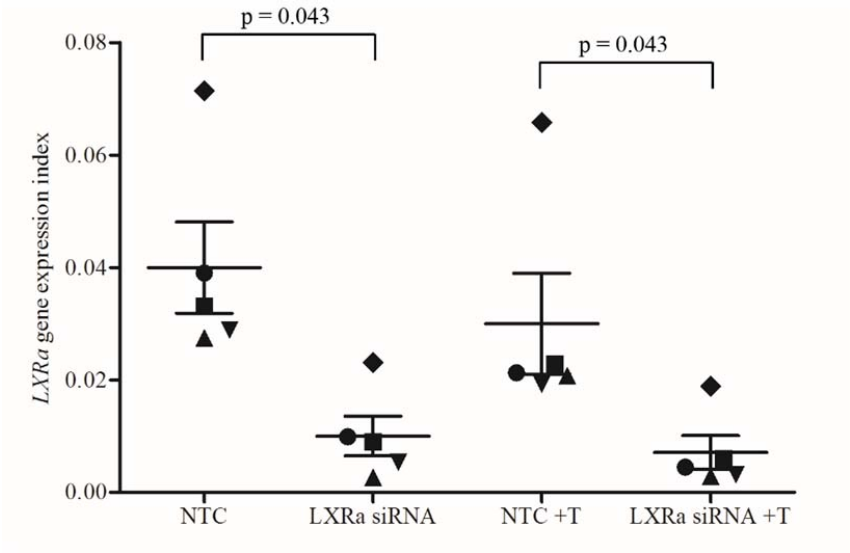

Figure 30: LXRa siRNA-mediated silencing of *LXRa* gene expression in hepatocytes in the absence and presence of T0901317.
Hepatocytes were first incubated with either 50nM of non-targeting control siRNA (NTC) or 50nM of LXRa siRNA for 24 hours, followed by the absence or presence of 5μM of T0901317 (T) for another 24 hours (n=5).

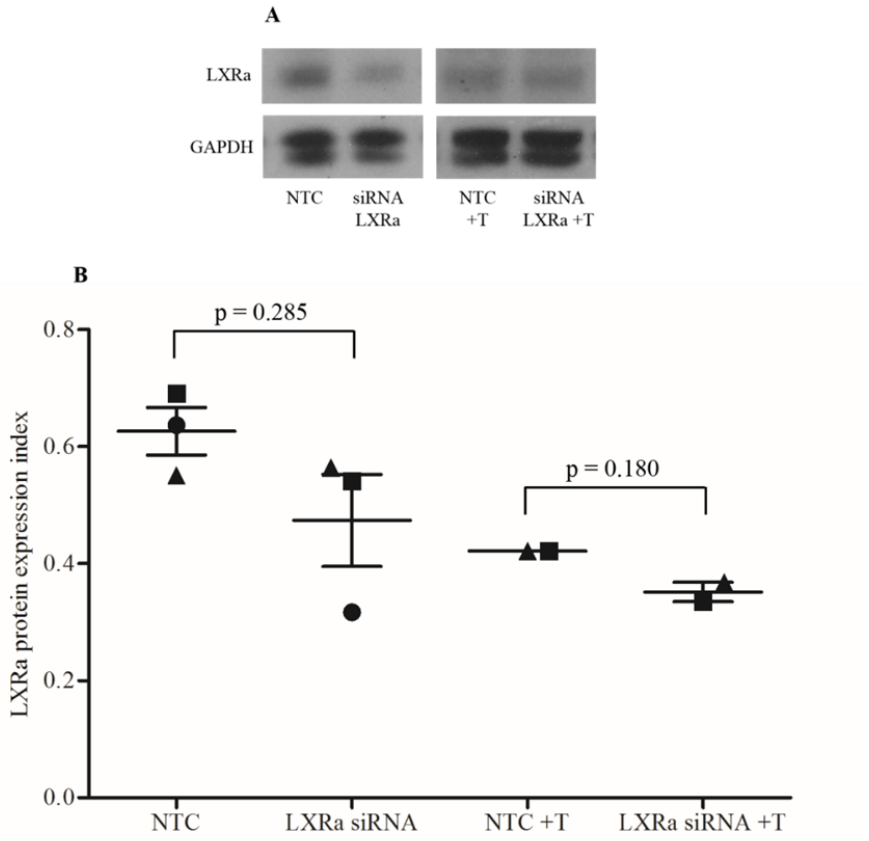

Figure 31: LXRa siRNA-mediated silencing of LXRa protein expression in hepatocytes in the absence and presence of T0901317.
Hepatocytes were first incubated with either 50nM of NTC or 50nM of LXRa siRNA for 24 hours, followed by the absence or presence of 5μM of T0901317 (T) for another 24 hours (n=2 or 3). Representative Western blot image of LXRa in NTC- and LXRa siRNA-transfected hepatocytes, in the absence and presence of T0901317, with GAPDH as loading control (A). Decreased protein expression of LXRa was observed in LXRa siRNA-transfected hepatocytes in the absence and presence of T0901317 (B).

Following LXRa siRNA transfection in hepatocytes, gene expressions of *ABCA1* (Figure 32) and *ABCG5* (Figure 33) were reduced compared to cells transfected with NTC, although this did not reach statistical significance.

To further clarify whether the regulation of ABCA1 and ABCG5 expressions was dependent on LXRa, we next examined the effect of *LXRa*-knockdown on T0901317-induced ABCA1 and ABCG5 expressions. Stimulation of NTC-

transfected hepatocytes with T0901317 resulted in a significant increase in gene expression levels of both *ABCA1* (Figure 32) and *ABCG5* (Figure 33) compared to unstimulated NTC-transfected cells, indicative of successful activation of LXRa. T0901317-induced mRNA expressions of *ABCA1* (Figure 32) and *ABCG5* (Figure 33) in the *LXRa*-knockdown hepatocytes were significantly reduced when compared to NTC-transfected cells stimulated with T0901317.

Validating its mRNA expression, increase in ABCA1 protein level was observed in T0901317-stimulated NTC-transfected hepatocytes compared to unstimulated NTC-transfected cells. Protein levels of ABCA1 were downregulated, although not significant due to small sample size, in the *LXRa*-knockdown hepatocytes compared to NTC-transfected cells, under both unstimulated and T0901317-stimulated conditions (Figure 34) (Appendix 5.6).

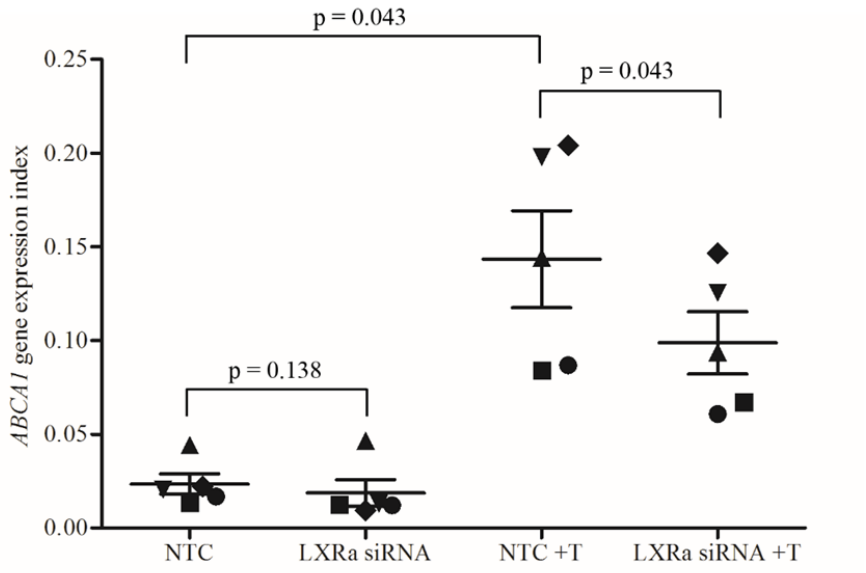

Figure 32: Effect of LXRa siRNA on T0901317-induced *ABCA1* gene expression level in hepatocytes.
Hepatocytes were first incubated with either 50nM of NTC or 50nM of LXRa siRNA for 24 hours, followed by the absence or presence of 5μM of T0901317 (T) for another 24 hours (n=5).

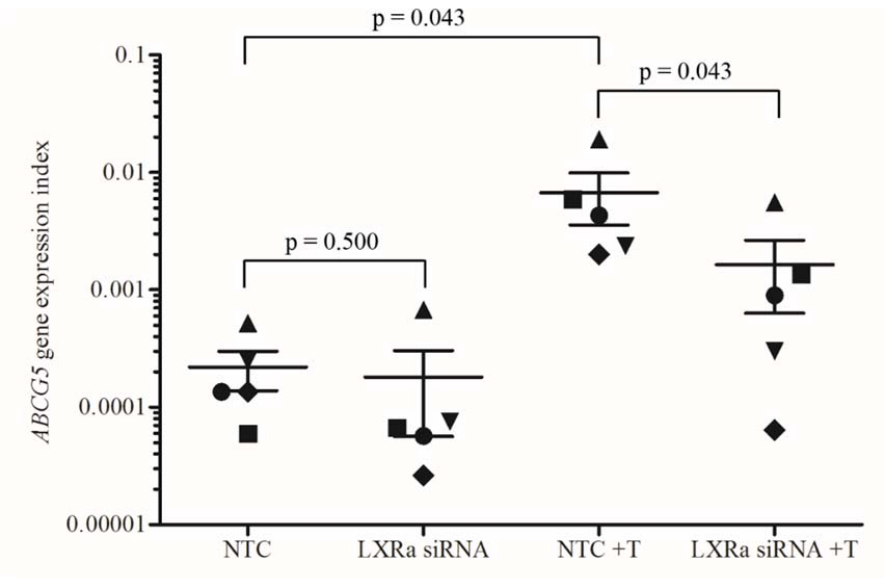

Figure 33: Effect of LXRa siRNA on T0901317-induced *ABCG5* gene expression level in hepatocytes.
Hepatocytes were first incubated with either 50nM of NTC or 50nM of LXRa siRNA for 24 hours, followed by the presence or absence of 5μM of T0901317 (T) for another 24 hours (n=5).

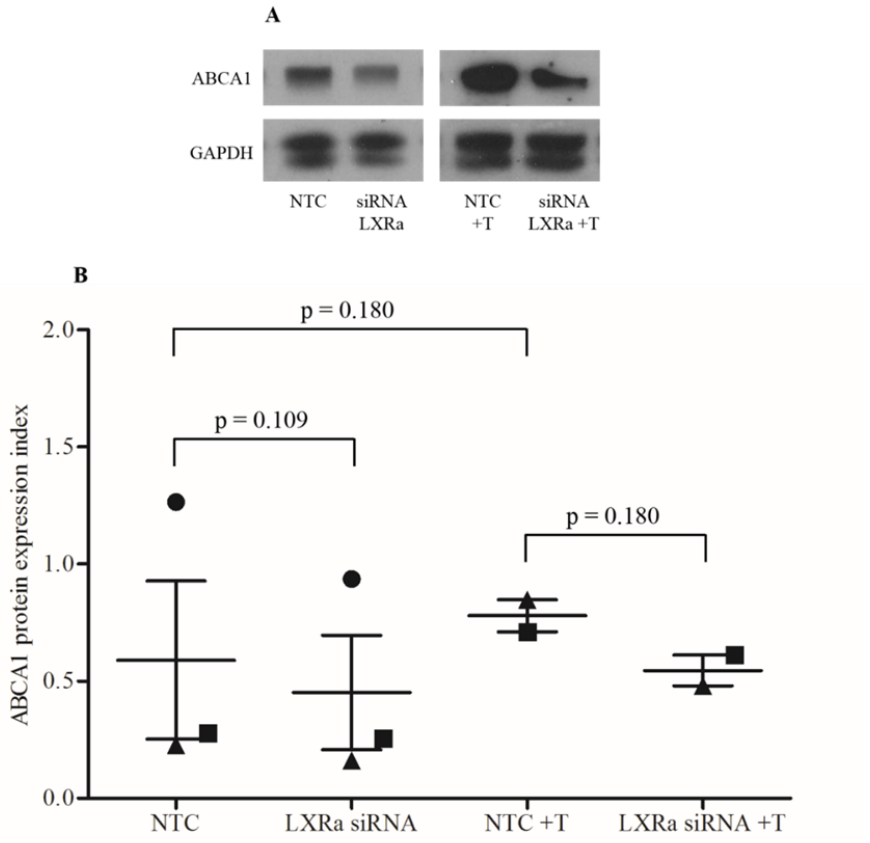

Figure 34: Effect of LXRa siRNA on T0901317-induced ABCA1 protein level in hepatocytes. Hepatocytes were first incubated with either 50nM of NTC or 50nM of LXRa siRNA for 24 hours, followed by the absence or presence of 5μM of T0901317 (T) for another 24 hours (n=2 or 3). Representative Western blot image of ABCA1 in NTC- and LXRa siRNA-transfected hepatocytes, in the absence and presence of T0901317, with GAPDH as loading control (A). Decreased protein expression of ABCA1 was seen in LXRa siRNA-transfected hepatocytes in the absence and presence of T0901317 (B).

5.4. Discussion

The hepatocyte is the major cell type involved in cholesterol regulatory pathways in the liver. Therefore rat primary hepatocyte cell culture was used in this chapter to study the direct effect of IL-13 in order to validate the findings of cholesterol dysregulation in the early and late events in the *IL-13* transfected rats.

Hepatocytes are highly polarized cells, and many of its liver-specific functions such as metabolite uptake, transport and excretion are highly dependent on cell polarity (Coleman and Roma, 2000; Treyer and Musch, 2013). The basolateral membrane in contact with the blood vessels contains transporter proteins responsible for the uptake of substrates to be metabolized within the cell. The apical membranes of adjoining hepatocytes form the bile canaliculi which contain export proteins to excrete free cholesterols and bile into the canaliculi after cellular cholesterol degradation (Tuschl et al., 2009).

Membrane polarity is lost during the isolation of hepatocytes. It is therefore imperative to re-establish their polarity for long-term functional maintenance *in vitro*. In this study, our rat primary hepatocyte cell culture achieved and maintained a functional polygonal shape with extensive cell-cell contacts and bile canaliculi network formation after overnight incubation and throughout the 48-hour study period.

The non-change in IL-13 receptor subunits *IL-4Ra* and *IL-13Ra1* gene expressions in our IL-13-stimulated rat hepatocyte culture was consistent with the results in our HC rats. This was also similar to the findings by David *et al.* in human keratinocyte cell line HaCaT, where no change was seen in the mRNA expressions of *IL-4Ra* and *IL-13Ra1* following incubation with IL-13 from 2 to 24 hours (David et al., 2001). However, gene expression of *IL-13Ra2* was upregulated and protein expression of pSTAT6 was only detected in IL-13-stimulated hepatocytes, demonstrating the occurrence of intracellular IL-13 signaling. This result was consistent with studies in monocytes, splenocytes and keratinocytes which have shown that IL-13 induced the expression of *IL-13Ra2* and triggered phosphorylation of STAT6 (Daines et al., 2006; David et al., 2001; Hebenstreit et al., 2006; Hershey, 2003).

The mRNA expression profile of the nine cholesterol metabolic genes selected for microarray validation by qPCR in the *IL-13* transfected nephrotic rats in Chapter 3 were investigated in the IL-13-stimulated rat primary hepatocyte cell culture.

With regards to the genes associated with cholesterol synthesis, we found a significant downregulation of gene expression of *HMGCR* in IL-13-stimulated hepatocytes, however transcription level of *SREBF2* was not different from unstimulated cells. SREBF2 is a transcriptional regulator of HMGCR and LDLR, and upon activation induces cholesterol synthesis. Therefore, the significant downregulation of *HMGCR* expression in IL-13-stimulated hepatocytes could not

be due to SREBF2 downregulation, but rather a direct effect of IL-13 or elevated cellular free cholesterol level. In our hepatocyte culture system, *ACAT2*, an enzyme which converts free cholesterols into cholesteryl esters for storage within the hepatocytes, was significantly upregulated in the presence of IL-13 incubation. ACAT2 is increased upon excess free cholesterols within the cell. Hence, the upregulation of *ACAT2* observed in IL-13-stimulated hepatocytes could either be a feedback mechanism or a direct effect of IL-13. The measured intracellular total cholesterol level was not significantly different between IL-13-stimulated hepatocytes and unstimulated cells. However, intracellular free cholesterol level was not measured, which could clarify if *HMGCR* and *ACAT2* were affected directly by IL-13 or were the result of the homeostatic response to an increased amount of intracellular free cholesterols.

The cholesterol metabolic genes involved in the degradation of cholesterol, namely *LXRa*, *RXRa* and *CYP7A1*, were all significantly downregulated in the hepatocytes stimulated with IL-13. Obligate heterodimer LXRa and RXRa regulates the mRNA expression of *CYP7A1*. Downregulation of cholesterol degradation genes could lead to the accumulation of cholesterols in the cell, which in turn could downregulate cholesterol synthesis via HMGCR and increase cholesterol storage via ACAT2.

IL-13 stimulation in the hepatocytes did not alter *LDLR* gene expression, which is involved in the hepatic uptake of circulatory cholesterols. This non-change in

LDLR level was in sync with the non-change in *SREBF2* level. On the other hand, *ABCA1* gene expression was downregulated following IL-13 stimulation. The significant downregulation in ABCA1 protein expression validated its gene expression level. Although there was significant elevation in *ABCG5* mRNA transcription level early following IL-13 stimulation of hepatocytes, its protein expression was not different from unstimulated cells. The temporal experiment on *ABCG5* gene expression levels showed that there was a progressive decrease in the difference between IL-13-stimulated and unstimulated hepatocytes over time. This together with the downregulation of ABCA1 gene and protein expressions, was associated with downregulation of *LXRa*, a known regulator of *ABCA1* and *ABCG5*. Moreover, our HC rats also showed downregulation of gene expressions of *LXRa*, *RXRa*, *ABCA1* and *ABCG5* as well as protein expressions of ABCA1 and ABCG5. The association between these genes was also demonstrated in the temporal experiment which showed that gene expressions of *LXRa* and *RXRa* were downregulated as early as 2 hours after IL-13 stimulation in the hepatocytes, whereas their target genes *ABCA1* and *CYP7A1* only showed significant downregulation after 6 hours and 24 hours respectively.

The roles of ABCA1 and ABCG5 in IL-13-induced cholesterol efflux were examined in our rat primary hepatocyte culture, whereby the presence of specific cholesterol acceptor in the culture medium activates specific membrane transporter for cholesterol efflux. To initiate cholesterol efflux via ABCA1, cholesterol acceptor apoA-I is required in the culture medium (Kim et al., 2012;

Li et al., 2010; Schwartz et al., 2000; Wang et al., 2000), while bile salt taurocholate is used as the cholesterol acceptor for ABCG5 (Johnson et al., 2010; Tachibana et al., 2007; Vrins et al., 2007).

IL-13-stimulated hepatocytes exhibited a significant decrease in the percentage of apoA-I-mediated cholesterol efflux as compared to unstimulated cells. This reduction in cholesterol efflux by hepatic ABCA1 into apoA-I could be due to the downregulation in both gene and protein expressions of ABCA1 in the IL-13-stimulated hepatocytes. Decreased hepatic ABCA1 has been linked to inefficient clearance of excess cholesterol in peripheral cells, especially macrophages, which could lead to foam cell formation and eventually atherosclerotic lesions.

Studies have demonstrated that the presence of bile salts as cholesterol acceptor was essential for ABCG5/G8 specific cholesterol efflux in cell models, and that other commonly known cholesterol acceptors such as apoA-I and HDL were not able to increase efflux via ABCG5/G8 (Tachibana et al., 2007; Vrins et al., 2007). Biologically, taurocholate is one of the major bile salts in mammalian bile, hence was used as cholesterol acceptor to induce cholesterol efflux in order to investigate ABCG5-mediated transport in the IL-13-stimulated hepatocytes. We have shown that the percentage of taurocholate-mediated cholesterol efflux was significantly reduced in IL-13-stimulated hepatocytes, suggesting that the efflux of cholesterol via ABCG5 could be reduced or impaired. ABCG5 represents one of the major pathways for cholesterol removal in the liver. Downregulation of

ABCG5-mediated cholesterol efflux hinders the effective clearance of cellular cholesterols within the liver. This could lead to hepatic intracellular cholesterol buildup, of which excess free cholesterols could downregulate the cholesterol biosynthetic enzyme HMGCR and activate ACAT2, as seen in the *HMGCR* downregulation and *ACAT2* upregulation in the IL-13-stimulated hepatocytes.

We went on to confirm the regulatory effect of *LXRa* on ABCA1 and ABCG5 expressions in our rat primary hepatocyte culture by using LXRa siRNA to knock down *LXRa*. Both gene and protein expressions of LXRa were successfully reduced upon LXRa siRNA transfection in our cultured rat hepatocytes under both T0901317-stimulated and unstimulated conditions. T0901317 is a well-established synthetic agonist of LXRa activity known to induce the transcription of LXRa target genes (Schultz et al., 2000). Stimulation of hepatocytes with T0901317 was able to significantly increase the expressions of *ABCA1* and *ABCG5* compared to unstimulated cells. Moreover, the significant decrease in *ABCA1* and *ABCG5* expressions in *LXRa*-knockdown hepatocytes compared to NTC-transfected cells in the presence of T0901317 demonstrated the direct regulation of LXRa on ABCA1 and ABCG5.

In summary, IL-13-stimulated hepatocytes showed a gene expression profile consistent with reduced cholesterol synthesis, degradation and efflux with downregulation of *LXRa*, *RXRa* and ABCA1 expression. Although there was significant increase in *ABCG5* gene expression in the IL-13-stimulated

hepatocytes throughout the temporal experiment, its gene expression showed a progressive decrease in the difference between stimulated and unstimulated cultures over time. In addition, ABCG5 protein expression showed similar levels in both IL-13-stimulated and unstimulated hepatocytes. Moreover, the reduced cholesterol efflux using apoA-I and taurocholate indicated that both efflux transporters ABCA1 and ABCG5 were functionally reduced, of which ABCA1 showed consistent downregulation in its gene and protein expressions. The effect of *LXRa*-knockdown on T0901317-induced hepatocytes confirmed that LXRa directly regulated both *ABCA1* and *ABCG5* gene expressions, and that its downregulation could lead to the decrease in ABCA1 and ABCG5, hence reducing the efflux of hepatic cholesterol *in vivo*. How these events could lead to hypercholesterolemia in the *IL-13* transfected rats will be discussed in the next chapter.

Chapter 6 Conclusion and future directions

6.1. Conclusion

In this study, we have elucidated distinct molecular mechanisms of hypercholesterolemia associated with our *IL-13* transfected rats in the early (in the absence of proteinuria) and late (in the presence of proteinuria) events.

The molecular signature of the hypercholesterolemia associated with *IL-13* transfected nephrotic rats (late event) is defined by DEGs highly involved in metabolism requiring NAD and NADP, characteristic of synthesis instead of catabolism. Pathway analysis of the DEGs identified 'ABC transporters' as the most relevant pathway in cholesterol metabolism, of which *ABCG5* expression showed the greatest downregulation validated by qPCR, suggesting possible involvement of ABC transporters in the genesis of hypercholesterolemia seen in the *IL-13* transfected nephrotic rats. Profiling of crucial cholesterol metabolic genes in these rats also showed *HMGCR* to be significantly upregulated.

In order to determine if the cause of the dysregulation of *ABCG5* and *HMGCR* was due to *IL-13* transfection in the rats or secondary to proteinuria, we went on to study the liver molecular profile and protein expression of the cholesterol metabolic genes in the early phase of our *IL-13* transfection rat model when hypercholesterolemia was first demonstrated, prior to the development of proteinuria (HC rats). The HC rats displayed reduction of ABCG5 expression, similar to that in the *IL-13* transfected nephrotic rats. This was accompanied by

downregulation of ABCA1, and their transcriptional regulator *LXRa* and its obligate binding partner *RXRa*. Moreover, a significant inverse correlation was observed between hepatic LXRa protein level and plasma total cholesterol in the HC rats, suggesting the possible role of *LXRa-ABCG5/ABCA1* pathway in the initiation of hypercholesterolemia following *IL-13* transfection.

In order to validate the role of this pathway in the genesis of hypercholesterolemia seen early in *IL-13* transfected rats, we then investigated the expression profile of cholesterol metabolic genes in an IL-13-stimulated rat primary hepatocyte cell culture system and compared this to the molecular signatures seen in the early and late events in the *IL-13* transfected rats.

Gene expressions of *SREBF2* and *LDLR* were not significantly different from controls across the *IL-13* transfected nephrotic rats, HC rats, as well as in the IL-13-stimulated hepatocytes. SREBF2 is a transcriptional regulator of *HMGCR* and *LDLR*. This could suggest that SREBF2-regulated cholesterol biosynthesis and LDLR-mediated cholesterol import do not play a major role in the hypercholesterolemia of IL-13-induced MCNS.

We have demonstrated significantly increased gene expression of *HMGCR* only in the liver of *IL-13* transfected nephrotic rats, but not early in the genesis of hypercholesterolemia prior to development of proteinuria in the HC rats. This finding was validated in our IL-13-stimulated rat hepatocytes where gene

expression of *HMGCR* was significantly downregulated compared to unstimulated hepatocytes. To determine whether the downregulation of *HMGCR* mRNA expression was secondary to an increased amount of hepatic intracellular cholesterols, we measured total cholesterol level in our IL-13-stimulated rat hepatocytes. However, there was no significant difference in the total cholesterol level between hepatocytes incubated with and without IL-13. This result was consistent with that observed in the HC rats, which also did not show any change in the liver total cholesterol level when compared to control rats. Further studies will have to be performed to determine the hepatic intracellular total cholesterol level at 48-hour post-IL-13-stimulation, as a 24-hour IL-13 incubation might be relatively short to detect any changes in the cholesterol concentration within the hepatocytes. In addition, the level of free cholesterols should be measured in our IL-13-stimulated hepatocytes, as it is the presence of excess free cholesterols binding to the sterol-sensing domain in HMGCR that results in its proteolytic degradation (Kuwabara and Labouesse, 2002).

These results suggested that *HMGCR* did not have a primary role in the initial genesis of hypercholesterolemia in the *IL-13* transfected rats, but upregulation of *HMGCR* was a late event phenomenon that perpetuates the hypercholesterolemia in nephrotic syndrome. HMGCR controls the rate-limiting step in the synthesis of endogenous cholesterol. The discrepant findings in *HMGCR* gene expression between the early and late events therefore suggest that hypercholesterolemia could possibly be further enhanced by another stimulus during the late event

upregulating *HMGCR* gene expression, namely the development of proteinuria. This finding is in contrast to the PAN rats with nephrotic syndrome, where studies have suggested that the transient increase in HMGCR was important in the initiation of hypercholesterolemia secondary to proteinuria (Vaziri and Liang, 1995).

The gene expression of *ACAT2* was significantly upregulated in the cultured hepatocytes following IL-13 stimulation. The role of ACAT2 in the hepatocyte is to convert free cholesterols into cholesteryl esters for storage within the cell. An increase in ACAT2 enzyme activity therefore occurs in the presence of excess intracellular free cholesterols. Vaziri and Liang have attributed part of the hypercholesterolemia in PAN rats to the increase in ACAT2, whereby its increase could have led to a reduction in hepatic intracellular free cholesterol level. The decrease in free cholesterol level in turn could activate hepatic SREBF2 and its downstream targets, HMGCR and LDLR, to synthesize more cholesterols, and eventually diminishing the hepatic uptake of circulatory cholesterols, resulting in hypercholesterolemia in the PAN rats (Vaziri and Liang, 2002). However this theory was not substantiated in our IL-13-stimulated hepatocytes as the initial upregulation of *ACAT2* occurred in association with *HMGCR* downregulation and normal levels of *SREBF2*. Furthermore, in the early event during the genesis of hypercholesterolemia in HC rats, *ACAT2* gene expression was not upregulated, but was in fact significantly downregulated. Even in the *IL-13* transfected nephrotic rats (late event), *ACAT2* gene expression was not upregulated. Hence,

the upregulation of *ACAT2* observed in IL-13-stimulated hepatocytes could either be a direct effect of IL-13 or secondary to a feedback mechanism following accumulation of hepatic free cholesterols.

Gene expression of *LXRa* was significantly downregulated in the IL-13-stimulated hepatocytes as compared to unstimulated condition, and this downregulation occurred as early as after 2 hours of IL-13 incubation, suggesting a direct effect of IL-13 on the regulation of *LXRa* expression. Expression of *RXRa*, the obligate binding partner of LXRa, also showed a similar temporal downregulation trend as *LXRa*. The decrease in both *LXRa* and *RXRa* was consistent with the decrease in the hepatic *LXRa* and *RXRa* expressions in HC rats. Moreover, protein expression of LXRa was unchanged in the IL-13-stimulated hepatocytes, similar to the observation in HC rats.

Gene expression of *ABCA1*, a target gene of LXRa, was significantly downregulated in hepatocytes stimulated with IL-13 as compared to controls, and this downregulation became significant after 6 hours of IL-13 incubation, and occurred after significant downregulation of *LXRa*. Protein expression of ABCA1 was also significantly reduced in the IL-13-stimulated hepatocytes. These findings suggested that IL-13 first induced the downregulation of *LXRa*, which subsequently resulted in downregulation of ABCA1. Similarly, expression of *ABCA1* was significantly downregulated in the HC rats but no change was seen in the *IL-13* transfected nephrotic rats, again consistent with the concept that the

LXRa-ABCG5/ABCA1 pathway is activated early in the genesis of hypercholesterolemia, following *IL-13* transfection. The downregulation of hepatic ABCA1 in our *IL-13* transfected rats was not accompanied by a decrease in plasma HDL-cholesterol level. This could be because the biogenesis of plasma HDL is multifactorial involving other molecules such as SR-BI and apoA-I.

Gene expression of *CYP7A1*, a key enzyme involved in cholesterol degradation, was significantly downregulated in the IL-13-stimulated hepatocytes. Downregulation of CYP7A1 causes the accumulation of cholesterols within the cell. Its temporal expression profile showed significant decrease only after 24 hours of IL-13 incubation. The downregulation of *CYP7A1* was not seen in both *IL-13* transfected nephrotic rats and HC rats. As *CYP7A1* is also a target gene of LXRa, this further supports the hypothesis that IL-13 acts on *LXRa*, which subsequently results in the downregulation of its target gene *CYP7A1*.

Although the gene expression of *ABCG5* in IL-13-stimulated hepatocytes was significantly upregulated, this *ABCG5* upregulation could not account for the reduction in taurocholate-mediated cholesterol efflux seen in our hepatocyte cell culture system, since taurocholate is known to activate cholesterol efflux via ABCG5/G8. In addition, the temporal expression of *ABCG5* showed a decreasing difference between IL-13-stimulated hepatocytes and unstimulated cells with time, suggesting a non-significant difference might be observed at a time point later than 24-hour. This was corroborated in the HC rats, where both gene and

protein expressions of ABCG5 were significantly downregulated, and this *ABCG5* gene downregulation was sustained in the *IL-13* transfected nephrotic rats.

In conclusion, the hypercholesterolemia observed early in the IL-13-induced rat model of MCNS (HC rats) could be due to IL-13-induced downregulation of *LXRa*, which subsequently led to the reduction in ABCA1 and ABCG5. The downregulation of hepatic ABCG5 could lead to reduced cholesterol efflux into bile canaliculi and hence inefficient removal of excess free cholesterols within the hepatocytes, bringing about an increased amount of intracellular cholesterols. Increased hepatic cholesterol level could inhibit the further uptake of circulatory cholesterols into the liver for excretion, leading to the hypercholesterolemia as seen in our *IL-13* transfected rats. Late event hypercholesterolemia seen in our *IL-13* transfected nephrotic rats could possibly be maintained by the continuous downregulation of ABCG5 and upregulation of HMGCR secondary to the gross proteinuria (Figure 35).

Our study has elucidated the gene molecular profile involved in the IL-13-induced hypercholesterolemia in the HC rats. Hence, to effectively bring down the elevated level of cholesterol to homeostatic level, targeted therapy could be developed to ameliorate the dysregulation of enzymes, transporters and/or regulators that are key in the pathogenesis of hypercholesterolemia in MCNS.

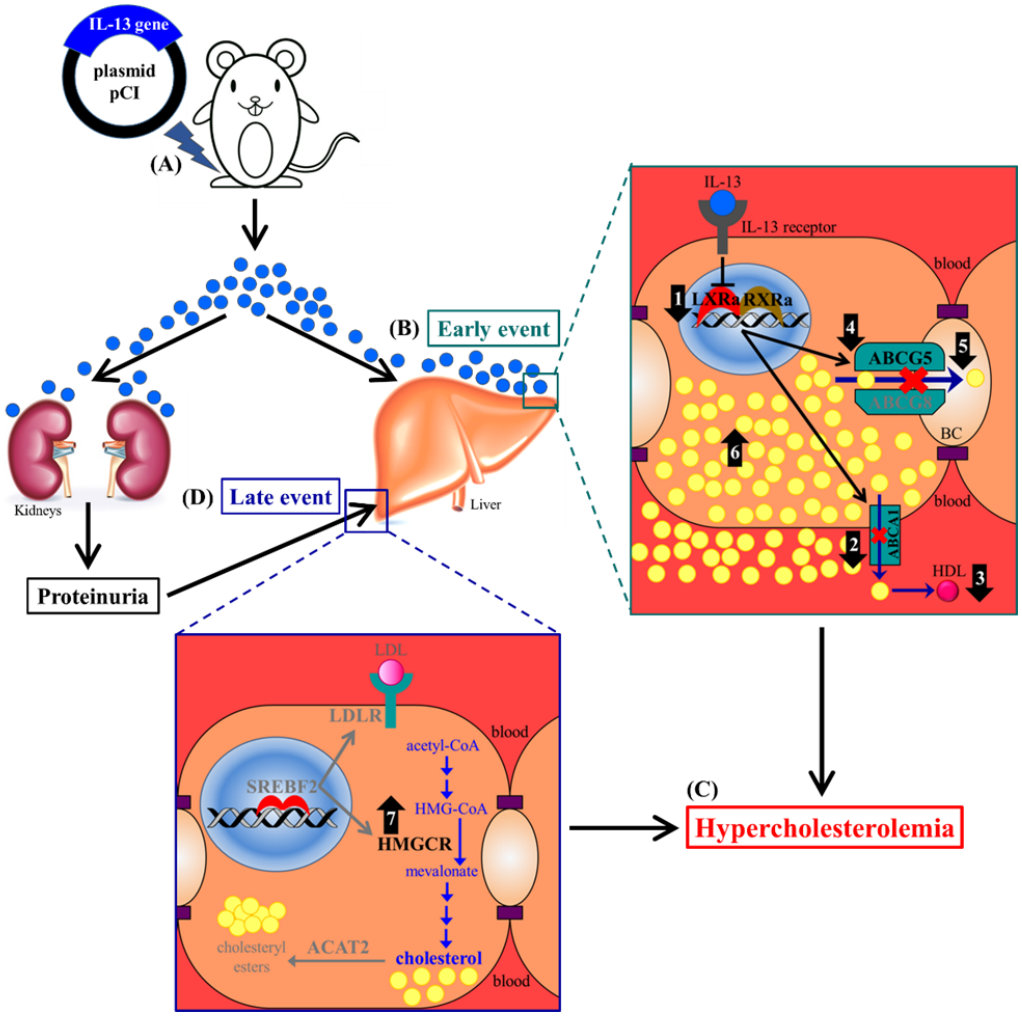

Figure 35: Proposed mechanism of hepatic cholesterol dysregulation in the IL-13-mediated hypercholesterolemia.

Plasma IL-13 was elevated upon *IL-13* transfection in the rat (A). In the early event (pre-proteinuric phase) (B), the increased circulatory IL-13 could act directly on the liver through IL-13 receptor binding, resulting in decreased *LXRa* expression (1), and the subsequent downregulation of its target genes ABCA1 (2) and ABCG5 (4). Reduction in ABCA1 decreases the amount of plasma HDL being synthesized (3). Decreased hepatic ABCG5 leads to reduced cholesterol efflux into bile canaliculi (BC) (5), and hence inefficient removal of excess cholesterols within the hepatocyte, bringing about an increased amount of intracellular free cholesterols (6). This could inhibit the further uptake of circulatory cholesterols into the liver for excretion, leading to the hypercholesterolemia as seen in our *IL-13* transfected rats (C). In the late event (D), the development of nephrotic range proteinuria resulted in the upregulation of *HMGCR* (7), and together with the continuous downregulation of ABCG5 (4), perpetuated the hypercholesterolemia seen in this disease (C).

6.2. Future directions

In order to prove that IL-13 has a direct downregulatory effect on LXRa, we will be performing antibody inhibitory experiments on the IL-13 receptor subunits in the cultured hepatocyte system, prior to incubation with IL-13. When IL-13 receptors are sufficiently blocked, IL-13 can no longer bind effectively to its receptors to trigger downstream signaling. The non-change in *LXRa* gene expression would prove the direct effect of IL-13 on *LXRa*.

To confirm the effect of IL-13 on the expression of genes regulated by LXRa, we will perform transfection studies in cultured hepatocytes using LXRa response element (LXRE)-luciferase vector construct. Since IL-13 downregulates *LXRa*, which in turn downregulates its target genes *ABCA1* and *ABCG5*, the activity of LXRE-linked luciferase should be significantly suppressed upon IL-13 stimulation, implying that IL-13 is able to suppress the expression of LXRE-regulated transcription in hepatocytes.

To determine whether the loss of LXRa is the sole factor responsible for the IL-13-mediated reduction in LXRE-driven gene transcription, we will cotransfect *LXRa* expression plasmid together with LXRE-linked luciferase plasmid construct in hepatocytes followed by IL-13 stimulation. Cotransfection experiment should show an increase in the LXRE-linked luciferase activity compared with hepatocytes transfected with only LXRE-linked luciferase plasmid construct in the presence of IL-13.

We could also overexpress *LXRa* in our *IL-13* gene overexpression rat model of MCNS and observe if *LXRa* overexpression could prevent the lipid abnormalities observed in our *IL-13* transfected rat model.

Upon establishing the molecular mechanism of IL-13-induced dysregulation of *LXRa* in the rat model of MCNS, validation of this pathway will also be carried out on human primary hepatocytes.

Although the regulation of cholesterol metabolism, such as production of endogenous cholesterol, mainly occurs in the liver, the intestine is also highly involved in regulating cholesterol metabolism. Intestinal cells also have very high expression levels of ABCG5/G8 (Lee et al., 2001), functioning to stimulate sterol secretion into the intestinal lumen for excretion. Transfection of *IL-13* in the rats could result not only in downregulation of ABCG5/G8 in the hepatocytes but also in the intestinal cells, and could conceivably result in increased uptake of dietary cholesterol into the circulation resulting in hypercholesterolemia. Therefore, we propose to conduct IL-13 stimulation experiments on human intestinal cell culture model system such as Caco-2 and HT-29, as well as primary human intestinal cells to investigate the expression of the *LXRa-ABCG5/ABCA1* pathway.

Finally to confirm that the free cholesterol secreted into the bile is indeed decreased after IL-13 transfection of the rats, we will also be measuring the bile content of the feces and compare this with the control rats.

Bibliography

1. Abbas, A.K., Murphy, K.M., Sher, A., 1996. Functional diversity of helper T lymphocytes. Nature 383, 787-793.
2. Adigun, M.O., Agbedana, E.O., Kadiri, S., Taylor, G.O., 1999. Increased high density lipoprotein cholesterol in adult nephrotic syndrome in Nigeria. African journal of medicine and medical sciences 28, 97-100.
3. Akaiwa, M., Yu, B., Umeshita-Suyama, R., Terada, N., Suto, H., Koga, T., Arima, K., Matsushita, S., Saito, H., Ogawa, H., Furue, M., Hamasaki, N., Ohshima, K., Izuhara, K., 2001. Localization of human interleukin 13 receptor in non-haematopoietic cells. Cytokine 13, 75-84.
4. al-Shurbaji, A., Humble, E., Rudling, M., Lindenthal, B., Berglund, L., 1998. Hepatic cholesterol metabolism in experimental nephrotic syndrome. Lipids 33, 165-169.
5. Alberti, S., Schuster, G., Parini, P., Feltkamp, D., Diczfalusy, U., Rudling, M., Angelin, B., Bjorkhem, I., Pettersson, S., Gustafsson, J.A., 2001. Hepatic cholesterol metabolism and resistance to dietary cholesterol in LXRbeta-deficient mice. The Journal of clinical investigation 107, 565-573.
6. Allain, C.C., Poon, L.S., Chan, C.S., Richmond, W., Fu, P.C., 1974. Enzymatic determination of total serum cholesterol. Clinical chemistry 20, 470-475.
7. Aoyagi, K., Shahrzad, S., Kuzure, Y., Koyama, A., Nakamura, K., Ienaga, K., 2000. The role of protein kinase C in the increased generation in isolated rat hepatocytes of the hydroxyl radical by puromycin aminonucleoside. Free radical research 32, 487-496.
8. Araya, C.E., Wasserfall, C.H., Brusko, T.M., Mu, W., Segal, M.S., Johnson, R.J., Garin, E.H., 2006. A case of unfulfilled expectations. Cytokines in idiopathic minimal lesion nephrotic syndrome. Pediatr Nephrol 21, 603-610.
9. Archibald, R.M., 1962. Reactions of creatinine with alkaline picrate. The Journal of biological chemistry 237, 612.
10. Back, S.S., Kim, J., Choi, D., Lee, E.S., Choi, S.Y., Han, K., 2013. Cooperative transcriptional activation of ATP-binding cassette sterol transporters ABCG5 and ABCG8 genes by nuclear receptors including Liver-X-Receptor. BMB reports 46, 322-327.
11. Berg, J.M., Tymoczko, J.L., Stryer, L., 2012. Biochemistry, 7th ed. W.H. Freeman, New York.
12. Berge, K.E., Tian, H., Graf, G.A., Yu, L., Grishin, N.V., Schultz, J., Kwiterovich, P., Shan, B., Barnes, R., Hobbs, H.H., 2000. Accumulation of dietary cholesterol in sitosterolemia caused by mutations in adjacent ABC transporters. Science 290, 1771-1775.

13. Bhattacharyya, A.K., Connor, W.E., 1974. Beta-sitosterolemia and xanthomatosis. A newly described lipid storage disease in two sisters. The Journal of clinical investigation 53, 1033-1043.
14. Bligh, E.G., Dyer, W.J., 1959. A rapid method of total lipid extraction and purification. Canadian journal of biochemistry and physiology 37, 911-917.
15. Brundert, M., Ewert, A., Heeren, J., Behrendt, B., Ramakrishnan, R., Greten, H., Merkel, M., Rinninger, F., 2005. Scavenger receptor class B type I mediates the selective uptake of high-density lipoprotein-associated cholesteryl ester by the liver in mice. Arteriosclerosis, thrombosis, and vascular biology 25, 143-148.
16. Brunham, L.R., Singaraja, R.R., Duong, M., Timmins, J.M., Fievet, C., Bissada, N., Kang, M.H., Samra, A., Fruchart, J.C., McManus, B., Staels, B., Parks, J.S., Hayden, M.R., 2009. Tissue-specific roles of ABCA1 influence susceptibility to atherosclerosis. Arteriosclerosis, thrombosis, and vascular biology 29, 548-554.
17. Cheung, W., Wei, C.L., Seah, C.C., Jordan, S.C., Yap, H.K., 2004. Atopy, serum IgE, and interleukin-13 in steroid-responsive nephrotic syndrome. Pediatr Nephrol 19, 627-632.
18. Chiang, J.Y., Kimmel, R., Stroup, D., 2001. Regulation of cholesterol 7alpha-hydroxylase gene (CYP7A1) transcription by the liver orphan receptor (LXRalpha). Gene 262, 257-265.
19. Cho, B.S., Yoon, S.R., Jang, J.Y., Pyun, K.H., Lee, C.E., 1999. Up-regulation of interleukin-4 and CD23/FcepsilonRII in minimal change nephrotic syndrome. Pediatr Nephrol 13, 199-204.
20. Chua, S.W., Vijayakumar, P., Nissom, P.M., Yam, C.Y., Wong, V.V., Yang, H., 2006. A novel normalization method for effective removal of systematic variation in microarray data. Nucleic acids research 34, e38.
21. Chugh, S.S., Clement, L.C., Mace, C., 2012. New insights into human minimal change disease: lessons from animal models. American journal of kidney diseases : the official journal of the National Kidney Foundation 59, 284-292.
22. Clement, L.C., Mace, C., Avila-Casado, C., Joles, J.A., Kersten, S., Chugh, S.S., 2014. Circulating angiopoietin-like 4 links proteinuria with hypertriglyceridemia in nephrotic syndrome. Nature medicine 20, 37-46.
23. Coleman, R., Roma, M.G., 2000. Hepatocyte couplets. Biochemical Society transactions 28, 136-140.
24. Crowther, J.R., 2001. The ELISA guidebook. Humana Press, Totowa, NJ.
25. Daines, M.O., Tabata, Y., Walker, B.A., Chen, W., Warrier, M.R., Basu, S., Hershey, G.K., 2006. Level of expression of IL-13R alpha 2 impacts receptor distribution and IL-13 signaling. J Immunol 176, 7495-7501.
26. David, M., Ford, D., Bertoglio, J., Maizel, A.L., Pierre, J., 2001. Induction of the IL-13 receptor alpha2-chain by IL-4 and IL-13 in human keratinocytes: involvement of STAT6, ERK and p38 MAPK pathways. Oncogene 20, 6660-6668.

27. Davies, R.W., Staprans, I., Hutchison, F.N., Kaysen, G.A., 1990. Proteinuria, not altered albumin metabolism, affects hyperlipidemia in the nephrotic rat. The Journal of clinical investigation 86, 600-605.
28. De Backer, G., Ambrosioni, E., Borch-Johnsen, K., Brotons, C., Cifkova, R., Dallongeville, J., Ebrahim, S., Faergeman, O., Graham, I., Mancia, G., Cats, V.M., Orth-Gomer, K., Perk, J., Pyorala, K., Rodicio, J.L., Sans, S., Sansoy, V., Sechtem, U., Silber, S., Thomsen, T., Wood, D., European Society of Cardiology Committee for Practice, G., 2003. European guidelines on cardiovascular disease prevention in clinical practice: third joint task force of European and other societies on cardiovascular disease prevention in clinical practice (constituted by representatives of eight societies and by invited experts). European journal of cardiovascular prevention and rehabilitation : official journal of the European Society of Cardiology, Working Groups on Epidemiology & Prevention and Cardiac Rehabilitation and Exercise Physiology 10, S1-S10.
29. Dennis, G., Jr., Sherman, B.T., Hosack, D.A., Yang, J., Gao, W., Lane, H.C., Lempicki, R.A., 2003. DAVID: Database for Annotation, Visualization, and Integrated Discovery. Genome biology 4, P3.
30. DK, D., Dnyanesh, S., Shenoy, V., 2014. A Study of Serum Lipids in Nephrotic Syndrome in Children. International Organization of Scientific Research 13, 1-6.
31. Eberle, D., Hegarty, B., Bossard, P., Ferre, P., Foufelle, F., 2004. SREBP transcription factors: master regulators of lipid homeostasis. Biochimie 86, 839-848.
32. European Association for Cardiovascular, P., Rehabilitation, Reiner, Z., Catapano, A.L., De Backer, G., Graham, I., Taskinen, M.R., Wiklund, O., Agewall, S., Alegria, E., Chapman, M.J., Durrington, P., Erdine, S., Halcox, J., Hobbs, R., Kjekshus, J., Filardi, P.P., Riccardi, G., Storey, R.F., Wood, D., Guidelines, E.S.C.C.f.P., Committees, 2011. ESC/EAS Guidelines for the management of dyslipidaemias: the Task Force for the management of dyslipidaemias of the European Society of Cardiology (ESC) and the European Atherosclerosis Society (EAS). European heart journal 32, 1769-1818.
33. Fiser, R.T., Arnold, W.C., Charlton, R.K., Steele, R.W., Childress, S.H., Shirkey, B., 1991. T-lymphocyte subsets in nephrotic syndrome. Kidney international 40, 913-916.
34. Fitzgerald, M.L., Mujawar, Z., Tamehiro, N., 2010. ABC transporters, atherosclerosis and inflammation. Atherosclerosis 211, 361-370.
35. Florido, J.F., Diaz Pena, J.M., Belchi, J., Estrada, J.L., Garcia Ara, M.C., Ojeda, J.A., 1992. Nephrotic syndrome and respiratory allergy in childhood. Journal of investigational allergology & clinical immunology 2, 136-140.
36. Fourcade, S., Ruiz, M., Camps, C., Schluter, A., Houten, S.M., Mooyer, P.A., Pampols, T., Dacremont, G., Wanders, R.J., Giros, M., Pujol, A., 2009. A key role for the peroxisomal ABCD2 transporter in fatty acid

homeostasis. American journal of physiology. Endocrinology and metabolism 296, E211-221.
37. Freeman, L.A., Kennedy, A., Wu, J., Bark, S., Remaley, A.T., Santamarina-Fojo, S., Brewer, H.B., Jr., 2004. The orphan nuclear receptor LRH-1 activates the ABCG5/ABCG8 intergenic promoter. Journal of lipid research 45, 1197-1206.
38. Friedewald, W.T., Levy, R.I., Fredrickson, D.S., 1972. Estimation of the concentration of low-density lipoprotein cholesterol in plasma, without use of the preparative ultracentrifuge. Clinical chemistry 18, 499-502.
39. Gai, J., Ji, M., Shi, C., Li, W., Chen, S., Wang, Y., Li, H., 2013. FoxO regulates expression of ABCA6, an intracellular ATP-binding-cassette transporter responsive to cholesterol. The international journal of biochemistry & cell biology 45, 2651-2659.
40. Garin, E.H., Boggs, K.P., 1987. Synergy of monocytes and lymphocytes from idiopathic minimal lesion nephrotic patients in relapse in the production of the supernatant factor that increases rat glomerular basement membrane sulfate uptake. The International journal of pediatric nephrology 8, 187-192.
41. Gbadegesin, R., Smoyer, W.E., 2008. CHAPTER 12 - Nephrotic Syndrome, in: Denis, F.G., Mb, Mrcp, Frcpc, Franz Schaefer, M.D. (Eds.), Comprehensive Pediatric Nephrology. Mosby, Philadelphia, pp. 205-218.
42. Gherardi, E., Rota, E., Calandra, S., Genova, R., Tamborino, A., 1977. Relationship among the concentrations of serum lipoproteins and changes in their chemical composition in patients with untreated nephrotic syndrome. European journal of clinical investigation 7, 563-570.
43. Gipson, D.S., Massengill, S.F., Yao, L., Nagaraj, S., Smoyer, W.E., Mahan, J.D., Wigfall, D., Miles, P., Powell, L., Lin, J.J., Trachtman, H., Greenbaum, L.A., 2009. Management of childhood onset nephrotic syndrome. Pediatrics 124, 747-757.
44. Graf, G.A., Yu, L., Li, W.P., Gerard, R., Tuma, P.L., Cohen, J.C., Hobbs, H.H., 2003. ABCG5 and ABCG8 are obligate heterodimers for protein trafficking and biliary cholesterol excretion. The Journal of biological chemistry 278, 48275-48282.
45. Han, S., Vaziri, N.D., Gollapudi, P., Kwok, V., Moradi, H., 2013. Hepatic fatty acid and cholesterol metabolism in nephrotic syndrome. American journal of translational research 5, 246-253.
46. Hebenstreit, D., Wirnsberger, G., Horejs-Hoeck, J., Duschl, A., 2006. Signaling mechanisms, interaction partners, and target genes of STAT6. Cytokine & growth factor reviews 17, 173-188.
47. Hershey, G.K., 2003. IL-13 receptors and signaling pathways: an evolving web. The Journal of allergy and clinical immunology 111, 677-690; quiz 691.
48. Holland, I.B., Blight, M.A., 1999. ABC-ATPases, adaptable energy generators fuelling transmembrane movement of a variety of molecules in organisms from bacteria to humans. Journal of molecular biology 293, 381-399.

49. Hu, P., Qin, Y.H., Lu, L., Hu, B., Jing, C.X., Lei, F.Y., Li, M.F., 2010. Genetic variation of apolipoprotein E does not contribute to the lipid abnormalities secondary to childhood minimal change nephrotic syndrome. International urology and nephrology 42, 453-460.
50. Huang da, W., Sherman, B.T., Lempicki, R.A., 2009. Systematic and integrative analysis of large gene lists using DAVID bioinformatics resources. Nature protocols 4, 44-57.
51. Ingulli, E., Tejani, A., 1991. Racial differences in the incidence and renal outcome of idiopathic focal segmental glomerulosclerosis in children. Pediatr Nephrol 5, 393-397.
52. ISKDC, 1978. Nephrotic syndrome in children: prediction of histopathology from clinical and laboratory characteristics at time of diagnosis. A report of the International Study of Kidney Disease in Children. Kidney international 13, 159-165.
53. Izawa, S., Okada, M., Matsui, H., Horita, Y., 1997. A new direct method for measuring HDL-cholesterol which does not produce any biased results. J. Medicine and Pharmaceutical Science 37, p1385-1388.
54. Jacobs, N.J., Vandemark, P.J., 1960. The purification and properties of the alpha-glycerophosphate-oxidizing enzyme of Streptococcus faecalis 10C1. Archives of biochemistry and biophysics 88, 250-255.
55. Johansson, A.C., Samuelsson, O., Attman, P.O., Haraldsson, B., Moberly, J., Knight-Gibson, C., Alaupovic, P., 2000. Dyslipidemia in peritoneal dialysis--relation to dialytic variables. Peritoneal dialysis international : journal of the International Society for Peritoneal Dialysis 20, 306-314.
56. Johnson, B.J., Lee, J.Y., Pickert, A., Urbatsch, I.L., 2010. Bile acids stimulate ATP hydrolysis in the purified cholesterol transporter ABCG5/G8. Biochemistry 49, 3403-3411.
57. Jones, A.L., Ruderman, N.B., Herrera, M.G., 1967. Electron microscopic and biochemical study of lipoprotein synthesis in the isolated perfused rat liver. Journal of lipid research 8, 429-446.
58. Kapp, U., Yeh, W.C., Patterson, B., Elia, A.J., Kagi, D., Ho, A., Hessel, A., Tipsword, M., Williams, A., Mirtsos, C., Itie, A., Moyle, M., Mak, T.W., 1999. Interleukin 13 is secreted by and stimulates the growth of Hodgkin and Reed-Sternberg cells. The Journal of experimental medicine 189, 1939-1946.
59. Kaysen, G.A., 1991. Hyperlipidemia of the nephrotic syndrome. Kidney international. Supplement 31, S8-15.
60. Kaysen, G.A., de Sain-van der Velden, M.G., 1999. New insights into lipid metabolism in the nephrotic syndrome. Kidney international. Supplement 71, S18-21.
61. Kaysen, G.A., Hoye, E., Jones, H., Jr., 1995. Apolipoprotein AI levels are increased in part as a consequence of reduced catabolism in nephrotic rats. The American journal of physiology 268, F532-540.
62. Keane, W.F., Kasiske, B.L., O'Donnell, M.P., Kim, Y., 1991. The role of altered lipid metabolism in the progression of renal disease: experimental

evidence. American journal of kidney diseases : the official journal of the National Kidney Foundation 17, 38-42.
63. Kim, C.H., Kim, H.J., Mitsuhashi, M., Vaziri, N.D., 2007. Hepatic tissue sterol regulatory element binding protein 2 and low-density lipoprotein receptor in nephrotic syndrome. Metabolism: clinical and experimental 56, 1377-1382.
64. Kim, J., Yoon, H., Ramirez, C.M., Lee, S.M., Hoe, H.S., Fernandez-Hernando, C., Kim, J., 2012. MiR-106b impairs cholesterol efflux and increases Abeta levels by repressing ABCA1 expression. Experimental neurology 235, 476-483.
65. Kimata, H., Fujimoto, M., Furusho, K., 1995. Involvement of interleukin (IL)-13, but not IL-4, in spontaneous IgE and IgG4 production in nephrotic syndrome. European journal of immunology 25, 1497-1501.
66. Klett, E.L., Lee, M.H., Adams, D.B., Chavin, K.D., Patel, S.B., 2004. Localization of ABCG5 and ABCG8 proteins in human liver, gall bladder and intestine. BMC gastroenterology 4, 21.
67. Koditschek, L.K., Umbreit, W.W., 1969. Alpha-glycerophosphate oxidase in Streptococcus faecium F 24. Journal of bacteriology 98, 1063-1068.
68. Kong, X., Yuan, H., Fan, J., Li, Z., Wu, T., Jiang, L., 2013. Lipid-lowering agents for nephrotic syndrome. Cochrane Database Syst Rev 12, CD005425.
69. Koskimies, O., Vilska, J., Rapola, J., Hallman, N., 1982. Long-term outcome of primary nephrotic syndrome. Archives of disease in childhood 57, 544-548.
70. Kovacs, A.L., Molnar, K., Seglen, P.O., 1981. Inhibition of autophagic sequestration and endogenous protein degradation in isolated rat hepatocytes by methylated adenosine derivatives. FEBS letters 134, 194-196.
71. Koyama, A., Fujisaki, M., Kobayashi, M., Igarashi, M., Narita, M., 1991. A glomerular permeability factor produced by human T cell hybridomas. Kidney international 40, 453-460.
72. Kozarsky, K.F., Donahee, M.H., Rigotti, A., Iqbal, S.N., Edelman, E.R., Krieger, M., 1997. Overexpression of the HDL receptor SR-BI alters plasma HDL and bile cholesterol levels. Nature 387, 414-417.
73. Kuwabara, P.E., Labouesse, M., 2002. The sterol-sensing domain: multiple families, a unique role? Trends in genetics : TIG 18, 193-201.
74. Lai, K.W., Wei, C.L., Tan, L.K., Tan, P.H., Chiang, G.S., Lee, C.G., Jordan, S.C., Yap, H.K., 2007. Overexpression of interleukin-13 induces minimal-change-like nephropathy in rats. Journal of the American Society of Nephrology : JASN 18, 1476-1485.
75. Lee, J.Y., Parks, J.S., 2005. ATP-binding cassette transporter AI and its role in HDL formation. Current opinion in lipidology 16, 19-25.
76. Lee, M.H., Lu, K., Hazard, S., Yu, H., Shulenin, S., Hidaka, H., Kojima, H., Allikmets, R., Sakuma, N., Pegoraro, R., Srivastava, A.K., Salen, G., Dean, M., Patel, S.B., 2001. Identification of a gene, ABCG5, important in the regulation of dietary cholesterol absorption. Nature genetics 27, 79-83.

77. Lehmann, J.M., Kliewer, S.A., Moore, L.B., Smith-Oliver, T.A., Oliver, B.B., Su, J.L., Sundseth, S.S., Winegar, D.A., Blanchard, D.E., Spencer, T.A., Willson, T.M., 1997. Activation of the nuclear receptor LXR by oxysterols defines a new hormone response pathway. The Journal of biological chemistry 272, 3137-3140.
78. Li, H., Zhao, Y., Zhou, S., Heng, C.K., 2010. Serum amyloid A activates peroxisome proliferator-activated receptor gamma through extracellularly regulated kinase 1/2 and COX-2 expression in hepatocytes. Biochemistry 49, 9508-9517.
79. Liang, K., Vaziri, N.D., 1999. Down-regulation of hepatic high-density lipoprotein receptor, SR-B1, in nephrotic syndrome. Kidney international 56, 621-626.
80. Liang, K., Vaziri, N.D., 2003. HMG-CoA reductase, cholesterol 7alpha-hydroxylase, LCAT, ACAT, LDL receptor, and SRB-1 in hereditary analbuminemia. Kidney international 64, 192-198.
81. Liang, K.H., Oveisi, F., Vaziri, N.D., 1996. Gene expression of hepatic cholesterol 7 alpha-hydroxylase in the course of puromycin-induced nephrosis. Kidney international 49, 855-860.
82. Lin, C.Y., Lee, B.H., Lin, C.C., Chen, W.P., 1990. A study of the relationship between childhood nephrotic syndrome and allergic diseases. Chest 97, 1408-1411.
83. Lombel, R.M., Gipson, D.S., Hodson, E.M., 2013. Treatment of steroid-sensitive nephrotic syndrome: new guidelines from KDIGO. Pediatr Nephrol 28, 415-426.
84. Low, H., Hoang, A., Sviridov, D., 2012. Cholesterol efflux assay. Journal of visualized experiments : JoVE, e3810.
85. Lowry, O.H., Rosebrough, N.J., Farr, A.L., Randall, R.J., 1951. Protein measurement with the Folin phenol reagent. The Journal of biological chemistry 193, 265-275.
86. Lu, K., Lee, M.H., Hazard, S., Brooks-Wilson, A., Hidaka, H., Kojima, H., Ose, L., Stalenhoef, A.F., Mietinnen, T., Bjorkhem, I., Bruckert, E., Pandya, A., Brewer, H.B., Jr., Salen, G., Dean, M., Srivastava, A., Patel, S.B., 2001. Two genes that map to the STSL locus cause sitosterolemia: genomic structure and spectrum of mutations involving sterolin-1 and sterolin-2, encoded by ABCG5 and ABCG8, respectively. American journal of human genetics 69, 278-290.
87. Ma, A.Z., Song, Z.Y., Zhang, Q., 2014. Cholesterol efflux is LXRalpha isoform-dependent in human macrophages. BMC cardiovascular disorders 14, 80.
88. Marsh, J.B., Drabkin, D.L., 1960. Experimental reconstruction of metabolic pattern of lipid nephrosis: key role of hepatic protein synthesis in hyperlipemia. Metabolism: clinical and experimental 9, 946-955.
89. Marshall, J.F., Apostolopoulos, J.J., Brack, C.M., Howlett, G.J., 1990. Regulation of apolipoprotein gene expression and plasma high-density lipoprotein composition in experimental nephrosis. Biochimica et biophysica acta 1042, 271-279.

90. Mathieson, P.W., 2003. Immune dysregulation in minimal change nephropathy. Nephrology, dialysis, transplantation : official publication of the European Dialysis and Transplant Association - European Renal Association 18 Suppl 6, vi26-29.
91. Mathieson, P.W., 2007. Minimal change nephropathy and focal segmental glomerulosclerosis. Seminars in immunopathology 29, 415-426.
92. Merouani, A., Levy, E., Mongeau, J.G., Robitaille, P., Lambert, M., Delvin, E.E., 2003. Hyperlipidemic profiles during remission in childhood idiopathic nephrotic syndrome. Clinical biochemistry 36, 571-574.
93. Michaeli, J., Bar-On, H., Shafrir, E., 1981. Lipoprotein profiles in a heterogeneous group of patients with nephrotic syndrome. Israel journal of medical sciences 17, 1001-1008.
94. Miettinen, T.A., 1980. Phytosterolaemia, xanthomatosis and premature atherosclerotic arterial disease: a case with high plant sterol absorption, impaired sterol elimination and low cholesterol synthesis. European journal of clinical investigation 10, 27-35.
95. Moorhead, J.F., Chan, M.K., El-Nahas, M., Varghese, Z., 1982. Lipid nephrotoxicity in chronic progressive glomerular and tubulo-interstitial disease. Lancet 2, 1309-1311.
96. Mundel, P., Reiser, J., 2010. Proteinuria: an enzymatic disease of the podocyte? Kidney international 77, 571-580.
97. Mundel, P., Shankland, S.J., 2002. Podocyte biology and response to injury. Journal of the American Society of Nephrology : JASN 13, 3005-3015.
98. Nakayama, M., Katafuchi, R., Yanase, T., Ikeda, K., Tanaka, H., Fujimi, S., 2002. Steroid responsiveness and frequency of relapse in adult-onset minimal change nephrotic syndrome. American journal of kidney diseases : the official journal of the National Kidney Foundation 39, 503-512.
99. Niaudet, P., 2004. Chapter 27 Steroid-Sensitive Idiopathic Nephrotic Syndrome in Children, 5th ed. Lippincott Williams & Wilkins, Philadelphia.
100. Niaudet, P., Boyer, O., 2009. Idiopathic Nephrotic Syndrome in Children: Clinical Aspects, in: Avner, E., Harmon, W., Niaudet, P., Yoshikawa, N. (Eds.), Pediatric Nephrology. Springer Berlin Heidelberg, pp. 667-702.
101. Oelkers, P., Behari, A., Cromley, D., Billheimer, J.T., Sturley, S.L., 1998. Characterization of two human genes encoding acyl coenzyme A:cholesterol acyltransferase-related enzymes. The Journal of biological chemistry 273, 26765-26771.
102. Oetliker, O.H., Mordasini, R., Lutschg, J., Riesen, W., 1980. Lipoprotein metabolism in nephrotic syndrome in childhood. Pediatric research 14, 64-66.
103. Ordonez, J.D., Hiatt, R.A., Killebrew, E.J., Fireman, B.H., 1993. The increased risk of coronary heart disease associated with nephrotic syndrome. Kidney international 44, 638-642.
104. Pahl, M.V., Oveisi, F., Khamiseh, G., Vaziri, N.D., 1998. Intestinal absorption and biliary secretion of cholesterol in rats with nephrotic

syndrome. Nephrology, dialysis, transplantation : official publication of the European Dialysis and Transplant Association - European Renal Association 13, 1446-1451.
105. Peet, D.J., Turley, S.D., Ma, W., Janowski, B.A., Lobaccaro, J.M., Hammer, R.E., Mangelsdorf, D.J., 1998. Cholesterol and bile acid metabolism are impaired in mice lacking the nuclear oxysterol receptor LXR alpha. Cell 93, 693-704.
106. Pruitt, K.D., Tatusova, T., Maglott, D.R., 2007. NCBI reference sequences (RefSeq): a curated non-redundant sequence database of genomes, transcripts and proteins. Nucleic acids research 35, D61-65.
107. Querfeld, U., 1999. Should hyperlipidemia in children with the nephrotic syndrome be treated? Pediatr Nephrol 13, 77-84.
108. Querfeld, U., Gnasso, A., Haberbosch, W., Augustin, J., Scharer, K., 1988. Lipoprotein profiles at different stages of the nephrotic syndrome. European journal of pediatrics 147, 233-238.
109. Remaley, A.T., Bark, S., Walts, A.D., Freeman, L., Shulenin, S., Annilo, T., Elgin, E., Rhodes, H.E., Joyce, C., Dean, M., Santamarina-Fojo, S., Brewer, H.B., Jr., 2002. Comparative genome analysis of potential regulatory elements in the ABCG5-ABCG8 gene cluster. Biochemical and biophysical research communications 295, 276-282.
110. Repa, J.J., Berge, K.E., Pomajzl, C., Richardson, J.A., Hobbs, H., Mangelsdorf, D.J., 2002. Regulation of ATP-binding cassette sterol transporters ABCG5 and ABCG8 by the liver X receptors alpha and beta. The Journal of biological chemistry 277, 18793-18800.
111. Repa, J.J., Mangelsdorf, D.J., 2000. The role of orphan nuclear receptors in the regulation of cholesterol homeostasis. Annual review of cell and developmental biology 16, 459-481.
112. Robinet, P., Wang, Z., Hazen, S.L., Smith, J.D., 2010. A simple and sensitive enzymatic method for cholesterol quantification in macrophages and foam cells. Journal of lipid research 51, 3364-3369.
113. Ruan, X.Z., Moorhead, J.F., Fernando, R., Wheeler, D.C., Powis, S.H., Varghese, Z., 2004. Regulation of lipoprotein trafficking in the kidney: role of inflammatory mediators and transcription factors. Biochemical Society transactions 32, 88-91.
114. Ryan, G.B., Karnovsky, M.J., 1975. An ultrastructural study of the mechanisms of proteinuria in aminonucleoside nephrosis. Kidney international 8, 219-232.
115. Sahali, D., Pawlak, A., Le Gouvello, S., Lang, P., Valanciute, A., Remy, P., Loirat, C., Niaudet, P., Bensman, A., Guellaen, G., 2001. Transcriptional and post-transcriptional alterations of IkappaBalpha in active minimal-change nephrotic syndrome. Journal of the American Society of Nephrology : JASN 12, 1648-1658.
116. Sahali, D., Pawlak, A., Valanciute, A., Grimbert, P., Lang, P., Remy, P., Bensman, A., Guellaen, G., 2002. A novel approach to investigation of the pathogenesis of active minimal-change nephrotic syndrome using

subtracted cDNA library screening. Journal of the American Society of Nephrology : JASN 13, 1238-1247.
117. Salen, G., Shore, V., Tint, G.S., Forte, T., Shefer, S., Horak, I., Horak, E., Dayal, B., Nguyen, L., Batta, A.K., et al., 1989. Increased sitosterol absorption, decreased removal, and expanded body pools compensate for reduced cholesterol synthesis in sitosterolemia with xanthomatosis. Journal of lipid research 30, 1319-1330.
118. Schultz, J.R., Tu, H., Luk, A., Repa, J.J., Medina, J.C., Li, L., Schwendner, S., Wang, S., Thoolen, M., Mangelsdorf, D.J., Lustig, K.D., Shan, B., 2000. Role of LXRs in control of lipogenesis. Genes & development 14, 2831-2838.
119. Schwartz, K., Lawn, R.M., Wade, D.P., 2000. ABC1 gene expression and ApoA-I-mediated cholesterol efflux are regulated by LXR. Biochemical and biophysical research communications 274, 794-802.
120. Seglen, P.O., 1976. Preparation of isolated rat liver cells. Methods in cell biology 13, 29-83.
121. Shalhoub, R.J., 1974. Pathogenesis of lipoid nephrosis: a disorder of T-cell function. Lancet 2, 556-560.
122. Sharples, P.M., Poulton, J., White, R.H., 1985. Steroid responsive nephrotic syndrome is more common in Asians. Archives of disease in childhood 60, 1014-1017.
123. Shefer, S., Hauser, S., Bekersky, I., Mosbach, E.H., 1970. Biochemical site of regulation of bile acid biosynthesis in the rat. Journal of lipid research 11, 404-411.
124. Shui, G., Cheong, W.F., Jappar, I.A., Hoi, A., Xue, Y., Fernandis, A.Z., Tan, B.K., Wenk, M.R., 2011. Derivatization-independent cholesterol analysis in crude lipid extracts by liquid chromatography/mass spectrometry: applications to a rabbit model for atherosclerosis. Journal of chromatography. A 1218, 4357-4365.
125. Skinnider, B.F., Elia, A.J., Gascoyne, R.D., Trumper, L.H., von Bonin, F., Kapp, U., Patterson, B., Snow, B.E., Mak, T.W., 2001. Interleukin 13 and interleukin 13 receptor are frequently expressed by Hodgkin and Reed-Sternberg cells of Hodgkin lymphoma. Blood 97, 250-255.
126. Skinnider, B.F., Kapp, U., Mak, T.W., 2002. The role of interleukin 13 in classical Hodgkin lymphoma. Leukemia & lymphoma 43, 1203-1210.
127. Srivastava, T., Simon, S.D., Alon, U.S., 1999. High incidence of focal segmental glomerulosclerosis in nephrotic syndrome of childhood. Pediatr Nephrol 13, 13-18.
128. Stanya, K.J., Jacobi, D., Liu, S., Bhargava, P., Dai, L., Gangl, M.R., Inouye, K., Barlow, J.L., Ji, Y., Mizgerd, J.P., Qi, L., Shi, H., McKenzie, A.N., Lee, C.H., 2013. Direct control of hepatic glucose production by interleukin-13 in mice. The Journal of clinical investigation 123, 261-271.
129. Staprans, I., Anderson, C.D., Lurz, F.W., Felts, J.M., 1980. Separation of a lipoprotein lipase cofactor from the alpha 1-acid glycoprotein fraction from the urine of nephrotic patients. Biochimica et biophysica acta 617, 514-523.

130. Staprans, I., Felts, J.M., Couser, W.G., 1987. Glycosaminoglycans and chylomicron metabolism in control and nephrotic rats. Metabolism: clinical and experimental 36, 496-501.
131. Stefanovic, V., Golubovic, E., Mitic-Zlatkovic, M., Vlahovic, P., Jovanovic, O., Bogdanovic, R., 1998. Interleukin-12 and interferon-gamma production in childhood idiopathic nephrotic syndrome. Pediatr Nephrol 12, 463-466.
132. Strauss, J., Zilleruelo, G., Freundlich, M., Abitol, C., 1987. Less commonly recognized features of childhood nephrotic syndrome. Pediatric clinics of North America 34, 591-607.
133. Sumi, K., Tanaka, T., Uchida, A., Magoori, K., Urashima, Y., Ohashi, R., Ohguchi, H., Okamura, M., Kudo, H., Daigo, K., Maejima, T., Kojima, N., Sakakibara, I., Jiang, S., Hasegawa, G., Kim, I., Osborne, T.F., Naito, M., Gonzalez, F.J., Hamakubo, T., Kodama, T., Sakai, J., 2007. Cooperative interaction between hepatocyte nuclear factor 4 alpha and GATA transcription factors regulates ATP-binding cassette sterol transporters ABCG5 and ABCG8. Molecular and cellular biology 27, 4248-4260.
134. Tachibana, S., Hirano, M., Hirata, T., Matsuo, M., Ikeda, I., Ueda, K., Sato, R., 2007. Cholesterol and plant sterol efflux from cultured intestinal epithelial cells is mediated by ATP-binding cassette transporters. Bioscience, biotechnology, and biochemistry 71, 1886-1895.
135. Tanaka, R., Yoshikawa, N., Nakamura, H., Ito, H., 1992. Infusion of peripheral blood mononuclear cell products from nephrotic children increases albuminuria in rats. Nephron 60, 35-41.
136. Teboul, M., Enmark, E., Li, Q., Wikstrom, A.C., Pelto-Huikko, M., Gustafsson, J.A., 1995. OR-1, a member of the nuclear receptor superfamily that interacts with the 9-cis-retinoic acid receptor. Proceedings of the National Academy of Sciences of the United States of America 92, 2096-2100.
137. Thabet, M.A., Challa, A., Chan, J.C., Pandak, W.M., Heuman, D.M., Vlahcevic, Z.R., 1993a. Studies of alteration of hepatic cholesterol metabolism in puromycin-induced nephrotic syndrome in rats. Kidney international 44, 789-794.
138. Thabet, M.A., Salcedo, J.R., Chan, J.C., 1993b. Hyperlipidemia in childhood nephrotic syndrome. Pediatr Nephrol 7, 559-566.
139. Tietz, N.W., Finley, P.R., Pruden, E., Amerson, A.B., 1990. Clinical guide to laboratory tests, 2nd ed. Saunders, Philadelphia.
140. Tremblay, A.J., Morrissette, H., Gagne, J.M., Bergeron, J., Gagne, C., Couture, P., 2004. Validation of the Friedewald formula for the determination of low-density lipoprotein cholesterol compared with beta-quantification in a large population. Clinical biochemistry 37, 785-790.
141. Treyer, A., Musch, A., 2013. Hepatocyte polarity. Comprehensive Physiology 3, 243-287.
142. Trinder, P., 1969. Annals of clinical biochemistry 6, 24-27.

143. Tsukahara, H., Haruki, S., Hiraoka, M., Hori, C., Sudo, M., 1997. Persistent hypercholesterolaemia in frequently relapsing steroid-responsive nephrotic syndrome. Journal of paediatrics and child health 33, 253-255.
144. Tuschl, G., Hrach, J., Walter, Y., Hewitt, P.G., Mueller, S.O., 2009. Serum-free collagen sandwich cultures of adult rat hepatocytes maintain liver-like properties long term: a valuable model for in vitro toxicity and drug-drug interaction studies. Chemico-biological interactions 181, 124-137.
145. Vaziri, N.D., 2003. Molecular mechanisms of lipid disorders in nephrotic syndrome. Kidney international 63, 1964-1976.
146. Vaziri, N.D., Gollapudi, P., Han, S., Farahmand, G., Yuan, J., Rahimi, A., Moradi, H., 2011. Nephrotic syndrome causes upregulation of HDL endocytic receptor and PDZK-1-dependent downregulation of HDL docking receptor. Nephrology, dialysis, transplantation : official publication of the European Dialysis and Transplant Association - European Renal Association 26, 3118-3123.
147. Vaziri, N.D., Liang, K., 2002. Up-regulation of acyl-coenzyme A:cholesterol acyltransferase (ACAT) in nephrotic syndrome. Kidney international 61, 1769-1775.
148. Vaziri, N.D., Liang, K., Parks, J.S., 2001. Acquired lecithin-cholesterol acyltransferase deficiency in nephrotic syndrome. American journal of physiology. Renal physiology 280, F823-828.
149. Vaziri, N.D., Liang, K.H., 1995. Hepatic HMG-CoA reductase gene expression during the course of puromycin-induced nephrosis. Kidney international 48, 1979-1985.
150. Vaziri, N.D., Liang, K.H., 1996. Down-regulation of hepatic LDL receptor expression in experimental nephrosis. Kidney international 50, 887-893.
151. Vernier, R.L., Papermaster, B.W., Good, R.A., 1959. Aminonucleoside nephrosis. I. Electron microscopic study of the renal lesion in rats. The Journal of experimental medicine 109, 115-126.
152. Voet, D., Voet, J.G., 2011. Biochemistry, 4th ed. John Wiley & Sons, Hoboken, NJ.
153. Vrins, C., Vink, E., Vandenberghe, K.E., Frijters, R., Seppen, J., Groen, A.K., 2007. The sterol transporting heterodimer ABCG5/ABCG8 requires bile salts to mediate cholesterol efflux. FEBS letters 581, 4616-4620.
154. Wang, N., Silver, D.L., Costet, P., Tall, A.R., 2000. Specific binding of ApoA-I, enhanced cholesterol efflux, and altered plasma membrane morphology in cells expressing ABC1. The Journal of biological chemistry 275, 33053-33058.
155. Wang, Y., Moser, A.H., Shigenaga, J.K., Grunfeld, C., Feingold, K.R., 2005. Downregulation of liver X receptor-alpha in mouse kidney and HK-2 proximal tubular cells by LPS and cytokines. Journal of lipid research 46, 2377-2387.

156. Warwick, G.L., Caslake, M.J., Boulton-Jones, J.M., Dagen, M., Packard, C.J., Shepherd, J., 1990. Low-density lipoprotein metabolism in the nephrotic syndrome. Metabolism: clinical and experimental 39, 187-192.
157. Warwick, G.L., Packard, C.J., Demant, T., Bedford, D.K., Boulton-Jones, J.M., Shepherd, J., 1991. Metabolism of apolipoprotein B-containing lipoproteins in subjects with nephrotic-range proteinuria. Kidney international 40, 129-138.
158. Wei, C.L., Cheung, W., Heng, C.K., Arty, N., Chong, S.S., Lee, B.W., Puah, K.L., Yap, H.K., 2005. Interleukin-13 genetic polymorphisms in Singapore Chinese children correlate with long-term outcome of minimal-change disease. Nephrology, dialysis, transplantation : official publication of the European Dialysis and Transplant Association - European Renal Association 20, 728-734.
159. Westerterp, M., Bochem, A.E., Yvan-Charvet, L., Murphy, A.J., Wang, N., Tall, A.R., 2014. ATP-binding cassette transporters, atherosclerosis, and inflammation. Circulation research 114, 157-170.
160. Willy, P.J., Umesono, K., Ong, E.S., Evans, R.M., Heyman, R.A., Mangelsdorf, D.J., 1995. LXR, a nuclear receptor that defines a distinct retinoid response pathway. Genes & development 9, 1033-1045.
161. Wittig, H.J., Goldman, A.S., 1970. Nephrotic syndrome associated with inhaled allergens. Lancet 1, 542-543.
162. Woo, K.T., Chan, C.M., Mooi, C.Y., H., L.C., Tan, H.K., Foo, M., Lee, G.S., Anantharaman, V., Lim, C.H., Tan, C.C., Lee, E.J., Chiang, G.S., Tan, P.H., Boon, T.H., Fook-Chong, S., Wong, K.S., 2010. The changing pattern of primary glomerulonephritis in Singapore and other countries over the past 3 decades. Clinical nephrology 74, 372-383.
163. Wu, J.E., Basso, F., Shamburek, R.D., Amar, M.J., Vaisman, B., Szakacs, G., Joyce, C., Tansey, T., Freeman, L., Paigen, B.J., Thomas, F., Brewer, H.B., Jr., Santamarina-Fojo, S., 2004. Hepatic ABCG5 and ABCG8 overexpression increases hepatobiliary sterol transport but does not alter aortic atherosclerosis in transgenic mice. The Journal of biological chemistry 279, 22913-22925.
164. Yan, K., Nakahara, K., Awa, S., Nishibori, Y., Nakajima, N., Kataoka, S., Maeda, M., Watanabe, T., Matsushima, S., Watanabe, N., 1998. The increase of memory T cell subsets in children with idiopathic nephrotic syndrome. Nephron 79, 274-278.
165. Yap, H.K., Cheung, W., Murugasu, B., Sim, S.K., Seah, C.C., Jordan, S.C., 1999. Th1 and Th2 cytokine mRNA profiles in childhood nephrotic syndrome: evidence for increased IL-13 mRNA expression in relapse. Journal of the American Society of Nephrology : JASN 10, 529-537.
166. Yap, H.K., Chia, K.S., Murugasu, B., Saw, A.H., Tay, J.S., Ikshuvanam, M., Tan, K.W., Cheng, H.K., Tan, C.L., Lim, C.H., 1990. Acute glomerulonephritis--changing patterns in Singapore children. Pediatr Nephrol 4, 482-484.
167. Yap, H.K., Murugasu, B., Saw, A.H., Chiang, G.S., Tay, J.S., Wong, H.B., Tan, C.L., Lim, C.H., 1989. Pattern of glomerulonephritis in Singapore

children--a renal biopsy perspective. Annals of the Academy of Medicine, Singapore 18, 35-39.
168. Yap, H.K., Yip, W.C., Lee, B.W., Ho, T.F., Teo, J., Aw, S.E., Tay, J.S., 1983. The incidence of atopy in steroid-responsive nephrotic syndrome: clinical and immunological parameters. Annals of allergy 51, 590-594.
169. Yokoyama, H., Kida, H., Abe, T., Koshino, Y., Yoshimura, M., Hattori, N., 1987. Impaired immunoglobulin G production in minimal change nephrotic syndrome in adults. Clinical and experimental immunology 70, 110-115.
170. Yu, L., Gupta, S., Xu, F., Liverman, A.D., Moschetta, A., Mangelsdorf, D.J., Repa, J.J., Hobbs, H.H., Cohen, J.C., 2005. Expression of ABCG5 and ABCG8 is required for regulation of biliary cholesterol secretion. The Journal of biological chemistry 280, 8742-8747.
171. Yu, L., Hammer, R.E., Li-Hawkins, J., Von Bergmann, K., Lutjohann, D., Cohen, J.C., Hobbs, H.H., 2002a. Disruption of Abcg5 and Abcg8 in mice reveals their crucial role in biliary cholesterol secretion. Proceedings of the National Academy of Sciences of the United States of America 99, 16237-16242.
172. Yu, L., Li-Hawkins, J., Hammer, R.E., Berge, K.E., Horton, J.D., Cohen, J.C., Hobbs, H.H., 2002b. Overexpression of ABCG5 and ABCG8 promotes biliary cholesterol secretion and reduces fractional absorption of dietary cholesterol. The Journal of clinical investigation 110, 671-680.
173. Yu, L., von Bergmann, K., Lutjohann, D., Hobbs, H.H., Cohen, J.C., 2004. Selective sterol accumulation in ABCG5/ABCG8-deficient mice. Journal of lipid research 45, 301-307.
174. Yu, L., York, J., von Bergmann, K., Lutjohann, D., Cohen, J.C., Hobbs, H.H., 2003. Stimulation of cholesterol excretion by the liver X receptor agonist requires ATP-binding cassette transporters G5 and G8. The Journal of biological chemistry 278, 15565-15570.
175. Zhou, Y., Zhang, X., Chen, L., Wu, J., Dang, H., Wei, M., Fan, Y., Zhang, Y., Zhu, Y., Wang, N., Breyer, M.D., Guan, Y., 2008. Expression profiling of hepatic genes associated with lipid metabolism in nephrotic rats. American journal of physiology. Renal physiology 295, F662-671.
176. Zilleruelo, G., Hsia, S.L., Freundlich, M., Gorman, H.M., Strauss, J., 1984. Persistence of serum lipid abnormalities in children with idiopathic nephrotic syndrome. The Journal of pediatrics 104, 61-64.

Appendices

Appendix 2.1: Protocol for rat urine albumin ELISA

Preparation of reagents

- 0.1M sodium carbonate buffer, pH 9.6

0.2M sodium carbonate (Na_2CO_3)	8ml
0.2M sodium bicarbonate ($NaHCO_3$)	17ml
ddH_2O	25ml

- 0.2M sodium carbonate (Na_2CO_3)

Sodium carbonate (Na_2CO_3)	21.2g
ddH_2O	1000ml

- 0.2M sodium bicarbonate ($NaHCO_3$)

Sodium bicarbonate ($NaHCO_3$)	16.8g
ddH_2O	1000ml

- Blocking solution

BSA	0.5g
Tween 20	25µl
1X PBS	50ml

- Diluent for standards and samples

1X PBS	500ml
Tween 20	250µl

- OPD substrate

Phosphate-citrate buffer, pH 5.0	6ml
OPD	300µl
30% H_2O_2 (Only add H_2O_2 just before use.)	3µl

- Phosphate-citrate buffer, pH 5.0

0.1M citrate buffer	24.3ml
0.2M phosphate buffer	25.7ml
ddH_2O	50ml

- 0.1M citrate buffer

Citric acid	3.84g
ddH_2O	200ml

- 0.2M phosphate buffer

Na_2HPO_4 (anhydrous)	5.68g
ddH_2O	200ml

Preparation of standards

- Dilute rat albumin stock solution of 20mg/ml to a working solution of 2µg/ml:
    1. Add 10µl rat albumin stock solution to 990µl diluent to get 200µg/ml solution.
    2. Add 50µl 200µg/ml solution to 4950µl diluent to get 2µg/ml solution.
- Make a 2X serial dilution from the 2µg/ml solution to obtain standard concentrations in ng/ml of 2000, 1000, 500, 250, 125, 62.5, 31.25, 15.625.

Preparation of samples

- Dilute urine samples sequentially:
    1. First dilute centrifuged urine samples 1/10 by adding 50µl urine sample to 450µl diluent.

2. Dilute the above diluted urine sample between 1/5 and 1/100 as shown in table below:

Second dilution (Final dilution)	Volume from first dilution / µl	Volume of diluent / µl
1/5 (1/50)	40	160
1/10 (1/100)	20	180
1/20 (1/200)	15	285
1/30 (1/300)	15	435
1/40 (1/400)	15	585
1/50 (1/500)	15	735
1/60 (1/600)	15	885
1/70 (1/700)	15	1035
1/80 (1/800)	15	1185
1/90 (1/900)	15	1335
1/100 (1/1000)	15	1485

Procedure

1. Coat 96-well EIA/RIA Clear Flat Bottom Polystyrene High Bind Microplate (Corning Inc., MA, USA) with 100µl rabbit antiserum to rat albumin diluted 1/2000 in 0.1M sodium carbonate buffer, pH 9.6. Incubate at 4°C overnight.
2. Aspirate coating antibody and wash microplate thrice with 1X PBS using a microplate washer (Tecan, Mannedorf, Switzerland).
3. Block wells with 100µl blocking solution at room temperature for 45 minutes.
4. Discard blocking solution without washing.
5. Add 50µl of diluent as blank, standards and diluted urine samples to each well in triplicate. Incubate at 37°C for 2 hours.
6. Aspirate and wash plate thrice with 1X PBS using microplate washer.
7. Incubate wells with 50µl HRP-conjugated sheep polyclonal antibody to rat albumin diluted 1/20000 in blocking solution at 37°C for 1 hour.
8. Aspirate and wash plate 4 times with 1X PBS.

9. Add 50µl OPD substrate in each well and incubate in darkness for color development at room temperature for 10 minutes.
10. Stop reaction with 60µl 4.5N sulphuric acid and mix gently. Incubate for 5 minutes.
11. Read absorbance at 490nm using microplate reader.

Appendix 2.2: Protocol for RNA purification and cleanup (RNeasy Mini Handbook, 4th Edition, 09/2010)

Preparation of reagents

- Buffer RPE is supplied as a concentrate. Before using it for the first time, add 4 volumes of absolute ethanol as indicated on the bottle to obtain a Buffer RPE working solution.
- Prepare DNase I stock solution before using the RNase-Free DNase Set for the first time. Dissolve the lyophilized DNase I (1500 Kunitz units) by injecting 550µl of the RNase-free water provided using RNase-free needle and syringe. Mix gently by inverting the vial. Do not vortex. Aliquot the stock solution into single-use volume and store at -20°C. Do not refreeze aliquots after thawing.

Procedure

1. Adjust the sample to a final volume of 100µl with RNase-free water.
2. Add 350µl Buffer RLT and mix well.
3. Add 250µl absolute ethanol to the mixture and mix well by pipetting.
4. Transfer the entire 700µl mixture to an RNeasy Mini spin column placed in a 2ml collection tube supplied. Centrifuge at 13000rpm for 15 seconds. Discard flow-through.
5. Add 350µl Buffer RW1 to the spin column. Centrifuge at 13000rpm for 15 seconds. Discard flow-through.

6. Add 10µl DNase I stock solution to 70µl Buffer RDD. Mix by gently inverting the tube and centrifuge briefly to collect residual liquid from the sides of the tube.
7. Add the 80µl DNase I incubation mix directly to the spin column membrane and incubate at room temperature for 15 minutes.
8. Add 350µl Buffer RW1 to the spin column. Centrifuge at 13000rpm for 15 seconds. Discard flow-through.
9. Add 500µl Buffer RPE to the spin column. Centrifuge at 13000rpm for 15 seconds. Discard flow-through.
10. Add 500µl Buffer RPE to the spin column. Centrifuge at 13000rpm for 2 minutes.
11. Place the spin column in a new 2ml collection tube supplied and discard the old collection tube with flow-through. Centrifuge at 13000rpm for 1 minute.
12. Place the spin column in a new 1.5ml collection tube supplied. Add 30µl RNase-free water directly to the spin column membrane. Centrifuge at 13000rpm for 1 minute to elute the RNA.
13. Repeat step 12 using the eluate from step 12 to obtain a higher RNA concentration. Reuse the collection tube from step 12.

Appendix 2.3: Protocol for RNA quantification and quality analysis (Agilent RNA 6000 Nano Kit Quick Start Guide, Edition 04/2007)

Preparation of reagents and equipment

- Adjust purified liver tissue RNA sample concentration to 150ng/µl using RNase-free water.
- Heat denature all RNA samples to minimize secondary structure and RNA 6000 Nano Ladder at 70°C for 2 minutes before use and keep on ice.
- Ensure chip priming station, IKA vortex mixer, 2100 Bioanalyzer and 2100 Expert Software are set up and ready to be used.
- Equilibrate all reagents in the RNA 6000 Nano Kit to room temperature before use.

Procedure

Preparing gel

1. Pipette 550µl RNA 6000 Nano Gel Matrix into a spin filter.
2. Centrifuge at 1500g at room temperature for 10 minutes.
3. Aliquot 65µl filtered gel into 0.5ml RNase-free microfuge tubes included in the kit. Store at 4°C and use within 1 month.

Preparing gel-dye mix

4. Protect RNA 6000 Nano Dye Concentrate from light when thawing to room temperature.
5. Vortex RNA 6000 Nano Dye Concentrate for 10 seconds and spin down.
6. Add 1µl RNA 6000 Nano Dye Concentrate to the 65µl filtered gel aliquot.

7. Vortex mixture thoroughly and centrifuge at 13000g at room temperature for 10 minutes. Protect gel-dye mix from light before use.

Loading gel-dye mix

8. Place a new RNA 6000 Nano Chip on the chip priming station.
9. Pipette 9µl gel-dye mix at the bottom of the well marked .
10. Ensure the plunger is positioned at 1ml and then close the chip priming station.
11. Press the plunger down until it is held by the clip.
12. Wait for exactly 30 seconds before releasing the clip.
13. Wait for 5 seconds and then slowly pull back the plunger to the 1ml position.
14. Open the chip priming station, and pipette 9µl gel-dye mix in each of the wells marked .

Loading RNA 6000 Nano Marker

15. Pipette 5µl RNA 6000 Nano Marker in all the 12 sample wells and in the well marked .

Loading ladder and samples

16. Pipette 1µl heat-denatured RNA ladder into the well marked .
17. Pipette 1µl heat-denatured sample into each of the 12 sample wells. Unused wells are to be filled with 1µl RNA 6000 Nano Marker to allow the chip to run properly.

18. Place the chip horizontally in the adapter of the IKA vortex mixer and vortex at 2400rpm for 1 minute.
19. Immediately insert the chip in the 2100 Bioanalyzer and start run within 5 minutes.

Data analysis

Major features of a successful ladder run should resemble Figure 1, displaying:

- 1 marker peak
- 6 RNA peaks (2100 Expert Software calls for 5 first ladder peaks only)
- All 7 peaks are well resolved
- Correct peak size assignment

Major features of a successful eukaryotic total RNA run should resemble Figure 2, displaying:

- 1 marker peak
- 2 ribosomal peaks (with successful sample preparation)

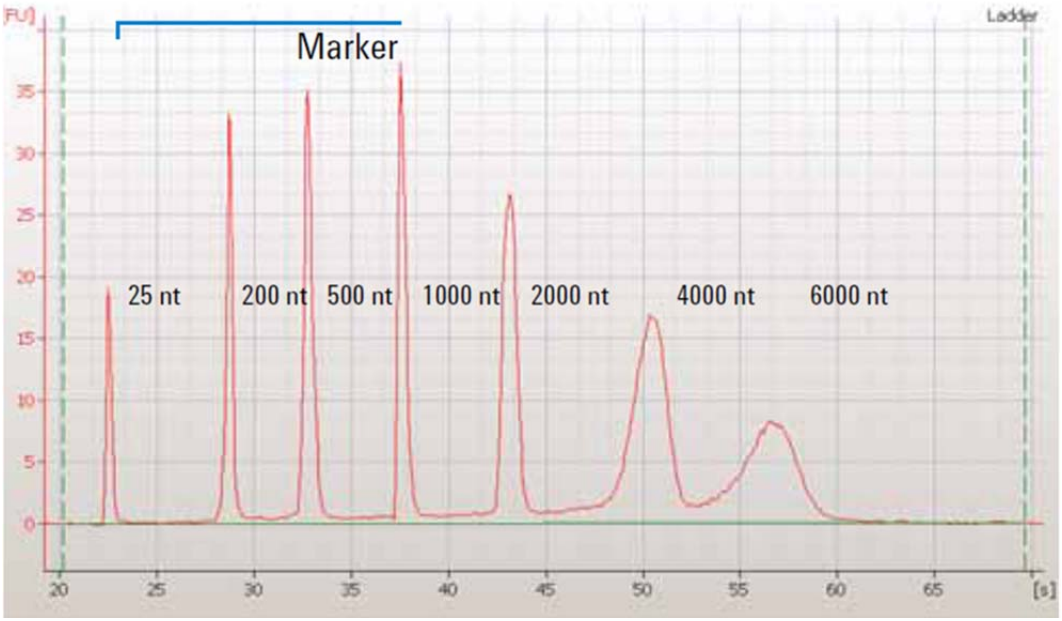

Figure 1: An electropherogram of a successful ladder run.

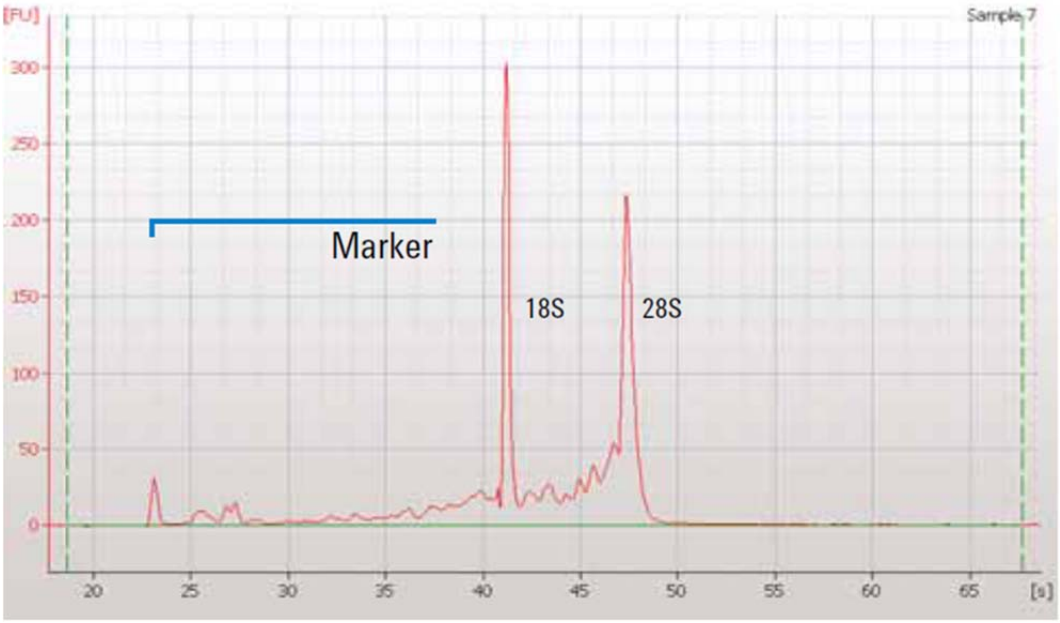

Figure 2: An electropherogram of a successful eukaryotic total RNA run.

By selecting the *Results* sub-tab in the 2100 Expert Software version B.02.02 or higher, values for the calculated RNA concentration, the ribosomal ratio and the RIN are displayed.

Appendix 2.4: Protocol for cRNA hybridization and array scanning (Illumina Whole-Genome Gene Expression for BeadStation)

Mix with Hyb reagents

1. Preheat the oven (with rocking platform) to 58°C.
2. To 750ng of cRNA, add RNase-free water up to 5µl and mix.
3. Incubate at room temperature for 10 minutes to resuspend cRNA.
4. Incubate GEX-HYB and GEX-HCB bottles in the 58°C oven for 10 minutes to dissolve any salt precipitation. If salt precipitation persists, incubate at 58°C for another 10 minutes.
5. Cool to room temperature and mix thoroughly before using.
6. Add 10µl GEX-HYB to each cRNA sample.

Set up hybridization

7. Place Hyb Chamber Gaskets into Hyb Chamber.
8. Dispense 200µl GEX-HCB into each of the 2 humidifying buffer reservoirs in each Hyb Chamber. Only add buffer to chambers that will be used.
9. Seal Hyb Chamber with lid and keep on bench at room temperature until ready to load BeadChips into Hyb Chamber.
10. Remove all BeadChips from their packages, using 3 fingers at the notches to release.
11. Holding BeadChip by cover seal tab with tweezers using powder-free gloved hands, slide BeadChip into Hyb Chamber Insert such that the barcode lines up with barcode symbol on the Hyb Chamber Insert.

12. Preheat cRNA sample at 65°C for 5 minutes.
13. Briefly vortex and then briefly centrifuge to collect liquid at the bottom of the tube. Allow sample to cool to room temperature before using.
14. Dispense 15µl sample immediately after cooling to room temperature onto the large sample port of each array, ensuring pipette tip does not touch array.
15. Load Hyb Chamber Inserts containing BeadChips into the Hyb Chamber with rocker speed at 5.
16. Seal lid onto the Hyb Chamber by applying the back of the lid first and then bringing it down to the front to avoid dislodging the Hyb Chamber Insert.
17. Incubate at 58°C for 18 hours.

Prepare 1X High-Temp Wash buffer with overnight incubation

18. Prepare 1X High-Temp Wash buffer by adding 50ml 10X High-Temp Wash buffer to 450ml RNase-free water.
19. Place Hybex Waterbath insert into heat block and add 500ml 1X High-Temp Wash buffer.
20. Set heat block temperature to 55°C and pre-warm High-Temp Wash buffer to that temperature.
21. Close heat block lid and leave overnight.

Prepare reagents

22. Prepare Wash E1BC solution by adding 6ml E1BC buffer to 2000ml RNase-free water.

23. Pre-warm Block E1 buffer (4ml/chip) to room temperature.

Room-Temp incubation

24. Remove Hyb Chamber from oven and disassemble.
25. Using powder-free gloved hands, remove BeadChips from Hyb Chamber and submerge them face up at the bottom of a container with 1000ml Wash E1BC solution. Observe for bubbles on BeadChips, and if any, locate them on the tracking sheet.
26. Using powder-free gloved hands, remove the cover seal from BeadChip in a zigzag manner, ensuring the entire BeadChip remains submerged during removal.
27. Using tweezers or powder-free gloved hands, transfer the peeled BeadChip into the slide rack submerged in the staining dish containing 250ml Wash E1BC solution.
28. Using the slide rack handle, transfer the slide rack into the Hybex Waterbath insert at 55°C containing High-Temp Wash buffer prepared previously.

High-Temp wash

29. Incubate static for 10 minutes with the Hybex lid closed.

First Room-Temp wash

30. During the 10-minute High-Temp Wash buffer incubation, add fresh 250ml Wash E1BC solution to a clean staining dish.

31. After the 10-minute High-Temp Wash buffer incubation is complete, immediately transfer the slide rack into the above prepared staining dish.
32. Briefly agitate using rack handle, then shake on orbital shaker at 110rpm for 5 minutes.

Ethanol wash

33. Transfer slide rack to a clean staining dish containing 250ml 100% ethanol.
34. Briefly agitate using rack handle, then shake on orbital shaker at 110rpm for 10 minutes.

Second Room-Temp wash

35. Transfer slide rack to a clean staining dish containing fresh 250ml Wash E1BC solution.
36. Briefly agitate using rack handle, then shake on orbital shaker at 110rpm for 2 minutes.

Block

37. Pipette 4ml Block E1 buffer into a BeadChip Wash Tray.
38. Transfer the BeadChip face up into BeadChip Wash Tray on rocker.
39. Rock at medium speed for 10 minutes.
40. Prepare Block E1 buffer (2ml/chip) with streptavidin-Cy3 (2µl of 1mg/ml stock per chip). Use a single conical tube for all BeadChips. Store in dark until detection step.

Detect

41. Pipette 2ml mixture of Block E1 buffer and streptavidin-Cy3 into a clean BeadChip Wash Tray.
42. Transfer the BeadChip face up into BeadChip Wash Tray on rocker.
43. Place BeadChip Tray Cover on BeadChip Wash Tray and rock at medium speed for 10 minutes.

Third Room-Temp wash

44. Add 250ml Wash E1BC solution to a clean staining dish.
45. Transfer the BeadChip into the slide rack submerged in the staining dish.
46. Briefly agitate using rack handle, and then shake at room temperature on orbital shaker for 5 minutes.

Dry

47. Prepare centrifuge with plateholders, paper towels and balance rack. Set speed to 270 rcf.
48. Transfer BeadChips in slide rack from staining dish to centrifuge and spin at room temperature for 4 minutes.
49. Store dry BeadChips in slide box until scanned.

Scanning

50. Scan the BeadChips with scan factor 1.5, PMT 531 using BeadArray™ Reader. Ensure the signal is strong enough, by looking out for the green color on the slot instead of red. Check that all the housekeeping genes and other parameters are normal.

Appendix 3.1: Profile of control and *IL-13* transfected nephrotic rats used for microarray analysis

Code	Sample	Serum IL-13 (pg/ml)	Serum albumin (g/l)	Serum cholesterol (mmol/l)	Serum creatinine (μmol/l)	Urine albumin excretion (μg/24hour)	Liver mass (g)
(3)C1	C1	0	37.9	1.81	89.5	398	12.5
(3)C2	C2	0	41.0	1.94	88.2	218	12.0
(3)C4	C4	0	56.9	1.63	67.2	194	12.4
(3)J2	J2	1578	27.9	7.80	69.7	2331	16.5
(3)J4	J4	376	29.3	5.83	89.5	3098	19.3
(4)J2	J8	232	28.3	4.82	53.1	7590	18.6
(4)J5	J11	28	29.0	4.30	70.5	2996	16.8
(4)J9	J15	336	29.3	4.45	67.6	6846	18.1
(4)J13	J19	1753	18.9	8.78	79.3	12087	9.0

Sample code with 'C' denotes control and 'J' denotes *IL-13* transfected nephrotic rats.

Appendix 3.2: List of downregulated DEGs

List of downregulated genes with fold change ≥ 1.5 and FDR < 0.05 differentially expressed in the livers of *IL-13* transfected nephrotic rats versus control rats.

Probe ID	Gene symbol	GenBank accession number	Gene description	Fold change
ILMN_1354422	Tor3a	NM_001009683	torsin family 3, member A	-7.39
ILMN_1651179	Hhip	NM_001191817	Hedgehog-interacting protein	-6.88
ILMN_1361259	Fabp7	NM_030832	fatty acid binding protein 7, brain	-6.37
ILMN_1361194	Rab30	NM_001015012	RAB30, member RAS oncogene family	-6.17
ILMN_1358631	Abcg5	NM_053754	ATP-binding cassette, sub-family G (WHITE), member 5	-6.00
ILMN_1350232	Hacl1	NM_053493	2-hydroxyacyl-CoA lyase 1	-5.39
ILMN_1360828	Acot5	NM_001079709	acyl-CoA thioesterase 5	-5.00
ILMN_1376848	Adh6	NM_001012084	alcohol dehydrogenase 6 (class V)	-4.60
ILMN_1369012	Mgll	NM_138502	monoglyceride lipase	-4.47
ILMN_1530388	Tor3a	NM_001009683	torsin family 3, member A	-4.21
ILMN_1350398	Lin7a	NM_053514	lin-7 homolog a (C. elegans)	-3.96
ILMN_1352829	Apol9a	NM_001025066	apolipoprotein L 9a	-3.66
ILMN_1360753	Umps	NM_001025402	uridine monophosphate synthetase	-3.57
ILMN_1367748	Plekhb1	NM_172033	pleckstrin homology domain containing, family B (evectins) member 1	-3.54
ILMN_1366852	Ifi47	NM_172019	interferon gamma inducible protein 47	-3.25
ILMN_1349962	Wasf1	NM_001025114	WAS protein family, member 1	-3.18
ILMN_1372579	Slc22a5	NM_019269	solute carrier family 22 (organic cation/carnitine transporter), member 5	-3.15
ILMN_1365923	Rbm48	NM_001024246	RNA binding motif protein 48	-3.09
ILMN_1362381	Gbp2	NM_133624	guanylate nucleotide binding protein 2	-3.01
ILMN_1351993	Cobll1	XM_001056368	Cobl-like 1	-2.96
ILMN_1370450	Decr1	NM_057197	2,4-dienoyl CoA reductase 1, mitochondrial, nuclear gene encoding mitochondrial protein	-2.95
ILMN_1372159	Stat1	NM_032612	signal transducer and activator of transcription 1, transcript variant alpha	-2.80
ILMN_1359709	RGD1562178	XM_575395	adenylate kinase 2, mitochondrial-like	-2.77
ILMN_1650864	Ak6	NM_001012463	adenylate kinase 6	-2.77
ILMN_1376733	Krt23	NM_001008753	keratin 23 (histone deacetylase inducible)	-2.76
ILMN_1349803	Shisa3	NM_001109087	shisa family member 3	-2.74
ILMN_1376951	Aco1	NM_017321	aconitase 1, soluble	-2.73
ILMN_1364915	LOC300760	XM_236308	similar to H3 histone, family 3B	-2.72
ILMN_1371397	Ptgds2	NM_031644	prostaglandin D2 synthase 2, hematopoietic	-2.71
ILMN_1366138	LOC306428	XM_224824	similar to Chain A, T13s Mutant Of Bovine 70 kDa Heat Shock Protein	-2.68
ILMN_1373487	RGD1562373	XM_001062085	similar to 3-ketoacyl-CoA thiolase B, peroxisomal precursor (Beta-ketothiolase B)	-2.65

ILMN_1361581	Sod3	NM_012880	superoxide dismutase 3, extracellular	-2.60
ILMN_1376900	Oas1i	NM_001009680	2' -5' oligoadenylate synthetase 1I	-2.57
ILMN_1375888	Coro2a	XM_575819	coronin, actin binding protein 2A	-2.54
ILMN_1349211	Fcn1	NM_031348	ficolin (collagen/fibrinogen domain containing) 1	-2.49
ILMN_1650649	LOC366608	XM_345665	similar to mKIAA0716 protein	-2.43
ILMN_1371171	Ppih	XM_001073803	peptidylprolyl isomerase H (cyclophilin H), transcript variant 1	-2.42
ILMN_1363976	Ak2	NM_030986	adenylate kinase 2, transcript variant 1	-2.42
ILMN_1355623	S100g	NM_012521	S100 calcium binding protein G	-2.41
ILMN_1650501	Ptgr2	NM_001015009	prostaglandin reductase 2	-2.41
ILMN_1361712	Lifr	NM_031048	leukemia inhibitory factor receptor alpha	-2.41
ILMN_1355010	Gemin6	NM_001009466	gem (nuclear organelle) associated protein 6	-2.41
ILMN_1370689	Peci	NM_001006966	peroxisomal delta3, delta2-enoyl-Coenzyme A isomerase	-2.40
ILMN_1650465	Sectm1a	NM_001013043	secreted and transmembrane 1A	-2.40
ILMN_1356675	Pank1	NM_001106373	pantothenate kinase 1	-2.37
ILMN_1362465	LOC290964	XM_214409	similar to RIKEN cDNA 8430426H19	-2.36
ILMN_1368814	Adi1	NM_199097	acireductone dioxygenase 1	-2.36
ILMN_1359094	Yc2	NM_001009920	glutathione S-transferase Yc2 subunit	-2.35
ILMN_1362365	Scml4	NM_001107638	sex comb on midleg-like 4 (Drosophila)	-2.34
ILMN_1360177	Ly6c	NM_020103	Ly6-C antigen	-2.34
ILMN_1367724	RGD1561455	XR_008037	similar to Ras GTPase-activating-like protein IQGAP2	-2.33
ILMN_1360549	Dyrk2	NM_001108100	dual-specificity tyrosine-(Y)-phosphorylation regulated kinase 2	-2.33
ILMN_1365281	Sh3gl3	NM_031238	SH3-domain GRB2-like 3	-2.33
ILMN_1364273	Nceh1	NM_001127524	neutral cholesterol ester hydrolase 1	-2.32
ILMN_1352135	Ceacam10	NM_173339	carcinoembryonic antigen-related cell adhesion molecule 10	-2.29
ILMN_1376808	Pdlim5	NM_053326	PDZ and LIM domain 5	-2.28
ILMN_1355553	Ddx6	XM_236192	DEAD (Asp-Glu-Ala-Asp) box polypeptide 6	-2.28
ILMN_1351495	LOC686213	XM_001072911	similar to DnaJ homolog subfamily B member 6 (Heat shock protein J2) (HSJ-2) (MRJ) (mDj4)	-2.28
ILMN_1364820	MGC108776	NM_001017466	Snf7 homologue associated with Alix 3	-2.27
ILMN_1351247	Ube2d1	NM_001108530	ubiquitin-conjugating enzyme E2D 1	-2.25
ILMN_1363239	Slc25a46	NM_001100515	solute carrier family 25, member 46	-2.25
ILMN_1360301	LOC497693	XM_579635	similar to P11 protein	-2.25
ILMN_1362787	Dnajc21	NM_138856	DnaJ (Hsp40) homolog, subfamily C, member 21	-2.21
ILMN_1350303	RGD1565165	XR_007875	similar to 60S ribosomal protein L7a	-2.20
ILMN_1369636	Cdk2ap1	NM_001113751	cyclin-dependent kinase 2 associated protein 1	-2.19
ILMN_1357234	Nrep	NM_178096	neuronal regeneration related protein	-2.18
ILMN_1366128	RGD1562311	XR_008266	similar to PIRA5	-2.17
ILMN_1363828	Pck1	NM_198780	phosphoenolpyruvate carboxykinase 1, cytosolic	-2.17
ILMN_1357078	Spred1	NM_001047089	sprouty-related, EVH1 domain containing 1	-2.15
ILMN_1369055	Disp1	NM_001105983	dispatched homolog 1 (Drosophila)	-2.15
ILMN_1351996	Hadhb	NM_133618	hydroxyacyl-Coenzyme A dehydrogenase/3-ketoacyl-Coenzyme A thiolase/enoyl-Coenzyme A hydratase (trifunctional protein), beta subunit, nuclear gene encoding mitochondrial protein	-2.15
ILMN_1374127	RGD1563348	NM_001114939	similar to Selenoprotein H	-2.14
ILMN_1360795	Slc11a1	NM_001031658	solute carrier family 11 (proton-coupled divalent metal ion transporters), member 1	-2.14
ILMN_1363947	Hmgcs2	NM_173094	3-hydroxy-3-methylglutaryl-Coenzyme A synthase 2 (mitochondrial), nuclear gene encoding	-2.13

			mitochondrial protein	
ILMN_1354480	Tusc2	NM_001109297	tumor suppressor candidate 2	-2.13
ILMN_1359983	Hist1h2bd	NM_001108414	histone cluster 1, H2bd	-2.13
ILMN_1357008	Fn3k	NM_001109051	fructosamine 3 kinase	-2.12
ILMN_1350981	Ripk1	NM_001107350	receptor (TNFRSF)-interacting serine-threonine kinase 1	-2.12
ILMN_1352627	LOC367191	XR_009207	poly(rC)-binding protein 2-like	-2.12
ILMN_1360891	Spin1	NM_001024796	spindlin 1	-2.12
ILMN_1372765	Nat1	NM_053853	N-acetyltransferase 1 (arylamine N-acetyltransferase)	-2.12
ILMN_1358768	LOC503192	XM_578715	zinc finger protein ZFP	-2.10
ILMN_1356825	Hrsp12	NM_031714	heat-responsive protein 12	-2.08
ILMN_1364518	Klhl25	NM_001039006	kelch-like 25 (Drosophila)	-2.08
ILMN_1350943	Cd163	NM_001107887	CD163 molecule	-2.08
ILMN_1350992	LOC498452	XM_573711	similar to ORF2 consensus sequence encoding endonuclease and reverse transcriptase minus RNaseH	-2.08
ILMN_1360060	Pla2g4a	NM_133551	phospholipase A2, group IVA (cytosolic, calcium-dependent)	-2.07
ILMN_1358826	Nudt15	NM_001106049	nudix (nucleoside diphosphate linked moiety X)-type motif 15	-2.07
ILMN_1374947	Bpnt1	NM_171990	bisphosphate 3'-nucleotidase 1	-2.06
ILMN_1371927	Srp54a	NM_053871	signal recognition particle 54A	-2.05
ILMN_2039303	Pelo	NM_001007634	pelota homolog (Drosophila)	-2.05
ILMN_1357590	Ascl2	NM_031503	achaete-scute complex homolog 2 (Drosophila)	-2.05
ILMN_1352469	Irf7	NM_001033691	interferon regulatory factor 7	-2.05
ILMN_1366496	Slc25a32	NM_001173334	solute carrier family 25 (mitochondrial folate carrier) , member 32	-2.04
ILMN_1363052	Pcgf6	NM_001013154	polycomb group ring finger 6	-2.04
ILMN_1372153	Lactb2	NM_001024247	lactamase, beta 2	-2.04
ILMN_1366226	Rbm47	NM_001005882	RNA binding motif protein 47	-2.03
ILMN_1366337	RGD1560687	XM_576192	ferritin light chain 1-like	-2.03
ILMN_1374066	Acot2	NM_138907	acyl-CoA thioesterase 2, nuclear gene encoding mitochondrial protein	-2.03
ILMN_1357358	Med4	NM_001024256	mediator complex subunit 4	-2.02
ILMN_1356599	Isg20l2	NM_001007741	interferon stimulated exonuclease gene 20-like 2	-2.02
ILMN_1356300	Nrbf2	NM_022186	nuclear receptor binding factor 2	-2.00
ILMN_1367993	Abcd2	NM_033352	ATP-binding cassette, sub-family D (ALD), member 2	-2.00
ILMN_1370477	Cdc40	NM_001108538	cell division cycle 40	-1.99
ILMN_1366288	March5	NM_001106372	membrane-associated ring finger (C3HC4) 5	-1.99
ILMN_1354725	LOC500490	XM_575855	similar to Retrovirus-related POL polyprotein	-1.98
ILMN_1651174	RGD1565965	XM_237746	hypothetical gene supported by NM_021262; AF171072	-1.98
ILMN_1357104	LOC498786	XM_574071	similar to GTP-binding protein NGB	-1.98
ILMN_1350310	Mecr	NM_017209	mitochondrial trans-2-enoyl-CoA reductase, nuclear gene encoding mitochondrial protein	-1.97
ILMN_1370862	Upp1	NM_001030025	uridine phosphorylase 1	-1.96
ILMN_1366946	LOC299262	XM_238465	hypothetical LOC299262	-1.95
ILMN_1376954	Uchl5	NM_001012149	ubiquitin carboxyl-terminal hydrolase L5	-1.95
ILMN_1372790	Scfd2	NM_001017499	sec1 family domain containing 2	-1.95
ILMN_1376652	Sh3glb1	NM_001011929	SH3-domain GRB2-like B1 (endophilin)	-1.93
ILMN_1358408	Xcl1	NM_134361	chemokine (C motif) ligand 1	-1.93
ILMN_1372785	MGC105647	XM_001079820	similar to Nur77 downstream protein 2	-1.92

ILMN_1351513	Asf1a	NM_001106389	anti-silencing function 1A histone chaperone	-1.92
ILMN_1364990	Nkrf	XM_233308	NFKB repressing factor	-1.91
ILMN_1372465	Trex1	NM_001024989	three prime repair exonuclease 1	-1.91
ILMN_1354716	Nupr1l	NM_001134570	nuclear protein, transcriptional regulator, 1-like	-1.91
ILMN_1376412	Gphn	NM_022865	gephyrin	-1.90
ILMN_1358752	Ndn	NM_001008558	necdin homolog (mouse)	-1.90
ILMN_1353110	Tmem167b	NM_001135260	transmembrane protein 167B	-1.90
ILMN_1350714	Oxr1	NM_057153	oxidation resistance 1, transcript variant 2	-1.90
ILMN_1363212	LOC498424	XM_573673	similar to 5330440M15Rik protein	-1.89
ILMN_1364624	LOC501605	XM_577005	similar to 40S ribosomal protein S2	-1.88
ILMN_1355426	Ppp1r10	NM_022951	protein phosphatase 1, regulatory subunit 10	-1.88
ILMN_1650500	Ccdc91	NM_001014061	coiled-coil domain containing 91	-1.88
ILMN_1364166	Prr16	NM_001108432	proline rich 16	-1.87
ILMN_1376472	Irgm	NM_001012007	immunity-related GTPase family, M	-1.87
ILMN_1367105	Cbr1	NM_019170	carbonyl reductase 1	-1.85
ILMN_1364885	Zdhhc6	NM_001037652	zinc finger, DHHC domain containing 6	-1.83
ILMN_1371910	Ube2e3	NM_001047857	ubiquitin-conjugating enzyme E2E 3	-1.83
ILMN_1352241	RGD1562392	XM_346007	similar to Sulfotransferase K1 (rSULT1C2)	-1.82
ILMN_1366967	RGD1562699	NM_001106141	RGD1562699	-1.82
ILMN_1355930	LOC497782	XM_579621	hypothetical gene supported by NM_133401	-1.81
ILMN_1367580	RGD1564026	XR_007667	similar to L-lactate dehydrogenase A chain (LDH-A) (LDH muscle subunit) (LDH-M)	-1.81
ILMN_1371172	LOC500734	XM_576113	similar to immunoglobulin heavy chain variable region	-1.80
ILMN_1360968	Arl5a	NM_053979	ADP-ribosylation factor-like 5A	-1.80
ILMN_1360638	LOC500903	XM_576305	similar to RIKEN cDNA 2210421G13	-1.80
ILMN_1372614	Ncald	NM_001024371	neurocalcin delta	-1.80
ILMN_1375936	Rangap1	XM_576313	RAN GTPase activating protein 1	-1.79
ILMN_1356037	LOC501413	XM_576825	similar to hypothetical protein	-1.79
ILMN_1350607	Siah2	NM_134457	seven in absentia 2	-1.79
ILMN_1650512	RGD1566244	XR_007720	similar to TatD DNase domain containing 1	-1.79
ILMN_1362688	Zfp191	NM_182955	zinc finger protein 191	-1.79
ILMN_1373470	Ctr9	XM_238127	Ctr9, Paf1/RNA polymerase II complex component, homolog (S. cerevisiae)	-1.78
ILMN_1366773	Sord	NM_017052	sorbitol dehydrogenase	-1.78
ILMN_1355396	Txndc17	NM_001105805	thioredoxin domain containing 17	-1.78
ILMN_1374122	LOC364763	XM_344621	similar to GTP-binding protein NGB	-1.78
ILMN_1354166	LOC687840	XM_001080312	similar to Glutathione S-transferase alpha-4 (Glutathione S-transferase Yk) (GST Yk) (GST 8-8) (GST K) (GST A4-4)	-1.78
ILMN_1373384	Dmn	XM_001055724	desmuslin, transcript variant 2	-1.78
ILMN_1376437	Zfand3	NM_001012175	zinc finger, AN1-type domain 3	-1.78
ILMN_1361429	Arih1	NM_001013108	ariadne ubiquitin-conjugating enzyme E2 binding protein homolog 1 (Drosophila)	-1.77
ILMN_1352032	Decr2	NM_171996	2,4-dienoyl CoA reductase 2, peroxisomal	-1.77
ILMN_1357381	Bet1	NM_019251	blocked early in transport 1 homolog (S. cerevisiae)	-1.77
ILMN_1358738	Ly86	NM_001106128	lymphocyte antigen 86	-1.76
ILMN_1355124	Galnt2	NM_001106196	UDP-N-acetyl-alpha-D-galactosamine:polypeptide N-acetylgalactosaminyltransferase 2 (GalNAc-T2)	-1.76
ILMN_1354435	Hnf4a	NM_022180	hepatocyte nuclear factor 4, alpha	-1.76
ILMN_1366222	LOC501416	XM_576827	similar to glutamate receptor, ionotropic, N-methyl D-aspartate-like 1A	-1.75

ILMN_1372464	Mb21d2	NM_001109056	Mab-21 domain containing 2	-1.75
ILMN_1369812	Zfp36l2	NM_001036626	zinc finger protein 36, C3H type-like 2	-1.75
ILMN_1357813	RGD1564594	XM_001055954	similar to pellino protein	-1.75
ILMN_1368635	Dst	NM_001108208	dystonin	-1.74
ILMN_1355986	Rab1	NM_031090	RAB1, member RAS oncogene family	-1.74
ILMN_1354213	Adh4	NM_017270	alcohol dehydrogenase 4 (class II), pi polypeptide	-1.74
ILMN_1651079	LOC500436	XM_575798	similar to heat shock protein 8	-1.74
ILMN_1376386	Pycrl	NM_001011993	pyrroline-5-carboxylate reductase-like	-1.74
ILMN_1349967	RGD1559924	XR_007622	similar to Eukaryotic translation initiation factor 1 (eIF1)	-1.74
ILMN_1374957	Mtfmt	NM_001009697	mitochondrial methionyl-tRNA formyltransferase, nuclear gene encoding mitochondrial protein	-1.73
ILMN_1376331	Hadha	NM_130826	hydroxyacyl-Coenzyme A dehydrogenase/3-ketoacyl-Coenzyme A thiolase/enoyl-Coenzyme A hydratase (trifunctional protein), alpha subunit	-1.73
ILMN_1374922	LOC499898	XM_575244	LOC499898	-1.73
ILMN_1351237	Txnrd1	NM_031614	thioredoxin reductase 1	-1.73
ILMN_2039089	Adh1	NM_019286	alcohol dehydrogenase 1 (class I)	-1.73
ILMN_1376965	Btbd1	XM_001067480	BTB (POZ) domain containing 1	-1.73
ILMN_1376462	Fxr1	NM_001012179	fragile X mental retardation, autosomal homolog 1	-1.72
ILMN_1363156	LOC684318	XM_001069848	similar to ubiquitin specific protease 12	-1.72
ILMN_1362861	Rwdd2b	NM_001100559	RWD domain containing 2B	-1.71
ILMN_1350341	Dnajc28	NM_001014124	DnaJ (Hsp40) homolog, subfamily C, member 28	-1.71
ILMN_1349542	Ssbp2	XM_342171	single-stranded DNA binding protein 2	-1.70
ILMN_1375183	Slc16a13	NM_001005530	solute carrier family 16, member 13 (monocarboxylic acid transporter 13)	-1.70
ILMN_1367476	LOC501326	XR_009028	similar to glutamate receptor, ionotropic, N-methyl D-aspartate-like 1A	-1.70
ILMN_1361326	Dhrs4	NM_153315	dehydrogenase/reductase (SDR family) member 4	-1.70
ILMN_1351249	Spast	NM_001108702	spastin	-1.70
ILMN_1366889	Timm21	NM_001008343	translocase of inner mitochondrial membrane 21 homolog (yeast)	-1.69
ILMN_1360190	Cd8a	NM_031538	CD8a molecule	-1.69
ILMN_1372394	Unc119	NM_017188	UNC-119 homolog (C. elegans)	-1.69
ILMN_1375869	Fbxo8	XM_573904	F-box only protein 8	-1.68
ILMN_1364233	Chfr	NM_001009258	checkpoint with forkhead and ring finger domains	-1.68
ILMN_1366519	Cdip1	NM_001008360	cell death-inducing p53 target 1	-1.68
ILMN_1359655	LOC683919	XM_001068058	similar to nudix-type motif 8	-1.68
ILMN_1355225	Rac1	NM_134366	ras-related C3 botulinum toxin substrate 1	-1.68
ILMN_1366255	Abca6	XM_001081607	ATP-binding cassette, subfamily A (ABC1), member 6	-1.68
ILMN_1363211	Cs	NM_130755	citrate synthase, nuclear gene encoding mitochondrial protein	-1.68
ILMN_1374215	Gpr89b	NM_001139486	G protein-coupled receptor 89B	-1.68
ILMN_1354598	Dexi	NM_001109026	dexamethasone-induced transcript	-1.67
ILMN_1376941	rnf141	NM_001001800	ring finger protein 141	-1.67
ILMN_1357860	Rpf1	NM_001100794	ribosome production factor 1 homolog (S. cerevisiae)	-1.67
ILMN_1361564	LOC501187	XM_576615	similar to putative RNA binding protein 1	-1.66
ILMN_1365812	Kbtbd4	NM_001107746	kelch repeat and BTB (POZ) domain containing 4	-1.66
ILMN_1365910	Etfa	NM_001009668	electron-transfer-flavoprotein, alpha polypeptide, nuclear gene encoding mitochondrial protein	-1.66
ILMN_1365109	LOC500343	XM_575695	similar to LRRGT00176	-1.65
ILMN_1357474	Ahcy	NM_017201	S-adenosylhomocysteine hydrolase	-1.65

ILMN_1373959	Map3k3	NM_001107058	mitogen activated protein kinase kinase kinase 3	-1.65
ILMN_1650897	Dnaaf2	NM_001014197	dynein, axonemal, assembly factor 2	-1.65
ILMN_1650940	Snrnp200	NM_001037766	small nuclear ribonucleoprotein 200 (U5)	-1.65
ILMN_1358108	Srm	NM_053464	spermidine synthase	-1.65
ILMN_1364242	Nanp	NM_001009409	N-acetylneuraminic acid phosphatase	-1.64
ILMN_1360282	Yars2	NM_001009627	tyrosyl-tRNA synthetase 2 (mitochondrial), nuclear gene encoding mitochondrial protein	-1.64
ILMN_1371034	Acsl4	NM_053623	acyl-CoA synthetase long-chain family member 4	-1.64
ILMN_1373367	Aar2	NM_001106535	AAR2 splicing factor homolog (S. cerevisiae)	-1.64
ILMN_2038784	Txn1	NM_053800	thioredoxin 1	-1.64
ILMN_1369091	Slc35e3	NM_001134687	solute carrier family 35, member E3	-1.63
ILMN_1359331	LOC687248	XR_009164	hypothetical protein LOC687248	-1.63
ILMN_1351590	Erich1	NM_001127680	glutamate-rich 1	-1.63
ILMN_1372726	Nub1	NM_001013925	negative regulator of ubiquitin-like proteins 1	-1.63
ILMN_1355168	Coa4	NM_001127655	cytochrome c oxidase assembly factor 4	-1.63
ILMN_1369530	Cat	NM_012520	catalase	-1.63
ILMN_1365458	Gtpbp10	NM_001100815	GTP-binding protein 10 (putative)	-1.62
ILMN_1366845	Auh	NM_001108407	AU RNA binding protein/enoyl-CoA hydratase	-1.62
ILMN_1371924	Utp14a	NM_001014113	UTP14, U3 small nucleolar ribonucleoprotein, homolog A (yeast)	-1.62
ILMN_1354803	Arcn1	NM_001007662	archain 1	-1.62
ILMN_1354808	Ncf4	NM_001127304	neutrophil cytosolic factor 4	-1.61
ILMN_1369424	Napg	NM_001107384	N-ethylmaleimide-sensitive factor attachment protein, gamma	-1.61
ILMN_1365599	Bphl	NM_001037206	biphenyl hydrolase-like (serine hydrolase)	-1.61
ILMN_1356247	RGD1564894	NM_001126278	similar to glycine-N-acyltransferase isoform a	-1.61
ILMN_1374995	Srp19	NM_001106157	signal recognition particle 19	-1.61
ILMN_1371355	RGD1309188	NM_001108129	similar to hypothetical protein BC011833	-1.60
ILMN_1360216	Id3	NM_013058	inhibitor of DNA binding 3	-1.60
ILMN_1366625	Slc17a5	NM_001009713	solute carrier family 17 (anion/sugar transporter), member 5	-1.60
ILMN_1361722	Rbm8a	XM_001059872	RNA binding motif protein 8A	-1.60
ILMN_1354675	Chrac1	NM_001134880	chromatin accessibility complex 1	-1.60
ILMN_1363823	Ccdc58	NM_001105875	coiled-coil domain containing 58	-1.60
ILMN_1368767	Polg	NM_053528	polymerase (DNA directed), gamma	-1.60
ILMN_1369087	RGD1304567	NM_001009711	similar to RIKEN cDNA A430005L14	-1.60
ILMN_1373798	Plcb1	NM_001077641	phospholipase C, beta 1 (phosphoinositide-specific)	-1.59
ILMN_1363987	Cndp1	NM_001007687	carnosine dipeptidase 1 (metallopeptidase M20 family)	-1.59
ILMN_1350248	Ryk	NM_080402	receptor-like tyrosine kinase	-1.59
ILMN_1353438	Mrps9	NM_001100549	mitochondrial ribosomal protein S9	-1.59
ILMN_1371849	Ccdc59	NM_001108090	coiled-coil domain containing 59	-1.59
ILMN_1364217	Isy1	NM_001014188	ISY1 splicing factor homolog (S. cerevisiae)	-1.58
ILMN_1353995	Mcee	NM_001106341	methylmalonyl CoA epimerase	-1.58
ILMN_1355224	Stk35	NM_001107773	serine/threonine kinase 35	-1.58
ILMN_1362897	Acadm	NM_016986	acyl-Coenzyme A dehydrogenase, C-4 to C-12 straight chain, nuclear gene encoding mitochondrial protein	-1.58
ILMN_1351976	Ifi44l	XM_227820	interferon-induced protein 44-like	-1.58
ILMN_1367456	C1qbp	NM_019259	complement component 1, q subcomponent binding protein, nuclear gene encoding mitochondrial protein	-1.58

ILMN_1365423	Mpc2	NM_001077643	mitochondrial pyruvate carrier 2	-1.58
ILMN_1354759	Fxn	NM_001191952	frataxin, nuclear gene encoding mitochondrial protein	-1.57
ILMN_1352941	Dusp12	NM_022248	dual specificity phosphatase 12	-1.57
ILMN_1374010	RGD1561310	XM_001068169	60S ribosomal protein L37-like	-1.57
ILMN_1362835	Rpain	NM_001033060	RPA interacting protein	-1.57
ILMN_1354159	LOC500420	XM_575783	similar to CG12279-PA	-1.56
ILMN_1358897	Glud1	NM_012570	glutamate dehydrogenase 1	-1.56
ILMN_1376836	Fut8	NM_001002289	fucosyltransferase 8 (alpha (1,6) fucosyltransferase)	-1.55
ILMN_1360039	Pafah1b3	NM_053654	platelet-activating factor acetylhydrolase, isoform 1b, alpha1 subunit	-1.55
ILMN_1650955	Ifi27	NM_203410	interferon, alpha-inducible protein 27	-1.55
ILMN_1349065	Iqcf6	NM_001109362	IQ motif containing F6	-1.55
ILMN_1353223	Nudt19	NM_001004258	nudix (nucleoside diphosphate linked moiety X)-type motif 19	-1.55
ILMN_1370151	Cdk7	XM_215467	cyclin-dependent kinase 7	-1.54
ILMN_1353778	RGD1564492	XM_574204	similar to hypothetical protein, 2-6	-1.54
ILMN_1353814	LOC689226	NM_001127573	similar to ubiquitin-conjugating enzyme E2R 2	-1.54
ILMN_1351644	LOC501311	XM_576724	hypothetical gene supported by BC088860	-1.53
ILMN_1353960	Idh1	NM_031510	isocitrate dehydrogenase 1 (NADP+), soluble	-1.53
ILMN_1373451	Slc37a2	XM_001061125	solute carrier family 37 (glycerol-3-phosphate transporter), member 2	-1.53
ILMN_1366497	Yipf6	NM_001025747	Yip1 domain family, member 6	-1.53
ILMN_1369440	Tinf2	NM_001006962	TERF1 (TRF1)-interacting nuclear factor 2	-1.53
ILMN_1362225	LOC497934	NM_001017474	similar to hypothetical protein FLJ20014	-1.52
ILMN_2040058	Chchd3	NM_001106588	coiled-coil-helix-coiled-coil-helix domain containing 3	-1.52
ILMN_1357565	Hdac1	NM_001025409	histone deacetylase 1	-1.52
ILMN_1373709	Trpm6	XM_219747	transient receptor potential cation channel, subfamily M, member 6	-1.52
ILMN_1359694	Lgals8	NM_053862	lectin, galactose binding, soluble 8	-1.51
ILMN_1375247	Fxyd2	NM_145717	FXYD domain-containing ion transport regulator 2, transcript variant a	-1.51
ILMN_1364467	RGD1561886	XR_008939	similar to ribosomal protein L27	-1.51
ILMN_1352039	Gsta4	NM_001106840	glutathione S-transferase alpha 4	-1.50

Appendix 3.3: List of upregulated DEGs

List of upregulated genes with fold change ≥ 1.5 and FDR < 0.05 differentially expressed in the livers of *IL-13* transfected nephrotic rats versus control rats.

Probe ID	Gene symbol	GenBank accession number	Gene description	Fold change
ILMN_1359586	Scd	NM_031841	stearoyl-CoA desaturase (delta-9-desaturase)	18.01
ILMN_1360317	Smoc2	NM_001106215	SPARC related modular calcium binding 2	15.01
ILMN_1360645	Gck	NM_012565	glucokinase	8.56
ILMN_1369135	Hsd11b1	NM_017080	hydroxysteroid 11-beta dehydrogenase 1	7.39
ILMN_1372932	LOC500504	XM_580077	LOC500504	6.11
ILMN_1360285	Mocos	NM_001108425	molybdenum cofactor sulfurase	5.79
ILMN_1373783	LOC360228	NM_001003706	WDNM1 homolog	5.75
ILMN_1373045	Cyp2c22	NM_138512	cytochrome P450, family 2, subfamily c, polypeptide 22	5.35
ILMN_1364575	Pfkfb1	NM_012621	6-phosphofructo-2-kinase/fructose-2,6-biphosphatase 1	5.20
ILMN_1357139	Ikbke	NM_001108854	inhibitor of kappa light polypeptide gene enhancer in B-cells, kinase epsilon	5.16
ILMN_1353346	Ltbp4	NM_001170336	latent transforming growth factor beta binding protein 4	5.03
ILMN_1365415	Prss8	NM_138836	protease, serine, 8 (prostasin)	5.00
ILMN_1352807	Vwf	NM_053889	von Willebrand factor	4.61
ILMN_1352810	Arhgef19	NM_001108692	Rho guanine nucleotide exchange factor (GEF) 19	4.36
ILMN_1367162	Gpm6a	NM_178105	glycoprotein m6a	3.97
ILMN_1365485	Pdgfa	NM_012801	platelet-derived growth factor alpha polypeptide	3.81
ILMN_1363044	C1qtnf2	XM_001067870	C1q and tumor necrosis factor related protein 2	3.78
ILMN_1366328	Nipal2	NM_001130559	NIPA-like domain containing 2	3.71
ILMN_1650259	Plod2	NM_175869	procollagen lysine, 2-oxoglutarate 5-dioxygenase 2	3.71
ILMN_1364908	Pmepa1	NM_001107807	prostate transmembrane protein, androgen induced 1	3.69
ILMN_1359113	Kifc3	NM_001103352	kinesin family member C3	3.69
ILMN_1359487	Mapk8ip3	NM_001100673	mitogen-activated protein kinase 8 interacting protein 3	3.67
ILMN_1366030	Cacna2d1	NM_012919	calcium channel, voltage-dependent, alpha2/delta subunit 1, transcript variant 1	3.62
ILMN_1365447	Cryab	NM_012935	crystallin, alpha B	3.60
ILMN_1366910	Acly	NM_016987	ATP citrate lyase	3.56
ILMN_1351428	Abcc3	NM_080581	ATP-binding cassette, sub-family C (CFTR/MRP), member 3	3.45
ILMN_1350619	Pdia5	NM_001014125	protein disulfide isomerase family A, member 5	3.40
ILMN_1355412	Olfml2b	NM_001107195	olfactomedin-like 2B	3.40
ILMN_1366054	Abcc8	NM_013039	ATP-binding cassette, sub-family C (CFTR/MRP), member 8	3.38
ILMN_1361494	LOC498901	XM_574188	similar to LRRGT00176	3.36
ILMN_1373203	Kif12	XM_001058042	kinesin family member 12	3.36
ILMN_1353477	LOC498907	XM_574196	similar to LRRGT00004	3.24
ILMN_1361779	Tcea3	NM_001015008	transcription elongation factor A (SII), 3	3.23

ILMN_1360221	Tacstd1	NM_138541	tumor-associated calcium signal transducer 1	3.17
ILMN_1367467	Per2	NM_031678	period homolog 2 (Drosophila)	3.14
ILMN_1355237	Cxcl1	NM_030845	chemokine (C-X-C motif) ligand 1 (melanoma growth stimulating activity, alpha)	3.13
ILMN_1373157	Wfdc2	NM_173109	WAP four-disulfide core domain 2	3.12
ILMN_1358074	Npdc1	NM_001004231	neural proliferation, differentiation and control, 1	3.02
ILMN_1376846	Loxl1	NM_001012125	lysyl oxidase-like 1	3.01
ILMN_1359236	Adamdec1	NM_001106046	ADAM-like, decysin 1	2.90
ILMN_1359468	Dhcr24	NM_001080148	24-dehydrocholesterol reductase	2.90
ILMN_1355149	Manba	NM_001031655	mannosidase, beta A, lysosomal	2.86
ILMN_1530405	Loxl1	NM_001012125	lysyl oxidase-like 1	2.81
ILMN_1364423	Synpo2	NM_001191963	synaptopodin 2	2.81
ILMN_1361143	Suv420h2	NM_001107475	suppressor of variegation 4-20 homolog 2 (Drosophila)	2.81
ILMN_1355110	Fbxl20	NM_022272	F-box and leucine-rich repeat protein 20	2.77
ILMN_1650719	Tmem106a	NM_001024967	transmembrane protein 106A	2.75
ILMN_1368538	Gria3	NM_032990	glutamate receptor, ionotropic, AMPA3 (alpha 3)	2.74
ILMN_1371681	Rcn3	NM_001008694	reticulocalbin 3, EF-hand calcium binding domain	2.73
ILMN_1354646	Tmem98	NM_001007672	transmembrane protein 98	2.71
ILMN_1374494	MGC116197	NM_001025755	similar to RIKEN cDNA 1700001E04	2.70
ILMN_1358691	Myadm	NM_183332	myeloid-associated differentiation marker	2.70
ILMN_1361132	Map2k6	NM_053703	mitogen-activated protein kinase kinase 6	2.69
ILMN_1365374	LOC295167	XM_227324	similar to CG13990-PA	2.62
ILMN_1360353	LOC500617	XM_575991	similar to LRRGT00014	2.54
ILMN_1368890	Wfikkn1	NM_001129776	WAP, follistatin/kazal, immunoglobulin, kunitz and netrin domain containing 1	2.52
ILMN_1354506	Icam1	NM_012967	intercellular adhesion molecule 1	2.50
ILMN_1365488	Cyp4f37	NM_001271352	cytochrome P450, family 4, subfamily f, polypeptide 37	2.45
ILMN_1354101	Dazap1	NM_001025742	DAZ associated protein 1	2.43
ILMN_1375844	Tia1	XM_575591	cytotoxic granule-associated RNA binding protein 1	2.43
ILMN_1355240	Pnoc	NM_013007	prepronociceptin	2.42
ILMN_1374674	LOC362882	XM_343210	similar to Lysozyme C, type 2 precursor (1,4-beta-N-acetylmuramidase C)	2.40
ILMN_1370728	Dctn1	NM_024130	dynactin 1	2.39
ILMN_1360715	LOC360303	XM_346531	hypothetical LOC360303	2.37
ILMN_1364747	Jub	NM_053503	jub, ajuba homolog (Xenopus laevis)	2.35
ILMN_1359746	Prpf38b	NM_001024305	pre-mRNA processing factor 38B	2.30
ILMN_1351912	RGD1304868	XR_009138	similar to RIKEN cDNA 2810443J12	2.28
ILMN_1360884	Arl13b	NM_001107101	ADP-ribosylation factor-like 13B	2.27
ILMN_1374266	Mgl1	NM_022393	macrophage galactose N-acetyl-galactosamine specific lectin 1	2.25
ILMN_1355272	Akap8	NM_053855	A kinase (PRKA) anchor protein 8	2.25
ILMN_1373875	Sparcl1	NM_012946	SPARC-like 1 (hevin)	2.23
ILMN_1352063	LOC499416	XM_574732	similar to transient receptor potential cation channel subfamily M member 2	2.22
ILMN_1370711	Plekha4	NM_199101	pleckstrin homology domain containing, family A (phosphoinositide binding specific) member 4	2.21
ILMN_1351742	Abcb9	NM_022238	ATP-binding cassette, sub-family B (MDR/TAP), member 9	2.21
ILMN_1364291	Spbc24	XM_001077474	spindle pole body component 24 homolog (S. cerevisiae)	2.21
ILMN_1357348	Nrg1	NM_031588	neuregulin 1	2.19
ILMN_1365562	LOC500974	XR_009636	similar to CDNA sequence BC024479	2.19

ILMN_1360746	Dmxl1	NM_001107388	Dmx-like 1	2.19
ILMN_1360523	Shroom1	XM_213289	shroom family member 1	2.19
ILMN_1350429	Setdb2	XM_224248	SET domain, bifurcated 2	2.19
ILMN_1375236	Pvrl2	XM_574380	poliovirus receptor-related 2 (herpesvirus entry mediator B)	2.18
ILMN_1355909	Tmem176b	NM_134390	transmembrane protein 176B	2.17
ILMN_1375690	Sept4	XM_001081164	septin 4	2.16
ILMN_1353007	Vtcn1	NM_001024244	V-set domain containing T cell activation inhibitor 1	2.16
ILMN_1368854	Gpx2	NM_183403	glutathione peroxidase 2	2.16
ILMN_1351420	RGD1305807	NM_001025276	hypothetical LOC298077	2.16
ILMN_1356327	Scarf1	NM_001107022	scavenger receptor class F, member 1	2.15
ILMN_1357400	Glt8d1	NM_001007683	glycosyltransferase 8 domain containing 1	2.14
ILMN_1356318	Cdc42ep5	NM_001108469	CDC42 effector protein (Rho GTPase binding) 5	2.11
ILMN_1372296	Zmym6	NM_001108681	zinc finger, MYM-type 6	2.11
ILMN_1368776	LOC498674	XM_579847	LOC498674	2.10
ILMN_1360376	App	NM_019288	amyloid beta (A4) precursor protein	2.09
ILMN_1350349	Sox4	NM_001271205	SRY (sex determining region Y)-box 4	2.09
ILMN_1352802	Cxadr	NM_053570	coxsackie virus and adenovirus receptor	2.08
ILMN_1366115	Cd151	NM_022523	CD151 molecule (Raph blood group)	2.07
ILMN_1651198	Zmynd11	NM_203366	zinc finger, MYND domain containing 11, transcript variant 1	2.02
ILMN_1355561	Cst3	NM_012837	cystatin C	2.01
ILMN_1376819	Sept4	XM_001081164	septin 4	2.01
ILMN_1356895	Ttc13	NM_001136162	tetratricopeptide repeat domain 13	2.00
ILMN_1369717	LOC682323	XM_001059807	similar to Splicing factor, arginine/serine-rich 3 (Pre-mRNA splicing factor SRP20) (X16 protein), transcript variant 1	2.00
ILMN_1374155	Nfkb2	NM_001008349	nuclear factor of kappa light polypeptide gene enhancer in B-cells 2, p49/p100	2.00
ILMN_1350234	Fbxw4	NM_001107600	F-box and WD repeat domain containing 4	1.98
ILMN_1364755	Snrpa	NM_001008303	small nuclear ribonucleoprotein polypeptide A	1.98
ILMN_1371901	Clk4	NM_001013041	CDC like kinase 4	1.97
ILMN_1351902	Abcg3	NM_001128311	ATP-binding cassette, subfamily G (WHITE), member 3	1.97
ILMN_1372684	Ppip5k2	NM_001025775	diphosphoinositol pentakisphosphate kinase 2	1.96
ILMN_1360455	Tmem110	NM_198774	transmembrane protein 110	1.95
ILMN_1355371	Jak3	NM_012855	Janus kinase 3	1.93
ILMN_1372351	Chrnb1	NM_012528	cholinergic receptor, nicotinic, beta 1 (muscle)	1.93
ILMN_1372737	Sfrs11	NM_001035255	splicing factor, arginine/serine-rich 11	1.93
ILMN_1352832	Slc39a13	NM_001039196	solute carrier family 39 (metal ion transporter), member 13	1.93
ILMN_1349593	Srrm2	NM_001277154	serine/arginine repetitive matrix 2	1.92
ILMN_1363056	Camta2	NM_001105801	calmodulin binding transcription activator 2	1.92
ILMN_1358401	Cygb	NM_130744	cytoglobin	1.92
ILMN_1365170	LOC689253	XM_001070133	similar to neurobeachin-like 1	1.91
ILMN_1361128	Acat2	NM_001006995	acetyl-Coenzyme A acetyltransferase 2	1.91
ILMN_1353902	Dennd1c	NM_001126289	DENN/MADD domain containing 1C	1.90
ILMN_1373158	Clec2l	NM_001044233	C-type lectin domain family 2, member L	1.90
ILMN_1363209	Efemp2	XM_001070338	EGF-containing fibulin-like extracellular matrix protein 2	1.89
ILMN_1360749	Aplf	NM_001173382	aprataxin and PNKP like factor	1.89
ILMN_1373978	Pcolce	NM_019237	procollagen C-endopeptidase enhancer	1.88

ILMN_1356806	Serpinh1	NM_017173	serine (or cysteine) peptidase inhibitor, clade H, member 1	1.87
ILMN_1375001	Col27a1	NM_198747	collagen, type XXVII, alpha 1	1.87
ILMN_1356512	Ap1g2	XM_214197	adaptor protein complex AP-1, gamma 2 subunit	1.87
ILMN_1349654	Crebl1	NM_001002809	cAMP responsive element binding protein-like 1	1.86
ILMN_1357732	Armc5	NM_001009455	armadillo repeat containing 5	1.86
ILMN_1359476	Nbeal2	XM_236649	neurobeachin-like 2	1.85
ILMN_1371992	Arv1	NM_001106197	ARV1 homolog (S. cerevisiae)	1.85
ILMN_1350517	Sfrs11	NM_001035255	splicing factor, arginine/serine-rich 11	1.84
ILMN_1368941	RGD1561145	NM_001134605	similar to novel protein	1.84
ILMN_1374618	Crb3	NM_001025661	crumbs homolog 3 (Drosophila)	1.84
ILMN_1353885	Zfp219	NM_001007681	zinc finger protein 219	1.84
ILMN_1367641	Git2	NM_001005553	G protein-coupled receptor kinase interacting ArfGAP 2	1.83
ILMN_1356069	Clk1	NM_001106913	CDC-like kinase 1	1.83
ILMN_1353448	LOC362725	XM_343047	similar to Retrovirus-related POL polyprotein	1.82
ILMN_1364845	RGD1305147	XR_009392	similar to RIKEN cDNA 1810048J11	1.82
ILMN_1374238	LOC690312	XM_001074055	similar to Fc receptor-like and mucin-like 1	1.82
ILMN_1362740	RGD1565059	NM_001127562	similar to hypothetical protein E130311K13	1.81
ILMN_1371331	Fnbp4	NM_001013159	formin binding protein 4	1.81
ILMN_1374027	Ppt1	NM_022502	palmitoyl-protein thioesterase 1	1.80
ILMN_1349485	LOC503197	XM_578721	similar to ATP synthase lipid-binding protein, mitochondrial precursor (ATP synthase proteolipid P1) (ATPase protein 9) (ATPase subunit C)	1.80
ILMN_1361731	Pabpn1	NM_001135008	poly(A) binding protein, nuclear 1	1.79
ILMN_1360269	Sfrs5	NM_019257	splicing factor, arginine/serine-rich 5	1.79
ILMN_1354884	Fstl1	NM_024369	follistatin-like 1	1.78
ILMN_1369730	Sidt2	NM_001108142	SID1 transmembrane family, member 2	1.78
ILMN_1360442	Yt521	NM_133423	splicing factor YT521-B	1.78
ILMN_1358403	Adcy4	NM_019285	adenylate cyclase 4	1.76
ILMN_1361299	Itgb1	NM_017022	integrin beta 1 (fibronectin receptor beta)	1.76
ILMN_1372853	LOC362985	XM_347091	similar to mKIAA3020 protein	1.76
ILMN_1366346	Emp3	NM_030847	epithelial membrane protein 3	1.75
ILMN_1357740	RGD1560636	XM_001063601	similar to novel protein	1.75
ILMN_1353961	Prpf3	NM_001108559	pre-mRNA processing factor 3	1.75
ILMN_1360410	U2surp	XM_001065014	U2 snRNP-associated SURP domain containing, transcript variant 2	1.75
ILMN_1349906	Casp2	NM_022522	caspase 2	1.75
ILMN_1368127	Tatdn3	NM_001105987	TatD DNase domain containing 3	1.74
ILMN_1376945	Tmem180	NM_001014030	transmembrane protein 180	1.74
ILMN_1373032	RGD1561715	XR_007960	similar to complement component 1, s subcomponent	1.74
ILMN_1354816	LOC497674	XM_579401	hypothetical gene supported by NM_017212	1.73
ILMN_1373348	Fas	NM_139194	Fas (TNF receptor superfamily, member 6)	1.73
ILMN_1351435	Anapc4	NM_001107220	anaphase promoting complex subunit 4	1.73
ILMN_1376672	Dync1h1	NM_019226	dynein cytoplasmic 1 heavy chain 1	1.72
ILMN_1373398	Tnfrsf4	NM_013049	tumor necrosis factor receptor superfamily, member 4	1.72
ILMN_1367561	LOC497794	XM_579477	hypothetical gene supported by NM_023103	1.72
ILMN_1364535	Rbm39	NM_001013207	RNA binding motif protein 39	1.72
ILMN_1355583	Bclaf1	NM_001047852	BCL2-associated transcription factor 1	1.71

ILMN_1361932	Kmt2e	NM_001100851	lysine (K)-specific methyltransferase 2E	1.71
ILMN_1375706	Rxrb	NM_206849	retinoid X receptor beta	1.71
ILMN_1370471	Cdc91l1	NM_181637	CDC91 cell division cycle 91-like 1 (S. cerevisiae)	1.71
ILMN_1352273	Klc1	NM_001081972	kinesin light chain 1, transcript variant A	1.70
ILMN_1369703	Naglu	XM_001081442	N-acetylglucosaminidase, alpha	1.70
ILMN_1376540	Spata7	NM_138862	spermatogenesis associated 7	1.69
ILMN_1368008	Mcoln1	NM_001105903	mucolipin 1	1.68
ILMN_1355376	Ercc5	NM_001106910	excision repair cross-complementing rodent repair deficiency, complementation group 5	1.68
ILMN_1373773	Pot1	NM_001024322	protection of telomeres 1	1.68
ILMN_1370484	Alms1	NM_001106604	Alstrom syndrome 1	1.67
ILMN_1352630	Sigirr	NM_001024887	single immunoglobulin and toll-interleukin 1 receptor (TIR) domain	1.66
ILMN_1375146	Cspp1	XM_001060285	centrosome and spindle pole associated protein 1	1.66
ILMN_1374672	Nol5	NM_021754	nucleolar protein 5	1.66
ILMN_1370339	Rarres2	NM_001013427	retinoic acid receptor responder (tazarotene induced) 2	1.64
ILMN_1358945	Kank3	NM_001108989	KN motif and ankyrin repeat domains 3	1.64
ILMN_1374578	RGD1307395	XM_001060221	similar to SR rich protein	1.64
ILMN_1363067	Slc9a1	NM_012652	solute carrier family 9 (sodium/hydrogen exchanger), member 1	1.63
ILMN_1352116	Ogt	NM_017107	O-linked N-acetylglucosamine (GlcNAc) transferase (UDP-N-acetylglucosamine:polypeptide-N-acetylglucosaminyl transferase)	1.63
ILMN_1649927	Tmem106c	NM_001008358	transmembrane protein 106C	1.62
ILMN_2039973	Bhmt	NM_030850	betaine-homocysteine methyltransferase	1.62
ILMN_1370376	LOC499031	XM_574321	similar to kinesin family member 25 isoform 1	1.61
ILMN_1355555	Taf1c	NM_001014155	TATA box binding protein (Tbp)-associated factor, RNA polymerase I, C	1.61
ILMN_1650076	Chtop	NM_001014175	similar to DKFZP547E1010 protein	1.61
ILMN_1650323	Vps33b	NM_022286	vacuolar protein sorting 33 homolog B (yeast)	1.60
ILMN_1352678	Knop1	NM_001134611	lysine-rich nucleolar protein 1	1.60
ILMN_1376513	Ctsb	NM_022597	cathepsin B	1.60
ILMN_1371937	LOC501139	XM_576559	similar to Ormdl1 protein	1.60
ILMN_1371416	Slc50a1	NM_001106445	solute carrier family 50 (sugar efflux transporter), member 1	1.59
ILMN_1376866	Znf18	NM_001012008	zinc finger protein 18	1.59
ILMN_1371270	Gpr56	NM_152242	G protein-coupled receptor 56	1.59
ILMN_1374214	Thoc1	XM_214625	THO complex 1	1.59
ILMN_1370972	Dtx2	NM_001107157	deltex homolog 2 (Drosophila)	1.59
ILMN_1367911	Abcg4	NM_001106816	ATP-binding cassette, subfamily G (WHITE), member 4	1.58
ILMN_1357995	RGD1559841	XR_009077	similar to expressed sequence AW413431	1.58
ILMN_1368568	Golga2	NM_022596	golgi autoantigen, golgin subfamily a, 2	1.58
ILMN_1376336	Mboat5	NM_001012189	membrane bound O-acyltransferase domain containing 5	1.58
ILMN_1359384	Topbp1	XM_236578	topoisomerase (DNA) II binding protein 1	1.58
ILMN_1362616	LOC497740	XM_579710	hypothetical gene supported by NM_178021	1.57
ILMN_1361040	Ostc	NM_001108566	oligosaccharyltransferase complex subunit (non-catalytic)	1.57
ILMN_1355605	Vkorc1	NM_203335	vitamin K epoxide reductase complex, subunit 1	1.56
ILMN_1362080	Klf6	NM_031642	Kruppel-like factor 6	1.56
ILMN_2040330	Tmed9	NM_001009703	transmembrane emp24 protein transport domain containing 9	1.56
ILMN_1353756	RGD1562094	XM_001080227	similar to RIKEN cDNA 2810426N06	1.56

ILMN_1368320	Tsc22d2	NM_001191960	TSC22 domain family, member 2	1.55
ILMN_1361346	RGD1564940	XM_575773	similar to RIKEN cDNA 3000004N20	1.55
ILMN_1371277	Pigq	NM_001007607	phosphatidylinositol glycan anchor biosynthesis, class Q	1.54
ILMN_1354877	LOC362587	XM_001055153	similar to microfilament and actin filament cross-linker protein isoform a	1.54
ILMN_1356051	RGD1560633	XM_218078	60S ribosomal protein L27a-like	1.54
ILMN_1358278	Tyro3	NM_017092	TYRO3 protein tyrosine kinase	1.54
ILMN_1364187	Tmem111	NM_001008355	transmembrane protein 111	1.54
ILMN_1374872	LOC499760	XM_575096	similar to serologically defined colon cancer antigen 3	1.53
ILMN_1349787	Tspo	NM_012515	translocator protein	1.53
ILMN_1357075	Myg1	NM_001005545	melanocyte proliferating gene 1	1.53
ILMN_1374816	Appl2	NM_001108741	adaptor protein, phosphotyrosine interaction, PH domain and leucine zipper containing 2	1.53
ILMN_1349757	Sirt5	NM_001004256	sirtuin (silent mating type information regulation 2 homolog) 5 (S. cerevisiae)	1.52
ILMN_1360062	Fam207a	NM_001008307	family with sequence similarity 207, member A	1.52
ILMN_1359049	Ilkap	NM_022606	integrin-linked kinase-associated serine/threonine phosphatase 2C	1.52
ILMN_1351625	Zpbp2	NM_001007011	zona pellucida binding protein 2	1.52
ILMN_1352750	Ccpg1	NM_001108770	cell cycle progression 1	1.51
ILMN_1349920	Mamdc2	XM_001078660	MAM domain containing 2	1.51

Appendix 4.1: Weekly profile of plasma IL-13 (pg/ml) in control and *IL-13* transfected rats

Batch	Rat	W0	W1	W2	W3	W4	W5	W6	W7	W8	W9	W10
B6	C1	69	21	37	27	0	9	30	19	24	26	44
B6	C2	91	29	36	47	76	27	34	27	30	39	26
B6	C3	42	71	27	16	24	8	17	16	28	22	30
B7	C1	47	18	45	84	47	21	41	0	15	22	20
B7	C2	28	31	25	26	22	26	22	18	19	15	32
B8	C1	83	70	13	40	20	50	42	44	47	22	D
B8	C2	38	97	34	92	111	66	D	D	D	D	D
B8	C3	50	43	42	D	D	D	D	D	D	D	D
B9	C1	43	NA	58	40	50	NA	41	12	NA	12	13
B9	C2	49	NA	55	31	115	NA	45	23	NA	18	18
B9	C3	71	NA	85	47	61	NA	46	23	NA	24	27
B10	C1	40	NA	44	36	34	NA	19	16	NA	20	13
B10	C2	41	NA	27	37	38	NA	31	31	NA	27	21
B10	C3	66	NA	25	49	48	NA	43	29	NA	32	13
B11	C1	52	19	27	31	D	D	D	D	D	D	D
B11	C2	14	18	10	NA	21	D	D	D	D	D	D
B11	C3	39	19	36	D	D	D	D	D	D	D	D
B11	C4	57	13	15	NA	13	NA	9	9	D	D	D
B12	C1	40	50	14	11	NA	10	13	9	NA	NA	19
B12	C2	16	13	13	10	NA	9	13	10	NA	NA	9
B12	C3	50	39	27	25	NA	49	10	16	NA	NA	15
B12	C4	35	42	19	11	NA	12	27	11	NA	NA	12
B12	C5	41	40	32	25	NA	11	10	24	NA	NA	15
B12	C6	71	61	40	46	26	D	D	D	D	D	D
B13	C1	29	11	NA	18	NA	10	8	D	D	D	D
B13	C2	24	14	NA	17	NA	10	17	NA	0	10	13
B13	C3	11	53	NA	11	NA	13	11	D	D	D	D
B13	C4	18	12	NA	16	NA	11	9	NA	10	11	10
B13	C5	33	40	NA	41	NA	48	31	D	D	D	D
B13	C6	10	27	NA	26	D	D	D	D	D	D	D
B14	C1	11	10	NA	28	NA	1	17	D	D	D	D
B14	C2	9	20	NA	31	29	D	D	D	D	D	D
B14	C3	12	13	NA	20	NA	19	24	D	D	D	D
B14	C4	18	14	NA	22	29	D	D	D	D	D	D
B14	C5	13	19	33	D	D	D	D	D	D	D	D
B14	C6	31	12	NA	42	NA	17	17	D	D	D	D
B15	C1	55	NA	55	88	55	NA	59	44	48	NA	49
B15	C2	45	NA	47	59	50	NA	51	29	15	NA	26
B15	C3	51	NA	44	92	55	D	D	D	D	D	D
B6	T1	61	62	43	37	21	319	99	97	D	D	D
B6	T2	62	77	530	548	389	294	398	137	D	D	D
B6	T3	38	43	36	48	41	282	232	250	D	D	D
B6	T4	54	23	36	31	65	362	921	912	560	395	788
B6	T5	47	205	81	50	69	111	26	82	52	39	29
B6	T6	61	35	65	40	51	809	393	272	110	91	155
B6	T7	47	43	229	278	195	136	422	874	399	556	536
B6	T8	248	71	51	40	47	214	763	655	370	546	447

B6	T9	72	65	383	202	280	266	70	508	66	112	81
B6	T10	103	73	28	33	4	188	588	165	57	62	137
B6	T11	67	56	87	56	101	209	153	81	30	27	39
B6	T12	47	58	72	106	167	147	128	68	124	68	187
B6	T13	40	39	21	25	65	84	40	364	152	524	725
B6	T14	65	65	55	55	30	199	80	54	46	305	361
B6	T15	35	28	210	172	99	74	41	90	71	43	708
B7	T1	15	995	266	114	612	1351	1881	1554	350	99	112
B7	T2	44	307	163	307	62	19	39	37	67	35	36
B7	T3	98	391	485	52	26	18	41	38	460	39	58
B7	T4	33	1145	714	317	127	87	156	47	66	44	63
B7	T5	29	950	998	101	869	464	100	44	43	67	74
B7	T6	26	3864	1263	879	3242	697	203	58	46	82	71
B7	T7	40	1497	1360	606	1387	250	111	39	50	66	61
B7	T8	81	1127	876	1418	935	602	114	64	112	82	79
B7	T9	140	1640	695	499	1812	D	D	D	D	D	D
B7	T10	30	729	2354	1067	1187	1646	5257	D	D	D	D
B8	T1	455	864	1414	D	D	D	D	D	D	D	D
B8	T2	43	877	992	170	83	518	D	D	D	D	D
B8	T3	21	273	136	759	983	958	767	829	841	606	1904
B8	T4	169	1021	911	805	614	167	94	898	113	113	74
B8	T5	12	845	478	368	1478	871	D	D	D	D	D
B8	T6	36	887	536	742	964	959	963	839	840	684	494
B8	T7	53	469	839	791	469	347	409	585	707	264	212
B8	T8	59	869	448	D	D	D	D	D	D	D	D
B8	T9	60	412	315	325	414	353	418	248	539	107	102
B9	T1	52	NA	571	773	94	NA	60	25	NA	10	33
B9	T2	52	NA	148	482	42	NA	41	32	NA	22	37
B9	T3	38	NA	184	704	634	NA	643	626	NA	170	316
B9	T4	86	NA	364	717	154	NA	86	78	NA	26	42
B9	T5	37	NA	121	673	848	NA	482	642	NA	493	1028
B9	T6	51	NA	480	977	735	NA	572	303	NA	153	210
B9	T7	84	NA	475	314	213	NA	85	261	NA	58	56
B9	T8	70	NA	129	1234	508	NA	151	510	NA	68	53
B9	T9	50	NA	116	449	92	NA	51	65	NA	14	25
B9	T10	37	NA	73	1214	558	NA	617	83	NA	997	374
B10	T1	30	NA	84	144	32	NA	32	26	NA	16	14
B10	T2	26	NA	47	72	43	NA	84	48	NA	544	612
B10	T3	34	NA	75	583	96	NA	45	35	NA	70	39
B10	T4	31	NA	621	182	79	NA	138	70	NA	162	63
B10	T5	49	NA	910	897	217	NA	223	259	NA	193	244
B10	T6	41	NA	386	65	66	NA	163	28	NA	51	28
B11	T1	13	491	1298	811	D	D	D	D	D	D	D
B11	T2	10	OVER	2040	D	D	D	D	D	D	D	D
B11	T3	25	906	479	NA	142	D	D	D	D	D	D
B11	T4	29	851	362	225	D	D	D	D	D	D	D
B11	T5	55	241	51	NA	55	NA	UNDER	85	D	D	D
B11	T6	27	54	672	NA	52	NA	219	292	D	D	D
B11	T7	36	UNDER	UNDER	NA	UNDER	D	D	D	D	D	D
B11	T8	17	2239	2161	D	D	D	D	D	D	D	D
B11	T9	43	1995	1170	D	D	D	D	D	D	D	D
B11	T10	83	369	128	1323	D	D	D	D	D	D	D
B11	T11	46	1115	363	NA	87	D	D	D	D	D	D
B11	T12	28	274	382	NA	61	NA	64	205	D	D	D

B12	T1	56	936	2032	592	NA	227	937	408	NA	NA	553
B12	T2	56	1176	1173	50	NA	43	23	33	NA	NA	71
B12	T3	54	887	273	69	413	D	D	D	D	D	D
B12	T4	53	175	57	387	NA	50	611	196	NA	NA	93
B12	T5	28	74	469	273	NA	216	76	43	NA	NA	188
B12	T6	53	1133	708	421	NA	157	257	104	NA	NA	170
B13	T1	16	214	NA	4420	D	D	D	D	D	D	D
B13	T2	19	106	NA	36	NA	258	56	NA	21	24	795
B13	T3	41	14970	NA	4853	D	D	D	D	D	D	D
B13	T4	37	57	NA	1154	NA	1028	1301	D	D	D	D
B13	T5	43	962	NA	279	NA	633	273	NA	778	808	302
B13	T6	35	452	NA	563	NA	150	304	NA	101	224	193
B14	T1	19	254	NA	4362	1742	D	D	D	D	D	D
B14	T2	12	1052	NA	235	NA	77	77	D	D	D	D
B14	T3	11	234	NA	165	NA	60	88	D	D	D	D
B14	T4	37	721	NA	582	NA	226	680	D	D	D	D
B14	T5	34	7186	1218	D	D	D	D	D	D	D	D
B14	T6	32	49	NA	155	NA	6	138	D	D	D	D
B15	T1	24	NA	591	306	339	NA	2401	290	77	NA	151
B15	T2	44	NA	13285	3074	1140	D	D	D	D	D	D
B15	T3	31	NA	604	199	338	NA	57	2233	558	NA	335
B15	T4	31	NA	388	393	69	NA	50	25	16	NA	60
B15	T5	34	NA	637	349	64	NA	44	22	20	NA	56
B15	T6	52	NA	94	105	543	NA	264	2244	832	NA	668
B15	T7	42	NA	147	10	15	NA	631	43	16	NA	70
B15	T8	25	NA	176	51	12	NA	43	11	9	NA	13
B15	T9	46	NA	209	45	51	NA	18	43	11	NA	45

'W' denotes week, 'C' denotes control rat, 'T' denotes *IL-13* transfected rat, 'NA' denotes not applicable and 'D' denotes dead. 'UNDER' denotes that IL-13 could not be detected in the plasma. 'OVER' denotes that IL-13 measured was above standard curve.

Appendix 4.2: Weekly profile of plasma cholesterol (mmol/l) in control and *IL-13* transfected rats

Batch	Rat	W0	W1	W2	W3	W4	W5	W6	W7	W8	W9	W10
B6	C1	2.50	1.99	2.71	2.77	2.98	2.63	3.15	3.02	2.47	2.93	2.65
B6	C2	2.27	1.43	2.31	2.59	3.43	2.64	3.02	2.99	2.43	2.77	2.87
B6	C3	2.53	1.71	2.21	2.82	2.93	2.19	2.66	2.43	1.91	2.07	2.05
B7	C1	2.02	2.07	2.14	2.67	2.12	2.39	2.67	2.49	2.35	1.98	1.89
B7	C2	2.02	1.76	2.10	2.07	1.74	2.12	2.05	1.29	1.69	1.79	1.65
B8	C1	1.75	2.09	2.31	2.18	2.56	2.50	2.61	2.09	2.52	2.21	1.82
B8	C2	1.95	2.10	2.51	2.67	2.40	2.35	D	D	D	D	D
B8	C3	2.10	1.98	2.27	D	D	D	D	D	D	D	D
B9	C1	2.10	NA	2.00	1.45	2.00	NA	2.05	2.10	NA	2.29	1.74
B9	C2	2.53	NA	2.12	1.82	2.48	NA	2.48	2.79	NA	3.23	2.41
B9	C3	2.10	NA	1.96	2.04	2.04	NA	1.75	1.87	NA	2.12	1.67
B10	C1	2.21	NA	2.16	2.07	2.55	NA	2.58	2.77	NA	2.49	2.88
B10	C2	2.04	NA	1.82	1.92	1.83	NA	1.96	1.86	NA	1.79	1.79
B10	C3	2.09	NA	1.33	2.06	2.06	NA	2.23	2.08	NA	2.01	2.03
B11	C1	1.95	1.67	1.72	NA	D	NA	D	D	D	D	D
B11	C2	1.74	1.28	1.57	NA	1.35	NA	D	D	D	D	D
B11	C3	2.07	1.92	1.65	NA	D	NA	D	D	D	D	D
B11	C4	1.82	1.60	1.67	NA	1.62	NA	1.71	1.85	D	D	D
B12	C1	1.57	1.48	1.64	1.97	NA	2.00	1.91	1.87	NA	1.91	1.87
B12	C2	1.90	1.86	1.97	2.29	NA	2.06	1.83	1.77	NA	2.20	1.96
B12	C3	1.99	2.07	1.82	2.04	NA	2.22	2.33	1.95	NA	2.18	2.00
B12	C4	2.02	1.70	1.67	1.93	NA	1.91	1.94	1.94	NA	2.10	1.93
B12	C5	1.86	1.54	1.79	1.88	NA	2.14	1.93	1.85	NA	1.73	1.63
B12	C6	1.83	1.66	1.73	1.87	1.88	D	D	D	D	D	D
B13	C1	1.92	1.83	NA	1.45	NA	2.36	1.94	D	D	D	D
B13	C2	1.32	1.38	NA	1.22	NA	1.48	1.54	NA	1.94	1.72	1.60
B13	C3	1.87	1.57	NA	1.45	NA	1.68	1.76	D	D	D	D
B13	C4	1.71	1.52	NA	1.63	NA	1.97	1.90	NA	2.37	2.10	2.03
B13	C5	1.61	1.20	NA	1.15	NA	1.65	1.51	D	D	D	D
B13	C6	1.36	1.26	NA	0.99	D	D	D	D	D	D	D
B14	C1	1.62	1.95	NA	1.81	NA	2.08	2.81	D	D	D	D
B14	C2	1.48	1.39	NA	1.35	1.73	D	D	D	D	D	D
B14	C3	1.97	1.76	NA	2.04	NA	2.09	2.13	D	D	D	D
B14	C4	1.44	1.60	NA	2.25	1.37	D	D	D	D	D	D
B14	C5	1.68	1.62	1.07	D	D	D	D	D	D	D	D
B14	C6	1.36	1.46	NA	1.37	NA	1.74	2.33	D	D	D	D
B15	C1	2.25	NA	2.03	1.87	1.76	NA	2.09	2.05	1.73	NA	2.01
B15	C2	2.15	NA	2.05	1.91	1.84	NA	2.10	2.10	1.83	NA	1.89
B15	C3	2.94	NA	3.20	2.74	2.93	D	D	D	D	D	D
B6	T1	2.73	2.01	2.84	2.93	3.55	2.60	3.09	2.40	D	D	D
B6	T2	2.39	1.87	2.52	2.15	3.84	2.99	3.08	2.77	D	D	D
B6	T3	2.12	1.80	2.17	2.28	2.96	2.34	2.43	2.40	D	D	D
B6	T4	1.93	1.68	2.12	2.00	3.15	2.30	3.12	3.64	3.53	3.21	3.54
B6	T5	2.82	1.55	2.26	3.02	3.53	2.66	2.90	2.77	2.16	2.39	2.09
B6	T6	1.79	1.61	1.88	2.54	2.16	2.16	2.41	2.27	2.09	2.32	1.96
B6	T7	2.77	1.91	2.58	3.49	2.98	2.63	2.82	2.77	2.35	3.03	3.00
B6	T8	2.04	1.58	2.30	2.13	3.20	2.60	3.09	2.92	2.87	2.73	2.94

B6	T9	1.77	0.84	1.76	2.26	2.32	2.28	2.54	2.71	2.36	2.16	2.31
B6	T10	2.03	1.51	1.95	2.32	2.89	2.79	3.11	2.81	2.31	2.23	2.29
B6	T11	1.85	1.15	2.29	2.33	3.15	2.77	3.53	2.72	2.62	2.45	2.42
B6	T12	1.89	1.29	2.09	2.34	3.14	2.19	2.41	2.82	2.25	2.28	2.33
B6	T13	2.50	1.74	2.34	2.34	3.01	2.17	2.45	2.60	2.30	2.45	2.80
B6	T14	2.29	1.89	2.20	2.37	2.87	2.17	2.45	2.51	2.16	2.51	1.92
B6	T15	1.95	1.65	1.98	2.21	2.87	2.56	3.33	2.91	2.36	2.48	2.52
B7	T1	1.19	2.00	2.08	1.87	2.26	2.23	2.73	2.49	2.29	2.51	2.61
B7	T2	2.35	2.11	2.57	2.32	2.41	2.30	2.77	2.27	2.26	2.35	2.72
B7	T3	2.59	2.20	3.05	3.00	2.79	2.76	2.76	2.41	3.24	2.79	3.26
B7	T4	2.46	2.48	2.18	2.83	2.22	2.33	2.64	2.15	1.90	2.25	1.28
B7	T5	2.70	2.75	3.05	2.91	2.61	3.44	4.22	2.99	3.06	3.41	2.97
B7	T6	2.26	3.01	3.14	2.83	4.10	3.64	4.50	3.75	3.48	3.87	3.51
B7	T7	1.67	2.49	4.33	4.50	5.81	5.92	5.60	6.93	6.60	6.60	6.37
B7	T8	2.13	2.33	2.75	2.58	3.09	3.65	3.34	3.04	3.01	2.86	2.54
B7	T9	2.24	2.70	3.53	2.94	6.34	D	D	D	D	D	D
B7	T10	2.57	2.13	3.07	2.93	2.93	3.03	3.54	D	D	D	D
B8	T1	1.76	2.90	2.67	D	D	D	D	D	D	D	D
B8	T2	1.01	1.43	2.47	2.72	2.32	2.53	D	D	D	D	D
B8	T3	1.38	1.78	2.62	2.51	2.14	2.06	2.31	2.08	2.93	2.35	2.27
B8	T4	1.88	2.16	2.43	1.69	2.56	2.78	2.38	2.99	3.32	2.75	2.46
B8	T5	2.25	2.49	2.86	2.44	3.18	3.40	D	D	D	D	D
B8	T6	1.59	2.17	2.51	1.95	2.43	2.21	2.36	2.27	2.78	2.55	2.22
B8	T7	1.92	1.98	2.56	2.50	2.89	2.85	1.76	2.59	3.25	2.09	2.82
B8	T8	1.95	3.05	3.02	D	D	D	D	D	D	D	D
B8	T9	2.04	2.42	2.88	2.64	2.60	2.62	1.85	3.22	3.61	2.55	2.93
B9	T1	2.77	NA	4.69	6.03	6.30	NA	6.09	6.63	NA	6.55	4.75
B9	T2	2.42	NA	1.78	1.81	2.11	NA	2.32	2.13	NA	2.35	1.52
B9	T3	1.81	NA	1.96	1.28	1.87	NA	1.82	1.94	NA	2.18	1.39
B9	T4	1.90	NA	1.90	0.82	2.11	NA	1.79	2.06	NA	2.27	1.16
B9	T5	2.89	NA	2.77	2.25	5.00	NA	4.70	4.99	NA	5.52	5.52
B9	T6	2.22	NA	2.23	1.81	2.11	NA	2.88	2.62	NA	2.26	1.98
B9	T7	2.35	NA	2.30	1.96	2.06	NA	1.94	2.36	NA	2.16	1.71
B9	T8	2.07	NA	2.40	2.43	2.43	NA	2.67	3.13	NA	2.62	1.46
B9	T9	2.58	NA	2.41	2.37	2.83	NA	2.58	2.74	NA	3.23	2.31
B9	T10	1.57	NA	1.90	2.78	3.24	NA	2.61	2.23	NA	3.71	2.41
B10	T1	2.50	NA	2.40	2.50	2.62	NA	3.02	3.04	NA	3.14	3.10
B10	T2	2.14	NA	1.90	2.22	2.33	NA	2.51	2.59	NA	2.24	2.47
B10	T3	1.77	NA	1.85	1.73	2.60	NA	1.82	2.22	NA	1.77	2.26
B10	T4	2.12	NA	2.17	3.24	3.03	NA	3.03	3.28	NA	2.88	3.13
B10	T5	2.04	NA	2.09	3.34	2.41	NA	2.72	2.49	NA	2.58	2.21
B10	T6	2.38	NA	2.14	3.74	2.55	NA	2.76	2.95	NA	3.10	2.83
B11	T1	1.57	1.78	1.89	NA	D	NA	D	D	D	D	D
B11	T2	2.17	3.88	5.07	NA	D	NA	D	D	D	D	D
B11	T3	2.10	2.24	2.08	NA	2.12	NA	D	D	D	D	D
B11	T4	1.81	1.50	1.44	NA	D	NA	D	D	D	D	D
B11	T5	2.43	1.87	1.72	NA	2.11	NA	1.99	1.93	D	D	D
B11	T6	2.43	2.01	2.09	NA	2.25	NA	2.41	2.50	D	D	D
B11	T7	2.04	1.91	1.87	NA	2.06	NA	D	D	D	D	D
B11	T8	2.20	4.23	4.63	NA	D	NA	D	D	D	D	D
B11	T9	1.79	3.31	3.05	NA	D	NA	D	D	D	D	D
B11	T10	2.42	1.84	1.79	NA	D	NA	D	D	D	D	D
B11	T11	3.37	3.96	3.27	NA	3.43	NA	D	D	D	D	D
B11	T12	2.03	1.67	1.45	NA	1.71	NA	1.87	1.79	D	D	D

B12	T1	2.05	1.79	1.78	2.11	NA	2.06	2.19	1.84	NA	2.25	1.84
B12	T2	1.77	1.56	1.34	2.13	NA	1.93	2.48	2.07	NA	1.92	1.64
B12	T3	2.19	1.94	2.06	2.42	2.37	D	D	D	D	D	D
B12	T4	1.62	1.58	1.58	1.88	NA	2.12	1.83	2.02	NA	2.27	1.72
B12	T5	1.76	1.82	1.72	2.01	NA	2.25	2.42	2.20	NA	2.47	2.08
B12	T6	1.52	1.67	1.58	2.01	NA	1.85	1.86	1.92	NA	1.88	1.56
B13	T1	1.44	1.31	NA	2.14	D	D	D	D	D	D	D
B13	T2	1.57	1.55	NA	1.45	NA	1.61	1.64	NA	1.76	1.76	1.80
B13	T3	1.68	1.78	NA	2.25	D	D	D	D	D	D	D
B13	T4	1.54	1.66	NA	1.63	NA	1.97	1.73	D	D	D	D
B13	T5	1.57	1.68	NA	1.54	NA	1.83	2.10	NA	2.45	2.63	2.15
B13	T6	1.61	1.52	NA	1.36	NA	1.60	1.65	NA	1.49	1.89	1.93
B14	T1	1.60	1.57	NA	3.05	3.04	D	D	D	D	D	D
B14	T2	2.10	2.48	NA	1.99	NA	2.76	3.45	D	D	D	D
B14	T3	1.71	1.60	NA	0.82	NA	2.20	2.36	D	D	D	D
B14	T4	1.61	1.81	NA	1.65	NA	1.87	2.36	D	D	D	D
B14	T5	1.83	2.72	3.30	D	D	D	D	D	D	D	D
B14	T6	1.48	1.78	NA	1.24	NA	1.91	1.79	D	D	D	D
B15	T1	1.97	NA	2.12	1.68	1.76	NA	2.12	2.12	1.92	NA	1.90
B15	T2	2.34	NA	3.54	6.74	11.71	D	D	D	D	D	D
B15	T3	2.06	NA	2.14	1.64	1.79	NA	2.00	2.63	1.93	NA	2.13
B15	T4	1.84	NA	2.21	2.30	2.23	NA	2.39	2.21	2.12	NA	2.17
B15	T5	2.18	NA	2.50	1.97	2.07	NA	2.04	1.89	2.01	NA	2.22
B15	T6	2.22	NA	2.86	2.61	2.65	NA	2.70	2.46	2.37	NA	2.53
B15	T7	1.94	NA	2.08	2.04	2.15	NA	2.34	2.25	2.30	NA	2.43
B15	T8	0.95	NA	1.67	1.58	2.03	NA	1.75	1.92	1.72	NA	1.89
B15	T9	3.24	NA	3.06	3.06	2.84	NA	2.76	2.95	2.67	NA	2.83

'W' denotes week, 'C' denotes control rat, 'T' denotes IL-13 transfected rat, 'NA' denotes not applicable and 'D' denotes dead.

Appendix 4.3: Weekly profile of urine albumin excretion (µg/24hour) in control and *IL-13* transfected rats

Batch	Rat	W0	W1	W2	W3	W4	W5	W6	W7	W8	W9	W10
B6	C1	363	644	396	610	1271	692	862	929	786	824	745
B6	C2	206	583	258	347	291	383	388	499	741	418	552
B6	C3	227	195	232	201	168	224	321	235	365	273	454
B7	C1	115	119	243	128	115	191	88	115	294	124	142
B7	C2	119	970	150	314	287	211	199	166	213	237	246
B8	C1	289	320	298	701	270	NA	118	182	140	167	NA
B8	C2	362	666	776	252	456	NA	D	D	D	D	D
B8	C3	745	404	436	D	D	D	D	D	D	D	D
B9	C1	261	NA	270	671	281	NA	183	287	NA	375	493
B9	C2	281	NA	698	2254	567	NA	553	508	NA	673	901
B9	C3	453	NA	547	1326	627	NA	499	548	NA	740	753
B10	C1	146	NA	261	224	563	NA	524	653	NA	344	566
B10	C2	693	NA	1081	1361	1047	NA	1153	712	NA	1364	615
B10	C3	1101	NA	448	718	494	NA	405	368	NA	359	591
B11	C1	916	233	226	NA	D	NA	D	D	D	D	D
B11	C2	364	277	621	NA	1233	NA	D	D	D	D	D
B11	C3	143	278	D	NA	D	NA	D	D	D	D	D
B11	C4	285	640	594	NA	362	NA	1005	324	D	D	D
B12	C1	149	147	154	NA	357	211	203	359	NA	194	133
B12	C2	146	236	248	NA	889	711	779	1188	NA	969	779
B12	C3	115	147	185	NA	457	425	397	489	NA	459	234
B12	C4	108	232	222	NA	173	382	412	445	NA	334	143
B12	C5	77	113	145	NA	270	355	731	99	NA	220	218
B12	C6	169	211	314	NA	353	D	D	D	NA	D	D
B13	C1	632	614	NA	549	NA	1036	1268	D	D	D	D
B13	C2	225	200	NA	292	NA	243	275	NA	450	342	162
B13	C3	255	241	NA	980	NA	259	605	D	D	D	D
B13	C4	90	196	NA	247	NA	163	142	NA	160	124	148
B13	C5	400	1012	NA	821	NA	2026	1566	D	D	D	D
B13	C6	253	333	NA	534	D	D	D	D	D	D	D
B14	C1	486	635	NA	1098	NA	865	1307	D	D	D	D
B14	C2	323	245	NA	479	396	D	D	D	D	D	D
B14	C3	386	699	NA	624	NA	1024	1539	D	D	D	D
B14	C4	552	652	NA	1510	922	D	D	D	D	D	D
B14	C5	242	308	575	D	D	D	D	D	D	D	D
B14	C6	349	188	NA	609	NA	693	1520	D	D	D	D
B15	C1	469	NA	258	527	331	NA	535	436	256	NA	250
B15	C2	453	NA	367	398	215	NA	264	363	354	NA	436
B15	C3	243	NA	463	554	510	D	D	D	D	D	D
B6	T1	364	346	365	620	584	394	540	445	D	D	D
B6	T2	3874	3443	2250	3540	705	1005	1466	1483	D	D	D
B6	T3	551	510	182	176	206	171	171	152	D	D	D
B6	T4	475	481	529	930	1603	2193	1462	785	674	687	1542
B6	T5	220	404	439	153	160	158	201	116	123	116	176
B6	T6	387	108	151	356	379	534	1147	1015	629	974	1718
B6	T7	409	474	630	307	299	224	205	191	162	130	180
B6	T8	2928	505	504	763	386	756	497	510	587	1107	868

B6	T9	282	402	311	600	714	334	601	713	747	550	1563
B6	T10	1196	292	210	247	207	243	246	165	163	132	170
B6	T11	6388	807	671	508	736	891	480	618	489	404	369
B6	T12	175	277	197	149	151	144	137	109	134	110	146
B6	T13	125	139	168	149	323	254	560	642	627	809	524
B6	T14	360	236	208	238	280	203	183	187	187	172	87
B6	T15	822	431	805	1393	480	940	1101	1185	826	881	3041
B7	T1	78	231	535	524	117	199	240	153	209	240	312
B7	T2	148	166	268	213	95	201	132	124	113	278	247
B7	T3	139	98	143	129	98	107	106	154	73	96	128
B7	T4	359	704	1006	248	326	284	238	185	162	289	213
B7	T5	311	1843	3618	5833	15053	1882	5792	9484	21357	37381	21015
B7	T6	125	238	293	103	126	177	173	138	208	249	1095
B7	T7	182	125	333	276	107	234	1273	391	637	1333	1067
B7	T8	86	114	149	94	92	126	120	148	144	140	165
B7	T9	129	77	110	5292	10042	D	D	D	D	D	D
B7	T10	216	369	451	719	484	281	520	D	D	D	D
B8	T1	1276	655	986	D	D	D	D	D	D	D	D
B8	T2	373	191	252	95	158	313	D	D	D	D	D
B8	T3	129	78	88	157	101	84	124	101	109	91	119
B8	T4	292	226	303	388	1608	737	833	1716	1757	4165	1378
B8	T5	163	131	149	167	197	178	D	D	D	D	D
B8	T6	826	307	415	227	274	125	290	329	176	147	190
B8	T7	226	323	196	329	286	98	164	407	230	222	516
B8	T8	400	329	645	D	D	D	D	D	D	D	D
B8	T9	346	398	597	866	348	346	283	1255	405	457	1015
B9	T1	157	NA	108	103	165	NA	249	327	NA	418	510
B9	T2	505	NA	270	329	209	NA	192	148	NA	179	179
B9	T3	164	NA	164	136	47	NA	65	118	NA	133	136
B9	T4	193	NA	295	203	925	NA	314	580	NA	559	465
B9	T5	188	NA	205	111	109	NA	190	145	NA	437	245
B9	T6	668	NA	886	907	1166	NA	1878	980	NA	1594	2206
B9	T7	215	NA	167	123	153	NA	117	113	NA	258	521
B9	T8	236	NA	606	535	901	NA	1355	1225	NA	2408	2211
B9	T9	168	NA	156	293	220	NA	268	242	NA	310	664
B9	T10	245	NA	197	70	72	NA	101	106	NA	200	197
B10	T1	251	NA	214	276	392	NA	639	600	NA	673	602
B10	T2	249	NA	241	196	312	NA	454	613	NA	854	652
B10	T3	434	NA	956	468	648	NA	520	355	NA	170	226
B10	T4	736	NA	593	158	385	NA	504	545	NA	576	546
B10	T5	368	NA	581	353	373	NA	558	322	NA	341	609
B10	T6	318	NA	606	1751	1883	NA	3281	6263	NA	3597	24487
B11	T1	165	268	199	NA	D	NA	D	D	D	D	D
B11	T2	484	202	D	NA	D	NA	D	D	D	D	D
B11	T3	293	197	225	NA	285	NA	D	D	D	D	D
B11	T4	237	452	544	NA	D	NA	D	D	D	D	D
B11	T5	182	198	244	NA	226	NA	607	548	D	D	D
B11	T6	516	440	337	NA	690	NA	2230	2576	D	D	D
B11	T7	211	232	226	NA	496	NA	D	D	D	D	D
B11	T8	242	275	D	NA	D	NA	D	D	D	D	D
B11	T9	380	269	D	NA	D	NA	D	D	D	D	D
B11	T10	352	191	232	NA	D	NA	D	D	D	D	D
B11	T11	237	427	522	NA	891	NA	D	D	D	D	D
B11	T12	229	340	180	NA	457	NA	311	1028	D	D	D

B12	T1	120	144	143	NA	210	257	341	316	NA	330	292
B12	T2	100	152	155	NA	291	307	1240	542	NA	479	459
B12	T3	193	197	215	NA	308	D	D	D	NA	D	D
B12	T4	155	356	355	NA	713	2021	2349	2013	NA	1997	1564
B12	T5	135	515	308	NA	487	1724	1380	1393	NA	7584	1729
B12	T6	177	451	577	NA	904	731	1059	1375	NA	1268	660
B13	T1	170	129	NA	104	D	D	D	D	D	D	D
B13	T2	512	1335	NA	2895	NA	1909	2548	NA	2946	1688	1050
B13	T3	452	270	NA	2633	D	D	D	D	D	D	D
B13	T4	250	323	NA	333	NA	808	176	D	D	D	D
B13	T5	331	264	NA	377	NA	348	145	NA	977	554	472
B13	T6	399	312	NA	495	NA	224	333	NA	NA	533	400
B14	T1	233	344	NA	308	268	D	D	D	D	D	D
B14	T2	179	200	NA	551	NA	1002	2322	D	D	D	D
B14	T3	544	1359	NA	555	NA	1577	1665	D	D	D	D
B14	T4	235	262	NA	213	NA	614	470	D	D	D	D
B14	T5	572	134	290	D	D	D	D	D	D	D	D
B14	T6	447	319	NA	1390	NA	719	302	D	D	D	D
B15	T1	251	NA	308	236	464	NA	784	1304	1956	NA	2318
B15	T2	216	NA	1234	1877	10239	D	D	D	D	D	D
B15	T3	343	NA	363	705	6064	NA	930	673	1235	NA	2502
B15	T4	203	NA	581	964	463	NA	679	1517	601	NA	1173
B15	T5	323	NA	377	579	327	NA	580	438	492	NA	656
B15	T6	229	NA	495	928	199	NA	486	630	1030	NA	935
B15	T7	1072	NA	1175	2638	1766	NA	2830	2823	2802	NA	2500
B15	T8	233	NA	1899	2342	5062	NA	2171	3277	2059	NA	3478
B15	T9	455	NA	176	352	353	NA	397	515	613	NA	613

‘W’ denotes week, ‘C’ denotes control rat, ‘T’ denotes IL-13 transfected rat, ‘NA’ denotes not applicable and ‘D’ denotes dead.

Appendix 4.4: Profile of control and HC rats

Batch	Rat	Plasma IL-13 (pg/ml)	Plasma total cholesterol (mmol/l)	Plasma albumin (g/l)	Plasma creatinine (μmol/l)	Urine albumin excretion (μg/24hour)	Body mass (g)	Liver mass (g)
B11	C3	36	1.65	31.0	81.1	278	196	8.4
B12	C1	19	1.87	44.1	70.5	133	241	10.0
B12	C3	15	2.00	36.3	96.4	234	284	10.1
B12	C4	12	1.93	35.6	114.1	143	300	9.9
B12	C6	26	1.88	44.2	95.2	353	241	8.8
B13	C2	13	1.60	35.0	91.1	162	311	10.3
B13	C4	10	2.03	36.0	91.1	148	251	7.4
B14	C2	29	1.73	34.3	116.9	396	222	7.7
B15	C2	26	1.89	37.8	106.8	436	270	10.5
B7	T1	112	2.61	44.2	94.0	312	278	13.6
B8	T2	518	2.53	42.3	83.5	313	259	11.1
B8	T3	1904	2.27	41.7	87.6	119	264	10.8
B8	T5	871	3.40	43.1	65.7	178	248	12.6
B8	T6	494	2.22	39.9	91.5	190	285	10.9
B8	T7	212	2.82	46.0	96.2	516	284	11.8
B8	T8	448	3.02	48.5	74.0	645	223	10.6
B11	T2	2040	5.07	46.6	89.3	202	221	14.0
B11	T8	2161	4.63	37.1	105.7	275	232	17.2
B11	T9	1170	3.05	36.0	88.6	269	214	11.5
B13	T1	4420	2.14	32.8	85.8	104	239	14.0
B13	T5	302	2.15	31.8	76.6	472	289	9.0
B14	T1	1742	3.04	37.1	61.8	268	245	11.8
B14	T4	680	2.36	38.1	65.8	470	236	9.0
B14	T5	1218	3.30	36.3	55.3	290	208	11.4

Rat column starting with ‘C’ represents control rat and ‘T’ represents HC rat.

Appendix 4.5: Plasma lipid profile of control and HC rats after overnight fasting

Batch	Rat	Total cholesterol (mmol/l)	LDL-cholesterol (mmol/l)	HDL-cholesterol (mmol/l)	Triglycerides (mmol/l)
B12	C6	1.88	1.23	0.43	0.49
B12	C1	1.87	0.81	0.52	1.18
B12	C3	2.00	1.41	0.33	0.55
B13	C2	1.60	0.86	0.56	0.39
B13	C4	2.03	1.18	0.64	0.45
B14	C2	1.73	1.19	0.32	0.48
B13	T1	2.14	1.33	0.52	0.62
B13	T5	2.15	1.41	0.53	0.44
B14	T5	3.30	2.30	0.71	0.62
B14	T1	3.04	1.89	0.90	0.56
B14	T4	2.36	1.46	0.76	0.31

Rat column starting with ‘C’ represents control rat and ‘T’ represents HC rat.

Appendix 4.6: Liver cholesterol profile of control and HC rats

Batch	Rat	Total cholesterol (mg/g liver)	Free cholesterol (mg/g liver)	Cholesteryl esters (mg/g liver)
B11	C3	1.46	1.19	0.28
B12	C1	0.77	0.66	0.11
B12	C3	0.82	0.68	0.14
B12	C4	1.07	0.79	0.27
B12	C6	0.93	0.70	0.23
B13	C2	1.05	0.93	0.12
B13	C4	1.12	0.97	0.15
B14	C2	0.91	0.74	0.17
B15	C2	0.83	0.74	0.10
B7	T1	0.79	0.69	0.11
B8	T2	0.86	0.68	0.19
B8	T3	0.87	0.74	0.14
B8	T5	0.92	0.72	0.20
B8	T6	0.84	0.72	0.12
B8	T7	0.88	0.74	0.14
B8	T8	0.95	0.67	0.28
B11	T2	1.17	0.94	0.23
B11	T8	1.14	0.92	0.21
B11	T9	0.89	0.69	0.21
B13	T1	0.71	0.62	0.10
B13	T5	1.11	0.89	0.22
B14	T1	0.83	0.69	0.15
B14	T4	1.01	0.84	0.17
B14	T5	0.82	0.64	0.19

Rat column starting with ‘C’ represents control rat and ‘T’ represents HC rat.

Appendix 4.7: Hepatic mRNA expression index was of IL-13 receptor subunits and cholesterol metabolic genes in control and HC rats

Batch	Rat	IL-4Ra	IL-13Ra1	IL-13Ra2	SREBF2	HMGCR	ACAT2	LXRa	RXRa	CYP7A1	LDLR	ABCA1	ABCG5
B11	C3	4.07E-01	1.16E-01	6.22E-03	1.90E-02	1.26E-01	2.43E-02	1.84E-01	8.80E-02	7.63E-02	2.03E-03	4.68E-02	1.40E-01
B12	C1	2.57E-01	2.85E-01	2.56E-03	3.57E-02	7.34E-02	3.93E-02	2.13E-01	1.79E-01	2.61E-02	4.34E-03	8.28E-02	2.62E-02
B12	C3	2.94E-01	3.33E-01	3.76E-03	5.01E-02	1.33E-01	3.15E-02	2.63E-01	2.13E-01	2.40E-02	6.98E-03	8.90E-02	3.80E-02
B12	C4	2.43E-01	3.03E-01	4.36E-03	4.74E-02	1.19E-01	4.06E-02	2.02E-01	1.49E-01	1.16E-02	5.43E-03	8.91E-02	1.29E-01
B12	C6	4.63E-01	4.94E-01	1.98E-02	5.16E-02	1.61E-01	3.90E-02	2.60E-01	2.44E-01	1.33E-01	5.70E-03	1.21E-01	2.01E-01
B13	C2	3.95E-01	5.14E-01	3.20E-02	3.75E-02	1.76E-01	3.81E-02	3.32E-01	2.01E-01	8.36E-02	4.29E-03	1.16E-01	3.40E-02
B13	C4	5.72E-01	4.48E-01	2.10E-02	3.11E-02	1.42E-01	4.51E-02	3.15E-01	1.79E-01	5.14E-02	2.80E-03	1.05E-01	1.03E-01
B14	C2	7.34E-01	6.60E-01	2.20E-02	4.68E-02	1.13E-01	4.69E-02	4.50E-01	2.47E-01	7.45E-02	1.47E-03	1.01E-01	1.41E-01
B15	C2	5.69E-01	5.40E-01	6.03E-03	5.40E-02	1.11E-01	5.50E-02	3.75E-01	2.32E-01	5.68E-02	7.08E-03	9.77E-02	7.18E-03
B7	T1	3.17E-01	3.34E-01	2.35E-02	3.29E-02	5.64E-02	2.96E-02	2.62E-01	1.07E-01	9.20E-02	3.14E-03	5.59E-02	1.50E-02
B8	T2	2.98E-01	2.81E-01	2.95E-02	3.57E-02	6.14E-02	3.22E-02	1.74E-01	1.19E-01	1.41E-02	4.87E-03	5.79E-02	2.92E-02
B8	T3	2.56E-01	3.10E-01	8.75E-02	3.70E-02	8.01E-02	2.19E-02	2.06E-01	1.20E-01	6.92E-02	5.81E-03	6.32E-02	1.26E-02
B8	T5	9.55E-01	2.37E-01	9.70E-02	3.67E-02	1.02E-01	2.22E-02	1.34E-01	9.71E-02	2.43E-02	6.64E-03	6.64E-02	6.40E-02
B8	T6	4.16E-01	3.68E-01	5.96E-02	7.06E-02	1.58E-01	3.82E-02	1.98E-01	1.38E-01	1.52E-01	8.78E-03	7.47E-02	1.55E-01
B8	T7	1.34E+00	3.61E-01	5.24E-02	4.28E-02	1.35E-01	3.55E-02	2.40E-01	1.73E-01	1.77E-01	8.25E-03	9.38E-02	5.50E-02
B8	T8	4.38E-01	2.54E-01	2.92E-02	2.52E-02	1.14E-01	2.58E-02	2.07E-01	1.49E-01	1.38E-02	3.23E-03	5.49E-02	9.37E-02
B11	T2	6.98E-01	2.23E-01	7.83E-02	2.95E-02	1.04E-01	3.51E-02	1.66E-01	9.85E-02	9.26E-02	2.92E-03	5.23E-02	2.25E-03
B11	T8	2.87E-01	1.33E-01	3.98E-02	2.28E-02	7.27E-02	2.22E-02	1.52E-01	8.50E-02	3.90E-02	1.79E-03	5.34E-02	7.73E-04
B11	T9	5.12E-01	1.69E-01	7.37E-02	2.13E-02	5.75E-02	2.29E-02	1.69E-01	1.19E-01	3.85E-02	1.24E-03	6.16E-02	1.75E-02
B13	T1	2.10E-01	3.39E-01	4.03E-01	2.81E-02	1.33E-01	2.99E-02	1.95E-01	1.17E-01	1.63E-01	3.00E-03	7.54E-02	9.99E-03
B13	T5	3.81E-01	3.04E-01	1.38E-01	1.67E-02	4.99E-02	2.26E-02	2.36E-01	1.36E-01	8.14E-03	1.51E-03	7.61E-02	1.39E-02
B14	T1	5.42E-01	4.79E-01	2.17E-01	3.22E-02	1.27E-01	3.43E-02	2.38E-01	1.96E-01	1.80E-01	1.67E-03	8.97E-02	2.47E-03
B14	T4	6.08E-01	6.03E-01	1.17E-01	3.12E-02	6.35E-02	2.92E-02	3.33E-01	2.87E-01	9.57E-02	2.03E-03	1.14E-01	7.51E-03
B14	T5	4.97E-01	6.62E-01	2.37E-01	3.80E-02	1.56E-01	3.25E-02	2.66E-01	2.10E-01	1.51E-01	2.48E-03	9.69E-02	9.19E-03

mRNA expression index was normalized against b-actin. Rat column starting with ‘C’ represents control rat and ‘T’ represents HC rat.

Appendix 4.8: Hepatic protein concentration of ABCG5 in control and HC rats

Batch	Rat	Concentration of liver ABCG5 (ng/ml)
B11	C3	340
B12	C1	299
B12	C3	258
B12	C4	365
B12	C6	426
B13	C2	334
B13	C4	499
B14	C2	484
B15	C2	306
B7	T1	192
B8	T2	237
B8	T3	301
B8	T5	265
B8	T6	251
B8	T7	260
B8	T8	245
B11	T2	270
B11	T8	264
B11	T9	254
B13	T1	218
B13	T5	494
B14	T1	359
B14	T4	448
B14	T5	290

Rat column starting with 'C' represents control rat and 'T' represents HC rat.

Appendix 4.9: Hepatic protein expression index was of IL-4Ra, IL-13Ra2, ABCA1 and LXRa in control and HC rats

Batch	Rat	IL-4Ra	IL-13Ra2	ABCA1	LXRa
B11	C3	0.68	0.45	2.24	0.57
B12	C1	0.50	0.61	NA	0.95
B12	C3	0.55	0.52	3.31	0.65
B12	C4	0.61	0.29	3.16	0.60
B12	C6	0.54	0.83	2.01	0.93
B13	C2	0.92	0.40	1.32	1.08
B13	C4	1.08	0.18	1.72	0.85
B14	C2	0.73	1.07	1.79	1.07
B15	C2	0.42	0.63	0.95	0.66
B7	T1	NA	NA	0.99	0.97
B8	T2	NA	NA	1.08	0.87
B8	T3	0.40	0.77	1.00	1.14
B8	T5	0.25	0.31	1.33	0.50
B8	T6	0.62	1.58	1.43	1.17
B8	T7	0.44	0.68	0.75	1.00
B8	T8	0.43	0.55	1.29	0.46
B11	T2	0.48	0.41	1.84	0.41
B11	T8	0.29	0.86	1.27	0.29
B11	T9	0.42	0.72	0.98	0.73
B13	T1	0.70	0.64	1.50	0.74
B13	T5	2.64	1.09	1.06	1.02
B14	T1	0.42	0.45	1.83	1.33
B14	T4	0.81	0.73	1.46	1.07
B14	T5	0.43	0.57	1.68	0.67

Protein expression index was normalized against GAPDH. Rat column starting with 'C' represents control rat and 'T' represents HC rat. 'NA' denotes not applicable.

Appendix 4:10: Correlation values for hepatic protein expression of LXRa and plasma total cholesterol in HC rats

Batch	Rat	Protein expression index was of LXRa	Plasma total cholesterol (mmol/l)
B7	T1	0.97	2.61
B8	T2	0.87	2.53
B8	T3	1.14	2.27
B8	T5	0.50	3.40
B8	T6	1.17	2.22
B8	T7	1.00	2.82
B8	T8	0.46	3.02
B11	T2	0.41	5.07
B11	T8	0.29	4.63
B11	T9	0.73	3.05
B13	T1	0.74	2.14
B13	T5	1.02	2.15
B14	T1	1.33	3.04
B14	T4	1.07	2.36
B14	T5	0.67	3.30

Appendix 5.1: mRNA expression index was of IL-13 receptor subunits and cholesterol metabolic genes in unstimulated and IL-13-stimulated hepatocytes

	IL-4Ra		IL-13Ra1	
Batch	Unstimulated	IL-13-stimulated	Unstimulated	IL-13-stimulated
H35	1.98E-01	1.98E-01	3.96E-02	2.99E-02
H38	2.12E-01	2.47E-01	3.88E-02	3.15E-02
H39	2.17E-01	2.17E-01	3.85E-02	3.00E-02
H42	2.42E-01	3.28E-01	3.33E-02	3.26E-02
H43	3.04E-01	3.38E-01	2.71E-02	2.79E-02

	SREBF2		HMGCR		ACAT2	
Batch	Unstimulated	IL-13-stimulated	Unstimulated	IL-13-stimulated	Unstimulated	IL-13-stimulated
H35	8.13E-03	7.45E-03	8.83E-02	4.40E-02	6.97E-03	8.43E-03
H38	7.40E-03	8.23E-03	5.66E-02	3.43E-02	5.81E-03	7.96E-03
H39	6.84E-03	6.85E-03	6.51E-02	3.47E-02	6.04E-03	7.19E-03
H42	7.93E-03	8.65E-03	6.25E-02	4.18E-02	7.18E-03	8.73E-03
H43	1.01E-02	9.95E-03	5.55E-02	3.51E-02	8.55E-03	1.02E-02

	LXRa		RXRa		CYP7A1	
Batch	Unstimulated	IL-13-stimulated	Unstimulated	IL-13-stimulated	Unstimulated	IL-13-stimulated
H35	9.48E-03	6.97E-03	2.56E-02	1.83E-02	5.63E-05	1.50E-05
H38	8.72E-03	4.93E-03	1.84E-02	1.35E-02	1.34E-04	9.68E-06
H39	5.36E-03	3.06E-03	1.79E-02	1.31E-02	1.16E-04	2.85E-05
H42	6.39E-03	4.80E-03	1.89E-02	1.43E-02	1.28E-05	4.21E-06
H43	1.05E-02	7.31E-03	3.54E-02	2.61E-02	2.03E-05	7.37E-06

	LDLR		ABCA1		ABCG5	
Batch	Unstimulated	IL-13-stimulated	Unstimulated	IL-13-stimulated	Unstimulated	IL-13-stimulated
H35	1.19E-03	1.29E-03	3.65E-02	1.96E-02	1.45E-04	4.49E-04
H38	1.60E-03	1.74E-03	1.47E-02	9.20E-03	1.04E-04	4.18E-04
H39	2.64E-03	2.60E-03	2.52E-02	1.73E-02	5.40E-05	2.13E-04
H42	3.02E-03	2.83E-03	1.63E-02	1.13E-02	5.98E-05	2.22E-04
H43	3.51E-03	3.25E-03	4.09E-02	1.90E-02	4.61E-05	9.37E-05

mRNA expression index was normalized against b-actin.

Appendix 5.2: Protein expression index was of LXRa and ABCA1, and protein concentration of ABCG5 in unstimulated and IL-13-stimulated hepatocytes

	LXRa	
Batch	Unstimulated	IL-13-stimulated
H16	0.72	0.47
H18	0.52	0.79
H20	0.81	0.94
H21	0.35	0.43
H29	0.66	0.68
H36	0.51	0.36

	ABCA1	
Batch	Unstimulated	IL-13-stimulated
H16	1.68	1.16
H18	0.69	0.81
H20	0.74	0.57
H21	0.71	0.50
H29	0.67	0.54
H36	0.69	0.41

	ABCG5 (ng/ml)	
Batch	Unstimulated	IL-13-stimulated
H76	87	105
H79	140	82
H81	95	76
H82	66	77
H87	87	92
H89	50	54

Protein expression index was normalized against GAPDH.

Appendix 5.3: Temporal mRNA expression index was of *LXRa*, *RXRa*, *ABCA1*, *ABCG5* and *CYP7A1* in unstimulated and IL-13-stimulated hepatocytes

LXRa	2H		4H		6H		8H	
Batch	Unstimulated	IL-13-stimulated	Unstimulated	IL-13-stimulated	Unstimulated	IL-13-stimulated	Unstimulated	IL-13-stimulated
H35	9.55E-03	7.37E-03	9.53E-03	8.86E-03	9.67E-03	8.82E-03	1.27E-02	1.08E-02
H38	6.88E-03	6.07E-03	8.09E-03	7.01E-03	9.19E-03	8.96E-03	9.20E-03	8.39E-03
H39	5.64E-03	4.81E-03	6.15E-03	5.23E-03	7.03E-03	6.06E-03	7.24E-03	5.57E-03
H41	4.58E-03	3.86E-03	5.28E-03	4.50E-03	6.08E-03	4.38E-03	5.31E-03	5.20E-03
H42	3.67E-03	3.64E-03	4.35E-03	3.49E-03	4.24E-03	3.13E-03	5.26E-03	3.39E-03

RXRa	2H		4H		6H		8H	
Batch	Unstimulated	IL-13-stimulated	Unstimulated	IL-13-stimulated	Unstimulated	IL-13-stimulated	Unstimulated	IL-13-stimulated
H35	2.85E-02	2.13E-02	2.37E-02	1.97E-02	2.33E-02	2.25E-02	2.68E-02	2.21E-02
H38	1.94E-02	1.86E-02	2.00E-02	1.84E-02	2.14E-02	1.95E-02	2.23E-02	1.97E-02
H39	1.88E-02	1.66E-02	1.78E-02	1.68E-02	1.74E-02	1.67E-02	1.90E-02	1.69E-02
H41	1.83E-02	1.75E-02	1.53E-02	1.51E-02	1.68E-02	1.27E-02	1.65E-02	1.42E-02
H42	2.04E-02	1.98E-02	1.76E-02	1.40E-02	1.62E-02	1.33E-02	1.59E-02	1.41E-02

ABCA1	2H		4H		6H		8H	
Batch	Unstimulated	IL-13-stimulated	Unstimulated	IL-13-stimulated	Unstimulated	IL-13-stimulated	Unstimulated	IL-13-stimulated
H35	5.60E-02	4.95E-02	5.38E-02	5.27E-02	5.40E-02	5.23E-02	4.71E-02	4.33E-02
H38	3.33E-02	3.42E-02	3.61E-02	3.72E-02	3.61E-02	3.07E-02	2.66E-02	2.16E-02
H39	4.61E-02	4.38E-02	4.54E-02	4.41E-02	4.06E-02	3.86E-02	3.45E-02	3.21E-02
H41	4.67E-02	4.57E-02	4.43E-02	4.62E-02	4.20E-02	3.62E-02	3.11E-02	2.84E-02
H42	4.57E-02	4.74E-02	4.64E-02	4.26E-02	4.32E-02	3.46E-02	3.40E-02	2.70E-02

ABCG5	2H		4H		6H		8H	
Batch	Unstimulated	IL-13-stimulated	Unstimulated	IL-13-stimulated	Unstimulated	IL-13-stimulated	Unstimulated	IL-13-stimulated
H35	6.71E-04	1.30E-03	5.98E-04	1.04E-03	4.41E-04	1.11E-03	3.36E-04	9.16E-04
H38	8.63E-04	1.38E-03	6.49E-04	1.42E-03	4.25E-04	1.33E-03	3.07E-04	1.12E-03
H39	3.50E-04	5.29E-04	2.42E-04	3.90E-04	1.63E-04	4.54E-04	1.10E-04	3.39E-04
H41	6.87E-04	1.22E-03	3.46E-04	8.91E-04	2.88E-04	6.05E-04	2.92E-04	7.02E-04
H42	5.22E-04	9.03E-04	3.67E-04	5.03E-04	2.28E-04	3.85E-04	1.96E-04	3.41E-04

CYP7A1	2H		4H		6H		8H	
Batch	Unstimulated	IL-13-stimulated	Unstimulated	IL-13-stimulated	Unstimulated	IL-13-stimulated	Unstimulated	IL-13-stimulated
H35	2.91E-04	4.41E-04	3.80E-04	3.27E-04	4.30E-04	2.53E-04	2.37E-04	2.06E-04
H38	1.45E-04	2.38E-04	1.28E-04	1.69E-04	8.23E-05	1.06E-04	5.91E-05	4.94E-05
H39	3.46E-04	4.62E-04	3.38E-04	3.05E-04	2.94E-04	2.16E-04	2.93E-04	1.57E-04
H41	5.66E-05	5.50E-05	2.18E-05	4.72E-05	3.07E-05	2.79E-05	2.67E-05	3.70E-05
H42	5.04E-05	2.58E-05	2.68E-05	1.75E-05	1.78E-05	1.32E-05	1.86E-05	1.12E-05

mRNA expression index was normalized against b-actin.

Appendix 5.4: Percentage of [^{3}H]-cholesterol efflux using apoA-I and taurocholate, and intracellular cholesterol level in unstimulated and IL-13-stimulated hepatocytes

5μg/ml ApoA-I-mediated [^{3}H]-cholesterol efflux (%)

Batch	Unstimulated	IL-13-stimulated
H100a	8.38	7.53
H100b	8.02	6.78
H102	8.02	5.49
H104	6.95	6.09
H105	7.88	5.37
H107	7.52	6.63

10mM Taurocholate-mediated [^{3}H]-cholesterol efflux (%)

Batch	Unstimulated	IL-13-stimulated
H76	13.51	12.02
H77	13.50	11.51
H78	14.99	11.19
H80	16.34	13.91
H81	17.97	16.32
H82	8.32	6.51
H83	13.71	12.99
H86	8.10	8.00
H90	15.30	14.92
H92	17.76	17.17

Intracellular cholesterol level (μg/mg)

Batch	Unstimulated	IL-13-stimulated
H1	188	187
H2	218	201
H3	308	257
H4	172	201
H5	226	215

Appendix 5.5: mRNA and protein expression index was of LXRa in NTC-transfected and *LXRa*-knockdown hepatocytes under unstimulated and T0901317-stimulated conditions

LXRa gene expression

Batch	NTC	LXRa siRNA	NTC +T	LXRa siRNA +T
H103a	3.90E-02	9.90E-03	2.13E-02	4.50E-03
H103b	3.31E-02	9.00E-03	2.29E-02	6.00E-03
H107	7.14E-02	2.31E-02	6.58E-02	1.89E-02
H116a	2.75E-02	2.70E-03	2.08E-02	2.90E-03
H116b	2.89E-02	5.40E-03	1.92E-02	3.20E-03

Gene expression index was normalized against b-actin.

LXRa protein expression

Batch	NTC	LXRa siRNA	NTC +T	LXRa siRNA +T
H101	6.37E-01	3.17E-01	NA	NA
H103a	6.91E-01	5.41E-01	4.22E-01	3.35E-01
H103b	5.51E-01	5.64E-01	4.22E-01	3.68E-01

Protein expression index was normalized against GAPDH. 'NA' denotes not applicable.

Appendix 5.6: mRNA and protein expression index was of ABCA1 and ABCG5 in NTC-transfected and *LXRa*-knockdown hepatocytes under unstimulated and T0901317-stimulated conditions

ABCA1 gene expression

Batch	NTC	LXRa siRNA	NTC +T	LXRa siRNA +T
H103a	1.69E-02	1.22E-02	8.69E-02	6.08E-02
H103b	1.34E-02	1.26E-02	8.40E-02	6.71E-02
H107	4.42E-02	4.66E-02	1.44E-01	9.37E-02
H116a	2.21E-02	9.30E-03	2.04E-01	1.47E-01
H116b	2.06E-02	1.29E-02	1.98E-01	1.26E-01

ABCG5 gene expression

Batch	NTC	LXRa siRNA	NTC +T	LXRa siRNA +T
H103a	1.35E-04	5.70E-05	4.33E-03	8.99E-04
H103b	6.00E-05	6.70E-05	5.92E-03	1.37E-03
H107	5.20E-04	6.76E-04	1.91E-02	5.56E-03
H116a	1.35E-04	2.60E-05	2.00E-03	6.40E-05
H116b	2.49E-04	7.60E-05	2.37E-03	3.00E-04

Gene expression index was normalized against b-actin.

ABCA1 protein expression

Batch	NTC	LXRa siRNA	NTC +T	LXRa siRNA +T
H101	1.27E+00	9.37E-01	NA	NA
H103a	2.78E-01	2.55E-01	7.11E-01	6.12E-01
H103b	2.27E-01	1.62E-01	8.48E-01	4.80E-01

Protein expression index was normalized against GAPDH. 'NA' denotes not applicable.